UNIVERSITY OF SOUTHAMPTON

FACULTY OF NATURAL AND ENVIRONMENTAL SCIENCES

CHEMISTRY

Coordination Complexes of Group 13 Halides: Towards a new Class of PET Imaging Agents

by

George Sanderson

Thesis for the degree of Doctor of Philosophy

April 2015

UNIVERSITY OF SOUTHAMPTON

ABSTRACT

FACULTY OF NATURAL AND ENVIRONMENTAL SCIENCES

Chemistry

Thesis for the degree of Doctor of Philosophy

Coordination Complexes of Group 13 Halides: Towards a new Class of PET Imaging Agents

George William Sanderson

Reaction of the triaza macrocycles RMe_2-tacn (R = Me, Bz) with the Group 13 chlorides MCl_3 gives the solvent free distorted octahedral adducts $[MCl_3(RMe_2\text{-tacn})]$ (M = Al, Ga, In). Reaction of the trichloro complexes with aqueous KF at room temperature yields the hydrated complexes $[MF_3(RMe_2\text{-tacn})]\cdot xH_2O$. The trifluoro complexes are formed in high yield, are stable under a range of conditions, and display significant H-bonding interactions between the coordinated fluoride ligands and the crystallised water molecules in the solid state, confirmed crystallographically.

The complex $[GaCl_3(BzMe_2\text{-tacn})]$ was successfully radiolabelled with aqueous $K^{18}F/^{19}F$ at room temperature to give the complex $[Ga^{18}F^{19}F_2(BzMe_2\text{-tacn})]$ with 30% incorporation in 45 minutes. The purified compound is stable in phosphate buffered saline at pH 7.5 and represents an exciting alternative route towards the ^{18}F radiolabelling of temperature sensitive biomolecules in PET imaging applications.

The complex $[GaF_3(BzMe_2\text{-tacn})]$ can act as a metalloligand towards alkali metal and ammonium salts via coordination of the metal fluoride fragment. Crystallographic analyses show that this results in a series of unusual supramolecular assemblies with Li^+, Na^+ and K^+.

Reaction of $Ga(NO)_3\cdot 9H_2O$ with 1-benzyl-1,4,7-triazacyclononane-4,7-dicarboxylic acid hydrochloride (L·HCl) gives the complex $[GaCl(L)]\cdot 2H_2O$. Treatment of this complex with carrier free $^{18}F^-$ at 80 ^oC gives the radiolabelled complex $[Ga^{18}F(L)]$ in high yield. The compound may be purified by a cartridge based method. The purified compound is stable up to at least pH 6, but loses fluoride at neutral pH.

Hydrothermal synthesis was used to access complexes of the poorly soluble hydrated Group 13 fluorides directly. Reaction of $MF_3\cdot 3H_2O$ (M = Al, Ga, In) with the tridentate imine ligand 2,2',2''-terpyridine gives the hydrated adducts *mer*-$[MF_3(terpy)]\cdot 3H_2O$. The complexes display extensive H-bonding interactions in the solid state. Attempts to access the ^{18}F labelled complex $[Ga^{18}F^{19}F_2(terpy)]$ *via* halide exchange from the preformed trichloro complex as an alternative complex type for potential use in PET imaging were not successful. Reaction of $MF_3\cdot 3H_2O$ with the bidentate imines 1,10-phenanthroline and 2,2′-bipyridine (L-L) under hydrothermal conditions gives the neutral complexes $[MF_3(L\text{-}L)(OH_2)]$.

A number of alternative tacn based ligands incorporating amide pendant arm functionality were synthesised and characterised as potential future architectures for metal complexes used in imaging applications.

Contents

List of tables

List of figures

List of accompanying materials

Appendix 1 General Experimental Techniques

Appendix 2 Crystallographic information files (cif) for structures discussed in this thesis

Definitions and Abbreviations

^{18}F	fluorine-18
bipy	2,2′-bipyridine
br	broad
Bu	butyl
Bz	benzyl
cyclam	1,4,11,14-tetraazacyclotetradecane
cyclen	1,4,7,10-tetraazacyclododecane
efg	electric field gradient
ESI	electrospray ionisation
Et	ethyl
fac	facial
GMP	good manufacturing practice
HSA	human serum albumin
IR	infra-red
m	multiplet
Me	methyl
mer	meridional
Mes	mesityl, (2,4,6-trimethyl)
MS	mass spectrometry
NMR	nuclear magnetic resonance
ORTEP	Oak Ridge thermal ellipsoid plot
PBS	phosphate buffered saline
PET	positron emission tomography
pmdta	N,N,N′,N′,N″-pentamethyldiethylenetriamine
qt	quartet
RCP	radiochemical purity
s	singlet
sh	sharp
tacn	1,4,7-triazacyclononane
^{t}Bu	*tert*-butyl
terpy	2,2’,2’’-terpyridine
thf	tetrahydrofuran
Ts	tosyl, p-toluenesulfonate
w	weak

DECLARATION OF AUTHORSHIP

I, **George William Sanderson** declare that this thesis entitled **Macrocyclic Complexes with Group 13 Halides; Towards a new Class of PET Imaging Agents** and the work presented in it are my own and has been generated by me as the result of my own original research.

I confirm that:

1. This work was done wholly or mainly while in candidature for a research degree at this University;

2. Where any part of this thesis has previously been submitted for a degree or any other qualification at this University or any other institution, this has been clearly stated;

3. Where I have consulted the published work of others, this is always clearly attributed;

4. Where I have quoted from the work of others, the source is always given. With the exception of such quotations, this thesis is entirely my own work;

5. I have acknowledged all main sources of help;

6. Where the thesis is based on work done by myself jointly with others, I have made clear exactly what was done by others and what I have contributed myself;

7. Parts of this work have been published as:

Triaza-macrocyclic complexes of aluminium, gallium and indium halides: fast 18F and 19F incorporation via halide exchange under mild conditions in aqueous solution, Bhalla, R.; Darby, C.; Levason, W.; Luthra, S. K.; McRobbie, G.; Reid, G; **Sanderson, G**.; Zhang, W. *Chem Sci*. **2014**, 5, 381-391

[GaF_3($BzMe_2$-tacn)] - a neutral 'metalloligand' towards alkali metal and ammonium cations in water, Bhalla, R.; Levason, W.; McRobbie, G.; Reid, G.; **Sanderson, G**; Zhang, W. *Chem Commun.* **2014**, 5, 12672-12675

Radiofluorination of a Pre-formed Gallium(III) Aza-macrocyclic Complex: Towards Next-Generation Positron Emission Tomography (PET) Imaging Agents, Bhalla, R.; Levason, W.; Luthra, S. K.; McRobbie, G.; Reid, R; **Sanderson, G**. *Chem. Eur. J*. **2015**, 21, 4688-4694

Hydrothermal synthesis of Group 13 metal trifluoride complexes with neutral N-donor ligands, Bhalla, R,; Levason, W.; Luthra, S. K.; McRobbie, G.; Monzittu, M. F.; Palmer, J.; Reid, G.; **Sanderson, G**.; Zhang, W. *Dalton. Trans.* **2015,** DOI: 10.1039/C5DT01120E

Signed: .....

Date:.....

Acknowledgements

A page doesn't seem long enough to express my thanks to all the people who have been part of my life for the last few years, and I'm sure I'll forget loads of them. While I am the one who has had to write this thing, there is no way I could have done it without the help and support of a huge number of people.

Firstly, I would like to thank my academic supervisors Professors Gillian Reid and William Levason. They have been an incredible source of guidance, knowledge, inspiration and time. Thank you for your belief in me and I only I hope I managed to meet their expectations for the project. I wish to offer huge thanks to Dr Graeme McRobbie and Dr Rajiv Bhalla from GE Healthcare who acted as fantastic industrial supervisors. In particular Graeme, who facilitated so many of my industrial visits and became a great source of advice, support, expertise and friendship. I shall miss our days in the lab together.

I would also like to thank current and past members of my research group for their constant support and advice…and for putting up with me! Davros, Martan, JEB, Andai, Sloth, Pepè and others, you have made it an amazing 3 years. But there is one man in particular who I must thank most from the group, Dr Wenjian Zhang, you are a legend! I cannot thank you enough for your guidance and advice in the early days, and you have remained an incredibly helpful and supportive colleague throughout my time here. I shall miss you terribly.

Thanks to the many 1000s of men (probably) who have played for SUCC over the years. You have all in your little way helped me de-stress and enjoy a life outside of the laboratory.

To my family…who don't have a bloody clue what this is about, thank you for always being there for me and supporting me in any way you could, it helped more than you know.

To the wolf pack, Jack, Pierre and Rick, thank you gents for some unbelievable weekends. Braai, golf and red wine, what more can a man ask for? And to Jack in particular, thank you for the evenings spent gribbling, the garage will be available for you to grow old in…

While I was blessed with some decent project students, there is one in particular who has gone on to change my life in a way I could never imagine. Jaz, you have been my rock throughout the last year or so and I can't tell you how lucky I am to have you. You have kept me fighting even when I was at my lowest and I will forever be so grateful to you…and you did some damn good chemistry!

Finally, thanks to the EPSRC and GE Healthcare for the dosh. It has been an absolute pleasure!

George Sanderson

April 2015

Chapter 1

Introduction

This thesis describes the development of new coordination chemistry of Group 13 metal halide complexes and their potential applications towards the formation of ^{18}F containing complexes for PET imaging agents. This chapter describes the current state of the art in regards to ^{18}F labelled compounds for PET imaging and an appreciation of their respective merits and limitations. The recent research towards an inorganic approach to ^{18}F labelled imaging agents is also shown. The Group 13 ions were identified as suitable candidates for the proposed application. The rationale for this is discussed, as well as their coordination chemistry. A number of characterisation methods were used in the identification of the complexes synthesised and are described in this chapter.

1.1 Positron Emission Tomography and ^{18}F

Positron emission tomography (PET) is an attractive medical imaging technique designed to map the position and severity of tumours and muscle tears.[1] The technique relies upon the radioactive decay of an atomic nucleus. As the nucleus decays, a positron (β^+) is emitted, which upon decay quickly interacts with an electron, resulting in an annihilation event. The annihilation emits two photons at 180 degrees to one another. Thus the source of photon emission may be tracked and mapped along a line of coincidence (Figure 1.1).[2]

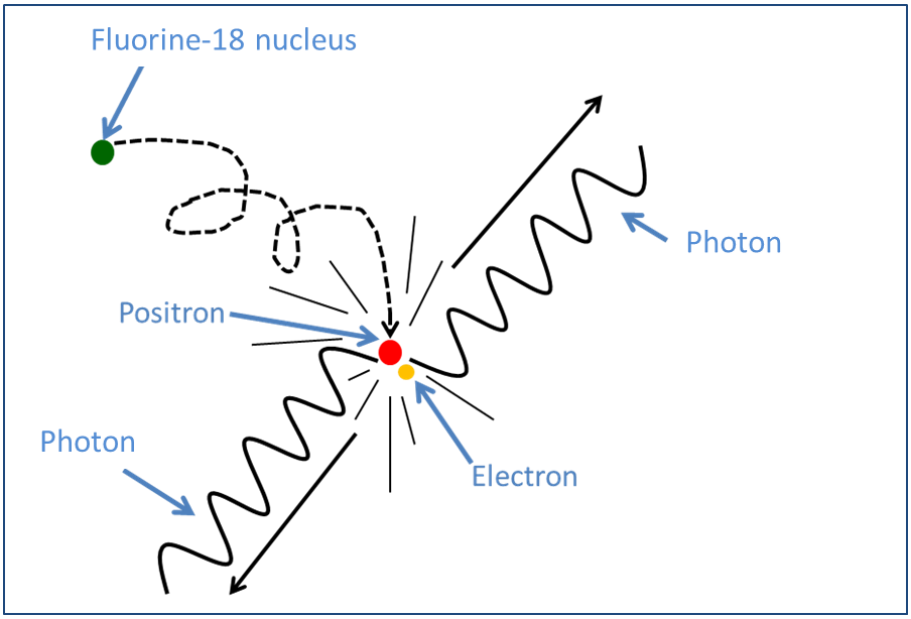

Figure 1.1: Diagram showing the decay process observed during positron emission.

The technique allows high quality 3D images to be obtained (Figure 1.2).

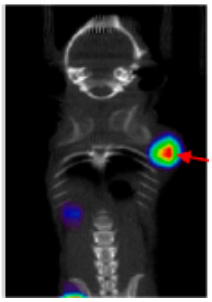

Figure 1.2: PET imaging scan showing the dynamic [^{18}F]-fluciclatide distribution in a mouse displaying a solid-core tumour.[3]

A number of positron emitting radio isotopes are utilised in PET imaging applications, their properties are summarised in Table 1.1.

Isotope	Half-life ($t_{1/2}$)	Energy of positron emission/ MeV
^{11}C	20.4 mins.	0.96
^{13}N	9.96 mins.	1.19
^{15}O	2.07 mins.	1.72
^{18}F	109.7 mins.	0.64
^{64}Cu	12.7 hours	0.66
^{68}Ga	67.7 mins.	1.90
^{89}Zr	78.5 hours	0.40

Table 1.1: Summary of properties of radio isotopes used in PET imaging applications.

Although there are several examples of radiopharmaceuticals utilising the radio isotopes shown above, the most widely used radio isotope in PET imaging is fluorine-18 (^{18}F). ^{18}F is a very suitable radio nuclide for PET applications due to the low energy of its positron emission, its safe decay route into the non-toxic ^{18}O isotope, and its moderately short half-life that minimises the amount of radioactive exposure received by the patient. The added benefit of ^{18}F is the availability and functionality of the cyclotron sources used to generate the isotope.

Current radiopharmaceutical production using ^{18}F is dominated by organofluorine chemistry.[4] Labelling carbon based molecules with ^{18}F is performed by reactions in which the ^{18}F reagent is either nucleophilic or electrophilic in nature.

The nucleophilic route is the most versatile. The nucleophilic fluoride is delivered from the cyclotron as [^{18}F]-fluoride in aqueous solution. This gives a bio-compatible, easy to handle reagent with no carrier added fluoride. However, the $^{18}F^-$ in aqueous solution is a poorer nucleophile due to the strong hydrogen bonding interactions with the solvent water molecules and tight hydration sphere. While most reactions may still be performed using aqueous $^{18}F^-$, on occasion more efficient labelling is achieved by the transfer of the fluoride into polar-aprotic conditions, commonly anhydrous MeCN. This is achieved by trapping the fluoride onto an ion exchange resin, followed by elution with Kryptofix 222, a bicyclic amino polyether, and potassium carbonate in MeCN (Figure 1.3).[5]

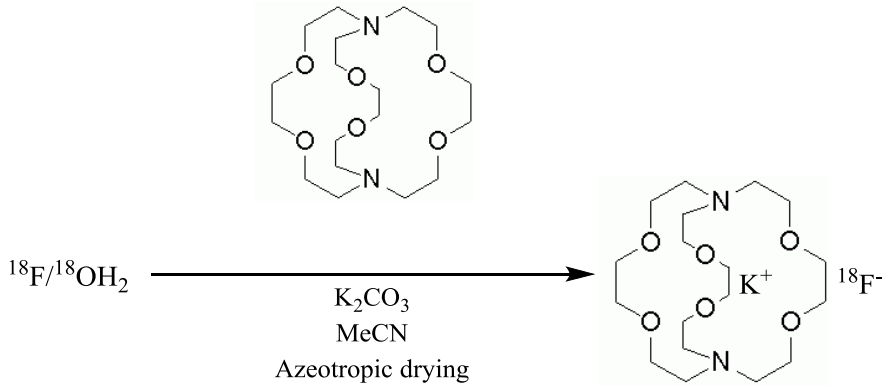

Figure 1.3: Synthesis of [K(2.2.2-crypt)]^{18}F

The most widely used PET radiopharmaceutical compound is fludeoxyglucose, ^{18}F-FDG (2-deoxy-2-(^{18}F)fluoro-*D*-glucose) (Figure 1.4) which is made via nucleophilic substitution.[6] The compound is highly active and is easily excreted as the ^{18}F decays to ^{18}O.

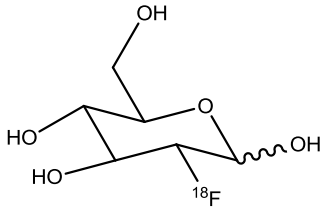

Figure 1.4: Structure of [^{18}F]-FDG.

The ^{18}F occupies the 2' position normally occupied the hydroxyl group. FDG is taken up in areas of high glucose concentration such as brain and kidney cells.

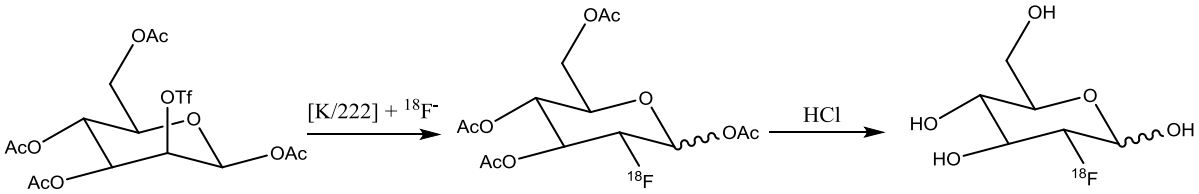

Figure 1.5: Synthesis of [^{18}F]-FDG by nucleophilic fluorination.[5]

Figure 1.5 demonstrates the challenges of nucleophilic fluorination. The procedure requires two synthetic steps, followed by a further purification step by preparative HPLC, which are time consuming and raise GMP (good manufacturing practice) issues in an industrial environment. Further, as the $^{18}F^-$ is not introduced at a late stage in the synthesis a considerable amount of initial activity is required in order to maintain a suitable dose for clinical applications.

The clinical importance and high volume production of [^{18}F]-FDG has made it worthwhile to perform this multi-step operation on a daily basis. Radiolabelling more complex and less robust molecules such as peptides and proteins, which are used less frequently using such methods are less economically attractive and more technically challenging.

Other examples of ^{18}F containing radiopharmaceuticals accessed via nucleophilic substitution of $^{18}F^-$ include Flutemetamol, developed by GE Healthcare as a diagnostic tool for Alzheimer's disease (Figure 1.6).[7, 8]

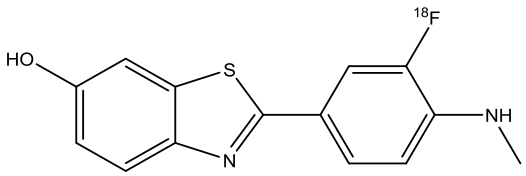

Figure 1.6: Structure of [^{18}F]-Flutemetamol

The alternative method of incorporating ^{18}F into carbon based molecules is via electrophilic fluorination. Currently, electrophilic ^{18}F is delivered as a highly reactive gas [^{18}F]-F_2 where the ^{18}F is significantly outnumbered by non-radioactive ^{19}F. ^{18}F incorporation by electrophilic routes tends to be non-specific resulting in a mixture of unwanted by-products. An example of electrophilic fluorination in the synthesis of a bioactive compound is shown in the preparation of [^{18}F]-FDOPA (2-fluoro-5-hydroxy-L-tyrosine) (Figure 1.7).[9]

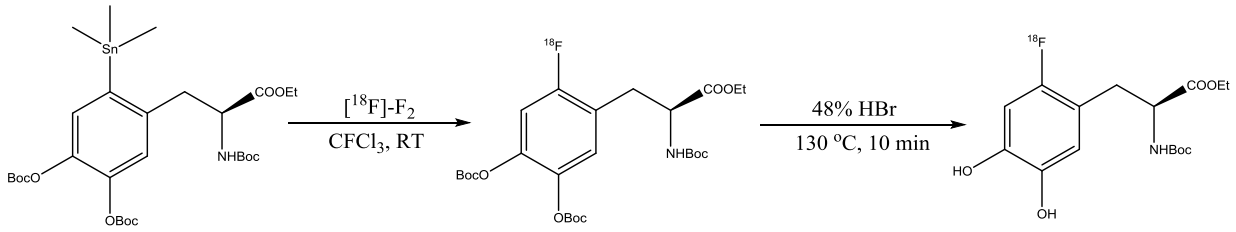

Figure 1.7: Synthesis of [^{18}F]-FDOPA using electrophilic ^{18}F.[9]

The challenging nature of using gaseous [^{18}F]-F_2 as a source of electrophilic ^{18}F has resulted in a number of elegant solutions to access electrophilic ^{18}F in the solution phase (see Chapter 1.2.1).

The limitations of organofluorine based ^{18}F PET imaging agents has resulted in a surge in the development of novel approaches to labelling compounds of biological interest *via* facile late stage nucleophilic fluorination under mild conditions incorporating alternative E-^{18}F (E = B, Si, Al) bond forming reactions (Chapter 1.2).[5]

This has led to a departure from traditional organic synthesis and the development of new inorganic approaches to the radiolabelling of biologically active molecules.

1.2 Inorganic Approaches to ^{18}F labelled radiopharmaceuticals

1.2.1 Transition metal catalysed electrophilic fluorination

There have been a number of novel routes towards solution based electrophilic fluorinating agents, which utilise transition metal containing coordination complexes.

Selected examples include catalytic fluorination and trifluoromethylation with palladium aryl complexes, as demonstrated by Buchwald *et al.*[10, 11] Groves and co-workers utilised a manganese(IV) porphyrin complex to catalyse alkyl fluorination by fluorine under mild conditions (Figure 1.8).[12]

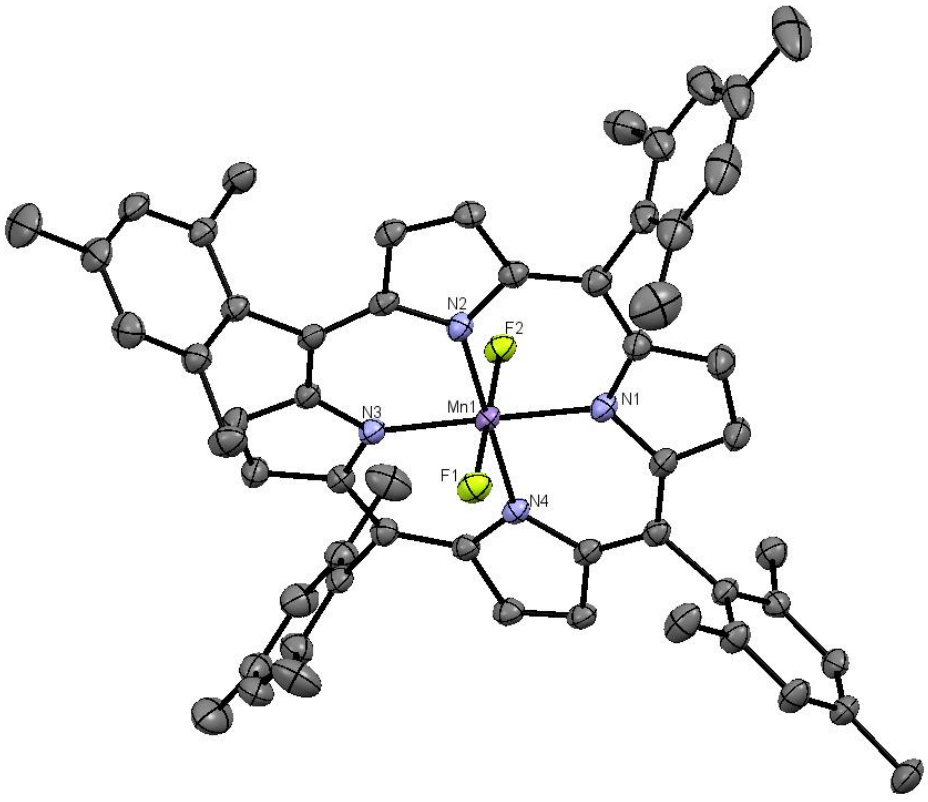

Figure 1.8: The crystal structure of [MnF_2(tmp)]. tmp = tetramesityl-porphryin.[12] Image redrawn from CCDC 893742

The six coordinate manganese(IV) complex with *trans* fluoride ligands was accessed directly from reaction of the corresponding [$MnCl_2$(tmp)] complex with excess AgF.

Recent work by Ritter *et al.* has demonstrated the ability to form electrophilic ^{18}F in solution by incorporating ^{18}F into a sterically encumbered palladium,[13] and more recently nickel[14] aryl complex (Figures 1.9 and 1.10). They have demonstrated the ability of these complexes to perform late stage electrophilic fluorination on a number of biologically active compounds.[15]

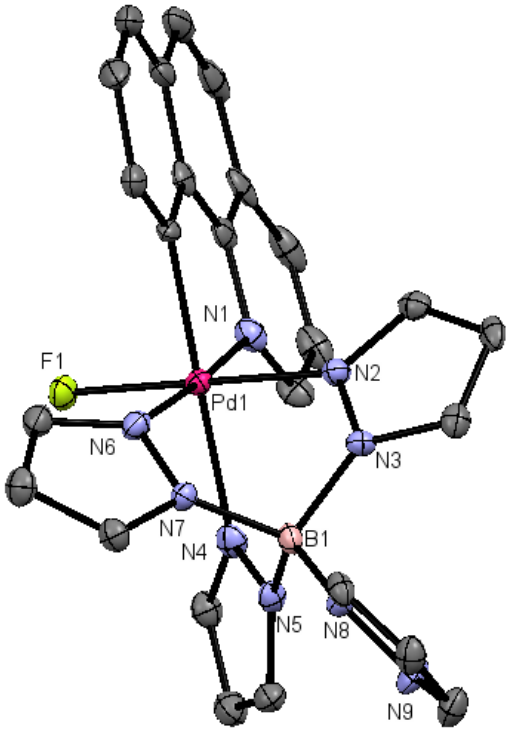

Figure 1.9: The crystal structure of the cationic palladium(IV) aryl complex utilised by Ritter *et al.* as a source of electrophilic fluorine.[13] Image redrawn from CCDC 829428.

The sterically bulky aryl substituents with electron withdrawing aromatic heterocyclic moieties on the Pd(IV) centre acts to direct any nucleophilic attack away from the metal centre and towards the fluorine ligand, forcing the fluorine ligand to act as the electrophile.[13] Subsequent reaction results in the reduction of the Pd(IV) centre to Pd(II) as the ^{18}F-biomolecule is cleaved.

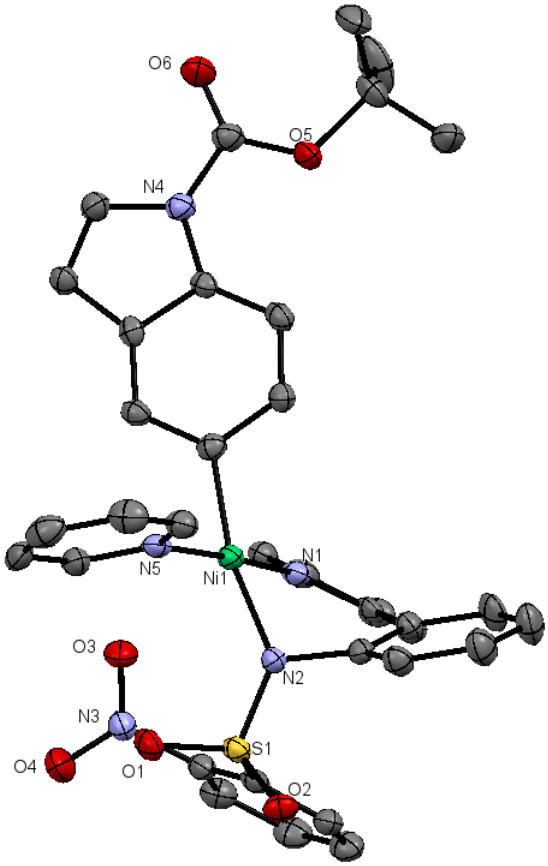

Figure 1.10: Crystal structure of the Ni(II) aryl complex utilised by Ritter *et al.* in their study of aqueous oxidative fluorination using ^{18}F towards PET imaging agents.[14] Image redrawn from CCDC 896034

The square planar nickel(II) aryl complex allows the use of aqueous fluoride ($^{18}F^-$), which greatly simplifies the synthetic procedure, and unlike the Pd(IV) complex discussed earlier, does not require a fluoride capture step. This rapidly accelerates the synthetic procedure, meaning lower activities of ^{18}F are required.[14]

The use of transition metal complexes as catalysts for the late stage fluorination of organic compounds under mild conditions has represented a significant shift in the field of organo-fluorine chemistry and continues to be an increasing area of research and development.[15]

1.2.2 B-^{18}F bond formation

B-F bonds are some of the most thermodynamically stable covalent interactions known (~613 kJmol^{-1}).[16] This makes them very suitable for use in imaging applications as there is less risk of the B-F bond being cleaved by biological processes. Most work on boron as a fluoride binding site for molecules has focused on the reaction of aryl boronic esters with fluoride containing synthons (Figure 1.11).[5, 17]

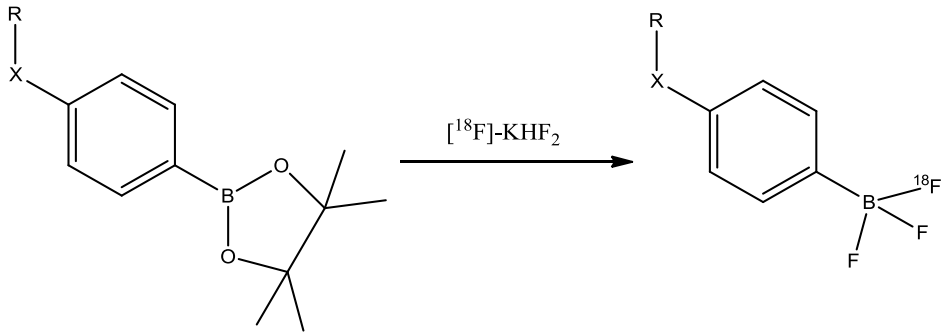

Figure 1.11: General synthetic route for the ^{18}F radiolabelling of boronic ester conjugates *via* reaction of nucleophilic ^{18}F (in the form of potassium hydrogen fluoride). X = an amide linker, R = biologically active compound.[5]

The groups of Perrin and Ting have produced numerous functionalised boronic ester bioconjugates as radiopharmaceutical precursors with the potential to be radiolabelled by conversion to the organotrifluoroborate derivative.[17-20]

This chemistry has several attractive features which make it a viable route to ^{18}F radiolabelled biomolecules, such as the fluorinations being accomplished under aqueous conditions, avoiding the need to undertake azeotropic drying. The labelling can be performed in a single radioactive step, thus reducing the initial activity of ^{18}F required. In addition the fluorination is specific to the boron site, meaning that fluorination is clean and multiple purification steps are not required. However, the fluorination (particularly with a KHF_2 carrier agent) is particularly slow, resulting in low radiochemical yields unless a high concentration of reagent is used. While this currently precludes a detailed commercial investigation, recent research has been dedicated to improving the radiochemical yield and shortening the reaction times involved in the formation of ^{18}F labelled aryltrifluoroborate bioconjugates.[21, 22 23, 24] A kit has also been developed indicating that B-^{18}F based radiopharmaceuticals may have clinical applications in the future.[21]

1.2.3 Si-^{18}F bond formation

The Si-F bond strength (570 $kJmol^{-1}$) is significantly stronger then the corresponding C-F bond (480 $kJmol^{-1}$)[16]. This makes Si-F containing bioconjugates an attractive new class of compounds for imaging applications.[25] Nucleophilic substitution of $^{18}F^-$ with a variety of alkoxy- and hydroxy-silanes gives the corresponding triorganofluorosilanes in acidic, aqueous media. The compounds remain stable for prolonged periods in acidic media. However, under physiological conditions the Si-^{18}F compounds rapidly hydrolyse to give the silanol.[26, 27]

Modification of the compounds to incorporate more sterically bulky alkyl groups resulted in trialkylfluorosilanes which were more resistant to hydrolysis under physiological pH.[5]

A further development was the formation of anionic alkyltetrafluorosilicates from the treatment of a trialkoxysilane derivative with $^{18}F/KHF_2$. The fluorination of a biotin derivative (Figure 1.12) by Perrin *et al.* was accomplished by this method in a matter of minutes at room temperature in partially aqueous solvent conditions.[17]

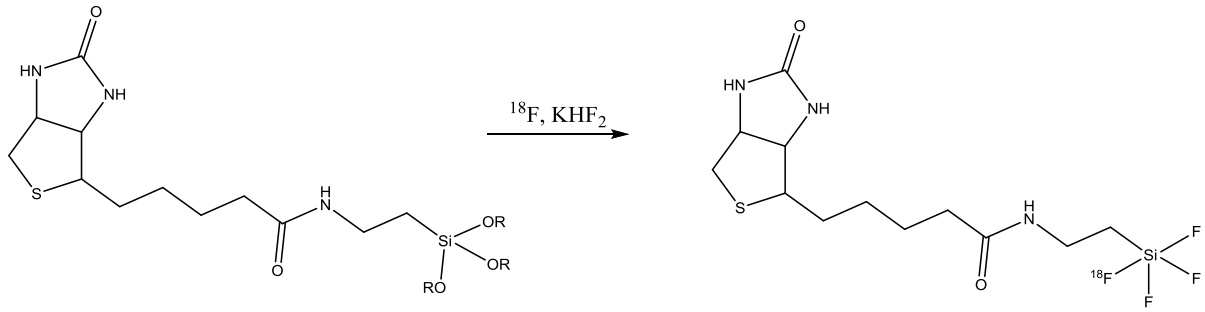

Figure 1.12: Labelling of a biotin trialkoxysilane derivative with ^{18}F to form an alkyltetrafluorosilicate. R = Et, Pr.[17]

However, as was the case for the triorganofluorosilane, the Si-^{18}F bond was rapidly cleaved under aqueous conditions.

Perhaps the most exciting development in Si-^{18}F bond formation research is the demonstration that ^{18}F may be incorporated into a trialkylfluorosilane via isotope exchange, instead of nucleophilic substitution of a hydroxy or alkoxy group (Figure 1.13).[28-30]

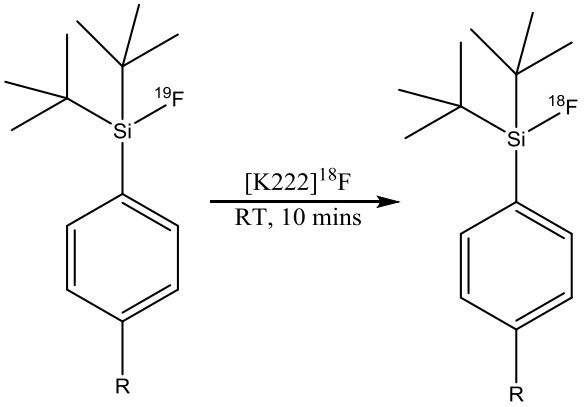

Figure 1.13: Synthesis of [^{18}F]-fluorodi-*tert*-butylphenylsilyl by $^{19}F/^{18}F$ isotope exchange. R = NCS, COOH.[29]

The isotope exchange for the above system is very efficient, with exchange occurring at room temperature in 15 minutes and in high radiochemical yield. The bulky *tert*-butyl substituents prevent the Si-F bond from hydrolysing. The nucleophilic exchange is very

efficient due to the low activation energy achieved through the associative formation of a pentacoordinate intermediate.[30]

This demonstrates the prospect of being able to produce preformed Si-^{19}F containing biomolecules and then incorporating ^{18}F at a late stage under mild conditions.

1.2.4 Al-^{18}F bond formation

While the reactions and molecules discussed in 1.2.2 and 1.2.3 demonstrated the value of inorganic element-fluorine bond formation in the preparation of organic based molecules, more recent studies has focussed on the use of metal chelate complexes to bind ^{18}F. In regards to the application proposed in this thesis; the development of PET imaging agents *via* the easy formation of M-^{18}F bonds (Chapter 1.3), the recent work on the design and synthesis of PET imaging agents based upon Al-^{18}F chelation is of particular interest, and provide examples for comparison with the systems discussed throughout this work.[31-33]

The interaction of fluoride with aluminium is particularly strong (> 670 kJmol^{-1}), and so provides a favourable driving force in the formation of stable Al-^{18}F containing chelates.[34] McBride and co-workers have used the inherent strength of the Al-F bond to create ^{18}F containing metal chelate complexes with the Al centre bound to a functionalised ligand based upon the triaza macrocycle 1,4,7-triazacyclononane. They have shown that chelation and Al-^{18}F bond formation can occur in aqueous solution (Figure 1.14).[35]

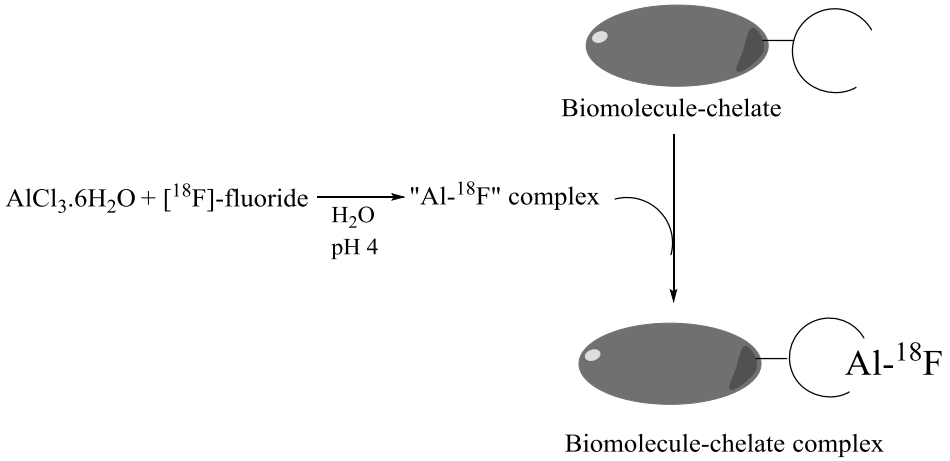

Figure 1.14: Biomolecule labelling using an aluminium(III) chelate as a binding site for $^{18}F^-$.

McBride and co-workers initially investigated Al-^{18}F chelation using the acyclic chelator diethylene triaminepentaacetic acid (DPTA) conjugated to a pre-targeting peptide (Figure 1.15).[35]

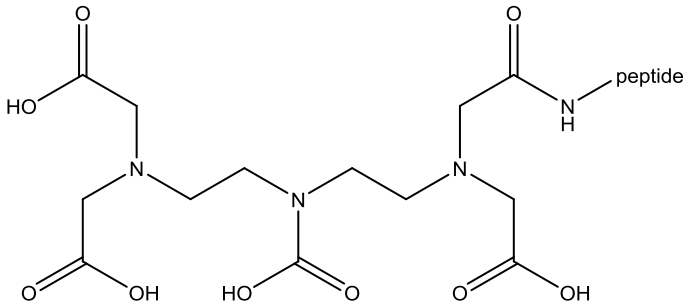

Figure 1.15: Structure of the DPTA based peptide conjugate utilised by McBride *et al.*[35]

After a short reaction time of 20 minutes, it was found that the incorporation of $^{18}F^-$ into the aluminium chelate was high (92%), however to achieve this heat (110 °C) was required. In addition, the labelled compound was found to be unstable in water at room temperature, with HPLC showing a 17% loss of compound over 40 minutes.[35]

Their focus then shifted towards a macrocyclic relative, 1,4,7-triazacyclononane-1,4,7-tricarboxylate (NOTA) as depicted in Figure 1.16.[36, 37]

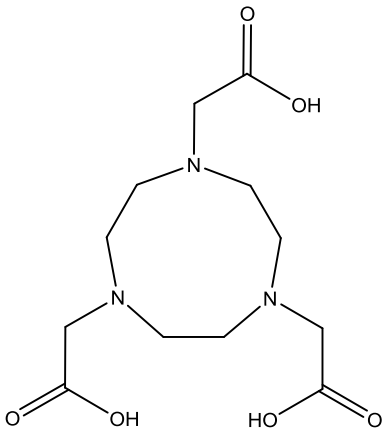

Figure 1.16: Structure of H_3-NOTA. A ligand used extensively in imaging applications and utilised by McBride *et al.* for Al-^{18}F chelation.[36, 37]

Early work with NOTA based chelates found that the labelling yields were low, likely due to the competition of $^{18}F^-$ *vs.* COO^- coordination to the metal centre.[36, 37] Nonetheless, they were able to demonstrate the labelling and subsequent stability both *in vivo* and *in vitro* of an Al-^{18}F NOTA chelate conjugated to an octreotide peptide.[36]

Further modification of the ligand framework identified the diacetate equivalent 1,4,7-triazacyclononane-1,4-dicarboxylate (NODA) as being an even more suitable ligand framework for the application, as it left a vacant coordination site on the aluminium centre in which the $^{18}F^-$ could bind.[38] McBride *et al*. used a NODA chelate appended with a methylphenylacetic acid group (see Chapter 4.1), which was shown to label in high yield (> 95%) and was stable *in vivo*.[38] This was also shown by Jeong *et al*. who used the NODA based ligand framework with a

benzyl substituent to demonstrate the high labelling yield and *in vivo* stability of this class of compound (discussed in more detail in Chapter 4.1).[39]

Having identified a suitable ligand framework, McBride has further developed the area of Al-^{18}F chelation through the design of a lyophilised kit for rapid radiofluorination of peptide chelates.[40] The work has now been developed to the point in which the system has been tested extensively, including under clinical conditions.[41-44]

While Al-^{18}F chelation has shown to be a highly effective new route towards ^{18}F labelled imaging agents, it does suffer from some disadvantages. The key disadvantage is the requirement to heat the reaction mixtures to high temperatures (110-115 °C) to promote the chelation. This currently makes this route unsuitable for the labelling of heat or temperature sensitive biomolecules, although recent efforts have sought to label heat sensitive molecules *via* a 2-step process.[45] Furthermore, it was found that the labelling reactions only proceeded in a narrow pH window (pH 4.0 ± 0.2). It would be desirable to eliminate both of these requirements. It would also be beneficial if the steps in the reaction were reversed so that ^{18}F labelling could be performed on the pre-formed aluminium chelate. This may allow for convenient labelling of thermally sensitive biomolecules and for the labelling reactions to occur over a wider pH range without a need to buffer the reaction mixture.[5]

1.3 Proposed Project: M-^{18}F Bond Formation *via* a Pre-formed Metal Complex

Unlike the work of McBride and Jeong in which the Al-^{18}F moiety is formed before the aluminium is coordinated to the chelate, this thesis in collaboration with GE healthcare aims to explore whether ^{18}F incorporation could be achieved rapidly under mild conditions *via* a ligand exchange reaction from a preformed metal chelate complex (Figure 1.17).

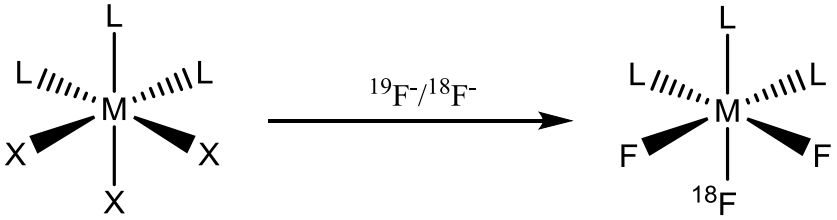

Figure 1.17: Schematic describing the generic route towards ^{18}F labelled metal complexes from a preformed metal chelate. L = strongly bound ligand, X = labile ligand in order to allow exchange reaction.

The precursor chelate could be synthesised in high yield and stored ready for use. The labile ligand should have a strong enough affinity for the metal centre to remain stable in solution, but should be labile enough to allow rapid ligand substitution. Careful choice of metal centre and labile ligand should allow the prospect of performing the ligand exchange at room

temperature, thus removing the heating step in the labelling process. In addition, the high affinity for the ligand exchange would result in clean substitution and minimal impurities, thus making purification more rapid. The ability to add the ^{18}F at a late stage of the process minimises the radioactive decay of the ^{18}F, meaning a smaller quantity of activity is required to undertake the labelling experiment. Furthermore, the ability to perform the halide exchange reaction in aqueous solution removes the need to azeotropically dry the $^{18}F^-$, a further significant time saving step.

In a clinical application, one envisages providing the preformed metal chelate, which a technician would dissolve into a pre-defined solvent regime, and add to the source of $^{18}F^-$. Post-reaction, a cartridge-based solid phase extraction (SPE) purification would isolate the desired ^{18}F labelled chelate ready for administration into the patient.

In order for a synthetic regime such as the one discussed above to be relevant to PET imaging applications, the complexes formed would likely require a certain number of fundamental chemical characteristics in order to be stable throughout the synthetic process and *in vivo.*

1.4 Complex Design and Rationale

With regards to the choice of metal one must consider both the ions affinity for fluoride in water and its stability in a wide pH range. On this basis, it would be reasonable to suggest that hard Lewis acids would be suitable candidates. A further requirement of the metal centre is to have a single preferred coordination number and limited redox chemistry. This will result in a tuneable and 'predictable' system. Additionally, a strong M-F bond is very desirable as this will provide a strong driving force in which the halide exchange reaction may proceed rapidly under mild conditions, and the resulting product would be expected to have good stability.

Based upon these considerations, the trivalent Group 13 ions Al^{3+}, Ga^{3+} and In^{3+} were identified as suitable metal ions.[46] Comparison of the M-X bond strengths show that the M-F bond dissociation enthalpy is large for all the ions, and is significantly larger than the corresponding M-Cl bond enthalpies (Table 1.2).[16] This provides a strong driving force in forming M-F interactions with the Group 13 ions, indicating that ^{18}F incorporation may be achieved rapidly under mild conditions, providing that the reaction kinetics are favourable.

Bond	Bond dissociation enthalpy/ kJ mol^{-1} *
Al-F	664
Al-Cl	494
Ga-F	577
Ga-Cl	481
In-F	506
In-Cl	439
Si-F	570
B-F	766
C-F	536

* Recorded at room temperature

Table 1.2: Table of selected bond dissociation enthalpies for some of the E-F interactions discussed in this work.[17, 34]

Another convenient advantage of these metals is their NMR active nuclei (^{27}Al, ^{71}Ga and ^{115}In), which allow detailed spectroscopic analysis to be undertaken in solution on a preparative scale.[47] Furthermore, the MX_3 salts (M = Al, Ga, In, X = Cl, Br, I) are soluble in a variety of organic solvents, such as MeCN, CH_2Cl_2, MeOH, and thus entry into the coordination chemistry can be gained more readily than the corresponding fluorides. Due to the greater ease of handling, the metal chloride chelates were identified as suitable precursor complexes.

The use of halide complexes of boron and thallium were not investigated. While the formation of B-F bonds has been investigated in order to produce organic radiopharmaceuticals (Chapter 1.2.2), the use of BX_3 as a Lewis acid in the proposed application is not possible as the small boron(III) centre (0.87 Å)[48] results in complexes that are almost exclusively tetrahedral, hence coordination of a multidentate ligand is not possible. [46] Thallium(III) is readily reduced to Th(I), which is labile in solution. This suggests that any complexes would be readily decomposed under physiological conditions.[46]

As shown by the work of McBride and Jeong, macrocyclic ligands are attractive candidates for this application.[32, 33, 39] They have well defined coordination modes and the complexes formed with them are kinetically stable due to the macrocyclic effect (Chapter 1.5). This imparts significant stability to the metal centre, creating robust complexes. Although macrocycles are somewhat challenging to synthesise (Chapter 1.6), once formed they are able to undergo further post synthetic modifications. One common modification is the addition of pendant arm functionality, useful for attaching peptides or to aid in stabilising the metal centre. In keeping with the requirements of the metal centre, macrocyclic ligands incorporating hard amine, carboxylate or even ether donor groups would be very suitable candidates. Given these requirements, and based on the work of McBride and others, the triaza macrocycle 1,4,7-

triazacyclononane (tacn) and its derivatives were identified as a suitable class of ligand. The tacn macrocycle coordinates in a *facial* arrangement which acts to cap one face of the metal centre, thus leaving one face in which to partake in ligand exchange chemistry. The hard N-donor atoms are compatible with the hard Group 13 ions which should result in robust coordination. Furthermore, the nitrogen atoms may be easily functionalised to incorporate a large variety of functionalised pendant arms.

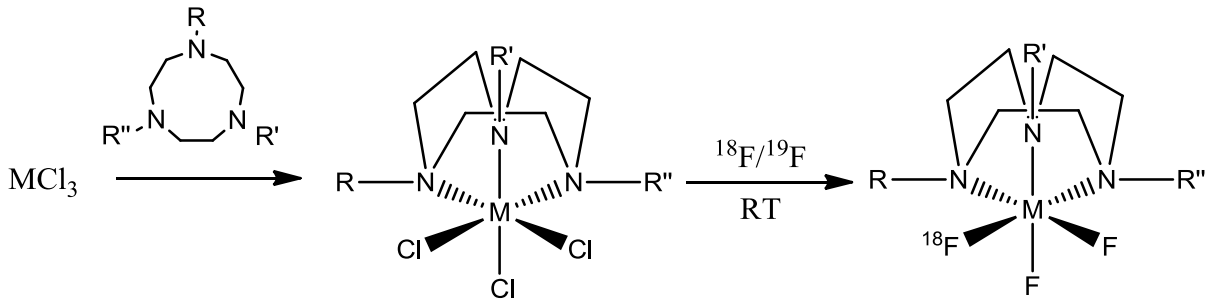

Figure 1.18: Synthetic route utilised to incorporate ^{18}F into metal chelate complexes. M = Al, Ga, In. The R groups would be a variety of substituents which could either stabilise the complex, or provide a linker in which a biomolecule or peptide could be conjugated.

1.5 Macrocyclic Chemistry

For the purposes of coordination chemistry, a macrocycle is usually defined as a cyclic molecule with three or more potential donor atoms in a ring of at least nine atoms.[49] Common donor atoms include nitrogen, oxygen and sulfur, although phosphorus, selenium and tellurium macrocycles have also been prepared.[50, 51]

Since Pedersen and Curtis' initial synthesis of the now ubiquitous crown ether and nitrato-amine compounds, there has been a huge expansion in the field of macrocyclic chemistry.[52, 53] While the initial impetus concerned the efficient synthesis of large ring compounds in high yield,[49, 54] later research focussed on the innate stability of the resulting complexes,[55, 56] leading to the advent of supramolecular chemistry[57-59] and a greater understanding of bioinorganic chemistry.[60, 61]

The enhanced stability of macrocyclic complexes is derived from the macrocyclic effect. This states that cyclic ligands form more stable complexes than those of the analogous open-chain ligand.[62] Investigations into the nature of the macrocyclic effect infer that the complex stability derives from both an entropic and enthalpic contribution.[63]

a) Entropic Contribution

Macrocyclic ligands have less rotational and translational degrees of freedom than their open-chain analogues, which is mainly due to the ring structure of the macrocycle. For a macrocycle which is compact and relatively rigid in its free form, coordination to a metal ion only leads to a small reduction in the rotational and vibrational degrees of freedom. However,

the open-chain analogue exhibits greater configurational entropy in its free form compared to its coordinated form. Thus, release of the open-chain ligand into solution results in a significant net gain in entropy.

b) Enthalpic Contribution

The magnitude of the enthalpic term is determined by a variety of factors including the ring size, metal ion and donor atom types.[64, 65] The different solvation energies of the open-chain and macrocyclic ligands play a crucial role in determining the enthalpic contribution. Solvation occurs more readily for the open-chain ligand compared to the analogous macrocycle, due to its greater flexibility in its free form.

c) Kinetic Effect

In addition to the enhanced thermodynamic stability exhibited by many macrocyclic complexes, they are also kinetically inert to dissociation.[66] Macrocyclic complexes have very high kinetic stability, greater than that of the analogous open-chain ligand complexes. The rates of formation and dissociation are both smaller for the macrocyclic species compared to the open chain complexes. The lower rate of formation is derived from the need for the cyclic ligand to orientate itself to allow endocyclic coordination to the metal ion. Dissociation requires elongation and cleavage of the M-L bonds, which is inhibited in macrocycle complexes due to the high degree of ligand distortion. In contrast, M-L cleavage in an open-chain polychelate is much easier as the lack of ligand distortion leads to an 'unzipping' mechanism.

Macrocyclic complexes are further stabilised by preorganization, depending upon the orientation of the lone pairs of the donor atoms of the ligand in its uncoordinated form. This preorganization 'pre-pays' some of the energetic cost of coordination.

The study of macrocyclic ligands and their complexes allows us to probe many of the more subtle aspects of the reactivity of coordination compounds which may not be possible in less stable complexes with non-cyclic ligands.

Neutral O-donor macrocycles, known as crown ethers, are used extensively in the selective binding of alkali metal cations, forming salts that are soluble in non-polar solvents. This therefore makes crown ethers useful as phase transfer catalysts, as shown in the 2·2·2-crypt ligand used to transfer $K^{18}F$ into organic media, as discussed in Chapter 1.1. The denticity of the polyether influences the affinity of the crown ether for various cations. For example, 18-crown-6 has high affinity for potassium cation (Figure 1.19), 15-crown-5 for a sodium cation, and 12-crown-4 for a lithium cation.

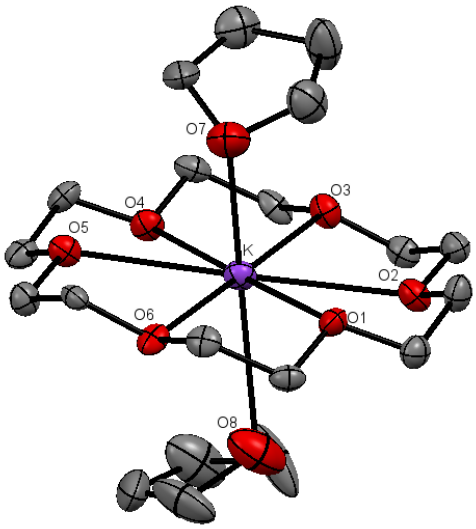

Figure 1.19: Crystal structure of the cation in [K(18-crown-6)(thf)$_2$][I] showing the spatial fit of the potassium cation in the hexadentate polyether.[67] Image redrawn from CCDC 227772.

Selected N-donor macrocycles include the triaza macrocycle tacn, (Chapter 1.6), [68] the tetrazamacrocycles 1,4,7,10-tetraazacyclododecane (cyclen) and 1,4,8,11-tetraazacyclotetradecane (cyclam) in which the latter two have found significant use in other medical imaging applications. Their main use being in MRI imaging applications, such as $[Gd(DOTA)]^{3+}$ in which the cyclen ring bears carboxylate pendant functions. (Figure 1.20).[69]

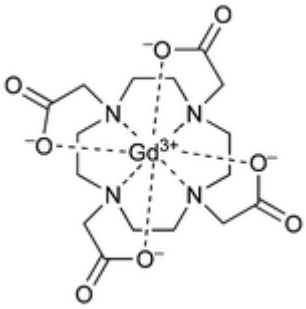

Figure 1.20: Schematic of $[Gd(DOTA)]^-$ the complex of choice for MRI contrast agents.[69]

1.6 Triazacyclononane: Synthesis and Selected Coordination Chemistry

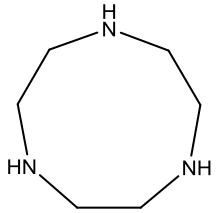

Figure 1.21: The structure of 1,4,7-triazacyclononane (tacn).

Tacn and its functionalised derivatives have been used extensively throughout coordination chemistry.[68] As briefly mentioned in Chapter 1.4, tacn has a number of features which makes it very suitable in coordination chemistry applications. The small tridentate ring results in almost exclusive *fac*-coordination to the metal centre. While stabilising the metal centre through the macrocyclic effect, the ligand acts to block one face of the metal centre, which allows the other face of the metal to undergo further chemistry such as ligand substitution. Furthermore, the small ring size tends to prevent the formation of sandwich compounds, particularly if the macrocycle has been functionalised. The N-donor atoms on the parent tacn ligand may be easily functionalised to provide a large library of derivatives which may be tuned towards a particular metal centre or application.

The parent tacn ligand was first reported in low yield in 1972 using high dilution synthesis techniques. The low yields and high expense of the chemicals were prohibitive to an extensive investigation of the ligand coordination chemistry.[70]

Richman *et al.* reported a more efficient synthesis in 1974 which did not require the use of high dilution conditions (Figure 1.22).[71]

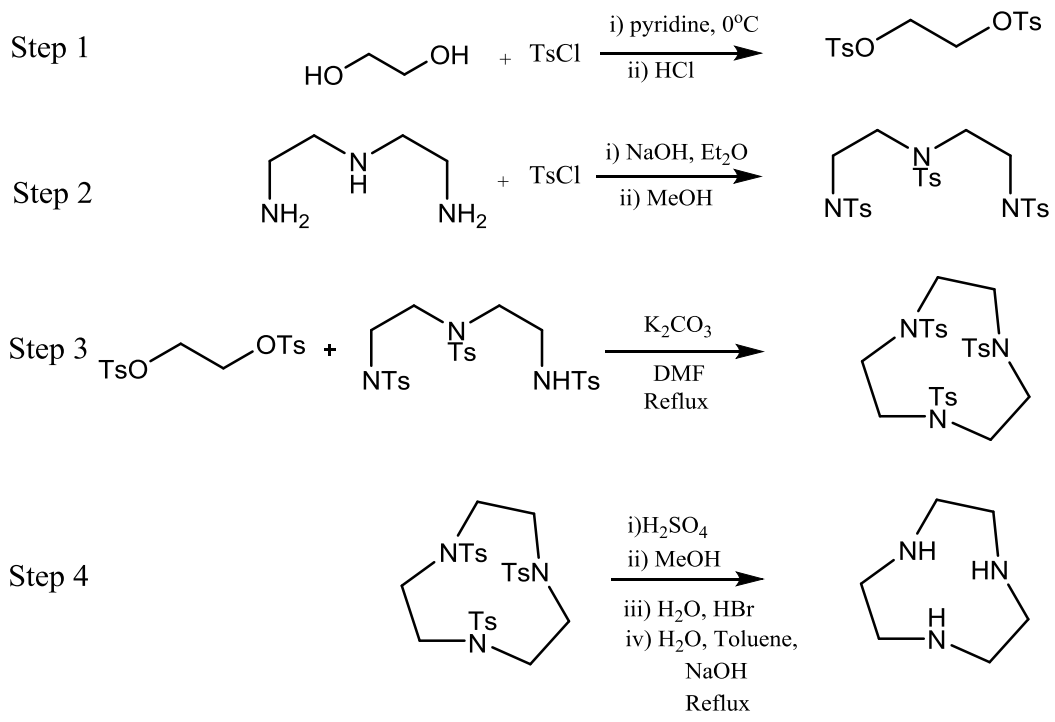

Figure 1.22: Synthesis of tacn.[71]

The synthesis proceeds *via* the coupling of a tosyl protected triamine with a tosyl activated diol under basic conditions. The resulting protected tacn ring is deprotected in the presence of sulfuric acid and protonated with HBr in water. Further functionalization of the parent tacn proceeds *via* a variety of synthetic techniques.[72, 73]

The coordination of tacn and its substituted variants have developed into a distinct branch of coordination chemistry with a rich and diverse range of structures and species. Its broad chemistry with transition metals has been reviewed elsewhere and is not discussed in detail here.[68]

The coordination chemistry of tacn and its derivatives with p-block elements has also been increasingly well developed in recent times. Tacn ligands bound to an aluminium(III) centre have found recent use in Al-^{18}F chelation as discussed in Chapters 1.2.4, 2.3 and 4.1. Gallium and indium(III) ions with tacn based ligands have found increasing use as potential PET imaging agents, and are described in more detail in Chapter 1.8. Other selected examples of tacn ligand complexes with Group 13 ions include [$GaBr_3$(Me_3-tacn)] (the first example of a six-coordinate gallium bromide complex)[74] and the novel hydroxy-bridged dinuclear complex [(Me_3-tacn)$_2$$Ga_2$(μ-OH)$_2$(μ-$CH_3CO_2$)]$^{3+}$ (Figure 1.23).[75]

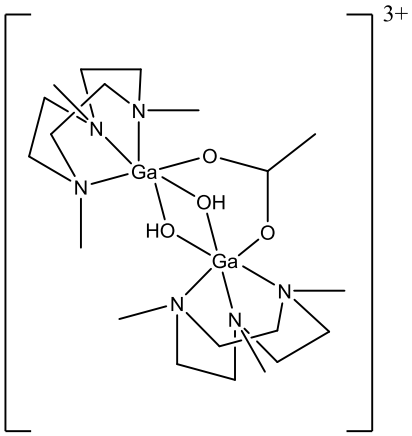

Figure 1.23: A schematic of the Ga(III) containing cation from the complex $[(Me_3\text{-tacn})_2Ga_2(\mu\text{-}OH)_2(\mu\text{-}CH_3CO_2)][I]^-_3$ as described by Wieghardt *et al.*[74]

Hydrolysis of $[InCl_3(tacn)]$ leads to the unusual tetranuclear indium cluster where four [In(tacn)] fragments are connected by bridging hydroxide ligands (Figure 1.24). The indium's large ionic radius (0.80 Å)[48] allows it to form the very sterically hindered $[L_4In_4(\mu\text{-}OH)_6]^{6+}$ complex.[76]

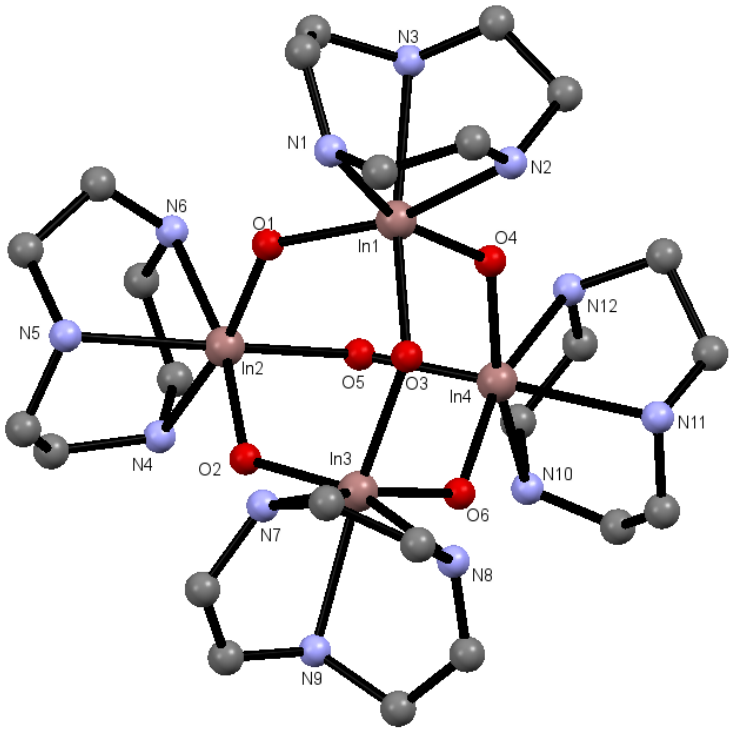

Figure 1.24: The crystal structure of In(III) containing cation $[L_4In_4(\mu\text{-}OH)_6]^{6+}$ described by Wieghardt *et al*. L = tacn.[75] H-atoms on the ligand and bridging hydroxide are omitted for clarity.

The In atoms are in a distorted octahedral environment of three *facially* coordinated N atoms of the macrocycle and three oxygen atoms of three μ-OH bridges.[76]

Wieghardt *et al.* also synthesised the first gallium fluoride adduct with a tacn ligand *via* reaction of $GaF_3 \cdot 3H_2O$ with the ligand 1,4,7-tris(2-amino-3,5-di-butylbenzyl)-1,4,7-triazacyclononane in refluxing EtOH over 15 hours. Recrystallisation of the resulting product from CH_2Cl_2/MeOH gave crystals of the complex [GaF_3{1,4,7-tris(2-amino-3,5-di-butylbenzyl)-1,4,7-triazacyclononane}]·6MeOH (Figure 1.25).[77]

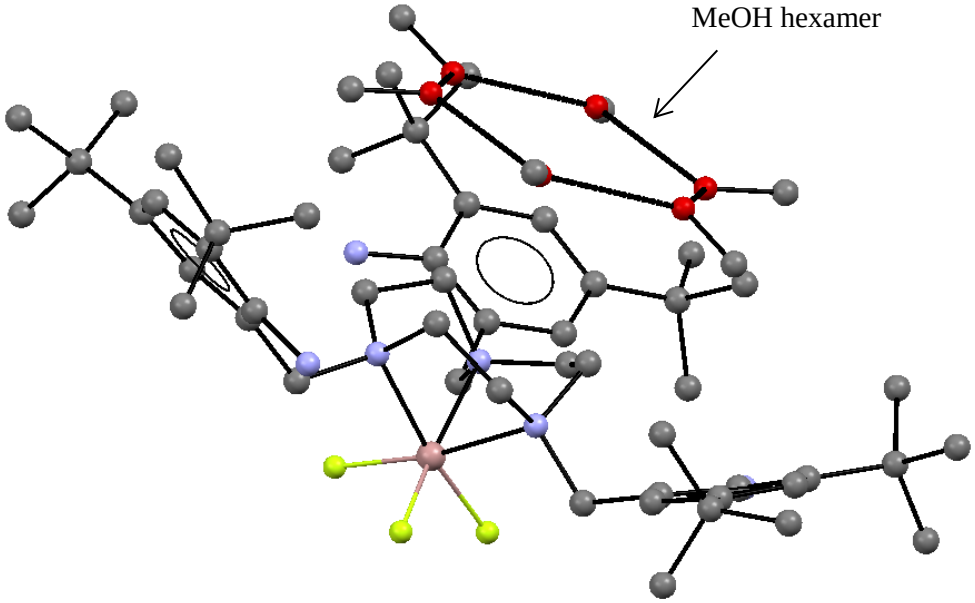

Figure 1.25: Crystal structure of [GaF_3{1,4,7-tris(2-amino-3,5-di-butylbenzyl)-1,4,7-triazacyclononane}]·6MeOH showing the methanol hexamer which crystallises in the hydrophobic cavity of the coordinated ligand. H-atoms and atom labels are omitted for clarity. Colour code: pink= Ga, yellow = F, blue = N, red = O, grey = C.[77] Image redrawn from CCDC 182797.

The octahedral complex shows *fac* coordination of the tacn ligand towards the Ga(III) centre. The coordination sphere around the gallium centre is completed by three fluoride ligands. The Ga-F bond lengths were shown to be in the range of 1.848(2)-1.850(3) Å. The fluoride ligands also partake in H-bonding interactions with three additional crystallised MeOH molecules (O-H···F = 2.58(1) Å). This is in keeping with the metal fluoride complexes discussed throughout this thesis, in which significant H-bonding is observed. The d(Ga-N) bond lengths were found to be the same length (2.147(2) Å). The bulky tertiary butyl groups of the ligand pendant arms are folded upwards towards the coordinated tacn ring to create a bowl shaped hydrophobic surface. Within the cavity, the methanol solvent crystallises into a hexamer held together by H-bonding interactions (O···O = 2.623(1) Å).[77] This complex demonstrates

that Group 13 fluoride complexes with functionalised tacn ligands may be accessed, but under rather forcing conditions. It also provides an example of a 'Ga-F' containing complex against which our new gallium fluoride complexes may be compared.

The preference of Me_3-tacn for tridentate coordination has been shown to promote substitution of fluoride even when the M-F bond is very strong. This is shown in the work by Levason *et al.* in which a Si-F bond is cleaved from SiF_4 as the ligand coordinates to produce the unique cation $[SiF_3(Me_3\text{-tacn})]^+$ (Figure 1.26).[78] Reaction of SiF_4 with Me_3-tacn in anhydrous CH_2Cl_2 gives the cationic species as the chloride salt *via* attack of the displaced 'naked' fluoride anion on the solvent.

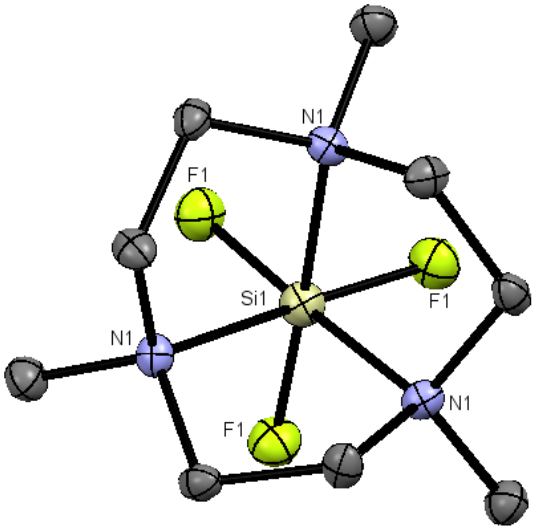

Figure 1.26: Crystal Structure of the Si(IV) containing cation in $[SiF_3(Me_3\text{-tacn})][Cl]$.[78] Image redrawn from CCDC 713184

The ability to abstract a fluoride ligand from the metal in order to form the *facially* coordinated cation was also demonstrated with the heavier germanium analogue giving the unusual $[GeF_3(Me_3\text{-tacn})]^+$ cation.[79] These examples demonstrate the ability of Me_3-tacn to impart unusual coordination geometries and stability upon Lewis acidic centres.

The work also highlighted the stability of the *fac*-$[MF_3(Me_3\text{-tacn})]$ unit. The silicon and germanium cations above were found to be extremely resistant to hydrolysis and to competition from donor solvent such as MeCN and thf. This implies that this complex type may prove very resistant to biological processes, a promising factor in the application proposed in this thesis. The use of the Group 13 metal ions will provide a neutral complex with the same coordination environment; which will provide further stability under physiological conditions.

1.7 Group 13 Metal Halides: Trends and Selected Coordination Chemistry

The coordination chemistry of the Group 13 halides with neutral ligands is rich and diverse. The chemistry is dominated by the M(III) oxidation state.[46] Al(I) may only be accessed in the gaseous phase at high temperatures. Gallium(I) may be accessed in solution but is very sensitive to oxidation. Although indium(I) and thallium(I) coordination chemistry has seen renewed development in recent times[80], only the chemistry of the M(III) oxidation state is discussed here. In addition, as mentioned in Chapter 1.4, as the chemistry of boron and thallium was not investigated, examples of their coordination complexes are not discussed here.

As might be expected as one descends the group the variety of coordination modes change. The smaller aluminium centre (ionic radius for Al(III) = 0.68 Å) means that it favours four coordinate tetrahedral, or six coordinate octahedral geometries.[46, 48] The larger gallium(III) (0.76 Å) and indium(III) (0.80 Å) centres have shown to form complexes with four to seven coordinate geometries and in the case of indium, depending upon the ligand donor type and steric requirements, eight coordinate species are known.[48, 81]

The chemistry is dominated by the Lewis acidity of the trivalent halides. The Lewis acidity of the Group 13 halides is generally accepted to fall F>Cl>Br>>I. Recent work has shown that the Lewis acidity trends between aluminium and gallium halides do not always follow the expected trend as indicated by gas phase DFT (density functional theory) calculations. The trends in Lewis acidity are far more subtle in the solid state, and are heavily influenced by factors such as H-bonding and the reorganisation energy of the metal halide salt. Timoshkin *et al.* have demonstrated that the Ga-N bond lengths in the complex $[GaBr_3(terpy)]$ (2.0265(18)-2.0965(18) Å) are shorter or equal to the Ga-N bond lengths in $[GaCl_3(terpy)]$ (2.0412(15)-2.1024(15) Å) in contrast to the generally accepted trends. It was postulated that the higher reorganisation energy in forming *mer*-octahedral complexes from the GaX_3 unit may promote this observation. The work also proposed that comparison of Ga-N bond lengths in the solid state may not be a reliable indicator of Lewis acidity.[82]

Timoshkin *et al.* also showed that the Al-N bond length in the complex $[AlBr_3(NEt_3)]$ (NEt_3 = triethylamine) was shorter than the corresponding $[AlCl_3(NEt_3)]$ complex (1.994(4) and 2.0181(16) Å respectively). This surprising result was proposed to arise from the differences in the intermolecular H····Cl and H····Br interactions in the two complexes. The influence of H-bonding interactions is an important consideration when discussing Lewis acidity trends and thus comparison of crystallographic data for complexes which contain these interactions should be treated with caution.[83]

The anhydrous Group 13 metal fluorides MF_3 (M = Al, Ga or In) are inert polymeric solids and generally unreactive towards neutral ligands, which has hindered attempts to explore their coordination chemistry.[84] The hydrates, $MF_3 \cdot 3H_2O$, are more reactive, but have very poor solubility in organic solvents or water.[84] Two structural forms of $AlF_3 \cdot 3H_2O$ are known, the α-

form with discrete $[AlF_3(OH_2)_3]$ molecules, and the β-form which is a polymer, $[\{AlF_2(OH_2)_2(\mu\text{-}F)\}_n]\cdot nH_2O$.[85] The structure of $GaF_3\cdot 3H_2O$ is unclear, but $InF_3\cdot 3H_2O$ is also a fluoride bridged polymer.[86] Adducts of the fluorides are relatively rare, except for the examples discussed in Chapters 1.6 and 6.1.

The metal trichloride salts MCl_3 are moisture sensitive solids at room temperature.[46] $AlCl_3$ adopts a layered cubic structure with six coordinate aluminium centres.[46] $GaCl_3$ adopts a dimeric Ga_2Cl_6 structure with chloride bridged tetrahedral gallium centres.[46] $InCl_3$ is a six coordinate ionic species with chlorides occupying one third of the octahedral holes.[46] The metal chlorides $AlCl_3$ and $GaCl_3$ are used extensively in organic synthesis as Lewis acid catalysts in Friedel Crafts acylation and other electrophilic aromatic substitutions.[87-89]

The Group 13 halide salts have a diverse coordination chemistry, they have been shown to not only form complexes with hard donor ligands such as ether, phosphine oxide or imine ligands but also with softer phosphine,[90, 91] thioether and selenoether ligands.[92-94] These include examples with neutral phosphine ligands such as the tetrahedral $[AlCl_3(PMe_3)]$ (Figure 1.27) and the six-coordinate octahedral cation $[AlCl_2\{o\text{-}C_6H_4(PMe_2)_2\}_2][AlCl_4]$,[90] Complexes with chalcogen donor ligands include $[GaCl_3(EMe_2)]$ (E = S, Se), and $[(GaI_3)_2\{\mu\text{-}MeS(CH_2)_2SMe\}]$ where a single chalcogen donor atom completes the coordination, with the neutral ligand acting as a bridging species (Figure 1.28).[95] These complexes typically form *via* reaction of MX_3 with ligand in anhydrous CH_2Cl_2. As might be expected for complexes in which the ligand interaction is weak, they are highly labile in solution.

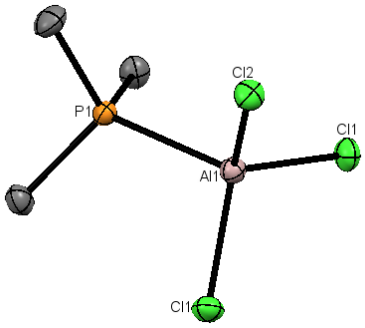

Figure 1.27: Crystal structure of $[AlCl_3(PMe_3)]$ as reported by Burt *et al.*[90] Image redrawn from CCDC 1005860.

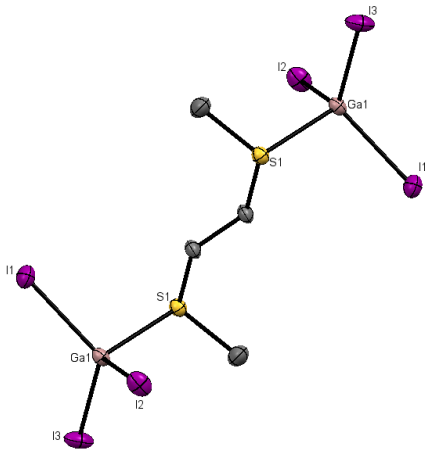

Figure 1.28: Crystal structure of the thioether bridged $[(GaI_3)_2\{\mu\text{-}MeS(CH_2)_2SMe\}]$ prepared by Gurnani *et al*.[94] Image redrawn from CCDC 691455.

InX_3 (X = Cl, Br, I) also form complexes with softer chalcogenoether ligands,[96] in which they display slightly more diverse coordination chemistry than the smaller aluminium and gallium analogues. Ligand structure, denticity and donor atom type play a more significant role in the structures formed. Examples include the four-coordinate species $[InX_3(SeMe_2)]$ and $[InX_3(TeMe_2)]$ (X = Cl, Br, I). However, upon addition of excess $SeMe_2$ to $InCl_3$, the distorted centrosymmetric dimer *cis*-$[\{In(\mu\text{-}Cl)Cl_2(SeMe_2)_2\}_2]$ is also shown to form.[96]

The metal chloride salts of gallium and indium have also shown to react with the thia-macrocycles [9]aneS_3 and [12]aneS_4 to give the neutral distorted octahedral cations $[GaCl_2([12]aneS_4)][GaCl_4]$ and $[InCl_2([12]aneS_4)][InCl_4]$ and the neutral octahedral complex $[InCl_3([9]aneS_3)]$.[96]

1.8 Group 13 Macrocyclic Complexes in Medical Imaging

While Al-^{18}F chelation is a recently developed use of the Al(III) ion in radiolabelling applications (Chapter 1.2.4), the Ga(III) and In(III) ions have been used extensively as alternative agents for PET imaging applications.[97] In particular the ^{68}Ga and ^{111}In radioisotopes are seeing increasing use in this application (see Table 1.1). ^{68}Ga is delivered as the salt $^{68}Ga(NO_3)_3$ in aqueous solution and ^{111}In as aqueous $^{111}InCl_3$. Many ^{68}Ga and ^{111}In containing compounds used in imaging applications are bound to aza-macrocyclic ligand frameworks. Coordination of the hard Lewis base to the hard Lewis acid results in a strongly bound metal complex which remains stable under physiological conditions. These complex types have been reviewed elsewhere, and so a small selection of examples is discussed below.[97]

Parker *et al.* reported the synthesis and crystal structure of the six coordinate [Ga(NOTA)] complex from reaction of the ligand H_3-NOTA with $Ga(NO_3)_3$ in 40 mM aqueous HNO_3 (Figure 1.29).[98] The complex was observed in the ^{71}Ga NMR spectrum under aqueous

conditions. The complex's stability to both acidic and neutral pH made it an exciting prospect as a potential radiopharmaceutical.

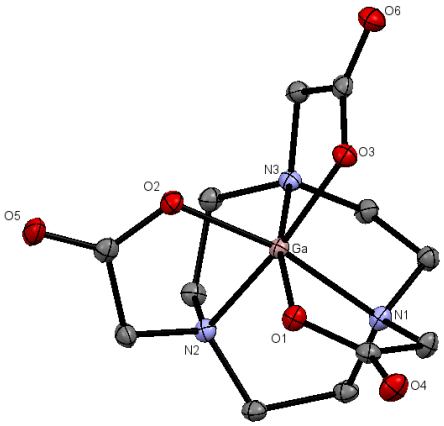

Figure 1.29: The crystal structure of the neutral six-coordinate [Ga(NOTA)] complex as reported by Parker *et al.*[98] The ligand is hexadentate with an N_3O_3 donor set.

Other complexes prepared for applications in ^{68}Ga based PET imaging agents include a *tris*-3-hydroxy-4-pyrone functionalised tacn derivative [Ga(NOKA)] (NOKA = 6,6,6″-(1,4,7-triazonane-1,4,7-triyl)*tris*(methylene)*tris*(5-hydroxy-2-(hydroxymethyl)-4H-pyran-4-one),[99] and complexes utilising tacn ligands functionalised with lyophilizing phosphinate groups, which have found use as a bone seeking agent in PET imaging.[100]

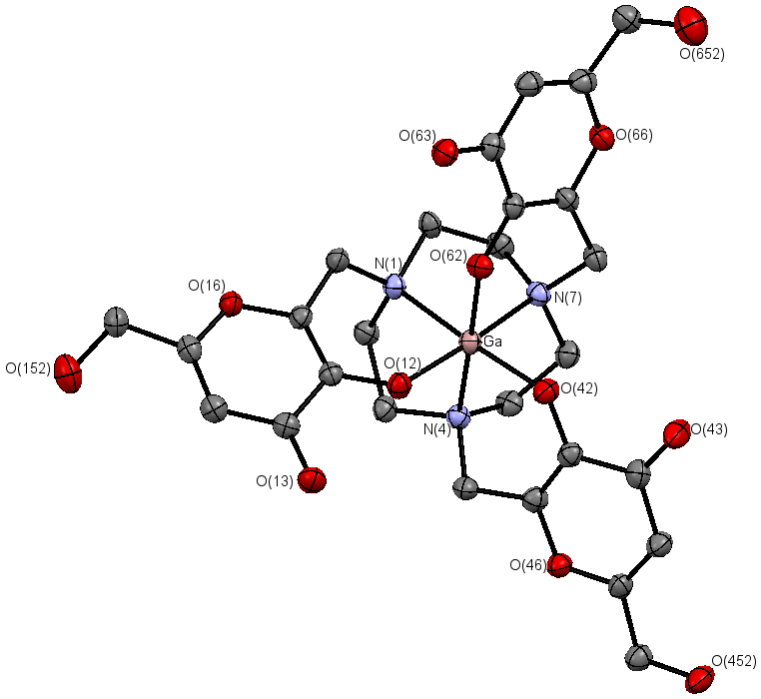

Figure 1.30: Crystal structure of [Ga(NOKA)].[101] Image redrawn from CCDC 766031.

There are few examples of the tetradentate azamacrocycles cyclen and cyclam coordinated to Ga(III) ions, and therefore the use of tetra azamacrocyclic based chelators as ligands for ^{68}Ga imaging applications has not been investigated.

The larger In(III) ion (ionic radius = 0.80 Å) allows for a wider range of coordination numbers,[48] which therefore presents a larger library of ligands with potential applications in ^{111}In based PET imaging agents. Reaction of $InCl_3$ with H-NOTA in buffered acetic acid (pH 5) affords the unusual 7-coordinate complex [InCl(NOTA)] (Figure 1.31), in which the metal centre adopts a pentagonal bipyramidal coordination environment.[102] The neutral complex is insensitive to metal or acid promoted dissociation *in vivo*. The ^{111}In labelled complex may be formed in > 97% radiochemical yield, in 30 minutes under ambient conditions.

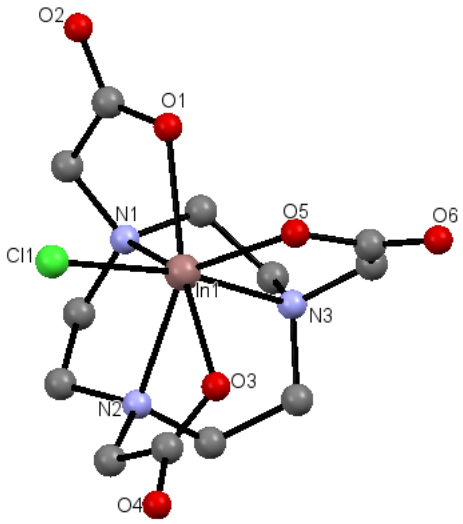

Figure 1.31: The crystal structure of the unusual 7-coordinate neutral complex [InCl(H-NOTA)], redrawn from Parker *et al.*[102]

The larger In(III) ion is capable of coordinating the octadentate DOTA ligand to form a neutral 8-coordinate complex which has grown to become a very useful ^{111}In radiopharmaceutical.[103]

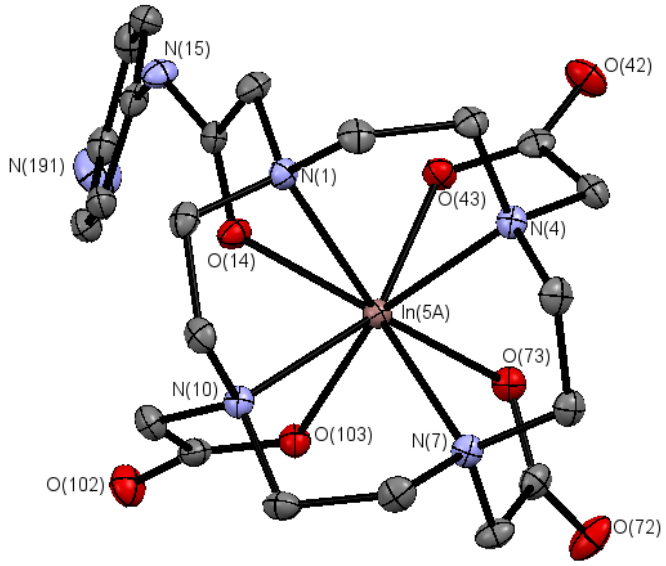

Figure 1.32: Crystal structure of the In(III) containing cation $[In(DOTA)]^{3+}$.[103] Image redrawn from CCDC 228929.

1.9 Characterisation Methods

A number of characterisation methods are available to provide compositional and structural data for the complexes synthesised in this work.

1.9.1 Infra-red spectroscopy

Infra-red (IR) spectroscopy is a characterisation technique used to determine the types of bonds present in the compound and the symmetry group to which the molecules belong. Radiation of a specific energy corresponding to vibrational transitions in the molecule is absorbed, resulting in a change of dipole moment. Subtraction of these absorptions from a pre-recorded background scan gives an IR spectrum characteristic of the compound.[104]

Infra-red spectroscopy is particularly useful in observing the M-X stretching frequencies in the halide complexes synthesised, as well as the organic functional groups present in the ligand. The number of observed bands may be used in combination with group theory calculations to determine the molecular symmetry present in the complex (see Chapter 2.2.1).

Infra-red spectroscopy is also a useful technique in determining whether the complex contains any H-bonded water molecules in the solid state, the broad ν O-H band at *ca.* 3500-3300 cm^{-1} and δ H-O-H band at 1650 cm^{-1} provides evidence of water being present.

Infra-red spectra are commonly recorded in the solid state as Nujol mulls, meaning that the complexes do not need to be soluble in common solvents. This offers a distinct advantage

over NMR spectroscopy, although unlike NMR spectroscopy, infra-red spectroscopy is a destructive technique.

1.9.2 NMR spectroscopy

Nuclear magnetic resonance (NMR) spectroscopy is a characterisation technique which exploits the magnetic properties of certain atomic nuclei to determine physical and chemical properties of atoms or the molecules in which they are contained.[47]

^{1}H, ^{19}F{^{1}H}, ^{27}Al, ^{71}Ga and ^{115}In NMR spectroscopy was used extensively throughout the project to help characterise the compounds produced (Table 1.3). The property of the nucleus responsible for the NMR effect is called nuclear spin (I). The ease with which NMR spectra may be obtained is affected by several factors, including the natural abundance of the isotope studied, the chemical shift range, and for nuclei with I >1/2, the magnitude of the quadrupole moment of the isotope being observed.[47] The ease in which NMR spectra may be obtained is also affected by the operating frequency; low frequency nuclei are difficult to detect. The sensitivity of the nucleus is also a factor.

Nuclei	**Spin**	**Natural Abundance/ %**	**Chemical Shift Range/ ppm**	**Quadrupole Moment/ 10^{-28} m^2**	**Resonant Frequency/ MHz**
^{1}H	1/2	100	13	n/a	100
^{19}F	1/2	100	700	n/a	94
^{27}Al	5/2	100	400	1.5 x10^{-1}	26.1
^{71}Ga	3/2	39.6	1436	1.2 x10^{-1}	30.6
^{115}In	9/2	95.7	unknown	8.3 x10^{-1}	22.0

Table 1.3: Selected properties of NMR nuclei utilised throughout this work.

Quadrupolar nuclei

An asymmetric environment surrounding the nucleus will lead to differences in the electron density, which causes an electric field gradient (efg). The nucleus will always try to orientate itself to the lowest energy. This is possible for nuclei in which I = 1/2, however, quadrupolar nuclei cannot find an orientation with minimum energy and therefore keep moving to orientate the nucleus, which results in an energetic loss. This energetic loss is rapid, which in turn means that the quadrupolar relaxation is very fast. The fast relaxation means that the lifetime of the excited state is very short, and thus the associated uncertainty of the lifetime is very small. This causes line broadening due to the Heisenberg uncertainty principle, which states that the more precisely the position of the particle is known, the less precisely its energy can be determined, and *vice versa*. As the uncertainty in the relaxation time is very small, there is an increase in the uncertainty in the position of the NMR signal, leading to line broadening.

Nuclei in a symmetric environment will have an efg close to zero, which results in a longer relaxation time. The longer relaxation time reduces the line broadening, which allows for sharper resonances to be observed. Tetrahedral (T_d) and octahedral (O_h) complexes containing quadrupolar nuclei may be observed in the NMR spectrum as the efg is zero, which allow couplings to be observed and sharp lines. Complexes with C_{3v} symmetry have an efg close to zero, which also allows couplings to be observed, although the line widths are typically quite large.

The ability to observe an NMR resonance with quadrupolar nuclei is also influenced by external factors such as temperature and solvent. For example, complexes dissolved in D_2O or CD_3OD may partake in H-bonding interactions with the solvent. These interactions affect the efg, and hence the rate of quadrupolar relaxation.

It is important to ensure that NMR resonances are correctly referenced. Typically ^{1}H NMR spectra are referenced to an internal standard such as the residual proton signals on a deuterated solvent and ^{19}F NMR spectra referenced to $CFCl_3$. ^{27}Al, ^{71}Ga and ^{115}In NMR spectra are usually referenced to an external standard of aqueous $[M(H_2O)_6]^{3+}$ at pH 1.[47]

Complexes are required to be highly soluble in order to obtain good NMR spectra. A variety of deuterated solvents are commercially available including D_2O, CD_3CN, CD_2Cl_2 and d^6-acetone. However many deuterated solvents are expensive and are therefore used sparingly. NMR spectroscopy allows a high level of structural elucidation to be sought, and is a non-destructive technique.

1.9.3 Single crystal X-ray diffraction

Single-crystal X-ray diffraction is a technique in which a beam of X-rays strikes a single crystal, producing scattered beams. The scattered beams are detected to produce a diffraction pattern as a series of spots; the strengths and angles of these beams are recorded as the crystal is gradually rotated. Each spot is called a reflection, since it corresponds to the reflection of the X-rays from one set of evenly spaced planes within the crystal. For single crystals of sufficient purity and regularity, X-ray diffraction data can determine the mean chemical bond lengths and angles to within a few thousandths of an angstrom and to within a few tenths of a degree, respectively.[105]

Crystals may be obtained from a number of methods; selected examples include slow evaporation of a solution of compound at ambient temperature and pressure, sublimation, vapour diffusion and recrystallisation. The key requirement is to prepare a crystal that is of sufficient purity and is ‘single’ (i.e. the crystal lattice is uniform throughout the sample without any defects). Crystals of highly reactive or moisture sensitive crystals may be handled under a stream of inert N_2 gas, but should be handled and mounted quickly. Crystals are mounted and

the structural information is acquired at 100 K, so as to minimise the thermal motion of the atoms in the crystal. The thermal motion of the atoms in the structure is quantified graphically using an Oak Ridge thermal ellipsoid plot (ORTEP) image.

Single crystal X-ray diffraction is an extremely useful tool in determining a compounds identity, giving a huge amount of structural information. However, the crystal structure obtained may not always be a true representative of the bulk product formed. In addition, despite the cooling of the crystal to 100 K, the motion of the atoms, and the ability of certain species such as $[BF_4]^-$ and $[PF_6]^-$ to adopt a number of geometries can give structures that are significantly disordered. Nonetheless, it is perhaps the single most useful technique in determining the identity of the compound formed in the solid state.

1.9.4 Elemental analysis

Elemental analysis is a technique in which a solid sample is analysed for its elemental composition. The most common form of elemental analysis is CHN analysis, in which a sample is combusted in an excess of oxygen. The combustion products (such as CO_2, H_2O, and N_2) are trapped and the mass of these gases present are used to calculate the elemental composition. Analyses in which the percentage compositions are ± 0.4% of the calculated percentage are considered suitable results. CHN analysis is a useful technique in understanding a compounds' composition in the bulk (provided that the compound contains organic constituents). However, compounds which are particularly sensitive to decomposition by air or moisture are difficult to transport and analyse effectively. In the context of the work described in this thesis, microanalysis may be useful in determining whether the complexes formed are solvent free, and if not, what degree of solvation may be present, if taken alongside evidence from other spectroscopic analysis.

1.9.5 Electrospray ionisation mass spectrometry

Mass spectrometry is an analytical technique that can provide both qualitative (structural) and quantitative (molecular mass or concentration) information on molecules after their conversion to ions. The molecules of interest are first introduced into the ionisation source of the mass spectrometer, where they are ionised to acquire positive or negative charges. The ions then travel through the mass analyser and arrive at different parts of the detector according to their mass/charge (*m/z*) ratio. After the ions make contact with the detector, useable signals are generated and recorded. The signals are displayed graphically as a mass spectrum showing the relative abundance of the signals according to their *m/z* ratio.

Electrospray ionisation (ESI) is a soft ionisation technique that is used extensively in the analysis of macromolecules, peptides, organometallics and other molecules which may be prone to fragmentation.[106] ESI uses electrical energy to assist the transfer of ions from solution into the

gaseous phase before they are subjected to mass spectrometric analysis. Ionic species in solution can thus be analysed by ESI-MS with increased sensitivity. Neutral compounds may also be converted to ionic form in solution or in gaseous phase by protonation or cationisation (such as from a metal cation), and hence can be studied by ESI-MS.

A solution containing the compound of interest is injected into the spectrometer, upon which a high voltage is passed through the sample which creates an aerosol. A stream of nitrogen gas acts to evaporate the solvent from the aerosol which leaves a concentrated droplet of charged species. These charged species are then ejected and the ion detected as detailed above.

As mentioned, ESI MS results in little fragmentation, which often allows the molecular ion to be observed. The instrument can be set to detect both positive and negative ions. In the work discussed in this thesis only positive ESI is used. In order to be observed using positive ESI, the compound analysed must be able to be readily protonated, or capable of forming interactions with a cationic species present within the mass spectrometer. ESI MS is a very sensitive technique, requiring only micro molar quantities of the compound to be analysed. Due to the requirement to evaporate the solvent, volatile solvents such as MeCN and MeOH are often mixed with water to produce the solution for injection. While ESI MS can provide evidence for the formation and purity of the sample analysed, it may be the case that only a small amount of an undesirable by-product is detected in the mass spectrum, giving a false impression as to the true identity of the compound. Nonetheless, in conjunction with other spectroscopic analysis, ESI MS is a very useful tool in analysing the complexes discussed in this thesis.

1.9.6 High performance liquid chromatography

High performance liquid chromatography (HPLC) is a chromatographic technique used extensively in radiochemistry. It allows the identification, quantification and purification of individual components of a reaction mixture.

HPLC relies on high pressure from mechanical pumps to push a liquid mobile phase through a chemical column. The chemical sample (dissolved in a suitable solvent) is injected onto the column and as the sample interacts with the column, separation occurs. The separated fractions will elute off at different retention times (Rt). The fractions are detected by UV/VIS spectroscopy or if handling radioactive species, radio detection as an intensity.

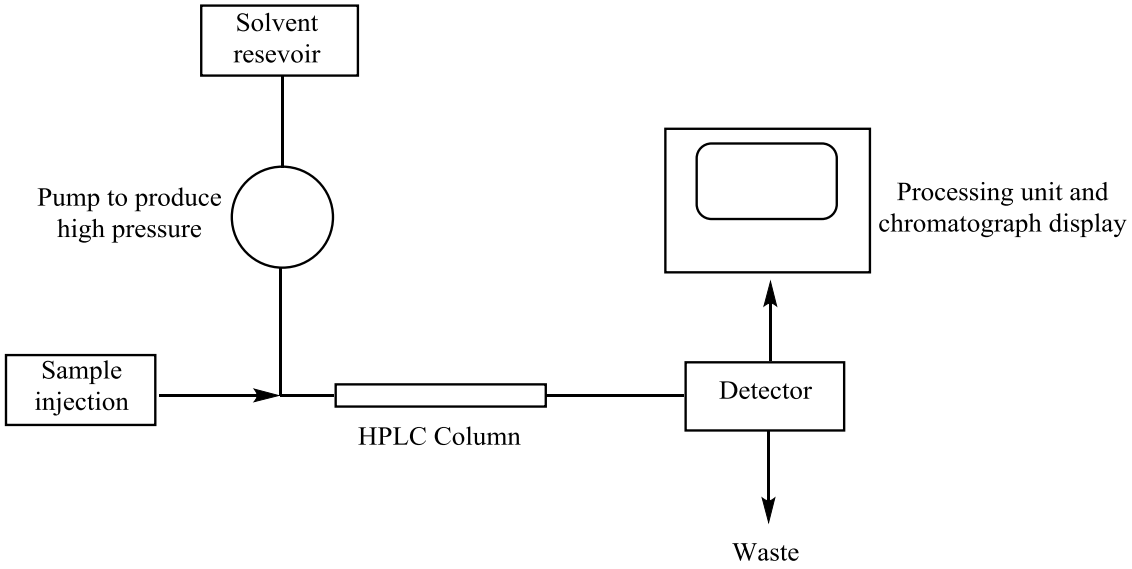

Figure 1.33: A basic schematic depicting the basic operation of a HPLC apparatus.

The speed of elution links to the retention time, species which interact strongly with the column are retained for longer. A high proportion of HPLC analysis is conducted with reverse phase columns. Reverse phase HPLC (RPHPLC) utilises an aqueous, moderately polar mobile phase with a polar stationary phase. The stationary phase is predominantly silica or alumina based which has undergone surface modification to incorporate long hydrophobic alkyl chains. Hydrophilic species do not interact strongly with the column and so will elute off with a short retention time (Rt), while more hydrophobic species interact strongly and are retained for longer. In the work discussed throughout this thesis, a reverse phase column was used, which allowed the lipophilic unreacted $^{18}F^-$ to be eluted off quickly, and thus allowed the desired compounds to elute off at a later retention time.

In radiochemical applications, HPLC is used extensively to determine whether the radionuclide has been incorporated during a reaction. A solution of the molecule of interest is injected into a solution of ^{18}F doped with a carrier agent (e.g. KF, KHF_2) and allowed to react. A sample of the reaction mixture is injected onto the HPLC where the separation is tracked by both UV/VIS and radio detection.

HPLC is a very sensitive technique; only small quantities of sample are required to be injected on to the column. The detectors are capable of detecting species in a nano or pico molar concentration, therefore any impurities in the sample are clearly observed. HPLC is also sensitive to the type of column and mobile phase used. For example, columns are available in several varieties based upon the length of the alkyl chains. If the sample being analysed is very hydrophilic, a column with long alkyl chains will elute off the sample too quickly to be detected. Conversely if a normal phase column were used, the sample would interact too strongly with the column, and would elute off too slowly.

In the work described in this thesis, a reverse phase column was used. This allowed any unreacted hydrophilic $^{18}F^-$ to be eluted off early in a run. A Luna C18 column was selected for the labelling experiments, which provided good separation of the species formed and without requiring long retention times.

1.10 Radiochemistry

Radiochemistry is the study of the chemistry of radioactive materials. Radioactivity is defined as the process by which the nucleus of an unstable atom loses energy by emitting ionising radiation. The radioactive decay of radioisotopes may be detected, and thus their incorporation in GE Healthcare's main radiochemical work concerns the incorporation of radioactive isotopes into a variety of biomolecules for imaging applications.

A large portion of their work involves the use of ^{18}F. $^{18}F^-$ is generated in a cyclotron by bombardment of a target of enriched $^{18}O/H_2O$ to provide $^{18}F^-$ as an aqueous solution.[107, 108] This aqueous solution is often of very high radioactivity (e.g. 60 GBq in 1 mL). To ensure that the activity is suitably low for use, the $^{18}F^-$ is diluted into water in a lead lined PET cell, and is sub-dispensed into N_2 pressurised vials. This allows for safe transfer of the radioactivity, and minimises the dose experienced by the handler.

The sub-dispensed fluoride is then further diluted into water, followed by addition of a carrier agent if required. The carrier agent, which is a ^{19}F fluoride source such as KF or KHF_2, aids in mechanical loss of the radionuclide. The loss of radionuclides during the analytical process due to adherence to container walls, solid phase extraction (SPE) cartridges and filters is minimised by the carrier agent competing to occupy these sites.

As one would expect, handling radiation involves rigorous containment and protection. Activity is transported in lead lined pots and all work is conducted in lead walled containment zones. The chemistry may then be performed manually if the amount of radioactivity is low. However, if large amounts of activity are used, the reactions may be performed on an automated synthesiser such as a GE FASTlab.

Reactions are typically undertaken in N_2 filled vials and supported in a lead pot. All syringes, vials etc. used in a 'hot' radioactive experiment are disposed into lead lined bins. Analysis of radiochemical products is performed on HPLC apparatus equipped with lead lined columns and detectors.

Researchers are permitted to receive a maximum of 20 mSv dosage per year. Therefore dosimeters are worn constantly, as are over-sleeves when handling activity. All researchers are measured for contamination after the experiment is completed.

1.11 Previous work in the group

Prior to the work discussed in this thesis, Dr Wenjian Zhang from the Reid/Levason group conducted an initial short feasibility study to ascertain whether the Group 13 metal halide complexes could be prepared with the neutral RMe_2-tacn ligands, and whether the halide exchange reaction with these complexes was possible. The work of Dr Zhang proved successful, providing some spectroscopic and structural data relating to some of the complexes discussed in parts of Chapters 2 and 3. While successful, the nature of the project meant that there were many gaps in the spectroscopy and very little understanding into the finer detail of the complexes prepared. Therefore the work in parts of Chapters 2 and 3 was repeated in greater detail by this author, the results of which are discussed herein. Dr Zhang collected a small number of crystal structures as part of the work; therefore any crystal structures collected by Dr Zhang have been included with his permission (and stated in the text) to aid in the discussion of the compounds formed. Where crystals of complexes previously synthesised by Dr Zhang were grown, unit cell determinations were performed to confirm the identity of the complexes formed.

1.12 Aims

This research project has five main aims;

(i) To develop a series of metal halide complexes based on the Group 13 ions Al, Ga and In with potential applications in PET imaging applications. This will invoke the use of the azamacrocycle tacn, functionalised with both neutral (Chapters 2, 3 and 5) and anionic pendant arms (Chapter 4).

(ii) To develop reaction methodology in which ligand exchange reactions may be performed to incorporate ^{18}F rapidly under mild conditions. This will involve investigation of the halide exchange under both anhydrous conditions using alkyl ammonium fluorides and under aqueous conditions using KF (Chapters 3 and 4).

(iii) To ^{18}F radiolabel the preformed metal chelates to demonstrate the utility of this new class of compound in potential PET imaging applications (Chapters 3 and 4);

(iv) To further develop the coordination chemistry of the Group 13 metal fluorides, an area which has been little explored. This involves the use of hydrothermal synthesis, a surprisingly little used method to access complexes of insoluble metal fluoride salts (Chapter 6).

(v) To synthesise a number of new tacn based ligands as potential future frameworks for imaging applications (Chapter 7).

1.13 References

1. Alauddin, M. M., *Am. J. Nucl. Med. Mol. Imaging.* **2012,** *2*, 55-76.
2. Phelps, M. E., *PET: physics, instrumentation, and scanners*. Springer: 2006.
3. Battle, M. R.; Goggi, J. L.; Allen, L.; Barnett, J.; Morrison, M. S., *J. Nucl. Med.* **2011,** *52*, 424-430.
4. Prakash, G. K. S.; Wang, F. In *Flourishing frontiers in organofluorine chemistry*, Wiley-VCH 2012; pp 413-476.
5. Smith, G. E.; Sladen, H. L.; Biagini, S. C. G.; Blower, P. J., *Dalton Trans.* **2011,** *40*, 6196-6205.
6. Ido, T.; Wan, C. N.; Casella, V.; Fowler, J. S.; Wolf, A. P.; Reivich, M.; Kuhl, D. E., *J. Labelled Compd. Radiopharm.* **1978,** *14*, 175-183.
7. Storey, A. E.; Jones, C. L.; Bouvet, D. R. C.; Lasbistes, N.; Fairway, S. M.; Williams, L.; Gibson, A. M.; Nairne, R. J.; Karimi, F.; Langstrom, B. Process for fluorination of anilides. WO2007020400A1, 2007.
8. Snellman, A.; Rokka, J.; Lopez-Picon, F. R.; Eskola, O.; Wilson, I.; Farrar, G.; Scheinin, M.; Solin, O.; Rinne, J. O.; Haaparanta-Solin, M., *Eur. J. Nucl. Med. Mol. Imaging* **2012,** *39*, 1784-1795.
9. S. Forsback, O. E., M. Haaparanta, J. Bergman, O.Solin, *Radiochima Acta.* **2010,** *96*, 845-850.
10. Lee, H. G.; Milner, P. J.; Buchwald, S. L., *J. Am. Chem. Soc.* **2014,** *136*, 3792-3795.
11. Watson, D. A.; Su, M.; Teverovskiy, G.; Zhang, Y.; Garcia-Fortanet, J.; Kinzel, T.; Buchwald, S. L., *Science.* **2009,** *325*, 1661-1664.
12. Liu, W.; Huang, X.; Cheng, M.-J.; Nielsen, R. J.; Goddard, W. A., III; Groves, J. T., *Science.* **2012,** *337*, 1322-1325.
13. Lee, E.; Kamlet, A. S.; Powers, D. C.; Neumann, C. N.; Boursalian, G. B.; Furuya, T.; Choi, D. C.; Hooker, J. M.; Ritter, T., *Science.* **2011,** *334*, 639-642.
14. Lee, E.; Hooker, J. M.; Ritter, T., *J. Am. Chem. Soc.* **2012,** *134*, 17456-17458.
15. Campbell, M. G.; Ritter, T., *Org. Process Res. Dev.* **2014,** *18*, 474-480.
16. Luo, Y.-R., *Handbook of Chemical Bond Energies*. CRC Press: 2007.
17. Ting, R.; Adam, M. J.; Ruth, T. J.; Perrin, D. M., *J. Am. Chem. Soc.* **2005,** *127*, 13094-13095.
18. Keller, U.; Bellac, C. L.; Li, Y.; Lou, Y.; Lange, P. F.; Ting, R.; Harwig, C.; Kappelhoff, R.; Dedhar, S.; Adam, M. J.; Ruth, T. J.; Benard, F.; Perrin, D. M.; Overall, C. M., *Cancer Res.* **2010,** *70*, 7562-7569.
19. Harwig, C. W.; Ting, R.; Adam, M. J.; Ruth, T. J.; Perrin, D. M., *Tetrahedron Lett.* **2008,** *49*, 3152-3156.

20. Ting, R.; Lo, J.; Adam, M. J.; Ruth, T. J.; Perrin, D. M., *J. Fluorine Chem.* **2008,** *129*, 349-358.
21. Liu, Z.; Li, Y.; Lozada, J.; Wong, M. Q.; Greene, J.; Lin, K.-S.; Yapp, D.; Perrin, D. M., *Nucl. Med. Biol.* **2013,** *40*, 841-849.
22. Liu, Z.; Radtke, M. A.; Wong, M. Q.; Lin, K.-S.; Yapp, D. T.; Perrin, D. M., *Bioconjugate Chem.* **2014,** *25*, 1951-1962.
23. Liu, Z.; Li, Y.; Lozada, J.; Pan, J.; Lin, K.-S.; Schaffer, P.; Perrin, D. M., *J. Labelled Compd. Radiopharm.* **2012,** *55*, 491-496.
24. Liu, Z.; Li, Y.; Lozada, J.; Schaffer, P.; Adam, M. J.; Ruth, T. J.; Perrin, D. M., *Angew. Chem., Int. Ed.* **2013,** *52*, 2303-2307.
25. Wangler, C.; Waser, B.; Alke, A.; Iovkova, L.; Buchholz, H.-G.; Niedermoser, S.; Jurkschat, K.; Fottner, C.; Bartenstein, P.; Schirrmacher, R.; Reubi, J.-C.; Wester, H.-J.; Wangler, B., *Bioconjugate Chem* **2010,** *21*, 2289-2296.
26. Walsh, J. C.; Flemming, L. M.; Satyamurthy, N.; Baario, J. R.; Phelps, M. E.; Gambhir, S. S.; Toyokuni, T., *J. Nucl. Med.* **2000,** *41*, 1098-1107.
27. Choudhry, U.; Martin, K.; Mainaard, D.; Biagini, S. C. G.; Blower, P. J., *Eur J. Nucl Med Mol Imaging.* **2006,** *33*, S306-S312.
28. Schirrmacher, E.; Wangler, C.; Schirrmacher, R., *Mini-Rev. Org. Chem* **2007,** *4*, 317-329.
29. Schirrmacher, E.; Wangler, B.; Cypryk, M.; Beadtmoller, G.; Schafer, M.; Eisenhut, M.; Jurkschat, K.; Schirrmacher, R., *Bioconjugate. Chem* **2007,** *18*, 2085-2089.
30. Schirrmacher, R.; Bradmoeller, G.; Schirrmacher, E.; Thews, O.; Tillmanns, J.; Siessmeier, T.; Bucholz, H. G.; Bartenstein, P.; Waengler, B.; Niemeyer, C. M.; Jurkschat, K., *Angew. Chem., Int. Ed.* **2006,** *45*, 6047-6050.
31. D'Souza, C. A.; McBride, W. J.; Goldenberg, D. M. Methods and compositions for F-18 labeling of proteins, peptides and other molecules. US20130315821A1, 2013.
32. Goldenberg, D. M.; Sharkey, R. M.; McBride, W. J.; Boerman, O. C., *J. Nucl. Med.* **2013,** *54*, 1170-1173.
33. McBride, W. J.; Sharkey, R. M.; Goldenberg, D. M., *EJNMMI Res.* **2013,** *3*, 36/1-36/11.
34. Dean, J. A., *Lange's Handbook of Chemistry. Section 4.* 15th ed.; 1999, 4.41-4.53.
35. McBride, W. J.; Sharkey, R. M.; Karacay, H.; D'Souza, C. A.; Rossi, E. A.; Laverman, P.; Chang, C.-H.; Boerman, O. C.; Goldenberg, D. M., *J. Nucl. Med.* **2009,** *50*, 991-998.
36. Laverman, P.; McBride, W. J.; Sharkey, R. M.; Eek, A.; Joosten, L.; Oyen, W. J. G.; Goldenberg, D. M.; Boerman, O. C., *J. Nucl. Med.* **2010,** *51*, 454-461.
37. McBride, W. J.; D'Souza, C. A.; Sharkey, R. M.; Karacay, H.; Rossi, E. A.; Chang, C.-H.; Goldenberg, D. M., *Bioconjugate Chem.* **2010,** *21*, 1331-1340.
38. D'Souza, C. A.; McBride, W. J.; Sharkey, R. M.; Todaro, L. J.; Goldenberg, D. M., *Bioconjugate Chem.* **2011,** *22*, 1793-1803.

39. Shetty, D.; Choi, S. Y.; Jeong, J. M.; Lee, J. Y.; Hoigebazar, L.; Lee, Y.-S.; Lee, D. S.; Chung, J.-K.; Lee, M. C.; Chung, Y. K., *Chem. Commun.* **2011,** *47*, 9732-9734.
40. McBride, W. J.; D'Souza, C. A.; Karacay, H.; Sharkey, R. M.; Goldenberg, D. M., *Bioconjugate Chem.* **2012,** *23*, 538-547.
41. Kiesewetter, D. O.; Guo, N.; Guo, J.; Gao, H.; Zhu, L.; Ma, Y.; Niu, G.; Chen, X., *Theranostics.* **2012,** *2*, 999-1009.
42. Dijkgraaf, I.; Franssen, G. M.; McBride, W. J.; D'Souza, C. A.; Laverman, P.; Smith, C. J.; Goldenberg, D. M.; Oyen, W. J. G.; Boerman, O. C., *J. Nucl. Med.* **2012,** *53*, 947-952.
43. Kiesewetter, D. O.; Gao, H.; Ma, Y.; Niu, G.; Quan, Q.; Guo, N.; Chen, X., *Eur. J. Nucl. Med. Mol. Imaging.* **2012,** *39*, 463-473.
44. Wan, W.; Guo, N.; Pan, D.; Yu, C.; Weng, Y.; Luo, S.; Ding, H.; Xu, Y.; Wang, L.; Lang, L.; Xie, Q.; Yang, M.; Chen, X., *J. Nucl. Med.* **2013,** *54*, 691-698.
45. McBride, W. J.; D'Souza, C. A.; Sharkey, R. M.; Goldenberg, D. M., *Appl. Radiat. Isot.* **2012,** *70*, 200-204.
46. Downs, A., *Chemistry of Aluminium, Gallium, Indium and Thallium*. Blackie Glasgow, 1993; Vol. 1.
47. Mason., J., *Multinuclear NMR*. Plenum Press: 1987; Vol. 1.
48. Shannon, R. D., *Acta Crystallogr., Sect. A* **1976,** *A32*, 751-767.
49. Constable, E., *Coordination Chemistry of Macrocyclic Compounds*. Oxford University Press: 1999.
50. Levason, W.; Reid, G., In *Comprehensive Coordination Chemistry II*, Meyer, T. J.; McCleverty, J. A., Eds. Pergamon: Oxford, 2003; pp 399-410.
51. Levason, W.; Reid, G., In *Comprehensive Coordination Chemistry II*, Meyer, T. J.; McCleverty, J. A., Eds. Pergamon: Oxford, 2003; pp 475-484.
52. Pedersen, C. J., *J. Am. Chem. Soc.* **1967,** *89*, 7017-7036.
53. Curtis, N. F.; Curtis, Y. M., *Inorg. Chem.* **1965,** *4*, 804-809.
54. Parker, D., *Macrocyclic Synthesis: A Practical Approach*. Oxford University Press: 1996; Vol. 2.
55. Raidt, M.; Neuburger, M.; Kaden, T. A., *Dalton Trans.* **2003**, 1292-1298.
56. Svobodova, I.; Lubal, P.; Plutnar, J.; Havlickova, J.; Kotek, J.; Hermann, P.; Lukes, I., *Dalton Trans.* **2006**, 5184-5197.
57. Bravo, J. A.; Raymo, F. M.; Stoddart, J. F.; White, A. J. P.; Williams, D. J., *Eur. J. Org. Chem.* **1998,** *1998*, 2565-2571.
58. Hasenknopf, B.; Lehn, J.-M.; Kneisel, B. O.; Baum, G.; Fenske, D., *Angew. Chem. Int. Ed.* **1996,** *35*, 1838-1840.
59. Lehn, J. M., *Science.* **1993,** *260*, 1762-1763.

60. Constable, E. C.; Housecroft, C. E.; Creus, M.; Gademann, K.; Giese, B.; Ward, T. R.; Woggon, W.-D.; Chougnet, A., *Chimia* **2010,** *64*, 846-847.
61. Karlin, K. D.; Zubieta, J., *Copper Coordination Chemistry: Biochemical and Inorganic Perspectives*. Adenine Press: New York, 1983.
62. Cabbiness, D. K.; Margerum, D. W., *J. Am. Chem. Soc.* **1969,** *91*, 6540-6541.
63. Dei, A.; Gori, R., *Inorg. Chim. Acta.* **1975,** *14*, 157-60.
64. Hancock, R. D.; Thom, V. J., *J. Am. Chem. Soc.* **1982,** *104*, 291-292.
65. Myers, R. T., *Inorg. Chem.* **1978,** *17*, 952-958.
66. Hinz, F. P.; Margerum, D. W., *Inorg. Chem.* **1974,** *13*, 2941-2949.
67. Liddle, S. T.; Clegg, W., *Acta Crystallogr., Sect. E* **2003,** *59*, m1184-m1186.
68. Chaudhuri, P.; Wieghardt, K., *Prog. Inorg. Chem.* **2007**, 329-436.
69. Chang, C. A.; Francesconi, L. C.; Malley, M. F.; Kumar, K.; Gougoutas, J. Z.; Tweedle, M. F.; Lee, D. W.; Wilson, L. J., *Inorg. Chem.* **1993,** *32*, 3501-3508.
70. Koyama, H.; Yoshino, T., *Bull. Chem. Soc. Jpn* **1972,** *45*, 481-484.
71. Richman, J. E.; Atkins, T. J., *J. Am. Chem. Soc.* **1974,** *96*, 2268-2270.
72. Lehn, J. M., *Pure Appl. Chem.* **1978,** *50*, 871-892.
73. Meade, T. J.; Busch, D. H., *Prog. Inorg. Chem.* **1985,** *33*, 59-126.
74. Willey, G. R.; Aris, D. R.; Beaumont, A. L.; Errington, W., *Main Group Met. Chem.* **1999,** *22*, 515-518.
75. Wieghardt, K.; Kleine-Boymann, M.; Nuber, B.; Weiss, J., *Z. Anorg. Allg. Chem.* **1986,** *536*, 179-186.
76. Wieghardt, K.; Kleine-Boymann, M.; Nuber, B.; Weiss, J., *Inorg. Chem.* **1986,** *25*, 1654-1659.
77. Penkert, F. N.; Weyhermuller, T.; Wieghardt, K., *Chem. Commun.* **1998**, 557-558.
78. Cheng, F.; Hector, A. L.; Levason, W.; Reid, G.; Webster, M.; Zhang, W., *Chem. Commun.* **2009**, 1334-1336.
79. Cheng, F.; Davis, M. F.; Hector, A. L.; Levason, W.; Reid, G.; Webster, M.; Zhang, W., *Eur. J. Inorg. Chem.* **2007**, 4897-4905.
80. McCleverty, J. A.; Meyer, T. J., *Comprehensive Coordination Chemistry II, Volume 3*. 2004.
81. Hsieh, W.-Y.; Liu, S., *Inorg. Chem.* **2004,** *45*, 6006-6014.
82. Kazakov, I. V.; Bodensteiner, M.; Timoshkin, A. Y., *Acta Crystallogr., Sect. C.* **2014,** *70*, 312-314.
83. Timoshkin, A. Y.; Bodensteiner, M.; Sevastianova, T. N.; Lisovenko, A. S.; Davydova, E. I.; Scheer, M.; Grassl, C.; Butlak, A. V., *Inorg. Chem.* **2012,** *51*, 11602-11611.
84. Aldridge, S.; Downs, A., *The Group 13 Metals, Aluminium, Gallium, Indium and Thallium: Chemical Patterns and Paculiarities*. Wiley: Chichester, 2011.

85. Kemnitz, E.; Gross, U.; Ruediger, S.; Scholz, G.; Heidemann, D.; Troyanov, S. I.; Morosov, I. V.; Lemee-Cailleau, M. H., *Solid State Sci.* **2006,** *8*, 1443-1452.
86. Bukovec, P.; Kaucic, V., *Inorg. Nucl. Chem. Lett.* **1978,** *14*, 79-81.
87. Heathcock, C. H., *Comprehensive Organic Synthesis: , Volume 2: Ch.3*. 1992.
88. Schreiber, S. L., *Comprehensive Organic Synthesis: Volume 1:* . Pergamon: 1992.
89. Semmelhack, M. F., *Comprehensive Organic Synthesis: Volume 4: Ch 1.8*. Pergamon: 1992.
90. Burt, J.; Levason, W.; Light, M. E.; Reid, G., *Dalton Trans.* **2014,** *43*, 14600-14611.
91. Cheng, F.; Codgbrook, H. L.; Hector, A. L.; Levason, W.; Reid, G.; Webster, M.; Zhang, W., *Polyhedron.,* **2007,** *26*, 4147-4155.
92. Gurnani, C.; Jura, M.; Levason, W.; Ratnani, R.; Reid, G.; Webster, M., *Dalton Trans.* **2009**, 1611-1619.
93. George, K.; Jura, M.; Levason, W.; Light, M. E.; Ollivere, L. P.; Reid, G., *Inorg. Chem.* **2012,** *51*, 2231-2240.
94. George, K.; Jura, M.; Levason, W.; Light, M. E.; Reid, G., *Dalton Trans.* **2014,** *43*, 3637-3648.
95. Gurnani, C.; Levason, W.; Ratnani, R.; Reid, G.; Webster, M., *Dalton Trans.* **2008**, 6274-6282.
96. Gurnani, C.; Jura, M.; Levason, W.; Ratnani, R.; Reid, G.; Webster, M., *Dalton Trans.* **2009**, 1611-1619.
97. Blower, P. J., *Dalton Trans.* **2015,** *44*, 4819-4844.
98. Craig, A. S.; Parker, D.; Adams, H.; Bailey, N. A., *J. Chem. Soc., Chem. Commun.* **1989**, 1793-1794.
99. Yang, C.-T.; Sreerama, S. G.; Hsieh, W.-Y.; Liu, S., *Inorg. Chem.* **2008,** *47*, 2719-2727.
100. Suzuki, K.; Satake, M.; Suwada, J.; Oshikiri, S.; Ashino, H.; Dozono, H.; Hino, A.; Kasahara, H.; Minamizawa, T., *Nucl. Med. Biol.* **2011,** *38*, 1011-1018.
101. Shetty, D.; Choi, S. Y.; Jeong, J. M.; Hoigebazar, L.; Lee, Y.-S.; Lee, D. S.; Chung, J.-K.; Lee, M. C.; Chung, Y. K., *Eur. J. Inorg. Chem.* **2010**, 5432-5438.
102. Craig, A. S.; Helps, I. M.; Parker, D.; Adams, H.; Bailey, N. A.; Williams, M. G.; Smith, J. M. A.; Ferguson, G., *Polyhedron* **1989,** *8*, 2481-2484.
103. Liu, S.; He, Z.; Hsieh, W.-Y.; Fanwick, P. E., *Inorg. Chem.* **2003,** *42*, 8831-8837.
104. Nakamoto, K., *Infrared Spectra of Inorganic and Coordination Compounds*. J. Wiley & Sons: 1985; Vol. 1.
105. Clegg, W., *Crystal Structure Determination*. Oxford University Press: 1998.
106. Barshick, C. M.; Duckworth, D. C.; Smith, D. H., *Inorganic Mass Spectrometry: Fundamentals and Applications*. Dekker: 2000.

107. Huszar, I.; Weinreich, R., *J. Radioanal. Nucl. Chem.* **1985,** *93*, 349-354.
108. Fowler, J. S.; Wolf, A. P., *The Synthesis of Carbon-11, Fluorine-18, and Nitrogen-13 Labeled Radiotracers for Biomedical Applications*. NTIS: 1983.

Chapter 2

Direct synthesis and characterisation of Group 13 metal halide complexes with neutral aza-macrocyclic ligands

2.1 Introduction

MCl_3, M = Al, Ga, In are moisture sensitive white solids at room temperature. $AlCl_3$ adopts a layered cubic structure with six coordinate aluminium centres.[1] $GaCl_3$ adopts a dimeric Ga_2Cl_6 structure with chloride bridged octahedral gallium centres.[1] $InCl_3$ is a six coordinate ionic species with indiums occupying one third of the octahedral holes.[1] These materials are indefinitely stable if stored under a dry and inert atmosphere. They are soluble in common organic solvents such as CH_2Cl_2, MeCN, and toluene. This allows their coordination chemistry to be extensively studied under mild synthetic conditions.

The metal chlorides $AlCl_3$ and $GaCl_3$ are used extensively in organic synthesis as Lewis acid catalysts in Friedel Crafts acylation and other electrophilic aromatic substitutions.[1]

The neutral tri-alkyl ligands 1,4,7-trimethyl-1,4,7-triazacyclononane (Me_3-tacn) and 1-benzyl-4,7-dimethyl-1,4,7-triazacyclononane ($BzMe_2$-tacn) are ligands used throughout coordination chemistry. The tri-alkylated ligand Me_3-tacn may be synthesised easily *via* post synthetic modification of the free base.[2] This proceeds via a simple Eschweiler Clarke reaction using excess formic acid and formaldehyde, followed by pH controlled work up (Figure 2.1).

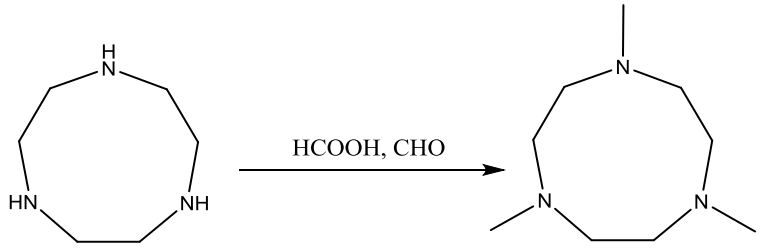

Figure 2.1: Synthesis of 1,4,7-trimethyl-1,4,7-triazacyclononane (Me_3-tacn).

The benzyl-dimethyl-tacn derivative is synthesised via a different route. The free base ligand cannot be alkylated *via* traditional protection and deprotection chemistry, as attempts to methylate the benzyl-tacn ligand results in quaternarization of the tacn nitrogen atoms. An alternative route is to cyclise two acyclic fragments containing each pendant arm functionality under dilution conditions followed by a $LiAlH_4$ mediated reduction (Figure 2.2).[3]

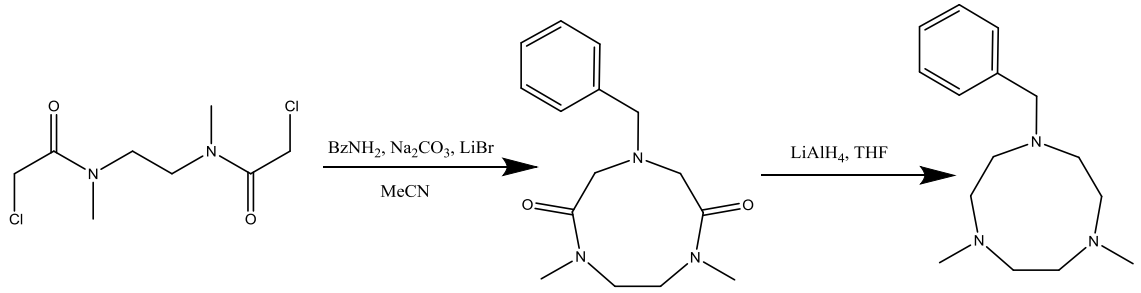

Figure 2.2: Synthesis of $BzMe_2$-tacn.

The Me_3-tacn ligand may be synthesised in high yield and easily purified by distillation. The $BzMe_2$-tacn is more challenging to synthesise, and is obtained in lower yield. This is due to the cyclisation reaction being difficult to control to gain the cyclised product, rather than the open chain compound. The $BzMe_2$-tacn ligand is of particular interest with regard to potential radiolabelling reactions as the benzyl substituent provides a UV chromophore which allows for the fate of the complex to be tracked by HPLC during labelling reactions. Further, the benzyl substituent can act as a site for a potential conjugation of peptides or bioactive compounds to create biologically active imaging agents.

Previous work in the group by Dr Wenjian Zhang had investigated the use of the heavier Group 13 halides MBr_3 to synthesise the precursor complexes. However formation of the chloride adducts was favoured over the bromide analogues due to the lower moisture sensitivity of the chloride complexes and ease of handling.[4]

2.2 Results and Discussion

2.2.1 General synthetic procedure towards the adducts [MCl_3(RMe_2-tacn)]

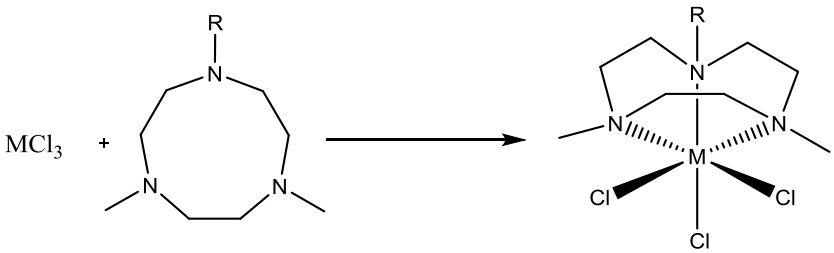

Figure 2.3: General synthetic route towards Group 13 chloride complexes.

Reaction of equimolar quantities of the appropriate metal trichloride with RMe_2-tacn (R = Me, Bz) in rigorously anhydrous MeCN (Al) or CH_2Cl_2 (Ga, In) at room temperature results in the rapid precipitation of the solvent free adducts *fac*-[MCl_3(RMe_2-tacn)]. The white solids were

isolated by filtration and washed with anhydrous hexane to remove any unreacted ligand (Figure 2.3).

The adducts may be isolated in very high yield and purity. The complexes are moderately moisture sensitive, but may be stored for many months without degradation in a dry N_2 filled glove box. The complexes are moderately soluble in MeCN and CH_2Cl_2.

2.2.2 Synthesis of [$AlCl_3$(RMe_2-tacn)] complexes

The infra-red spectra of the complexes (recorded between CsI plates) indicate the presence of two IR active bands in the Al-Cl region (a_1, e). This is expected for *facially* coordinated octahedra with C_{3V} symmetry (Table 2.1).[5]

Complex	ν M-Cl/ cm^{-1}
[$AlCl_3$(Me_3-tacn)]	375, 346
[$AlCl_3$($BzMe_2$-tacn)]	384, 349
[$GaCl_3$(Me_3-tacn)]	278, 245
[$GaCl_3$($BzMe_2$-tacn)]	280, 260
[$InCl_3$(Me_3-tacn)]	287, 269
[$InCl_3$($BzMe_2$-tacn)]	288, 272

Table 2.1: Table of infra-red stretching frequencies for the M-Cl bond in the complexes [MCl_3(RMe_2-tacn)].

The ^{1}H NMR spectrum of the complex [$AlCl_3$(Me_3-tacn)] displays two second order multiplets assigned to the methylene protons in the coordinated Me_3-tacn ring system, as well as a sharp singlet corresponding to the methyl protons on the Me_3-tacn. This is due to facial coordination of the Me_3-tacn locking the ring geometry. This places the methylene protons into two distinct environments; one pointing towards the metal centre and one away from the metal centre. This creates two distinct resonances in the NMR spectrum. The second factor is the effect of the quadrupolar aluminium nucleus. The ^{27}Al centre will couple to the methylene protons resulting in the multiplet formation. The substituent methyl protons are equivalent giving a singlet to high frequency of the Me_3-tacn ligand.

The ^{1}H NMR spectrum of [$AlCl_3$($BzMe_2$-tacn)] also displays this characteristic splitting pattern, suggesting that *facial* tridentate coordination of the ligand to the metal centre gives this unusual NMR spectrum.

^{27}Al NMR spectroscopy (I = 5/2, Q = 0.15 x10^{-28} m^2)[6] was also used as a probe to characterise the complexes. The complexes gave strong resonances in the NMR spectrum (Figure 2.4) consistent with six-coordinate aluminium.[7, 8] Both complexes also appeared insensitive towards a variety of weak donor solvents such as anhydrous MeCN, CH_2Cl_2, thf and acetone. However when dissolved in more strongly coordinating solvents such as DMF or DMSO, the complexes decompose and the resonance associated with [$AlCl_3$(RMe_2-tacn)] is

lost. This is also the case when water is added to a solution of the complex in MeCN upon which a resonance appears at δ = 0 ppm corresponding to $[Al(H_2O)_6]^{3+}$. This shows that the aluminium complexes are hydrolytically unstable, and that the RMe_2-tacn residue is relatively weakly bound.

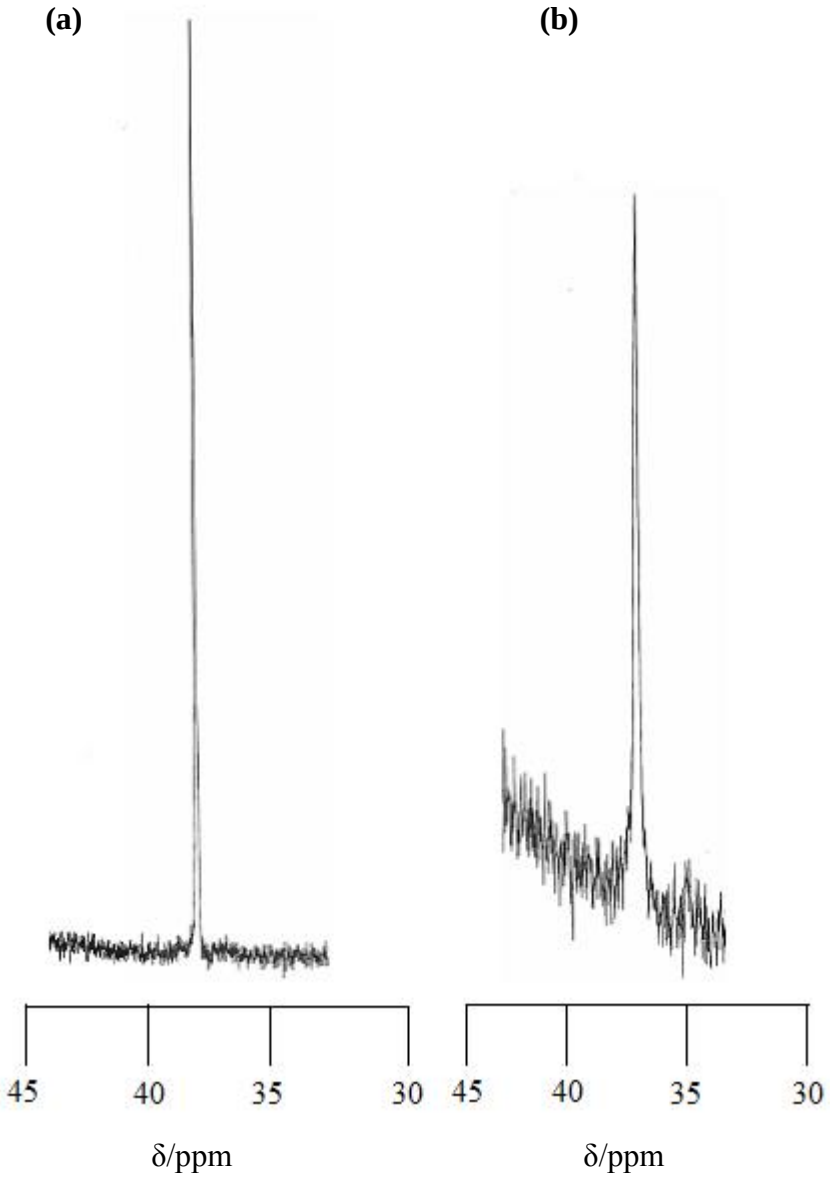

Figure 2.4: ^{27}Al NMR spectra of $[AlCl_3(Me_3\text{-tacn})]$ (a) δ 34.5 ppm. $W_{1/2}$ = 30 Hz and $[AlCl_3(BzMe_2\text{-tacn})]$ (b) δ 36.5 ppm. $W_{1/2}$ = 45 Hz.

The complex was also synthesised by Dr Wenjian Zhang, who through cooling of the reaction filtrate managed to obtain colourless crystals of $[AlCl_3(Me_3\text{-tacn})]$ suitable for single crystal X-ray diffraction.

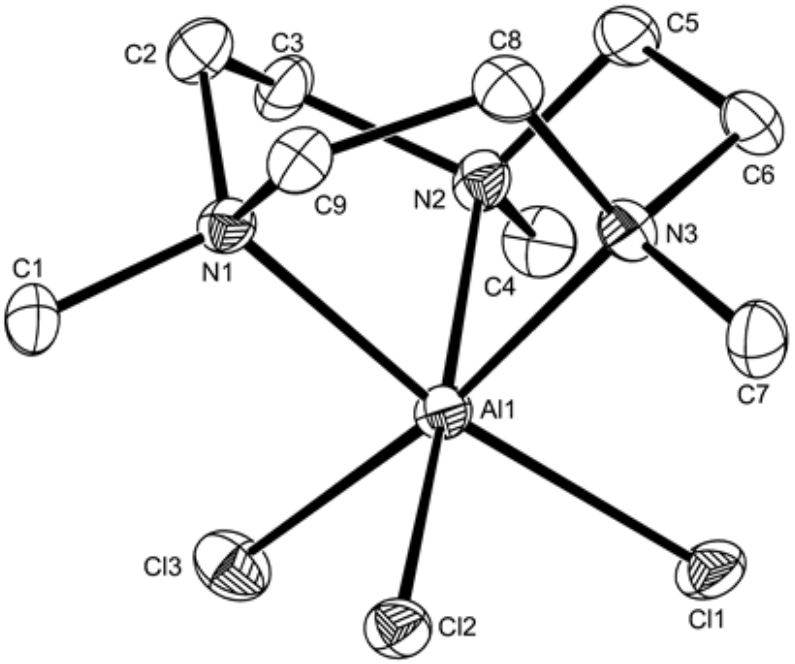

Figure 2.5: Crystal structure of the complex [$AlCl_3$(Me_3-tacn)]. Ellipsoids are drawn at 50% probability level. H-atoms are omitted for clarity. Monoclinic, $P2_1/c$. Image recopied with permission from Dr W. Zhang. Al1-N1 2.133(5), Al1-N2 2.148(5), Al1-N3 2.114(5), Al1-Cl1 2.279(2), Al1-Cl2 2.264(2), Al1-Cl3 2.272(2) Å. N3-Al1-N1 82.93(14), Cl2-Al1-Cl1 93.78(7), N1-Al1-N2 81.60(14), Cl2-Al1-Cl3 94.10(6), N3-Al1-N2 81.739(14), Cl3-Al1-Cl1 94.21(7)°.

The structure (Figure 2.5) reveals a distorted octahedral aluminium centre with the tridentate Me_3-tacn ligand coordinating *facially*. The d(Al-N) in the complex ranges from 2.114(5) – 2.148(5) Å. The lack of crystallographically characterised *facially* coordinated complexes with neutral N-donor ligands makes detailed comparisons difficult. Comparison of the complex *mer*-[$AlCl_3(py)_3$] shows the d(Al-N) are significantly shorter (2.087(3) – 2.0958(5) Å) than the [$AlCl_3$(Me_3-tacn)] complex. While the geometry of the complex and donor ability of the pyridine ligand must be taken into account, it shows that the macrocyclic ring is limiting the approach of the N-donor atoms. The requirement to accommodate three chloride ligands (ionic radius Cl^- = 1.81 Å) onto the small aluminium metal centre (ionic radius of six-coordinate Al(III) = 0.68 Å) also contributes to the elongated Al-N bond lengths. The complex does not crystallise with any co-solvent, in stark contrast to the corresponding fluoride complexes discussed in Chapters 3.2.3 and 3.2.4.

2.2.3 Synthesis of [$GaCl_3$(RMe_2-tacn)] complexes

Combination of anhydrous $GaCl_3$ with RMe_2-tacn (R = Me, Bz) in anhydrous MeCN at room temperature yields the solvent free adducts [$GaCl_3$(RMe_2-tacn)] as off white solids. Like the aluminium complexes they have a distorted octahedral geometry, with the tacn ligand binding *facially* to the metal centre. The IR spectrum of the complexes indicates the presence of two IR active bands for Ga-Cl in the region of around 280-245 cm^{-1}. This observation is as expected for *facially* coordinated octahedra with C_{3V} symmetry.

The ^1H NMR spectrum of the complex [$GaCl_3$(Me_3-tacn)] indicates a similar pattern to that observed in the aluminium system, specifically the two second order multiplets corresponding to the methylene protons as well as a sharp singlet corresponding to the methyl protons on the Me_3-tacn. The ^1H NMR of [$GaCl_3$($BzMe_2$-tacn)] (Figure 2.6) also displays this characteristic splitting pattern, although there are more methylene CH_2 environments as a result of the unsymmetrical benzyl substituent, which results in different proton environments within the tacn ring.

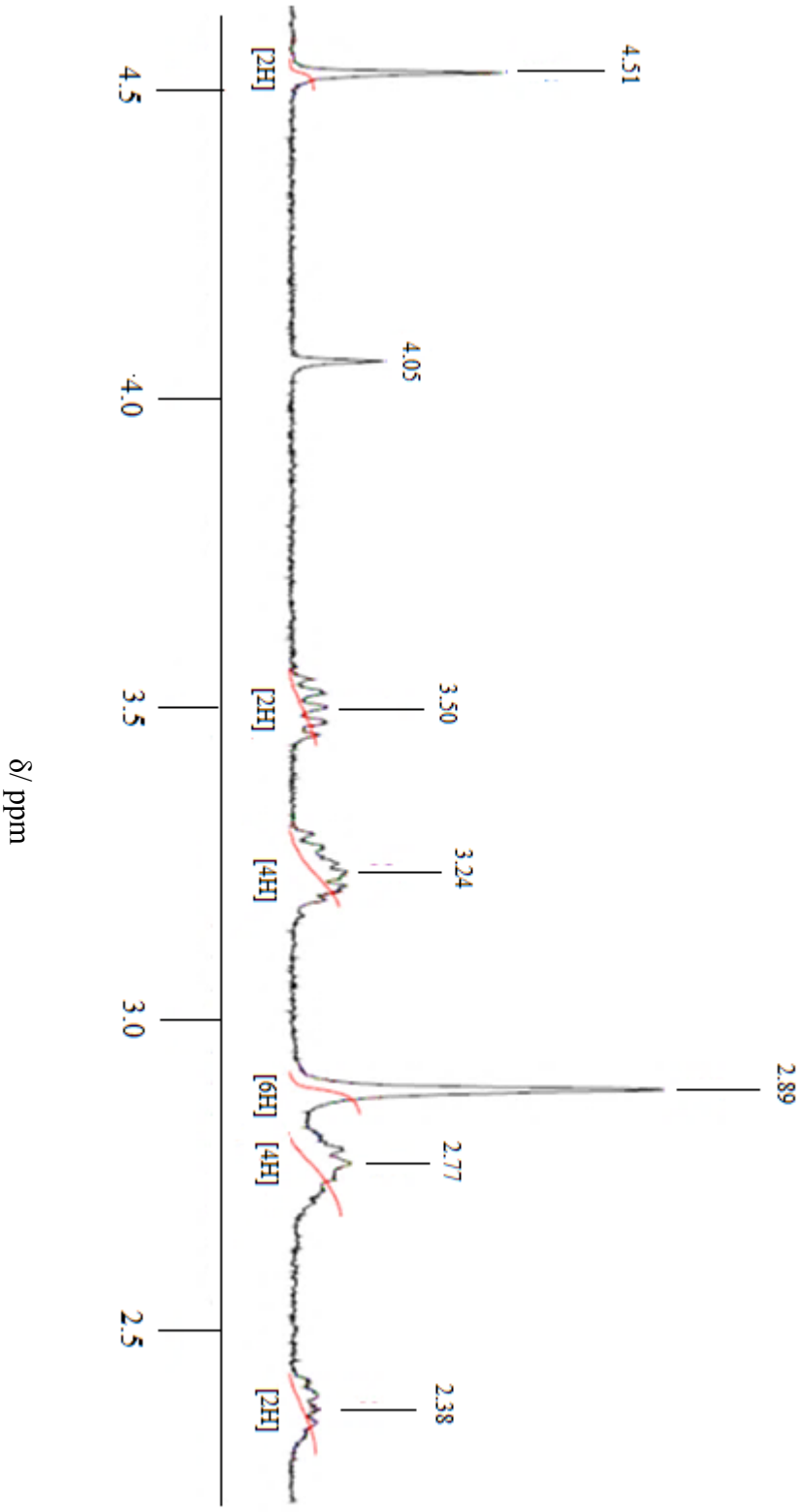

Figure 2.6: ^{1}H NMR spectrum of [$GaCl_3$($BzMe_2$-tacn)] recorded in CD_3CN. It shows the benzyl singlet at 4.51 ppm, the second order multiplets related to the methylene protons in the tacn ring (3.50, 3.24, 2.77, 2.36 ppm) and the singlet related to the methyl (2.89 ppm). A minor impurity peak is also present at δ = 4.05 ppm. Aromatic protons are not depicted.

^{71}Ga NMR spectroscopy was also used as a probe to characterise the complexes. Both complexes [$GaCl_3$(Me_3-tacn)] and [$GaCl_3$($BzMe_2$-tacn)] exhibit a broad singlet at δ 93 and 94 ppm respectively.[9-11]

Dissolution of [$GaCl_3$(Me_3-tacn)] in anhydrous MeCN, followed by slow evaporation in the glovebox yielded large colourless block crystals suitable for analysis by single crystal X-ray diffraction (Figure 2.7).

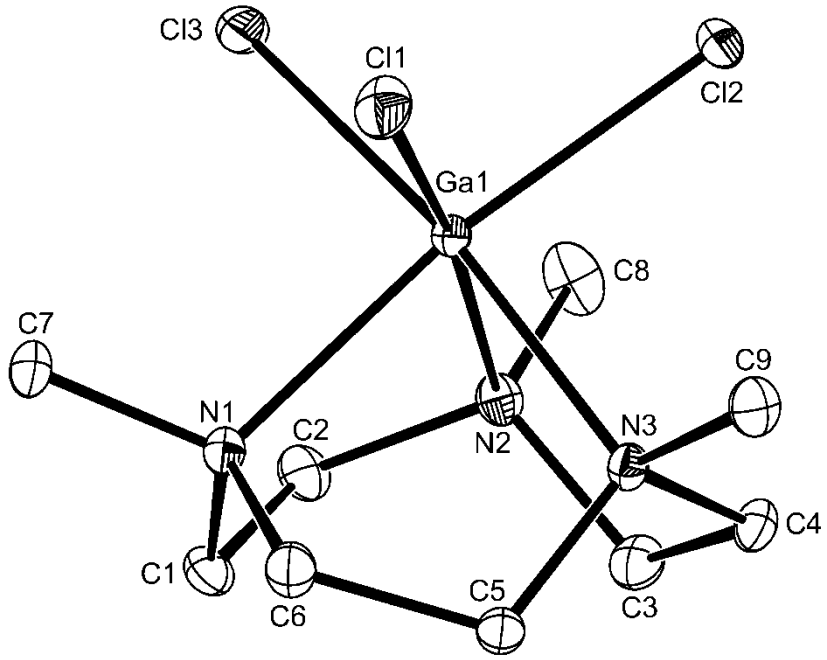

Figure 2.7: The crystal structure of the complex [$GaCl_3$(Me_3-tacn)]. Ellipsoids are drawn at 50% probability level. H-atoms are omitted for clarity. Ga1-Cl1 2.3177(8), Ga1-Cl2 2.3087(4), Ga1-Cl3 2.3217(3), Ga1-N1 2.1755(3), Ga1-N2 2.1960(7), Ga1-N3 2.1644(3)Å. N3-Ga1-N1 81.90(5), Cl3-Ga1-Cl1 93.98(2), N1-Ga1-N2 80.83(5), Cl2-Ga1-Cl3 93.98(2), N3-Ga1-N2 91.72(5), Cl2-Ga1-Cl1 94.38(2)°.

The structure shows a distorted octahedral gallium centre with *facial* coordination of the Me_3-tacn ligand. The complex is iso-structural with the aluminium analogue. The d(M-N) and d(M-Cl) only show a small (0.05 Å) increase in the gallium complex compared to those of the aluminium analogue. This is slightly less than would be expected for the change in ionic radii from Al(III) to Ga(III) (0.68 to 0.76 Å). This suggests that the slightly larger Ga(III) centre might provide a better spatial fit for both the chloride ligands and the triaza-macrocycle.

Previous work in the group showed that prolonged exposure to moisture (such as in the freezer) led to a small number of crystals of a hydrolysis product. While the complex is stable in water over a short period (^{1}H NMR spectroscopic analysis indicates that the complex remains unchanged over a period of about 4 hours), prolonged exposure to moisture results in the minor decomposition of the molecular species to form a hydroxy-bridged dimeric species. Dr Wenjian Zhang collected the original structural data (Figure 2.8, discussed below) but unit cell determinations of crystals grown under similar conditions matched those of the complex shown in Figure 2.8.

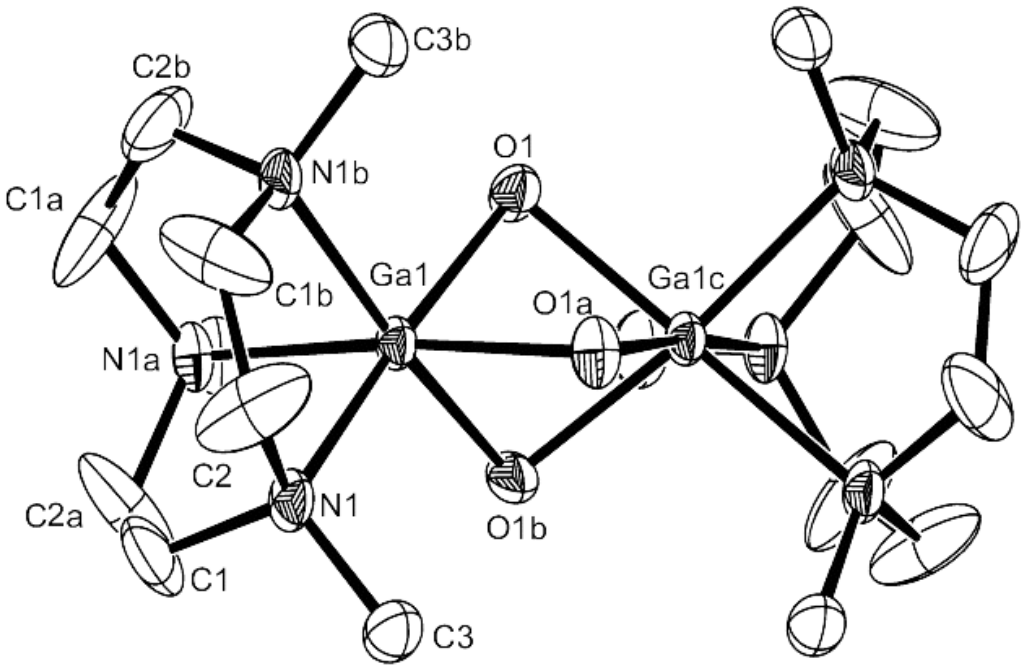

Figure 2.8: Crystal structure of the cation $[(Ga_2(Me_3\text{-tacn}))_2(\mu OH)_3]^{3+}$. Ellipsoids are drawn at 50% probability level. H-atoms are omitted for clarity. Image copied with permission from Dr W. Zhang. Ga1-O 1.955(4), Ga1-N 2.078(4) Å. O1-Ga1-O1a 78.58(18), O1-Ga1-N1 173.0(2), O1-Ga1-N1a 94.70(19) °. Symmetry operations: a = 1–y, x–y, z ; b = 1–x+y, 1–x, z ; c = x, y, 1/2–z.

The structure shows a centrosymmetric dimer with a distorted octahedral geometry around each gallium centre, which are bridged by three *facially* occupied hydroxide ligands (d(Ga-O) = 1.955 (4) Å). The Me_3-tacn moiety is coordinated *facially* to the metal centre via three M-N interactions (d(Ga-N) 2.078 (4) Å). This structure mimics the structures observed by Wieghardt *et al.* in their work on indium di-nuclear species.[2, 12] It is likely that if the compound was left for a longer period of time in a moist atmosphere, the oxo-bridged species would form.

2.2.4 Synthesis of [$InCl_3(RMe_2$-tacn)] complexes

Combination of anhydrous $InCl_3$ with RMe_2-tacn (R = Me, Bz) in anhydrous CH_2Cl_2 at room temperature yields the mildly moisture sensitive adducts [$InCl_3(RMe_2$-tacn)] as white solids. The complexes have a distorted octahedral geometry, with the RMe_2-tacn ligand binding on one face. The complexes remain stable for several months if stored under an inert atmosphere. The complexes are sparingly soluble in MeCN and chlorocarbons.

Unlike the ^{1}H NMR spectra of [$MCl_3(Me_3$-tacn)] (M = Al, Ga), where the proton environments of the tacn ligand are distinct, the ^{1}H NMR spectrum of the indium chloride complexes shows overlap of proton environments (Figure 2.9).

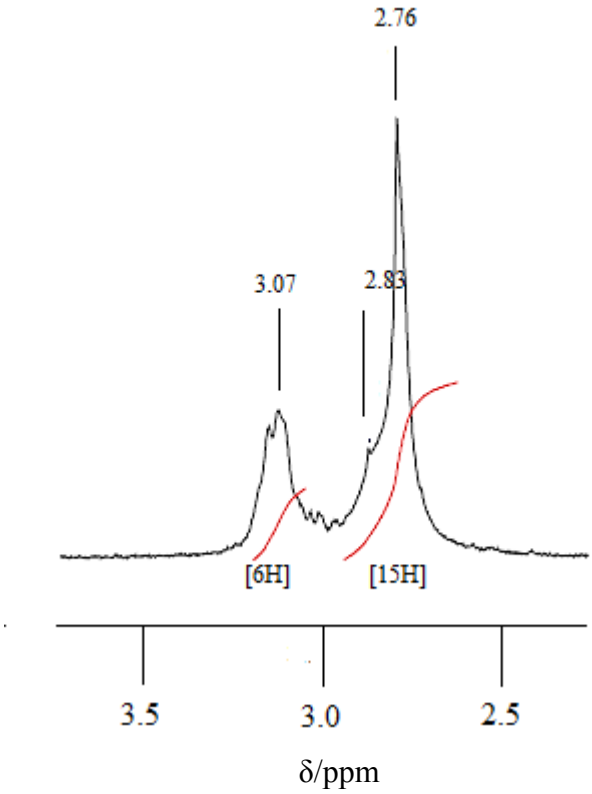

Figure 2.9: ^{1}H NMR spectrum of [$InCl_3(Me_3$-tacn)].

The second order splitting pattern of the methylene protons in the Me_3-tacn ring overlaps with the singlet derived from the methyl pendant arms to result in a broad peak which integrates to 15 protons.

^{115}In NMR spectroscopy (I = 9/2, Q = 0.83 x10^{-28} m^2, 95.7%) was used as a probe to study the indium species formed if the complexes were of high enough symmetry.[6] [$InCl_3(Me_3$-tacn)] and [$InCl_3(BzMe_2$-tacn)] gave signals at δ = 270 and 265 ppm respectively. The signals are broadened significantly ($W_{1/2}$ = 800 and 2200 Hz respectively). Microanalytical measurements

confirmed the formulation as solvent free molecular adducts [$InCl_3(RMe_2$-tacn)]. Layering of the CH_2Cl_2 filtrate with hexane yielded a small number of crystals suitable for single crystal X-ray diffraction.

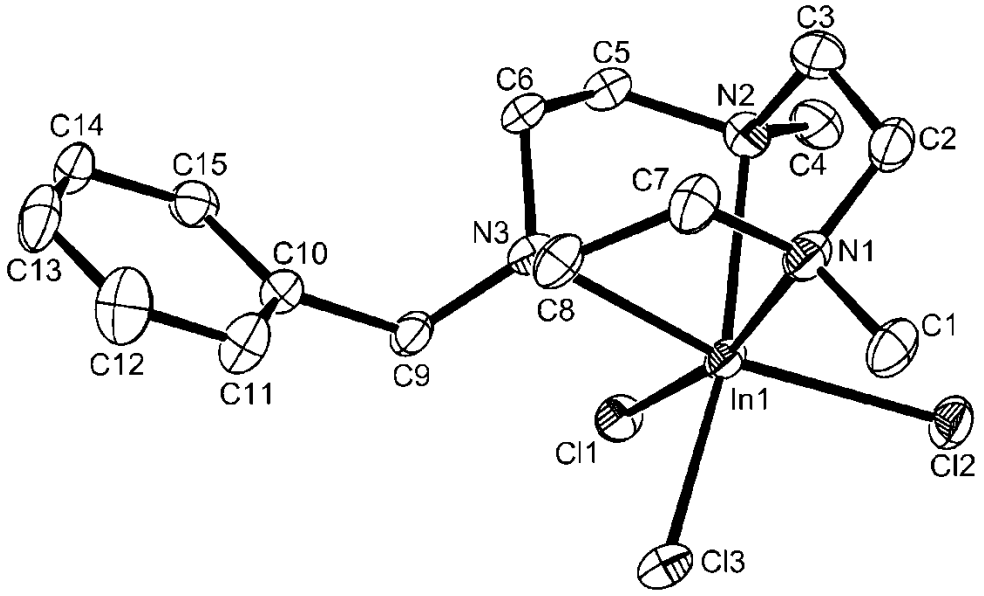

Figure 2.10: The crystal structure of [$InCl_3(BzMe_2$-tacn)]. Ellipsoids are drawn at 50% probability level. H-atoms are removed for clarity. In1-Cl1 2.4547(2), In1-Cl2 2.4506(2), In1-Cl3 2.4447(3), In1-N1 2.2962(3), In1-N2 2.3381(2), In1-N3 2.3618(2) Å. Cl1-In1-Cl2 97.69(2), N2-In1-N3 76.44(5), Cl1-In1-Cl3 96.26(2), N3-In1-N1 78.11(5), Cl2-In1-Cl3 95.45(2), N2-In1-N1 76.61(5)°.

The crystal structure (Figure 2.10) shows the indium centre in a particularly distorted octahedral coordination sphere with the $BzMe_2$-tacn moiety coordinated *facially* to the indium centre. The chloride ligands lie *trans* to the $BzMe_2$-tacn ligand.

Comparison of the crystal structure of [$InCl_3(BzMe_2$-tacn)] with those of the bromo complexes [$InBr_3(Me_3$-tacn)][13] and [$InBr_3(BzMe_2$-tacn)]·$2CH_2Cl_2$ show that the mean d(In-X) decreases by 0.15 Å in the chloride complex (d(In-Cl) = 2.450(2) Å, d(In-Br) = 2.602(8) Å). This decrease in bond length is in keeping with the change in ionic radius between the chloride (1.67 Å) and bromide (1.82 Å) ion. Perhaps more surprisingly the d(In-N) shows very little difference between the chloride and bromide complexes. This would infer that the interaction of the metal centre to the tacn ligand is not as heavily influenced by the halide ligands as is the case for the smaller aluminium and gallium analogues.

2.3 Hydrothermal synthesis of the trifluoro adducts [MF_3(Me_3-tacn)]·xH_2O

Having demonstrated the ability to form the neutral chloride adducts [MCl_3(RMe_2-tacn)] in high yield it was postulated whether the corresponding fluoride complexes could be accessed. As discussed in Chapter 1.7, the binary metal fluorides of the Group 13 elements are insoluble in organic solvents and water. Therefore complexes are difficult to obtain under mild synthetic conditions.

Recent work from Lightfoot *et al.* demonstrated the utility of hydrothermal synthesis as a method to access fluoroscandate complexes with amine ligands in the presence of HF.[14] This is in addition to the hydrothermal synthesis of the polymeric [GaF_3(4,4-bipy)] from GaF_3·3H_2O, aqueous 2% HF and ligand as described by Petrosyants *et al*.[15] This led to the possibility of being able to use the hydrated fluoride salts MF_3·3H_2O in combination with the ligand Me_3-tacn under hydrothermal conditions to yield the [MF_3(Me_3-tacn)] adducts. This would provide a spectroscopic fingerprint in which the halide exchange reactions discussed in Chapters 3.2.1 and 3.2.2 could be tracked and compared.

2.3.1 General Synthetic Procedure

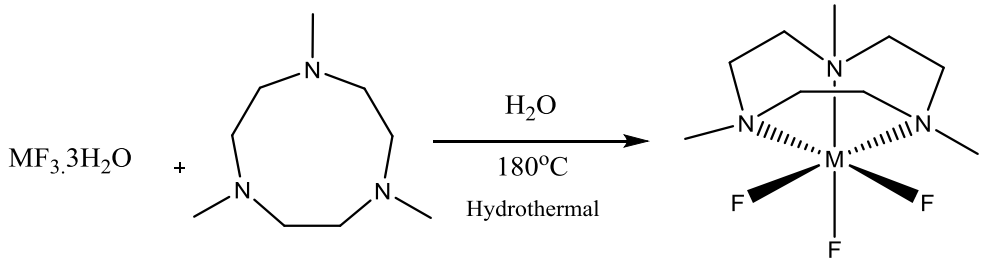

Figure 2.11: General synthetic procedure towards the formation of the complexes [MF_3(Me_3-tacn)]·4H_2O. M = Al, Ga, In.

Hydrothermal reactions utilise Teflon containers in stainless steel pressure vessels equipped with bursting discs. However, aside from this the general synthetic procedure is straightforward (Figure 2.11).

The hydrated salt MF_3·3H_2O (M = Al, Ga, In) was combined with 1 molar equivalent of Me_3-tacn in freshly distilled H_2O. The resulting suspension was transferred into a Teflon cup, and placed into the stainless steel vessel. The mixture was heated to 180 °C for 15-18 hours. The resulting yellow solutions were filtered to remove insoluble particulates. Removal of the volatiles under high vacuum, followed by washing with hexane yields the desired complexes as off-white solids. The reactions are high yielding, and the unreacted MF_3·3H_2O is conveniently removed by filtration. The solids are stable indefinitely in the solid state, and as discussed in more detail in Chapter 2.3.3, are stable for a prolonged period in aqueous solution.

Perhaps surprisingly the formation of the complexes was favoured over protonation of the ligand. The Me_3-tacn macrocycle has demonstrated a propensity to protonate if exposed to moisture.[16] However it is likely that the formation of a kinetically inert complex, bound to the strongly Lewis acidic MF_3 moiety provides the driving force for complexation.

2.3.2 Synthesis of $[AlF_3(Me_3\text{-tacn})]\cdot xH_2O$

Reaction of $AlF_3\cdot 3H_2O$ with Me_3-tacn yields the distorted octahedral complex $[AlF_3(Me_3\text{-tacn})]\cdot 4H_2O$. Slow evaporation of the reaction solution yielded crystals suitable for single crystal X- ray diffraction (Figure 2.12).

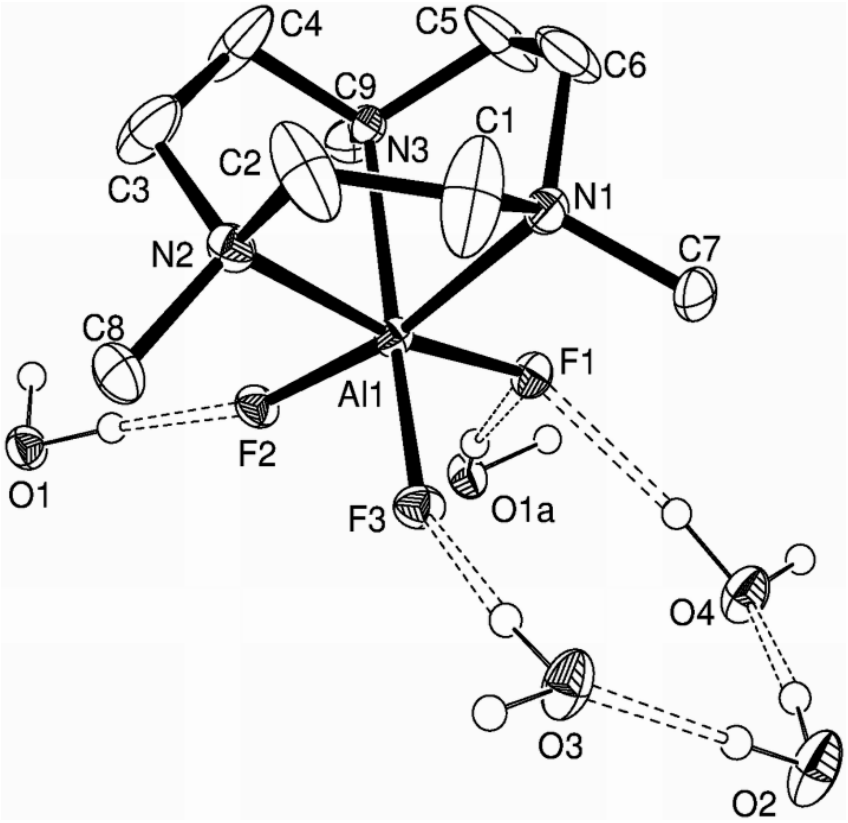

Figure 2.12: The crystal structure of $[AlF_3(Me_3\text{-tacn})]\cdot 4H_2O$ showing the atom labelling scheme. Ellipsoids are drawn at the 40% probability level. The H-atoms in the Me_3-tacn ring are omitted for clarity. Al1-F1 1.7568(2), Al1-F2 1.7396(2), Al1-F3 1.7444(2), Al1-N1 2.1145(2), Al1-N2 2.1060(2), Al1-N3 2.0982 (3) Å. F1-Al1-F2 96.65(12), F1-Al1-F3 96.00(11), F2-Al1-F3 95.81(12), N2-Al1-N3 82.20(13), N3-Al1-N1 82.13(13), N2-Al1-N1 82.37(13)°.

The crystal structure shows a distorted octahedral structure, with an aluminium centre *facially* bound by the Me_3-tacn ligand. The fluoride ligands lie *trans* to the N-donor atoms of the

Me_3-tacn ligand. The complex crystallises as a tetrahydrate. The solvent water molecules participate in significant H-bonding interactions with one another, and with the trifluoride face of the metal complex. The extended structure shows a supramolecular assembly based on significant H-bonding interactions between the MF_3 unit and the lattice water molecules (F····H-OH and O····H-O). These interactions form a sheet like structure of metal complexes held by the co-crystallised water molecules (Figure 2.13).

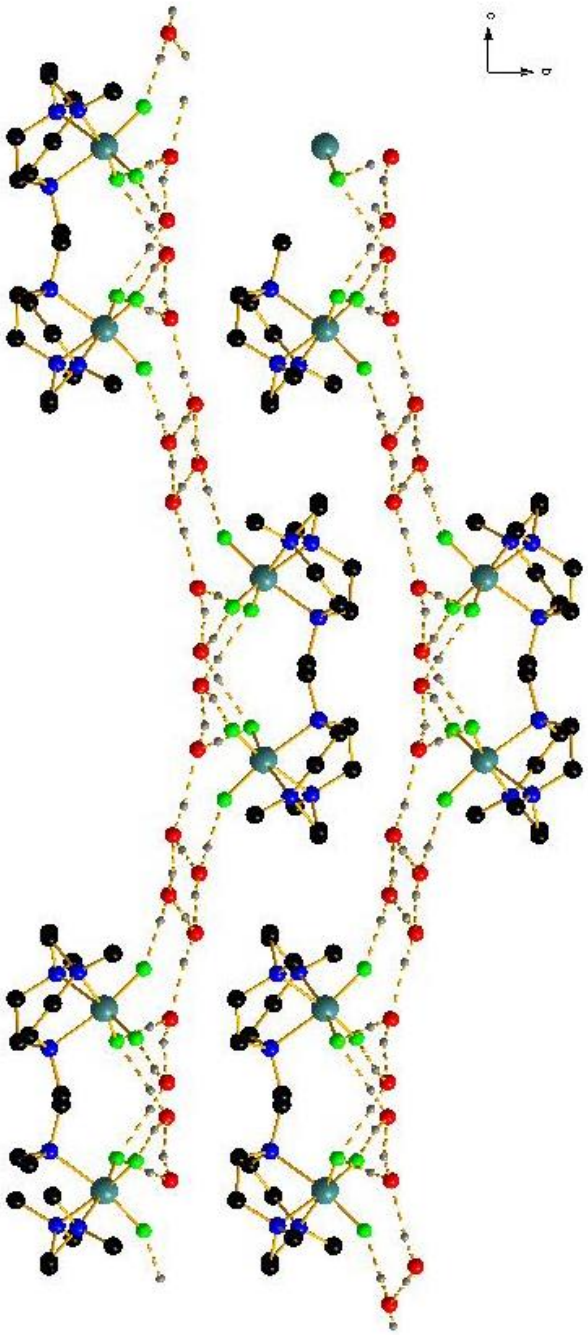

Figure 2.13: A portion of the extended structure of the complex $[AlF_3(Me_3\text{-tacn})]\cdot 4H_2O$ viewed down the *a*-axis. It shows the supramolecular assembly derived from hydrogen bonding waters being held in place by the interaction with the fluoride ligands in the aluminium complex.

The difference between the average Al-Cl (2.272 Å) and Al-F (1.748 Å) bond lengths in the complexes $[AlX_3(Me_3\text{-tacn})]$ is 0.524 Å, significantly greater than would be expected for a change in the textbook bond lengths Al-Cl to Al-F.[1] This therefore infers that the formation of the fluoride complex places less steric demand on the aluminium centre, as one would expect given the smaller ionic radius of the fluoride ion (1.19 Å) compared to that of the chloride ion

(1.67 Å).[17] The release of steric strain allows a stronger interaction to occur. This is an important consideration when considering the halide exchange in the aluminium systems discussed in Chapter 3.2.2.

The remaining reaction solution was worked up *via* removal of the reaction solvent *in vacuo* and washing with hexane, yielding an off-white solid. The ^{1}H NMR spectrum of the complex depicts the second order multiplet splitting pattern observed previously for the chloride complex (see Chapter 2.2.2). The $^{19}F\{^{1}H\}$ NMR spectrum showed a single, fairly sharp resonance at -176.1 ppm. One would expect a six line splitting pattern with lines of equal intensity, however the significant hydrogen bonding within the system likely broadens the couplings, hence the resonance appear as a singlet. The ^{27}Al NMR spectrum depicted a single species at 19 ppm. Again the absence of a splitting pattern could be derived from the significant hydrogen bonding in the complex. Microanalytical measurements of the bulk solid gave the formulation $[AlF_3(Me_3\text{-tacn})]\cdot 3H_2O$, indicating that the complex partially dehydrates during the vacuum drying to gain the bulk solid.

The data acquired confirms that the complex $[AlF_3(Me_3\text{-tacn})]\cdot xH_2O$ may be accessed under hydrothermal conditions.

2.3.3 Synthesis of $[GaF_3(Me_3\text{-tacn})]\cdot xH_2O$

Reaction of $GaF_3\cdot 3H_2O$ with Me_3-tacn under hydrothermal conditions yields a grey-white solid after work up.

Analysis of the bulk material confirmed the formation of the desired complex $[GaF_3(Me_3\text{-tacn})]\cdot xH_2O$. The infra-red spectrum of $[GaF_3(Me_3\text{-tacn})]\cdot xH_2O$ indicated two Ga-F bands at ν 478, 462 cm^{-1}, consistent with the expected C_{3V} symmetry adopted by the complex. The infra-red spectrum also showed evidence for H-bonding water (broad band at ν 3488 cm^{-1}).

The ^{1}H NMR spectrum of $[GaF_3(Me_3\text{-tacn})]\cdot xH_2O$ shows the second order tacn-CH_2 multiplets as observed for the analogous chloride complex, coupled with a small positive chemical shift, likely a reflection of the Me_3-tacn being bound to the harder GaF_3 moiety.

The $^{19}F\{^{1}H\}$ NMR spectrum recorded in CD_3CN gives a collapsed quartet at δ -182.5 ppm (Figure 2.14). This coupling pattern is observed as a result of the fluorides in the complex coupling to both ^{69}Ga and ^{71}Ga (both NMR active), with the resulting signals overlapping one another. The appearance of the multiplicity in the solution phase is due to the high symmetry of the complex, giving a small electric field gradient, which allows the couplings to be observed.

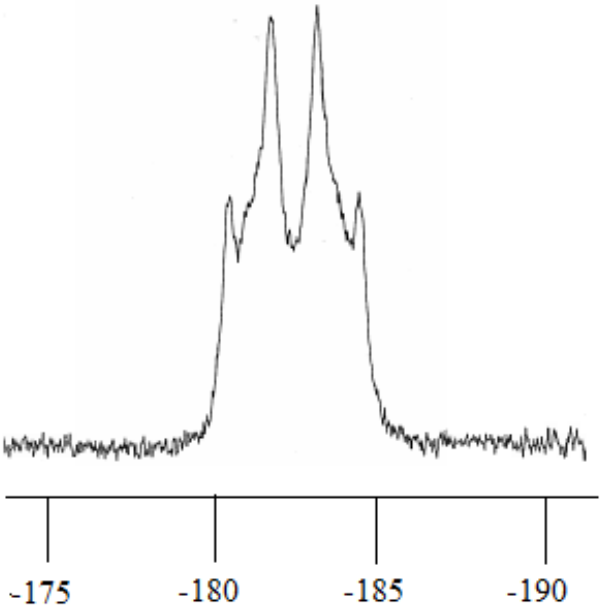

Figure 2.14: The $^{19}F\{^{1}H\}$ NMR spectrum of $[GaF_3(Me_3\text{-tacn})]$ recorded in CD_3CN, δ = -182.5 ppm. The spectrum depicts a pseudo-quartet peak. This observation is derived from the fluorides in the complex coupling to both ^{69}Ga and ^{71}Ga nuclei. The resulting signal overlaps one another to give the splitting observed. ^{19}F NMR (I = 1/2, 100%). ^{69}Ga (I = 3/2, 60.4%, Q = 0.19 x 10^{-28} m^2), ^{71}Ga (I = 3/2, 39.6%, Q = 0.12 x 10^{-28} m^2).

The ^{71}Ga NMR spectrum depicted a formal quartet at δ 41.3 ppm (Figure 2.15). The unusual observation of coupling in the solution phase ^{71}Ga NMR is derived from the three equivalent fluorides coupling to the ^{71}Ga centre ($J_{Ga\text{-}F}$ 490 Hz). The lower quadrupolar moment in ^{71}Ga (Q =0.12 x10^{-28} m^2, 39.6%)[6] coupled with the very high symmetry of the complex resulting in slower quadrupolar relaxation.

Figure 2.15: ^{71}Ga NMR Spectrum of [GaF_3(Me_3-tacn)]. δ = 41.3 ppm. J_{Ga-F} 490 Hz. ^{71}Ga NMR (I = 3/2, Q = 1.2 x10^{-28} m^2, 39.6%) ^{19}F NMR (I = 1/2, 100%).

Microanalytical measurements indicate that the proposed formulation is [GaF_3(Me_3-tacn)]·1H_2O, suggesting that the complex partially dehydrates upon drying under high vacuum. Slow evaporation of the reaction solution gave crystals suitable for single crystal X-ray diffraction.

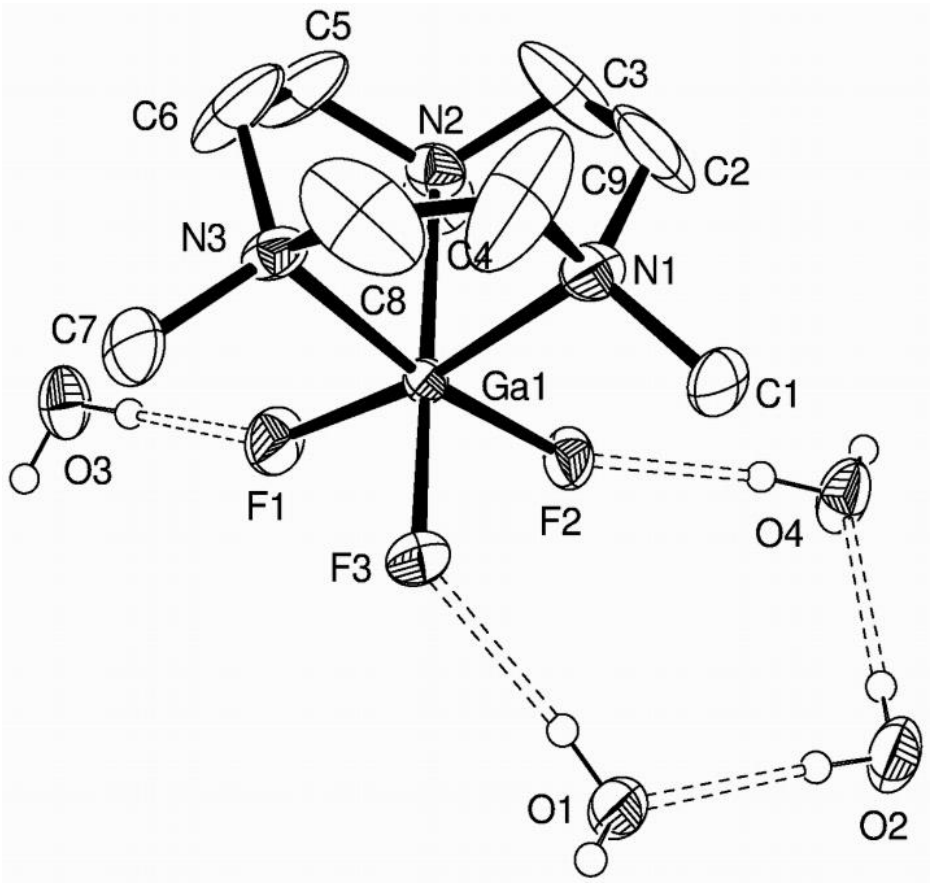

Figure 2.16: Ortep representation of the crystal structure of $[GaF_3(Me_3\text{-tacn})]\cdot 4H_2O$. Ellipsoids are drawn at 50% probability level. H-atoms on the Me_3-tacn are omitted for clarity. Ga1-F1 1.851(3), Ga1-F2 1.858(3), Ga1-F3 1.882(3), Ga1-N1 2.140(4), Ga1-N2 2.126(4), Ga1-N3 2.126(4) Å. F1-Ga1-F2 95.81(12), F1-Ga1-F3 94.87(2), F2-Ga1-F3 94.23(12), N2-Ga1-N1 82.4(13), N3-Ga1-N1 81.6(2), N2-Ga1-N3 82.2(1)°.

The crystal structure confirms that the gallium occupies a distorted octahedral coordination sphere (Figure 2.16). The tridentate Me_3-tacn ligand binds *facially* via three nitrogen atoms to the metal centre. The d(Ga-F) in the complex ranges from 1.851(3) to 1.882(3) Å, which are 0.45 Å shorter than the corresponding d(Ga-Cl) in the $[GaCl_3(Me_3\text{-tacn})]$ complex. This is slightly less than the difference in the ionic radii of chloride (1.67 Å) and fluoride (1.19 Å) ion. This shows that the smaller, harder fluoride ion is capable of forming a stronger interaction with the gallium centre, although the effect of the H-bonded water molecules on the Ga-F bond lengths may have an effect. Subsequent to this work, the $[GaF_3(Me_3\text{-tacn})]$ complex was synthesised by Weyhermüller *et al.* as part of their study on metal fluoride complexes as constituents of bimetallic clusters as magnetic refrigerants (see Chapter 1.8 and 5.1.2).[18] The atomic coordinates of their crystal structure were in strong agreement to those gained here. Much like the analogous aluminium complex, $[GaF_3(Me_3\text{-tacn})]$ crystallises as a tetrahydrate with an extensive H-bonding array involving intermolecular OH-O···F and

O···H-OH interactions. The extended structure also shows the supramolecular networks produced from these H-bonding interactions (Figure 2.17).

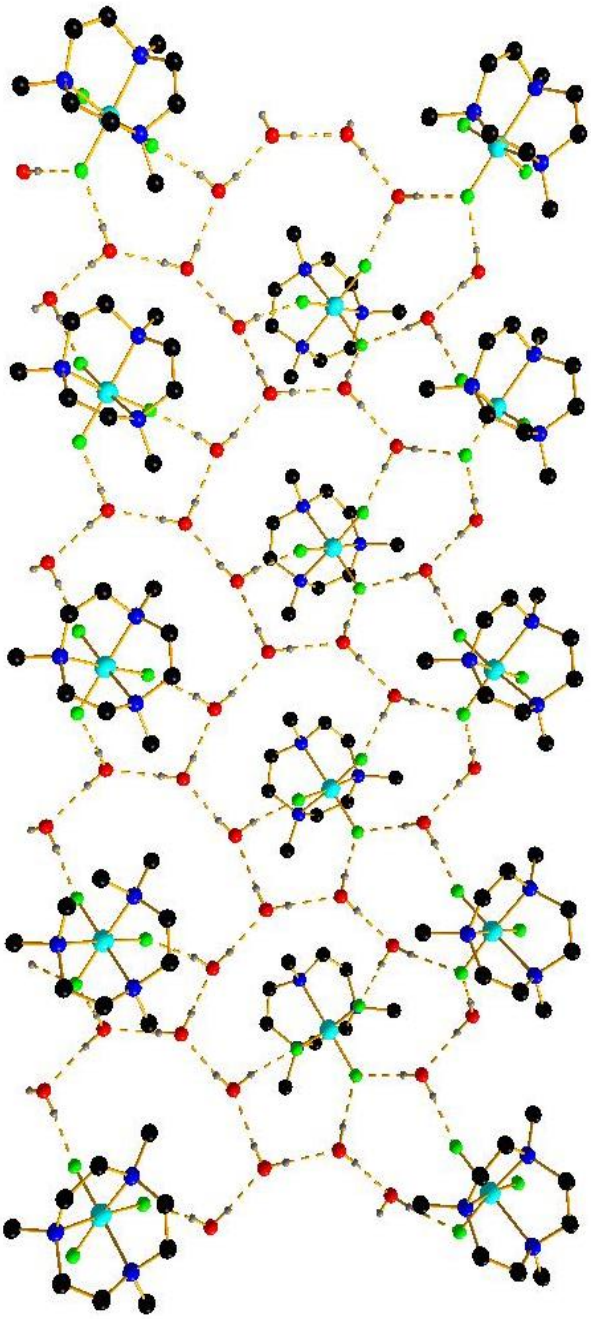

Figure 2.17: A portion of the extended structure of the complex $[GaF_3(Me_3\text{-tacn})]\cdot 4H_2O$ viewed down the *c*-axis showing the supramolecular assembly derived from hydrogen bonded waters being held in place by the interaction with the fluoride ligands on the gallium complex.

The H-bonding of the waters of crystallisation results in the stabilisation of the M-F bond by providing multiple H-bonding interactions. The added stabilisation provided by the H-bonding interactions means the likelihood of the M-F bond dissociating is lessened.

The complex $[GaF_3(Me_3\text{-tacn})]$ displays remarkable stability under a number of conditions. It is stable indefinitely in the solid state and for at least six weeks in aqueous solution (no visible degradation in the ^1H, $^{19}F\{^1H\}$ NMR spectrum). It is also resistant to acid, the treatment of $[GaF_3(Me_3\text{-tacn})]$ with 1.0 M HBF_4 (pH 1) leads to no visible degradation in the $^{19}F\{^1H\}$ NMR spectrum. Additionally, the complex proves stable to decomposition when formulated into a 10% EtOH/PBS solution, at pH 7.5. This implies a strong Ga-F interaction, and could prove to be stable under physiological conditions.

2.3.4 Synthesis of $[InF_3(Me_3\text{-tacn})]\cdot xH_2O$

Reaction of $InF_3\cdot 3H_2O$ with Me_3-tacn under hydrothermal conditions yields an off-white solid which was determined spectroscopically as the complex *fac*-$[InF_3(Me_3\text{-tacn})]\cdot xH_2O$. The complex is isolated in high yield and purity.

The infra-red spectrum shows the formation of two In-F bands, consistent with the approximate C_{3V} symmetry of a *fac*-isomer (Table 2.2).

Complex	**ν M-F/ cm^{-1}**
$[AlF_3(Me_3\text{-tacn})]\cdot 4H_2O$	633, 613
$[GaF_3(Me_3\text{-tacn})]\cdot 4H_2O$	530, 492
$[InF_3(Me_3\text{-tacn})]\cdot 4H_2O$	478, 443

Table 2.2: Table showing the stretching frequencies for the M-F bonds in the complexes synthesised hydrothermally.

The ^1H NMR spectrum of $[InF_3(Me_3\text{-tacn})]$ indicates an approximate 0.5 ppm increase in the chemical shift upon formation of the fluoride complex compared to those of the corresponding $[InCl_3(Me_3\text{-tacn})]$ – although there is little change in the pattern observed.

The ^{115}In NMR spectrum of $[InF_3(Me_3\text{-tacn})]\cdot xH_2O$ provides a rare example of an In-F coupling pattern in solution.[19-21] Figure 2.18 depicts a quartet of intensity 1:3:3:1 at δ = 65 ppm ($J_{In\text{-}F}$ = 600 Hz).

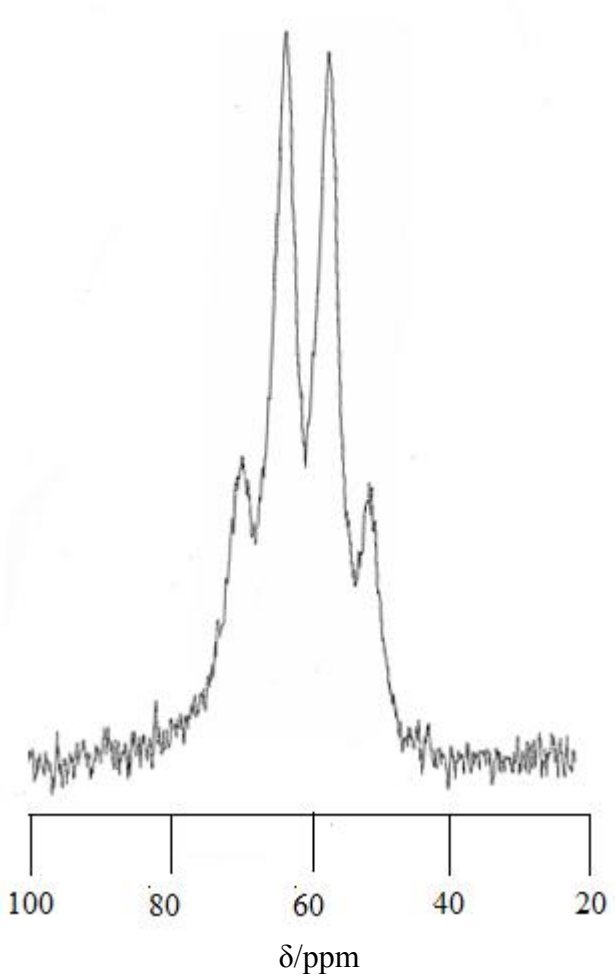

Figure 2.18: ^{115}In NMR spectrum of [InF_3(Me_3-tacn)]. δ 64 ppm. J_{In-F} 600 Hz. ^{19}F (I = 1/2 100%), ^{115}In (I = 9/2, Q = 0.83 x10^{-28} m^2, 95.7%).

The splitting pattern observed is derived from the coupling of three equivalent fluorine atoms to the indium centre. Coupling patterns are rare in solution phase indium NMR studies – the large quadrupolar moment of the indium nucleus results in extreme line broadening. However the highly symmetric molecular symmetry in the complex results in an electric field gradient of almost zero which thus allows the coupling to be observed. When the complex was dissolved into D_2O, no signal appeared in the ^{115}In NMR, the polar solvent results in extreme line broadening thus the resonance is not observed.

Confirmation of the expected formulation was gained through single crystal X-ray analysis of a crystal formed from the slow evaporation of the reaction solvent (Figure 2.19).

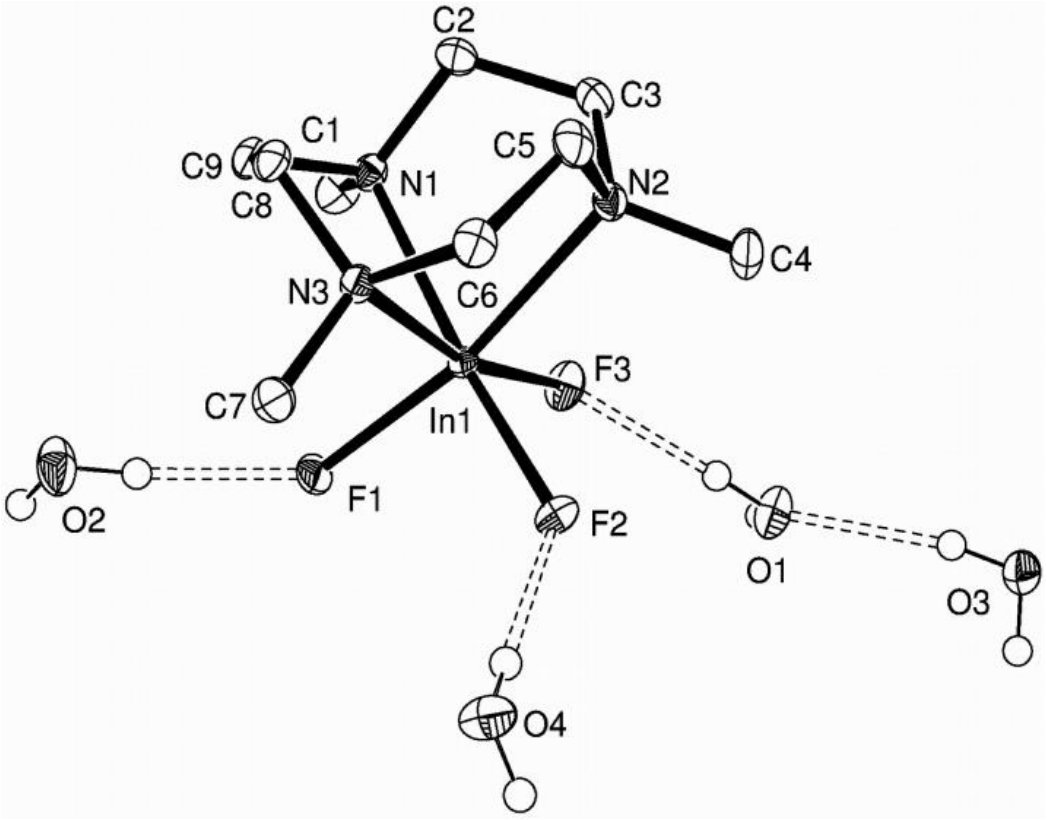

Figure 2.19: ORTEP representation of the crystal structure of $[GaF_3(Me_3\text{-tacn})]\cdot 4H_2O$. Ellipsoids are drawn at 50% probability level. H-atoms on the Me_3-tacn are omitted for clarity. In1-F1 2.0318(11), In1-F2 2.0391(12), In1-F3, 2.0570(11), In1-N1 2.287(2), In1-N2 2.289(2), In1-N3 2.291(2) Å. F1-In1-F2 96.33(5), F1-In1-F3 95.04(5), F2-In1-F3 94.79(5), N1-In1-N2 78.68(6), N1-In1-N3 78.91(6), N2-In1-N3 78.44(6)°.

The structure shows an octahedral In(III) centre coordinated by the tridentate Me_3-tacn ligand in a *fac*-arrangement. Although not directly analogous, comparison of the M-X bond lengths in $[InF_3(Me_3\text{-tacn})]$ with $[InCl_3(BzMe_2\text{-tacn})]$ show a decrease in the In-F lengths of *ca.* 0.40 Å, less than would be expected for the change in ionic radii (0.48 Å). The effect of the H-bonding interactions with the solvent water molecules are likely to have an effect on the In-F bond lengths and thus detailed comparisons of the bond lengths are treated with caution. As observed in the lighter Group 13 complexes discussed above, the complex is heavily hydrated, crystallising as a tetrahydrate. This results in significant F···H–OH hydrogen-bonding between the fluoride ligand and the lattice water molecules.

The trend in X–M–X and N–M–N angles across the series correlates with the trends in bond distances (Table 2.3). In all cases the angles involving halide ligands are ~94–98°, with no obvious trend with changing X or M. In contrast, the N–M–N angles in the Al^{3+} and Ga^{3+}

complexes are essentially invariant (~82°), while those involving In^{3+} are rather more acute, ~77°, reflecting the elongated In–N bond distances.

The complexes $[MF_3(Me_3\text{-tacn})]\cdot 4H_2O$ (M = Al, Ga, In) are isostructural, but not isomorphous, the H-bonded networks are different in each case.

Complex	**d(M–X)/Å**	**d(M–N)/Å**	**<(X–M–X)/°**	**<(N–M–N)/°**
$[AlF_3(Me_3\text{-tacn})]\cdot 4H_2O$	1.7396(2) 1.7444(2) 1.7568(2)	2.0982(2) 2.1060(2) 2.1145(3)	96.65(12) 96.00(11) 95.81(12)	82.20(13) 82.13(13) 82.37(13)
$[AlCl_3(Me_3\text{-tacn})]$	2.267(2) 2.274(2) 2.276(2)	2.111(3) 2.126(4) 2.141(4)	94.03(7) 93.74(6) 94.21(7)	83.03(14) 81.64(14) 81.97(14)
$[GaF_3(Me_3\text{-tacn})]\cdot 4H_2O$	1.851(3) 1.858(3) 1.881(3)	2.126(4) 2.126(4) 2.140(4)	95.81(12) 94.87(13) 94.23(12)	82.2(1) 82.4(2) 81.6(2)
$[GaCl_3(Me_3\text{-tacn})]$	2.3087(5) 2.3177(9) 2.3217(5)	2.1644(13) 2.1755(13) 2.1960(14)	94.38(2) 93.98(2) 94.49(2)	81.90(5) 80.80(5) 80.83(5)
$[InF_3(Me_3\text{-tacn})]\cdot 4H_2O$	2.0318(11) 2.0391(12) 2.0570(11)	2.287(2) 2.289(2) 2.291(2)	96.33(5) 95.04(5) 94.79(5)	78.68(6) 78.91(6) 78.44(6)
$[InF_3(BzMe_2\text{-tacn})]\cdot H_2O$	2.0585(12) 2.0501(12) 2.0176(13)	2.3359(16) 2.2948(16) 2.2995(14)	96.72(5) 96.72(5) 98.24(5)	77.96(6) 77.14(6) 77.80(6)
$[InCl_3(BzMe_2\text{-tacn})]$	2.4547(2) 2.4506(2) 2.4447(3)	2.2962(3) 2.3381(2) 2.3618(2)	95.32(5) 96.26(5) 98.31(5)	77.1(2) 77.4(2) 76.3(2)

Table 2.3: Table of bond lengths and angles of the crystal structures discussed in Chapters 2 and 3.

2.4 Conclusions

This chapter has discussed the successful synthesis and full characterisation of the well-defined precursor complexes [MCl_3(RMe_2-tacn)], M = Al, Ga, In, R = Me, Bz in high purity and yield. The synthesis of the chloride adducts was favoured over the bromide analogues due to the lower moisture sensitivity and ease of handling. The complexes were characterised in full using infra-red, ^{1}H and multinuclear NMR spectroscopy, elemental analysis and where possible, single crystal X-ray diffraction. These complexes provide an exciting option as a defined precursor towards potential ^{18}F radiolabelled complexes through a halide exchange reaction (discussed further in Chapter 3).

The high yielding synthesis of the complexes [MF_3(Me_3-tacn)]·$4H_2O$ via hydrothermal synthesis has demonstrated an alternative route towards complexes based upon the insoluble Group 13 metal fluoride, furthering the chemistry of this little explored area. The synthesis demonstrated that the triamine Me_3-tacn does not protonate under these conditions. The complexes synthesised were characterised fully by infra-red, ^{1}H, ^{19}F{^{1}H} and multinuclear NMR spectroscopy, elemental analysis and single crystal X-ray diffraction. The detailed spectroscopic fingerprint provided allow comparison with the species formed for the halide exchange reactions discussed in Chapter 3. The complexes [MF_3(Me_3-tacn)] crystallise as tetrahydrates. This results in extensive H-bonding interactions between the fluoride ligands and the solvent water molecules. This produces supramolecular assemblies based upon the H-bonded interactions. This observation might suggest that the use of the facial MF_3 moiety could have potential to form other interesting supramolecular assemblies.

2.5 Experimental

For full details of experimental methods and techniques see Appendix 1. The ligands H_3-tacn[22], Me_3-tacn[2] and $BzMe_2$-tacn[3] were synthesised as described in the literature and purified by distillation before use. The anhydrous metal salts MCl_3 (M = Al, Ga, In) were used as received in a dry N_2 purged glovebox. The hydrated metal fluoride salts MF_3·$3H_2O$ (M = Al, Ga, In) were used as received.

[$AlCl_3$(Me_3-tacn)]: A solution of Me_3-tacn (0.10 g, 0.113 mL, 0.6 mmol) in anhydrous MeCN (5 mL) was treated with $AlCl_3$ (0.07 g, 0.6 mmol) to form a colourless solution. Stirring at room temperature for 30 minutes afforded a white precipitate. The solid was isolated via removal of the solvent *in vacuo*. The solid was washed with 5 mL hexane, collected via filtration and dried *in vacuo*. Yield: 0.11 g, 72%. Required for $C_9H_{21}A1_1Cl_3N_3$·$0.2CH_2Cl_2$: C, 34.4; H, 6.7; N, 13.1. Found: C, 34.2; H, 7.2; N, 13.9%. IR(Nujol, ν/cm^{-1}) 375, 346 (Al-Cl). ^{1}H NMR (CD_3CN, 298 K) δ = 3.23 (m, [6H], tacn CH_2), 2.86 (m, [9H], CH_3), 2.67 (m, [6H], tacn CH_2). ^{27}Al{^{1}H} NMR

(104 MHz, 298 K) δ = 34.54 (s) in CH_2Cl_2-CD_2Cl_2, δ 34.85 (s) in dmf-CD_3CN, δ 34.54 (s) in dmso-CD_3CN, δ 35.18 (s) in acetone-CD_3CN, 35.54 (s) in thf-CD_3CN, 35.54 (s) in CH_3CN-CD_3CN. Retention of the reaction filtrate in the freezer yielded colourless crystals suitable for X-ray diffraction.

[$AlCl_3$(BzMe_2-tacn)]: $AlCl_3$ (0.050 g, 0.4 mmol) was added to a solution of BzMe_2-tacn (0.10 g, 0.4 mmol) in anhydrous CH_2Cl_2 (5 mL) resulting in a colourless solution. The solution was stirred at room temperature for 2 hours. Removal of the solvent *in vacuo* gave a white solid, which was washed with a 5mL of hexane, collected by filtration and dried in vacuo. Yield: 0.13 g, 68%. Required for $C_{15}H_{25}A1Cl_3N_3$: C, 47.3; H, 6.6; N, 11.0. Found: C, 47.0; H, 6.7; N, 11.2%. IR(Nujol, ν/cm^{-1}) 384, 349 (Al-Cl). ^{1}H NMR (CD_3CN, 297 K) δ = 7.31 (m, [5H], C_6H_5), 4.57 (m, [2H], benzyl CH_2), 3.54 (m, [2H], tacn CH_2), 3.29 (m, [4H], tacn CH_2), 2.92 (m, [6H], CH_3), 2.65 (m, [4H], tacn CH_2), 2.28 (m, [2H], tacn CH_2). ^{27}Al NMR (297 K): δ = 36.47 (s) in CH_2Cl_2-CD_2Cl_2, δ 35.97 (s) in dmf-CD_3CN, δ 35.73 (s) in dmso-CD_3CN, δ 36.18 (s) in acetone-CD_3CN, 36.76 (s) in thf-CD_3CN, 35.79 (s) in CH_3CN-CD_3CN. Retention of the reaction filtrate in the freezer yielded colourless crystals suitable for X-ray diffraction.

[$GaCl_3$(Me_3-tacn)]: $GaCl_3$ (0.105 g, 0.6 mmol) was added to a solution of Me_3-tacn (0.10 g, 0.118 mL, 0.6 mmol) in anhydrous CH_2Cl_2 (5 mL). Stirring at room temperature for 30 minutes afforded a white precipitate. The solid was isolated via removal of the solvent *in vacuo.* The solid was washed with 5 mL hexane, collected via filtration and dried *in vacuo.* Yield 0.110g, 60%. Required for $C_9H_{21}Cl_3GaN_3$: C, 31.1; H, 6.1; N, 12.1. Found: C, 31.2; H, 5.9; N, 12.1%. IR (Nujol, ν/cm^{-1}) 278, 245 (Ga-Cl). ^{1}H NMR (CD_3CN, 298 K) δ = 3.19 (m, [6H], tacn CH_2), 2.83 (m, [9H], CH_3), 2.62 (m, [6H], tacn CH_2). ^{71}Ga NMR (CD_3CN, 298 K) δ = 94 (s). Dissolution of the complex in anhydrous MeCN followed by slow evaporation in the glovebox yielded large colourless crystals suitable for X-ray diffraction.

[$GaCl_3$(BzMe_2-tacn)]: A solution of BzMe_2-tacn (0.100 g, 0.4 mmol) in anhydrous CH_2Cl_2 was treated with $GaCl_3$ (0.07 g, 0.4 mmol) to form a colourless solution. Stirring at room temperature for 2 hours resulted a white precipitate. The solvent was removed *in vacuo.* The white solid was washed with 5 mL hexane, collected by filtration and dried *in vacuo*. Yield 0.092 g, 55%. Required for $C_{15}H_{25}Cl_3GaN_3$: C,42.6; H, 6.0; N, 9.9. Found: C,42.2; H, 6.0; N, 9.6%. IR (Nujol, ν/cm^{-1}) 280, 260 (Ga-Cl). ^{1}H NMR (CD_3CN, 298 K) δ = 7.38 (m, [5H], C_6H_5), 4.71 (s, [2H], benzyl CH_2), 3.68 (m, [3H], tacn CH_2), 3.41 (m, [4H], tacn CH_2), 3.08 (s, [6H], CH_3), 2.78 (m, [4H], tacn CH_2), 2.32 (m, [3H], tacn CH_2). ^{71}Ga NMR (CD_3CN, 298 K) δ = 93 (s), $W_{1/2}$ = 300 Hz.

[$InCl_3(Me_3$-tacn)]: $InCl_3$ (0.22 g, 1.0 mmol) was added to a solution of Me_3-tacn (0.175 g, 1.0 mmol) in anhydrous CH_2Cl_2 (5 mL) resulting a cloudy suspension solution. This was stirred at room temperature for 12 hours. The solid was isolated via removal of the solvent *in vacuo*. The solid was washed with 5 mL hexane, collected via filtration and dried *in vacuo.* Yield 0.112 g, 50%. Required for $C_9H_{21}Cl_3InN_3$: C,27.5; H, 5.4; N, 10.7. Found C,27.8; H, 5.5; N, 10.9%. IR (Nujol, ν/cm^{-1}) 287, 269 (In-Cl). ^1H NMR (CD_3CN, 298 K) δ = 3.12 (m, [6H], tacn CH_2) 2.77 (m, [15H], tacn CH_2 and CH_3). ^{115}In NMR (CD_3CN, 298 K) δ = 270 (s), $W_{1/2}$ = 800 Hz. Slow evaporation of the reaction filtrate yielded colourless crystals suitable for X-ray diffraction.

[$InCl_3(BzMe_2$-tacn)]: Combination of $InCl_3$ (0.09 g, 0.4 mmol) with $BzMe_2$-tacn (0.10 g, 0.4 mmol) in anhydrous 5 mL CH_2Cl_2 resulted a colourless solution. Stirring at room temperature for 12 hours yielded a white solid which was isolated by removal of the solvent in vacuo. The solid was washed with hexane, collected by filtration and dried *in vacuo.* Yield 0.106 g, 52%. Required for $C_{15}H_{25}N_3Cl_3In$: C, 38.6; H, 5.4; N, 8.9. Found C,38.8; H, 5.8; N, 8.7%. IR (Nujol, ν/cm^{-1}) 288, 272 (In-Cl). ^1H NMR (CD_3CN, 298 K) δ =7.52-7.35 (m, [5H], C_6H_5), 4.96 (s, [4H], tacn-CH_2), 4.88 (m, [6H], CH_3), 4.77 (m, [4H], tacn-CH_2), 4.57 (m, [4H], tacn-CH_2). ^{115}In NMR (CD_3CN, 298 K) δ = 265 (br, m), $W_{1/2}$ = 2200Hz.

[$AlF_3(Me_3$-tacn)]·$4H_2O$: $AlF_3{\cdot}3H_2O$ (0.100 g, 0.73 mmol) was suspended in freshly distilled water (7 mL). Me_3-tacn (0.125 g, 0.73 mmol) was added to the suspension. The pale yellow suspension was transferred into a Teflon container and loaded into a stainless steel bomb. The bomb was heated to 180^{o}C for 15 hours overnight. The bomb was removed from the oven and allowed to cool. A dark yellow-brown solution had formed. An aliquot of the reaction solution was retained to grow crystals. The remaining reaction solvent was removed *in vacuo* giving a white brown solid which was washed with hexane and filtered. The white solid was dried *in vacuo.* Yield 0.125 g, 70%. Required for $C_9H_{27}AlF_3N_3O_3$, C; 34.9, H; 8.8, N; 13.6. Found C; 34.6, H; 8.9, N; 14.6%. IR (Nujol, ν/cm^{-1}) 633, 613, 604 (Al-F). ^1H NMR (CD_3CN, 298 K) δ = 2.84-2.76 (m, [6H], tacn-CH_2), 2.72-2.65 (m, [6H], tacn-CH_2), 2.55 (s, [12H], CH_3). ^{19}F NMR (CD_3CN, 298 K) δ = -176.1 (s). ^{27}Al NMR (CD_3CN, 298 K) δ = 19.0 (s). Slow evaporation of the reaction solvent gave brown crystals suitable for X-ray diffraction.

[$GaF_3(Me_3$-tacn)]·$4H_2O$: $GaF_3{\cdot}3H_2O$ (0.150 g, 0.83 mmol) was suspended in freshly distilled water (7 mL). Me_3-tacn (0.142 g, 0.83 mmol) was then added and the pale yellow suspension was transferred into a Teflon container and loaded into a stainless steel high pressure vessel and heated to 180 ^{o}C for 15 h. The vessel was then allowed to cool. A yellow-brown solution formed. A small aliquot of the reaction solution was retained to grow crystals. For the remaining reaction mixture the volatiles were removed *in vacuo,* giving a light brown solid which was washed with hexane and filtered. The resulting white solid was dried *in vacuo.* Yield 0.21 g,

84%. Anal. Required for $C_9H_{27}F_3GaN_3O_3$: C, 30.7; H, 7.7; N, 11.9. Found: C, 30.6; H, 6.9; N, 11.0%. IR (Nujol, ν/cm^{-1}) 529, 492 (Ga–F). ^{1}H NMR (CD_3CN, 298 K) δ = 2.84 (m[6H], tacn-CH_2), 2.72 (m[6H], tacn-CH_2), 2.63 (s[9H], CH_3). ^{19}F NMR (CD_3CN, 298 K) δ = -182.5 (qt). ^{71}Ga NMR (CD_3CN, 298 K) δ = 41.3 (qt), J_{Ga-F} 488 Hz.

[InF_3(Me_3-tacn)]·4H_2O: A Teflon reactor vessel was charged with freshly distilled water (7 mL), $InF_3.3H_2O$ (0.200 g, 0.90 mmol) and Me_3-tacn (0.154 g, 0.90 mmol). The Teflon container was loaded into a stainless steel high pressure vessel (Parr instrument company, part no 276AC-T304-04 1 10) and heated to 180 °C for 15 hours. The vessel was then allowed to cool. A dark yellow-brown solution had formed. A small aliquot of the reaction solution was retained to grow crystals. For the remaining reaction mixture the volatiles were removed *in vacuo*, giving a light brown gum which was washed with hexane. The hexane was decanted and the remaining volatiles removed *in vacuo* to give a light brown solid. Yield 0.246 g, 69%. Required for $C_9H_{23}F_3InN_3O$: C, 29.9; H, 6.4; N, 11.6. Found: C, 29.9; H, 6.1; N, 11.5%. IR (Nujol, ν/cm^{-1}) 478, 462, 443 (In-F). ^{1}H NMR (CD_3CN, 298 K) δ = 2.96-2.87 (m, [12H], tacn-CH_2), 2.71 (s, [9H], CH_3). ^{19}F NMR (CD_3CN, 298 K) δ = -196.0 (m). ^{115}In NMR (CD_3CN, 298 K) δ = 64 (qt) J_{In-F} 600 Hz.

Table 2.4: Table of crystallographic data for the crystal structures discussed in Chapter 2.[a]

Compound	**$[AlCl_3(Me_3\text{-tacn})]$**	**$[GaCl_3(Me_3\text{-tacn})]$**	**$[InCl_3(BzMe_2\text{-tacn})]$**
Formula	$C_9H_{21}AlCl_3N_3$	$C_9H_{21}Cl_3GaN_3$	$C_{15}H_{25}Cl_3InN_3$
M	304.62	347.36	468.55
crystal system	Monoclinic	Monoclinic	Monoclinic
Space group	$P2_1/c$ (no. 14)	$P2_1/c$ (no. 14)	$P2_1/c$ (no. 14)
a [Å]	12.128(5)	12.173(3)	7.2893(15)
b[Å]	7.185(2)	7.2253(10)	15.026(4)
c [Å]	15.695(6)	15.696(6)	18.528(4)
α [deg]	90	90	90
β [deg]	90.07(5)	90.239(6)	100.924(15)
γ [deg]	90	90	90
U [$Å^3$]	1367.7(8)	1380.5(6)	1992.5(8)
Z	4	4	4
μ(Mo Kα) [mm^{-1}]	0.713	2.552	1.588
total reflns	8994	6378	19924
unique reflns	3059	3150	4522
R_{int}	0.053	0.022	0.057
R_1 [$I_o > 2\sigma(I_o)$][b]	0.058	0.021	0.053
R_1 [all data]	0.078	0.024	0.0758
wR_2 [$I_o > 2\sigma(I_o)$][b]	0.107	0.052	0.096
wR_2 [all data]	0.119	0.053	0.107

[a] Common items: temperature = 100 K; wavelength (Mo-K_α) = 0.71073 Å;

[b] $R_1 = \Sigma \big| \, |F_o| - |F_c| \, \big| / \Sigma |F_o|$; $wR_2 = [\Sigma w(F_o^2 - F_c^2)^2 / \Sigma wF_o^4]^{1/2}$

Table 2.5: Table of crystallographic data for the crystal structures discussed in Chapter 2.[a]

Compound	**$[AlF_3(Me_3\text{-tacn})]\cdot 4H_2O$**	**$[GaF_3(Me_3\text{-tacn})]\cdot 4H_2O$**	**$[InF_3(Me_3\text{-tacn})]\cdot 4H_2O$**
Formula	$C_9H_{29}AlF_3N_3O_4$	$C_9H_{29}F_3GaN_3O_4$	$C_9H_{29}F_3InN_3O_4$
M	327.33	370.07	415.17
crystal system	Orthorhombic	Monoclinic	Monoclinic
Space group	Pbca (no. 61)	$P2_1/c$ (no. 14)	$P2_1/n$ (no. 14)
a [Å]	8.8131(15)	13.420(4)	6.8679(10)
b [Å]	13.356(2)	8.871(2)	20.187(4)
c [Å]	26.551(5)	13.542(3)	12.014(2)
α [deg]	90	90	90
β [deg]	90	97.816(15)	99.482(10)
γ [deg]	90	90	90
U [$Å^3$]	3125.3(10)	1597.3(7)	1642.8(5)
Z	8	4	4
μ(Mo Kα) [mm^{-1}]	0.178	1.769	1.484
total reflns	8255	12911	19404
unique reflns	3570	3645	3750
R_{int}	0.051	0.049	0.028
R_1 [$I_o > 2\sigma(I_o)$] [b]	0.079	0.058	0.0219
R_1 [all data]	0.124	0.076	0.0254
wR_2 [$I_o > 2\sigma(I_o)$] [b]	0.168	0.124	0.044
wR_2 [all data]	0.196	0.133	0.046

[a] Common items: temperature = 100 K; wavelength (Mo-K_α) = 0.71073 Å;

[b] $R_1 = \Sigma \big| |F_o| - |F_c| \big| / \Sigma |F_o|$; $wR_2 = [\Sigma w(F_o^2 - F_c^2)^2 / \Sigma wF_o^4]^{1/2}$

2.6 References

1. *The Group 13 Metals, Aluminium, Gallium, Indium and Thallium: Chemical Patterns and Paculiarities*. Wiley: Chichester, 2011.
2. Wieghardt, K.; Chaudhuri, P.; Nuber, B.; Weiss, J., *Inorg. Chem.* **1982,** *21*, 3086-3090.
3. Belousoff, M. J.; Duriska, M. B.; Graham, B.; Batten, S. R.; Moubaraki, B.; Murray, K. S.; Spiccia, L., *Inorg. Chem.* **2006,** *45*, 3746-3755.
4. Bhalla, R.; Darby, C.; Levason, W.; Luthra, S. K.; McRobbie, G.; Reid, G.; Sanderson, G.; Zhang, W., *Chem. Sci.* **2014,** *5*, 381-391.
5. Nakamoto, K., *Infrared Spectra of Inorganic and Coordination Compounds*. J. Wiley & Sons: 1985; Vol. 4.
6. Mason., J., *Multinuclear NMR*. Plenum Press: 1987; Vol. 1.
7. George, K.; Jura, M.; Levason, W.; Light, M. E.; Reid, G., *Dalton Trans.* **2014,** *43*, 3637-3648.
8. Burt, J.; Levason, W.; Light, M. E.; Reid, G., *Dalton Trans.* **2014,** *43*, 14600-14611.
9. Bandoli, G.; Dolmella, A.; Tisato, F.; Porchia, M.; Refosco, F., *Coord. Chem. Rev.* **2009,** *253*, 56-77.
10. Parker, D.; Waldron, B. P.; Yufit, D. S., *Dalton Trans.* **2013,** *42*, 8001-8008.
11. Zhou, Q.; Henoumont, C.; Vander Elst, L.; Laurent, S.; Muller, R. N., *Contrast Media Mol. Imaging* **2011,** *6*, 165-167.
12. Wieghardt, K.; Walz, W.; Nuber, B.; Weiss, J.; Ozarowski, A.; Stratemeier, H.; Reinen, D., *Inorg. Chem.* **1986,** *25*, 1650-1654.
13. Willey, G. R.; Aris, D. R.; Haslop, J. V.; Errington, W., *Polyhedron.*, **2001,** *20*, 423-429.
14. Stephens, N. F.; Lightfoot, P., *Solid State Sci* **2006,** *8*, 197-202.
15. Petrosyants, P.; Ilyukhin, A. B., *Zh. Neorg. Khim.*, **2010,** *55*, 33-39.
16. Wieghardt, K.; Brodka, S.; Peters, K.; Peters, E. M.; Simon, A., *Z. Naturforsch., B: Chem. Sci.* **1987,** *42*, 279-281.
17. Shannon, R. D., *Acta Crystallogr., Sect. A* **1976,** *A32*, 751-767.
18. Pedersen, K. S.; Lorusso, G.; Morales, J. J.; Weyhermueller, T.; Piligkos, S.; Singh, S. K.; Larsen, D.; Schau-Magnussen, M.; Rajaraman, G.; Evangelisti, M.; Bendix, J., *Angew. Chem., Int. Ed.* **2014,** *53*, 2394-2397.
19. Colton, R.; Dakternieks, D.; Hauenstein, J., *Aust. J. Chem.* **1981,** *34*, 949-955.
20. McGarvey, B. R.; Trudell, C. O.; Tuck, D. G.; Victoriano, L., *Inorg. Chem.* **1980,** *19*, 3432-3436.
21. Malyarick, M. A.; Petrosyants, S. P., *Inorg. Chem.* **1993,** *32*, 2265-2268.
22. Richman, J. E.; Atkins, T. J., *Inorg. Chem* **1974,** *96*, 2268-2278.

Chapter 3

Synthesis and Characterisation of Group 13 Metal Fluoride Complexes with Neutral Aza-macrocyclic Ligands *via* Halide Exchange Reactions

3.1 Introduction

The work discussed in Chapter 2 described the successful synthesis and characterisation of the neutral Group 13 chloride complexes [$MCl_3(RMe_2$-tacn)] (M = Al, Ga, In, R = Bz, Me) and the novel hydrothermal synthesis of the neutral trifluoride analogues [$MF_3(Me_3$-tacn)]·$4H_2O$. While the hydrothermal reactions provided a useful route into the fluoride containing complexes, and thus provided a detailed spectroscopic fingerprint as well as an indication of the solubility of the complexes and their stability under a range of conditions, the key priority to the successful development of ^{18}F containing agents for PET imaging applications is the ability to access the fluoride complexes *via* halide exchange from the pre-formed chloride containing precursors.

The work in this chapter describes the successful synthesis of the complexes [$MF_3(Me_3$-tacn)] (M = Ga, In) *via* a chloride/fluoride exchange reaction using NR_4F (R = Bu, Me) at room temperature from the complexes [$MCl_3(Me_3$-tacn)]. The synthesis of the complexes [$MF_3(RMe_2$-tacn)] (M = Al, Ga, In, R = Me, Bz) using aqueous KF are discussed and the spectroscopic characterisation of the complexes is described. The ease in which the halide exchange is accomplished for each metal is summarised and placed into context for the proposed application. The radio synthesis, purification and analysis of the complex [$Ga^{18}F^{19}F_2(BzMe_2$-tacn)] is demonstrated and its stability in PBS buffer solution shown.

3.2 Results and Discussion

3.2.1 Halide exchange with NR_4F (R = Me, Bu)

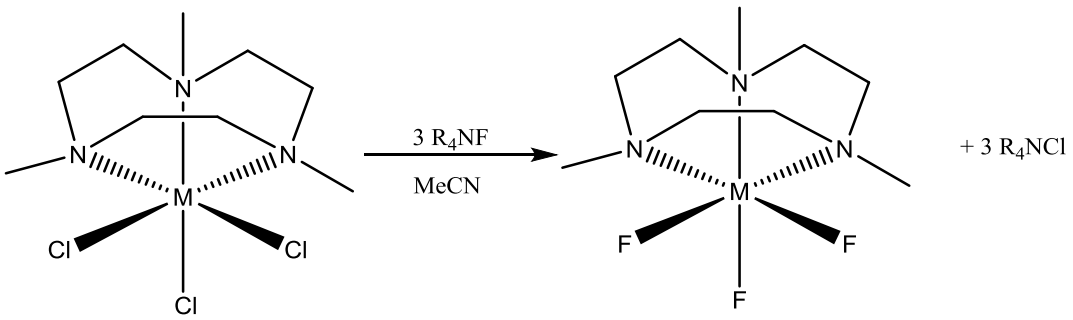

Figure 3.1: Synthetic route to [$MF_3(Me_3$-tacn)] (M = Ga, In) using tetraalkylammonium fluoride salts. R = Me, Bu.

Due to the belief that the metal chloride complexes were hydrolytically sensitive, the initial halide exchange reactions were investigated using the tetraalkylammonium fluoride salts NBu_4F and NMe_4F (Figure 3.1). Tetrabutylammonium fluoride (NBu_4F) is a highly viscous, strongly nucleophilic oil in its pure form. It is supplied commercially as a 1.0 $moldm^{-3}$ solution in thf, giving a convenient, organic soluble source of fluoride ion. The highly electronegative fluoride ion is extremely hydrophilic, and thus is a strong H-bond acceptor. This results in the incorporation of a significant amount of hydrogen bonded water molecules, and despite drying under vacuum, the salt retains a large proportion of water.[1,2] Vigorous drying (i.e. under vacuum at 150 °C) results in decomposition to the tetrabutylammonium bifluoride salt.[1]

Tetramethylammonium fluoride (NMe_4F) is a hygroscopic solid, which like the tetrabutylammonium analogue retains a high proportion of water. However, anhydrous NMe_4F was accessed *via* azeotropic drying of the commercial sample in benzene, followed by prolonged drying under vacuum at 150 °C.[3] The infra-red spectrum of the dried sample showed no evidence of H-bonded water (loss of a broad peak at ν 3240 cm^{-1}). The sample may be stored for short periods under the dry N_2 atmosphere of the glove box. However, due to the very hygroscopic nature of the compound, trace water was readily incorporated into the sample. The salt in its anhydrous form is soluble in anhydrous MeCN – although it has been shown that after prolonged exposure the fluoride salt is capable of deprotonating the solvent to form CH_2CN^- and HF. As the compound degrades to its hydrated form, the solubility in MeCN decreases.[3]

The halide exchange reaction was investigated initially with the complexes [MCl_3(Me_3-tacn)] (M = Al, Ga, In) as the corresponding trifluoride complexes had been synthesised and characterised fully *via* the hydrothermal route discussed in Chapter 2.3. Once the details of the halide exchange had been established, the corresponding complexes [MF_3($BzMe_2$-tacn)] were synthesised and characterised similarly.

Attempted halide exchange reaction with [$AlCl_3$(Me_3-tacn)] and NR_4F

A suspension of the complex [$AlCl_3$(Me_3-tacn)] in anhydrous MeCN was treated with three molar equivalents of NBu_4F. Addition of the fluoride source resulted in the dissolution of the precursor complex. The mixture was stirred at room temperature for one hour. However analysis of the product formed indicated that no reaction had occurred. The infra-red spectrum showed two Al-Cl bands at 375 and 346 cm^{-1}, and showed no evidence of the formation of the Al-F bands at 600-650 cm^{-1}.[4] The ^1H NMR spectrum also matched that of the [$AlCl_3$(Me_3-tacn)] precursor. A further indication that no reaction had occurred was observed in the $^{19}F\{^1H\}$ NMR spectrum recorded in CD_3CN, in which the only peak present corresponded to unreacted NBu_4F (-118 ppm).[1] This implied that the reaction had not proceeded at room temperature. This result was not entirely unexpected; the work of McBride discussed in Chapter 1.2.4, while not

analogous to the work discussed here, required heating to drive the formation of the Al-^{18}F bonds.[5-9]

The reaction was therefore repeated with heating to 40 °C for 30 minutes. Under these conditions, while a reaction did occur, the desired fluoride adduct [AlF_3(Me_3-tacn)] did not form. Instead the Me_3-tacn was liberated and the stable, tetrahedral tetrafluoroaluminate salt [NBu_4][AlF_4] had formed.[10] The infra-red spectrum showed the loss of the Al-Cl bands and the formation of a single strong band at 760 cm^{-1} indicative of the [AlF_4]$^-$ ion.[10] The ^{1}H NMR spectrum indicated the presence of free Me_3-tacn (two singlets [12H], [9H] indicative of the methylene CH_2 protons in the tacn ring and the methyl CH_3's in the pendant arm). The ^{19}F{^{1}H} NMR spectrum (recorded in CD_3CN) revealed a six line coupling pattern of equal intensity at -194 ppm (Figure 3.2).[10] The splitting arises from the coupling of the four fluorine atoms to the quadrupolar aluminium centre (I = 5/2) to give a six line pattern of equal intensity. Confirmation of the formation of [AlF_4]$^-$ was found in the ^{27}Al NMR spectrum, in which a single broad peak was present at 49 ppm.[10] One would expect to observe a quintet, due to the coupling of the four fluoride ligands to the aluminium centre. However this was not the case, instead a broad peak was observed. It is likely that the ability to observe couplings in the sensitive ^{27}Al nucleus is concentration dependent.

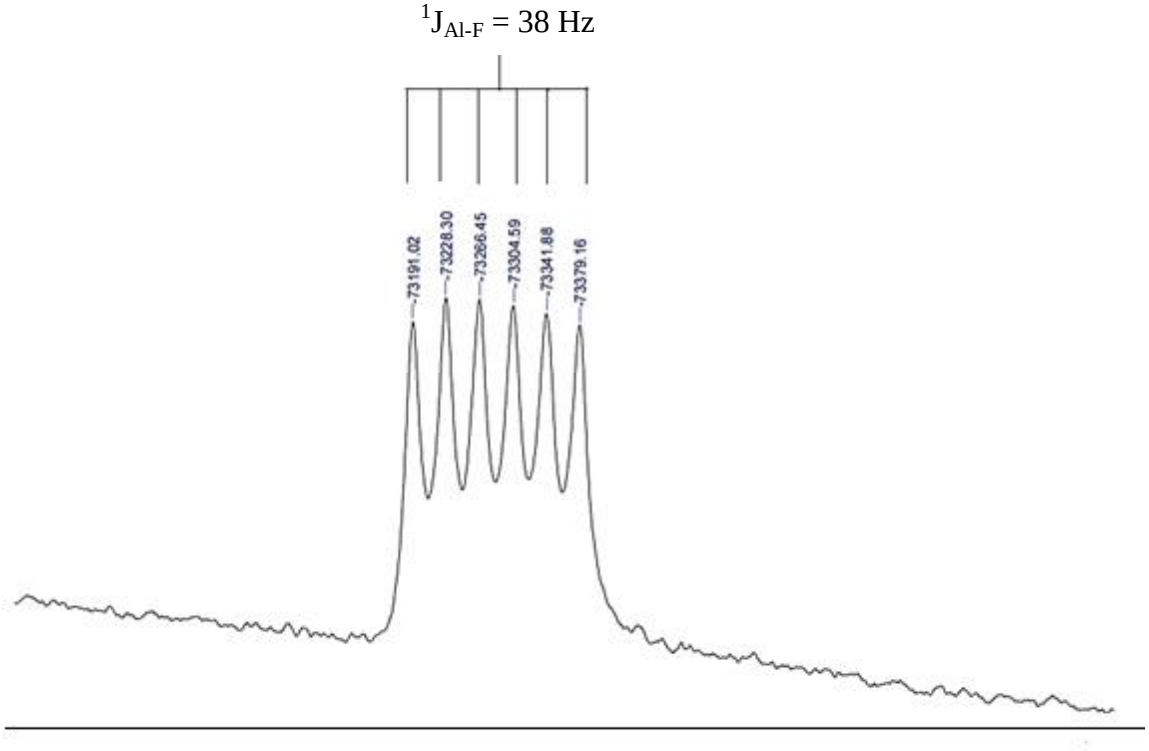

Figure 3.2: $^{19}F\{^1H\}$ NMR spectrum of $[NMe_4][AlF_4]$ recorded in CD_3CN showing the splitting pattern arising from the $[AlF_4]^-$ anion. $^1J_{Al-F}$ 38 Hz.

The results observed using the NBu_4F was replicated with the NMe_4F, which implies that it is not the effect of the alkyl groups which is inhibiting the successful chloride/fluoride exchange.

Comparison of the Al–N bond distances in $[AlF_3(Me_3\text{-tacn})]\cdot 4H_2O$ synthesised hydrothermally (Chapter 2.3) with those in $[AlCl_3(Me_3\text{-tacn})]$ (Chapter 2.2.2) reveals a very small increase in d(Al-N) of only ~0.02 Å. If one compares this to the corresponding gallium system, the d(Ga–N) distances are *ca.* 0.04–0.05 Å shorter in the $[GaF_3(Me_3\text{-tacn})]\cdot 4H_2O$ than in $[GaCl_3(Me_3\text{-tacn})]$. This indicates that the Me_3-tacn ligand might be too large for optimal binding to the octahedrally coordinated aluminium centre. This results from the small Al^{3+} ion (ionic radius 0.68 Å).[11] Therefore to accommodate a six coordinate geometry with a *facially* coordinated Me_3-tacn moiety; the Al-N bonds lengthen to decrease the steric strain.

It has been shown that in aqueous media, ligand substitution mechanisms in the six coordinate Al(III) ions proceed *via* an I_d mechanism in which the activation process is dominated by a bond breaking step.[12-14] This is supported by the belief that for metal ions with ionic radii less than 0.6 Å the associative pathway is favoured.[15 4] However, under the solvent

conditions utilised in the halide exchange reaction for the [$AlCl_3$(Me_3-tacn)] precursor, the mechanism may proceed *via* an I_a step. It seems that the attack of the fluoride ligand on the [$AlCl_3$(Me_3-tacn)] complex forms a pseudo 7-coordinate transition state.[16] This imparts too much steric strain on the Al(III) centre resulting in the liberation of the weakly bound macrocyclic ligand. Once the steric strain has been released the exchange of the halides proceeds, thus forming the tetrahedral $[AlF_4]^-$.

Halide exchange reaction with [$GaCl_3$(Me_3-tacn)]

Treatment of a suspension of [$GaCl_3$(Me_3-tacn)] in anhydrous MeCN with three molar equivalents of NBu_4F/thf at room temperature results in the rapid dissolution of the precursor complex. Analysis of the resulting product showed that the spectroscopic data was identical to that obtained for the [GaF_3(Me_3-tacn)] complex synthesised hydrothermally. This confirmed complete halide exchange, leading to full conversion to the neutral trifluoride complex [GaF_3(Me_3-tacn)]. This was confirmed by infra-red spectroscopy, where the bands for the Ga-Cl stretching vibrations were lost, and the corresponding Ga-F bands appeared at 530 and 492 cm^{-1}. The ^1H NMR spectrum showed the characteristic resonances (see Chapter 2.3.3) corresponding to the fluoride complex. There was no evidence in the ^1H NMR spectrum for unreacted [$GaCl_3$(Me_3-tacn)] or free Me_3-tacn. Both the $^{19}F\{^1H\}$ and ^{71}Ga NMR spectra showed no evidence for fluorogallate anions such as $[GaF_4]^-$ and only showed one observable 'Ga-F' containing species, which matched that observed from the hydrothermal reaction discussed in Chapter 2.3.3.

The exchange reaction proceeds very quickly at room temperature, as confirmed by *in situ* $^{19}F\{^1H\}$ and ^{71}Ga NMR experiments. A solution of [$GaCl_3$(Me_3-tacn)] in CD_3CN was treated with three molar equivalents of NBu_4F and the $^{19}F\{^1H\}$ and ^{71}Ga NMR spectra recorded. The spectra showed the formation of the expected [GaF_3(Me_3-tacn)] complex. The complex had formed in 5 minutes, the time in which it was possible to record the NMR spectra. On the basis of these results the gallium system was identified to be well suited to performing halide exchange reactions on a radiochemical scale (Chapter 3.2.6).

Halide exchange reaction with [$InCl_3$(Me_3-tacn)]

Addition of three molar equivalents of NBu_4F/thf to a suspension of [$InCl_3$(Me_3-tacn)] in anhydrous MeCN at room temperature resulted in rather slow dissolution of the precursor complex, in stark contrast to the gallium analogue. After 10-15 minutes of vigorous stirring the chloride precursor complex did dissolve.

The halide exchange reaction is slower in the [$InCl_3$(Me_3-tacn)] complex compared to the [$GaCl_3$(Me_3-tacn)]. In fact at room temperature the halide exchange reaction took up to an hour to complete. Given the need for the halide exchange reaction to occur swiftly on a

radiochemical scale, this was viewed as a disadvantage. Upon heating to 80 °C under N_2, the halide exchange reaction proceeded more quickly (*ca.* 30 minutes), fully converting the chloride precursor to [InF_3(Me_3-tacn)]. While heating demonstrated that the chloride/fluoride exchange could be accomplished faster than at room temperature in the indium system, the time required to accomplish the reaction was significantly longer than for the gallium analogue. This implies that for this ligand type, the indium(III) ion is less well suited. This may be due to the smaller difference between the In-Cl (439 $kJmol^{-1}$) and In-F (506 $kJmol^{-1}$) bond enthalpies, which might mean a larger driving force may be required to complete the halide exchange. The key factor which might affect the halide exchange with [$InCl_3$(Me_3-tacn)] is the apparently poorer solubility of the precursor in MeCN; the halide exchange cannot occur until the precursor enters solution.

3.2.2 Halide exchange reaction using $KF_{(aq)}$

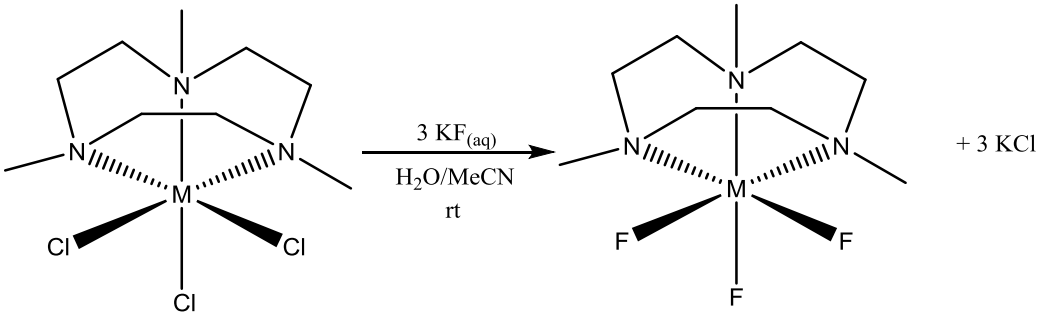

Figure 3.3: Synthetic route to the complexes [MF_3(Me_3-tacn)] (M = Ga, In) using aqueous KF.

While the synthesis of [MF_3(Me_3-tacn)] (M = Ga, In) was successfully accomplished *via* chloride/fluoride exchange using the tetraalkylammonium fluoride salts NMe_4F and NBu_4F, the synthetic route had some challenges. It proved difficult to remove the NR_4Cl by-product, particularly for NBu_4Cl. While the NMe_4Cl analogue proved a little easier to remove, the requirement to have the NMe_4F rigorously anhydrous before use to allow solubility in MeCN was time consuming.

When considering the potential use of this class of compound as ^{18}F containing radiopharmaceuticals for imaging applications, it would be more beneficial to introduce the fluoride in aqueous solution; the $^{18}F^-$ that is produced in the cyclotron is delivered as an aqueous solution and to remove the need for azeotropic drying of the $^{18}F^-$ is considered a significant time saving in the synthetic process.[17] Therefore the halide exchange reaction was investigated using aqueous potassium fluoride (KF) as the source of fluoride (Figure 3.3). While the fluoride complexes [MF_3(Me_3-tacn)]·$4H_2O$ are stable in aqueous solution, the corresponding chlorides are more hydrolytically unstable as evidenced by the [(Ga_2(Me_3-tacn))$_2$($\mu OH)_3$]$^{3+}$ compound

produced through hydrolysis of [$GaCl_3$(Me_3-tacn)] (Chapter 2.2.3). Therefore, the key to the utility of these compounds is for the chloride/fluoride exchange reaction to proceed faster than the competing hydrolysis reaction.

Treatment of a suspension of [$AlCl_3$(Me_3-tacn)] in anhydrous MeCN with three molar equivalents of $KF_{(aq)}$ at room temperature followed by removal of the volatiles under high vacuum gave a white solid. The KCl by-product is conveniently removed by washing the solid with MeCN and filtering off the salt by-product. Analysis of the resulting product confirmed the complex was [AlF_3(Me_3-tacn)]·$4H_2O$, based upon comparison of the spectroscopic data obtained for the hydrothermal reaction discussed in Chapter 2.2.3. This shows that complete exchange of chloride for fluoride is achieved under mild conditions in aqueous MeCN. This was unexpected given the observations from the halide exchange reaction using NR_4F. This implies that under these solvent conditions the substitution may proceed *via* a dissociative (D) or interchange (I_d) mechanism, as suggested by Patterson and others.[14, 18] This mechanistic pathway would proceed *via* the bond breaking and loss of the chloride ligand, thus releasing the steric strain on the aluminium centre through the formation of a five-coordinate transition state. This then allows the smaller fluoride ligand to coordinate in a step wise process.[16]

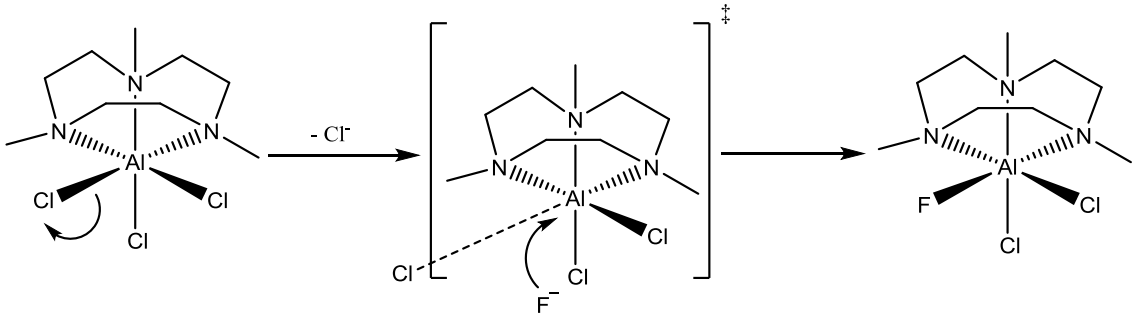

Figure 3.4: Proposed I_d mechanism for the chloride/fluoride exchange reaction in [$AlCl_3$(Me_3-tacn)].

The halide exchange reaction is complete in *ca.* 10 minutes at room temperature. While not directly analogous, the work of McBride *et al.* discussed in Chapter 1.2.4 and 4.1.1 uses elevated temperatures (115 °C) and reaction times (*ca.* 20 minutes) to achieve Al-F bond formation.[5-7, 9, 19] The difference between the enthalpy of bond formation between Al-F (664 $kJmol^{-1}$) and Al-Cl (494 $kJmol^{-1}$) probably drives the rapid formation of the [AlF_3(Me_3-tacn)] complex under mild conditions.[20]

The chloride/fluoride exchange reaction of [$AlCl_3$(Me_3-tacn)] with $KF_{(aq)}$ was shown to be quicker than any competing hydrolysis reaction using ^{27}Al NMR spectroscopy. The ^{27}Al NMR nucleus is referenced to $[Al(H_2O)_6]^{3+}$ in water.[21] Treatment of [$AlCl_3$(Me_3-tacn)] with D_2O gives

a resonance at 0 ppm after 5 minutes, and no evidence of any other high symmetry aluminium-containing species. This shows that the formation of $[AlF_3(Me_3\text{-tacn})]$ under aqueous conditions is more rapid and favoured over the competing hydrolysis reaction.

The chloride/fluoride halide exchange using $KF_{(aq)}$ was also investigated with the analogous $[MCl_3(Me_3\text{-tacn})]$ (M Ga, In) complexes. As observed using the NR_4F salts, the complex $[GaF_3(Me_3\text{-tacn})]$ was formed rapidly (5 minutes) at room temperature. The indium analogue proceeded more slowly (*ca.* 45-60 minutes). Heating the indium system to 80 °C under N_2 did appear to accelerate the halide exchange reaction (20 minutes). Despite heating, halide exchange using $[InCl_3(Me_3\text{-tacn})]$ is still slower than the corresponding aluminium and gallium systems. It is likely that the prolonged exchange reaction is derived from the lower solubility of $[InCl_3(Me_3\text{-tacn})]$.

As with $[AlCl_3(Me_3\text{-tacn})]$, the chloride/fluoride exchange reaction was favoured over any competing hydrolysis reaction using $[GaCl_3(Me_3\text{-tacn})]$. Treatment of $[GaCl_3(Me_3\text{-tacn})]$ with D_2O alone gives a single resonance at 0 ppm in the ^{71}Ga NMR spectrum, corresponding to the $[Ga(H_2O)_6]^{3+}$ cation.[21] Treatment with KF/D_2O leads to the observation of a broad resonance at 41 ppm, consistent with the complex $[GaF_3(Me_3\text{-tacn})]$. There was no evidence of the quartet observed from the compound formed hydrothermally, but it is likely that this is because the polar water solvent molecules hydrogen bond strongly to the complex, broadening the resonance.

The ability to perform the halide exchange reaction in aqueous media is a significant advantage in the development of these complexes as potential agents for PET imaging. The use of KF is approved by the federal drug agency (FDA) which removes any regulatory issues related to the use of other fluoride salts.[22] From a chemical standpoint, the use of aqueous fluoride removes the need to dry the $^{18}F^-$ from the cyclotron, greatly simplifying the synthetic procedure.

3.2.3 Synthesis of $[MF_3(BzMe_2\text{-tacn})]\cdot H_2O$ (M = Al, Ga, In) *via* halide exchange

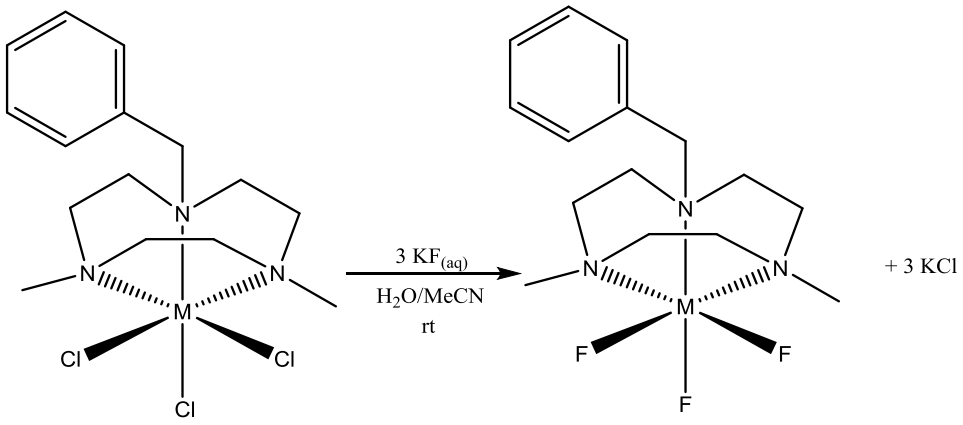

Figure 3.5: Synthetic route towards the neutral complexes $[MF_3(BzMe_2\text{-tacn})]$ (M = Al, Ga, In) via chloride/fluoride exchange with $KF_{(aq)}$.

Based upon the success of the chloride/fluoride exchange reactions conducted with the $[MCl_3(Me_3\text{-tacn})]$ (M = Al, Ga, In) complexes using $KF_{(aq)}$, the synthesis of the corresponding $[MF_3(BzMe_2\text{-tacn})]$ (M = Al, Ga, In) complexes was attempted similarly. As mentioned in Chapter 2.1, the $BzMe_2$-tacn ligand has some advantages over the Me_3-tacn, namely the UV active chromophore on the benzyl substituent allows the complexes to be detected with the UV detector in the HPLC and could potentially act as a tether in which peptides or bioactive molecules may be attached to the ligand scaffold.

The complex $[AlF_3(BzMe_2\text{-tacn})]$ was successfully synthesised *via* chloride/fluoride exchange using $KF_{(aq)}$. The infra-red spectrum showed two Al-F stretching vibration bands at 635, 601 cm^{-1}, and no evidence of Al-Cl bands at 375 and 349 cm^{-1}. The ^1H NMR spectrum showed the complex second order peak pattern discussed in Chapter 2.3. The $^{19}F\{^1H\}$ NMR spectrum recorded in CD_3CN showed two peaks at δ −149.4 (m) and −150.4 (m) in a ratio of 1:2 reflecting the inequivalent fluoride environments which arise through the unsymmetrical substituents on the $BzMe_2$-tacn ligand. The ^{27}Al NMR spectrum gave a broad singlet at δ 20 ppm. The benzyl substituent on the tacn ligand breaks the local symmetry around the molecule, which lowers the electric field gradient. This results in couplings too broad to be observed. This was the only ^{27}Al resonance observed, suggesting the complex was the only high symmetry aluminium complex present in the sample. Despite repeated attempts, crystals of the complex of suitable quality to perform single crystal X-ray diffraction were not obtained.

$[GaF_3(BzMe_2\text{-tacn})]$ was readily accessed *via* the halide exchange reaction with aqueous KF. The infra-red spectrum proved similar to the related $[GaF_3(Me_3\text{-tacn})]$ complex synthesised *via* halide exchange with $KF_{(aq)}$, with two bands at 527 and 485 cm^{-1} indicating a complex with an approximate C_{3V} symmetry. The ^1H NMR spectrum of $[GaF_3(BzMe_2\text{-tacn})]$ showed a slight shift in the resonances to a higher chemical shift in comparison to the $[GaCl_3(BzMe_2\text{-tacn})]$

complex. Unlike $[GaF_3(Me_3\text{-tacn})]\cdot 4H_2O$, neither the $^{19}F\{^1H\}$ or ^{71}Ga NMR spectra showed any couplings. This is due to the lower symmetry of the complex which creates a higher efg. This results in faster relaxation which broadens the peaks, meaning a loss of resolved couplings. However the chemical shifts observed were consistent with those seen in the $[GaF_3(Me_3\text{-tacn})]$ analogue, demonstrating that the desired neutral octahedral complex had formed. Slow evaporation of a MeCN solution of the complex yielded crystals suitable for single crystal X-ray diffraction (Figure 3.6).

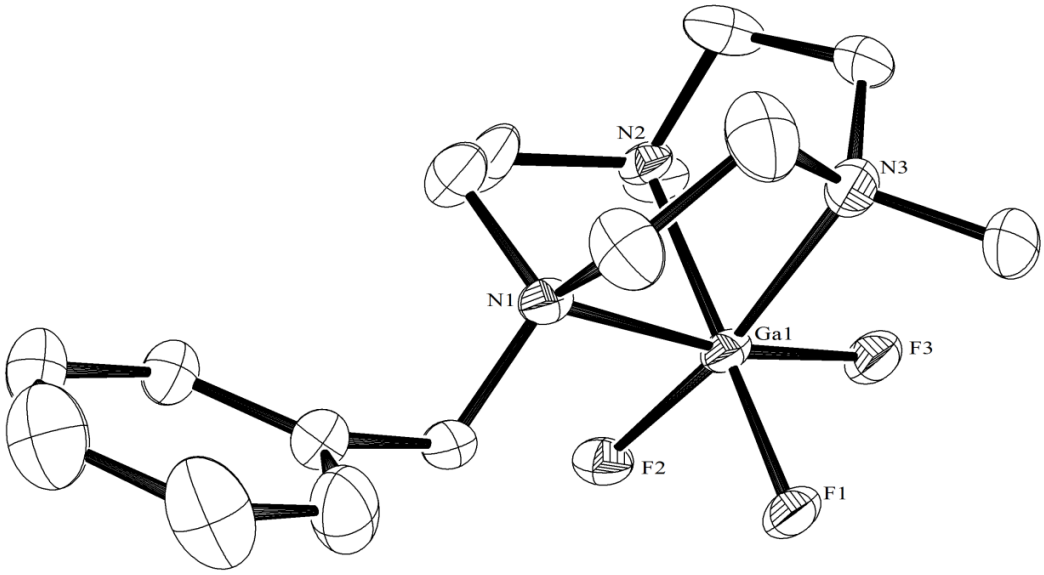

Figure 3.6: ORTEP representation of the crystal structure of *fac*-$[GaF_3(BzMe_2\text{-tacn})]\cdot 2H_2O$. Ellipsoids are drawn at 50% probability level. Lattice water molecules and H-atoms are omitted for clarity. Ga1-F1 1.841(2), Ga1-F2 1.849(3), Ga1-F3 1.870(2), Ga1-N1 2.151(4), Ga1-N2 2.133(4), Ga1-N3 2.137(4) Å. F1-Ga1-F2 94.68(11), F1-Ga1-F3 96.62(11), F2-Ga1-F3 94.48(12), N2-Ga1-N1 82.61(13), N3-Ga1-N1 82.83(14), N2-Ga1-N3 82.73(14)°.

The crystal structure confirms the expected *fac* octahedral coordination to the Ga(III) centre with the tridentate $BzMe_2$-tacn ligand coordinated on one face. The fluoride ligands lie *trans* to the $BzMe_2$-tacn ligand nitrogen donor atoms. Comparison with both the 'Ga-F' hexamer prepared by Wieghardt *et al.* and the $[GaF_3(Me_3\text{-tacn})]$ analogue reveals very little difference between the two structures in terms of the d(Ga-F) and d(Ga-N), implying that the benzyl substituent has little effect on the metal coordination.[23]

The complex crystallised as a dihydrate in contrast to the $[GaF_3(Me_3\text{-tacn})]\cdot 4H_2O$ complex discussed in Chapter 2.3.3. This could be due to the hydrophobic benzyl substituent, which acts to prevent more lattice water molecules from crystallising with the complex. Like the analogous

Me_3-tacn complex, $[GaF_3(BzMe_2\text{-tacn})]\cdot 2H_2O$ exhibits extensive H-bonding array involving intermolecular HO-H····F (2.744(2) Å) and O-H····O (2.809(2) Å) interactions (Figure 3.7).

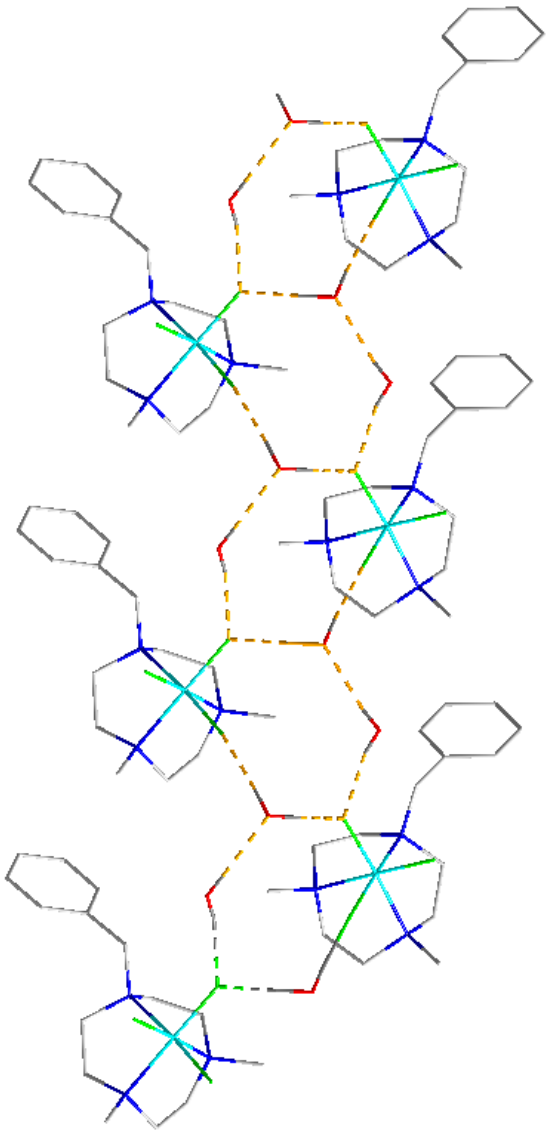

Figure 3.7: View of the portion of the extended structure of the complex *fac*-$[GaF_3(BzMe_2\text{-tacn})]\cdot 2H_2O$ depicting the H-bonded network derived from intermolecular F····O and O····O interactions. H-bonds denoted by dashed yellow lines. Colour key: turquoise = Ga, green = F, blue = N, red = O, grey = C.

Microanalytical measurements on the bulk sample confirmed the expected formulation.

Like the analogous $[GaF_3(Me_3\text{-tacn})]$complex, $[GaF_3(BzMe_2\text{-tacn})]\cdot 2H_2O$ formed rapidly at room temperature under the reaction conditions employed. *In situ* $^{19}F\{^1H\}$ NMR studies indicated that the chloride/fluoride exchange reaction occurred within 5 minutes at room temperature. $^{19}F\{^1H\}$ NMR spectroscopy also indicated that $[GaF_3(BzMe_2\text{-tacn})]$ was remarkably stable for long periods (at least four weeks) in a variety of solvents including H_2O,

thf, MeCN and MeOH, and was stable to both gentle (40 ^{o}C) and vigorous (80 ^{o}C, heat gun) heating in MeCN. This was demonstrated through the observation that no change was observed in the $^{19}F\{^{1}H\}$ resonance at -173 ppm, and no evidence of formation of a new fluorine containing species. It also proved resistant to competition reactions from a number of anions such as acetate (NaOAc) at pH 4, and in phosphate buffered saline (PBS) at pH 7.5. Given the rapid exchange kinetics and its stability in solution, the complex [GaF_3($BzMe_2$-tacn)] was selected as the first model compound to attempt to be radiolabelled (Chapter 3.2.4).

Formation of the complex [InF_3($BzMe_2$-tacn)] *via* halide exchange with aqueous KF at room temperature took significantly longer than the aluminium and gallium analogues, taking about 45-60 minutes to reach completion, based upon *in situ* $^{19}F\{^{1}H\}$ NMR spectroscopy . This was also observed in the formation of [InF_3(Me_3-tacn)]. The infra-red spectrum of [InF_3($BzMe_2$-tacn)] showed the presence of two In-F stretching vibrations consistent with an octahedral complex with C_{3V} symmetry (a_1 + e). As was seen for all the fluoride complexes discussed in Chapter 2.3, the infra-red spectrum gave evidence of H-bonded water in the complex (υ O-H = 3450 cm^{-1}, δ HO-H = 1657 cm^{-1}) . A signal could not be observed in the ^{115}In NMR spectrum of the [InF_3($BzMe_2$-tacn)]·H_2O. This observation arises from the increase in the efg through the reduced molecular symmetry, combined with the large quadrupolar moment associated with the indium nucleus. The $^{19}F\{^{1}H\}$ NMR spectrum of [InF_3($BzMe_2$-tacn)] depicted a very broad multiplet at δ = -220 ppm. Slow diffusion of Et_2O into a MeCN solution of the complex gave crystals suitable for single crystal X-ray diffraction.

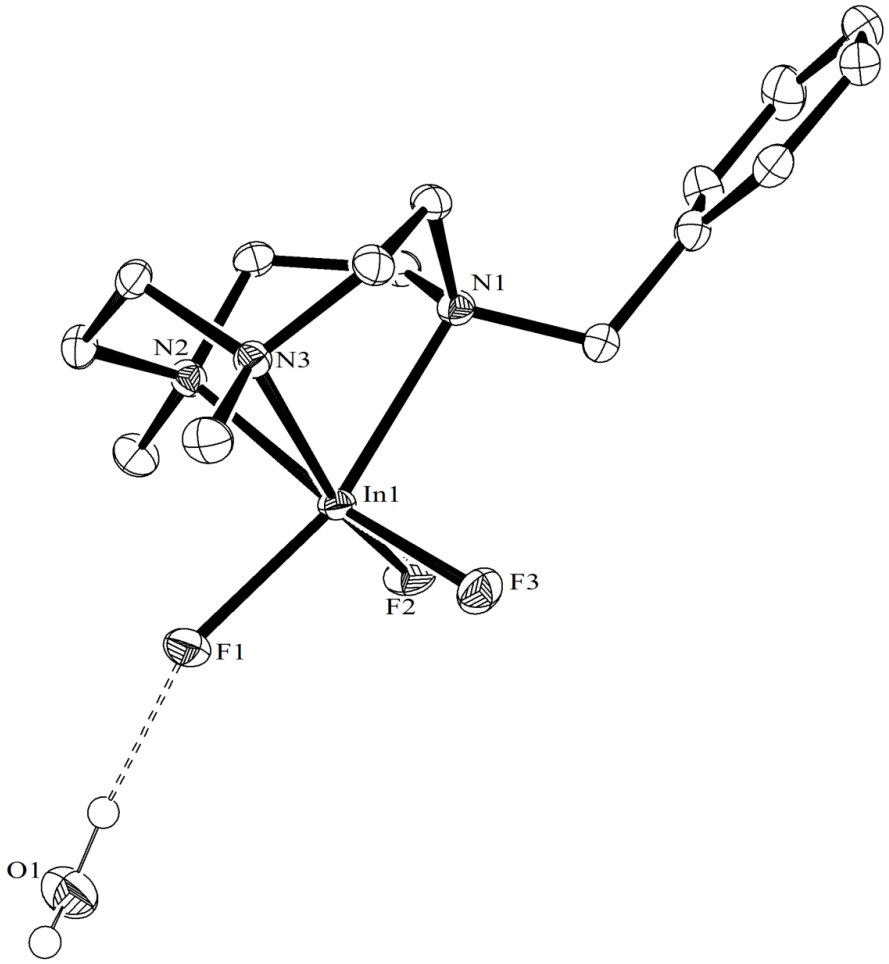

Figure 3.8: ORTEP representation of the crystal structure of *fac*-[$InF_3(BzMe_2$-tacn)]·H_2O. Ellipsoids are drawn at 50% probability level. H-atoms on the $BzMe_2$-tacn ligand are omitted for clarity. In1-F1 2.0585(12), In1-F2 2.0501(12), In1-F3 2.0176(12), In1-N1 2.3359(16), In1-N2 2.2948(16), In1-N3 2.2995(4) Å. F1-In1-F2 98.24(5), F1-In1-F3 96.71(5), F2-In1-F3 96.72(5), N2-In1-N1 77.81(6), N3-In1-N1 77.15(6), N2-In1-N3 77.81(6)°.

The structure (Figure 3.8) confirms the distorted octahedral In(III) with the tridentate tacn ligand coordinated *facially*. The coordination sphere is completed by three fluoride ligands coordinated *trans* to the $BzMe_2$-tacn ligand. Comparison with [$InCl_3(BzMe_2$-tacn)] shows that the mean d(In-F) is 0.4079(12) Å shorter than the d(In-Cl). This is less than the difference in the ionic radii between chloride and fluoride. This might suggest that the halide ligands are more tightly bound in the fluoride complex than the chloride, perhaps a reflection on the stronger electronegativity of the fluoride ion and its stronger Lewis acidity towards the indium centre. Comparison with [$InF_3(Me_3$-tacn)]·$4H_2O$ shows little difference between the In-F and In-N bond lengths between the two complexes, although the heavily hydrated [$InF_3(Me_3$-tacn)]·$4H_2O$ may mask any differences in the In-F bond lengths. The [$InF_3(BzMe_2$-tacn)] complex crystallises as a monohydrate which contrasts with the [$GaF_3(BzMe_2$-tacn)] complex which crystallises as a

dihydrate. Further, while all the fluoride complexes with the Me_3-tacn ligand [$MF_3(Me_3$-tacn)] crystallised as tetra-hydrates, the corresponding $BzMe_2$-tacn complexes showed more variety in the number of crystallised water molecules in the lattice. This may be due to the packing affects from the benzyl substituent on the ligand. The crystallised lattice water molecules also participate in H-bonding interactions with the fluoride ligands of the [$InF_3(BzMe_2$-tacn)] complex.

Complex	**δ^{27}Al/^{71}Ga/^{115}In/ppm; ($W_{1/2}$ / Hz)**	**δ^{19}F{^{1}H} (ppm)**	**Solvent**
[$AlF_3(Me_3$-tacn)]	19.0 (60) 18.5 (52)	–176.1 –169.9	MeCN D_2O
[$AlCl_3(Me_3$-tacn)]	34.5 (30)	-	MeCN
[$GaF_3(Me_3$-tacn)]	42.0 (q, $^1J_{GaF}$ ~ 490 Hz) 44.6 (br q)	–180.9 (two br q) –173 (br)	MeCN D_2O
[$GaCl_3(Me_3$-tacn)]	93.9 (60)	-	CH_2Cl_2
[$InF_3(Me_3$-tacn)]	64 (q, $^1J_{InF}$ ~ 600 Hz) n.o.	–215 (br) –192.5 (br)	MeCN D_2O
[$InCl_3(Me_3$-tacn)]	268 (750)	-	CH_2Cl_2
[$AlF_3(BzMe_2$-tacn)]	19.8 (100)	–161.5 (F), –161.7 (2F)	MeCN
[$AlCl_3(BzMe_2$-tacn)]	36.5 (45)	-	CH_2Cl_2
[$GaF_3(BzMe_2$-tacn)]	44.9 (q $^1J_{GaF}$ ~ 445Hz)	–172.8 (br)	D_2O
[$GaCl_3(BzMe_2$-tacn)]	92.8 (360)	-	MeCN
[$InF_3(BzMe_2$-tacn)]	n.o. [a]	–220 (br)	MeCN
[$InCl_3(BzMe_2$-tacn)]	265 (2200)	-	MeCN

Table 3.1: Table summarising all relevant multinuclear NMR data from the complexes discussed in Chapters 2 and 3.

3.2.4 Synthesis of $[GaF_3(Me_3\text{-tacn})]$ from $Ga(NO_3)_3{\cdot}9H_2O$

While the use of the metal chloride based chelates as precursors towards $^{18}F^-$ labelled compounds was successful with this class of compound, the use of the moisture sensitive MCl_3 (M = Al, Ga, In) as a starting material when performing reactions on a sub-milligram quantity (e.g. for peptide conjugated chelates) is expected to be very challenging. Therefore it would be advantageous to identify an aqueous source of the trivalent metal – one in which the anion could be easily exchanged for fluoride during radiolabelling.

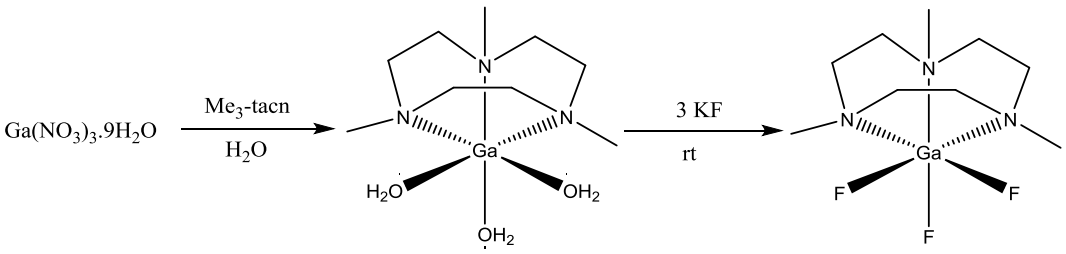

Figure 3.9: Proposed synthetic route and intermediate towards $[GaF_3(Me_3\text{-tacn})]$ from aqueous $Ga(NO_3)_3{\cdot}9H_2O$.

Given the favourable halide exchange reaction and the stability of the resultant complex, gallium was identified as the metal of choice. The water soluble salt gallium nitrate $Ga(NO_3)_3$ was chosen, which has been identified as a nona-hydrate in the solid state. The salt is extensively dissociated in solution with a six coordinate octahedral $[Ga(OH_2)_6]^{3+}$ cation with three $[NO_3]^-$ ions charge balancing and a further three water molecules crystallised in the lattice.[24] Therefore, $Ga(NO_3)_3{\cdot}9H_2O$ is used as the reference standard in ^{71}Ga NMR spectroscopy. When dissolved in water the aquo ion $[Ga(OH_2)_6]^{3+}$ signal is set at 0 ppm.[21] ^{71}Ga NMR spectroscopy can be used to track reactions at the gallium centre provided the compounds formed are of high enough symmetry to allow the resonances to be observed. The complex $[GaF_3(Me_3\text{-tacn})]$ was observable in the ^{71}Ga NMR spectrum, in both MeCN and H_2O (see Chapter 2.3.3). Therefore if the complex $[GaF_3(Me_3\text{-tacn})]$ could be prepared *in-situ* from $Ga(NO_3)_3{\cdot}9H_2O$, it would be identifiable by ^{71}Ga NMR spectroscopy.

Dissolution of $Ga(NO_3)_3{\cdot}9H_2O$ into D_2O gave the expected resonance at 0 ppm in the ^{71}Ga NMR spectrum. The $Ga(NO_3)_3{\cdot}9H_2O$ solution was then treated with one molar equivalent of Me_3-tacn. The ^{71}Ga NMR spectrum of this solution showed the loss of the resonance at 0 ppm, but no evidence of a new resonance appearing. This would suggest that the gallium salt had reacted with the Me_3-tacn to likely form the highly labile $[Ga(OH_2)_3(Me_3\text{-tacn})]^{3+}$ complex. The highly labile nature of the complex gives rise to a dynamic system in solution, which raises the electric field gradient resulting in fast

quadrupolar relaxation and the loss of observable resonances.

The solution was treated with three molar equivalents of KF and stirred at room temperature for 10 minutes. The ^{71}Ga NMR spectrum of the solution gave a single broad resonance at δ = 45.0 ppm, which matched that seen for the complex [GaF_3(Me_3-tacn)] when recorded in D_2O. This demonstrated that the complex [GaF_3(Me_3-tacn)] may be accessed from the water soluble $Ga(NO_3)_3 \cdot 9H_2O$. Subsequent work-up of the reaction solution and spectroscopic analysis indicated that the desired complex had been formed (spectroscopic data matched that discussed in Chapter 2.3.3). This establishes the ability to use an inert, water soluble source of Ga(III) as a route to $^{18}F^-$ labelled complexes for imaging applications, and sets up the work discussed in Chapter 4.

3.2.5 Radiolabelling of [$GaCl_3$($BzMe_2$-tacn)]

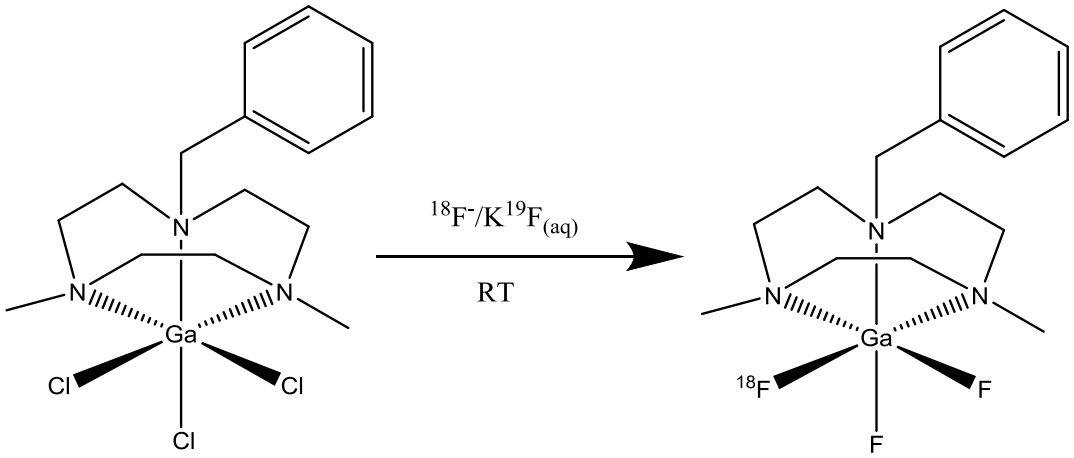

Figure 3.10: Synthetic strategy towards the radiolabelling of [$GaCl_3$($BzMe_2$-tacn)].

The radiolabelling of [$GaCl_3$($BzMe_2$-tacn)] was accomplished using an ^{18}F doped solution of ($K^{19}F$) at room temperature. The quantity of $^{18}F^-$ which is produced from the cyclotron is very small in terms of chemical quantity (e.g. 1 GBq $^{18}F^-$ in 0.2 mL $H_2{}^{18}O$). This, and the requirement to exchange three chloride ligands with three fluoride ligands meant that a carrier agent was required. Given the success of the halide exchange reaction on the preparative scale, $K^{19}F$ was used as the carrier agent.

The radiolabelling was performed on a 1 mg scale (2.36 μmol of [$GaCl_3$($BzMe_2$-tacn)]) to allow enough quantity of material to thoroughly analyse the products formed. While the labelling reaction was performed on a significantly lower concentration than on a synthetic scale, it was still higher than the concentrations used in clinical applications, which are usually administered on a nano-molar scale.

[$GaCl_3$($BzMe_2$-tacn)] was dissolved in 0.6 mL aqueous MeCN, followed by addition of 2.99 mol. equivalents of aqueous $K^{19}F$ and 0.4 mL of $^{18}F^-$ (100-500 MBq). The reaction mixture was shaken and allowed to stand at room temperature for between 30 and 60 minutes. The crude reaction solution was diluted into water so that approximately 10% of the solution contained the organic MeCN. The crude mixture was purified by preparative HPLC using a water/MeCN mobile phase (Figure 3.11). This gave a single product peak at Rt = 9.1 mins (*ca.* 30% incorporation after one hour).

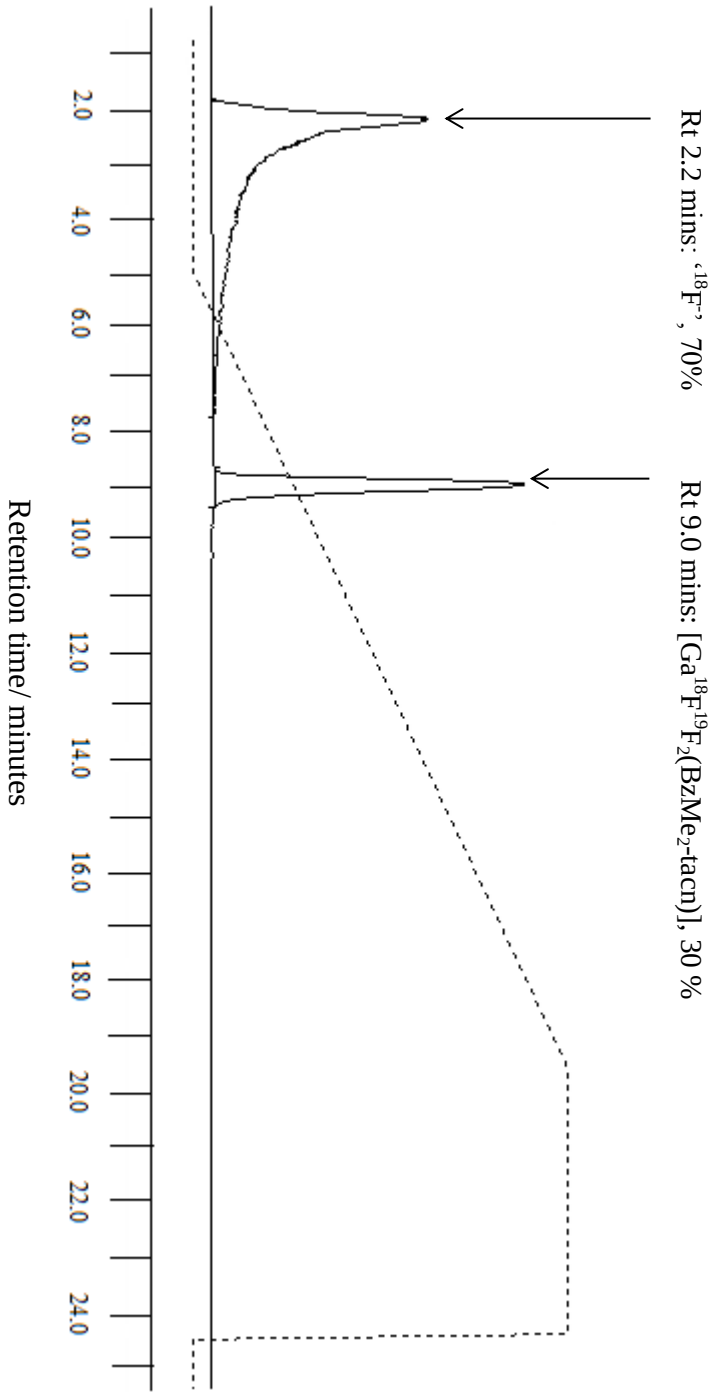

Figure 3.11: Preparative HPLC radio trace of the crude reaction mixture for the labelling of $[GaCl_3(BzMe_2\text{-tacn})]$ with $^{18}F/K^{19}F$. Peak 1: R_t 2.1 mins. ($^{18}F^-$). Peak 2: Rt 9.0 mins. ($[Ga^{18}F^{19}F_2(BzMe_2\text{-tacn})]$).

The purified species was eluted through an analytical HPLC system using a 10 mM aq. NH_4OAc/MeCN mobile phase, giving a single peak in the radio-chromatograph at Rt = 6.2 minutes (Figure 3.12).

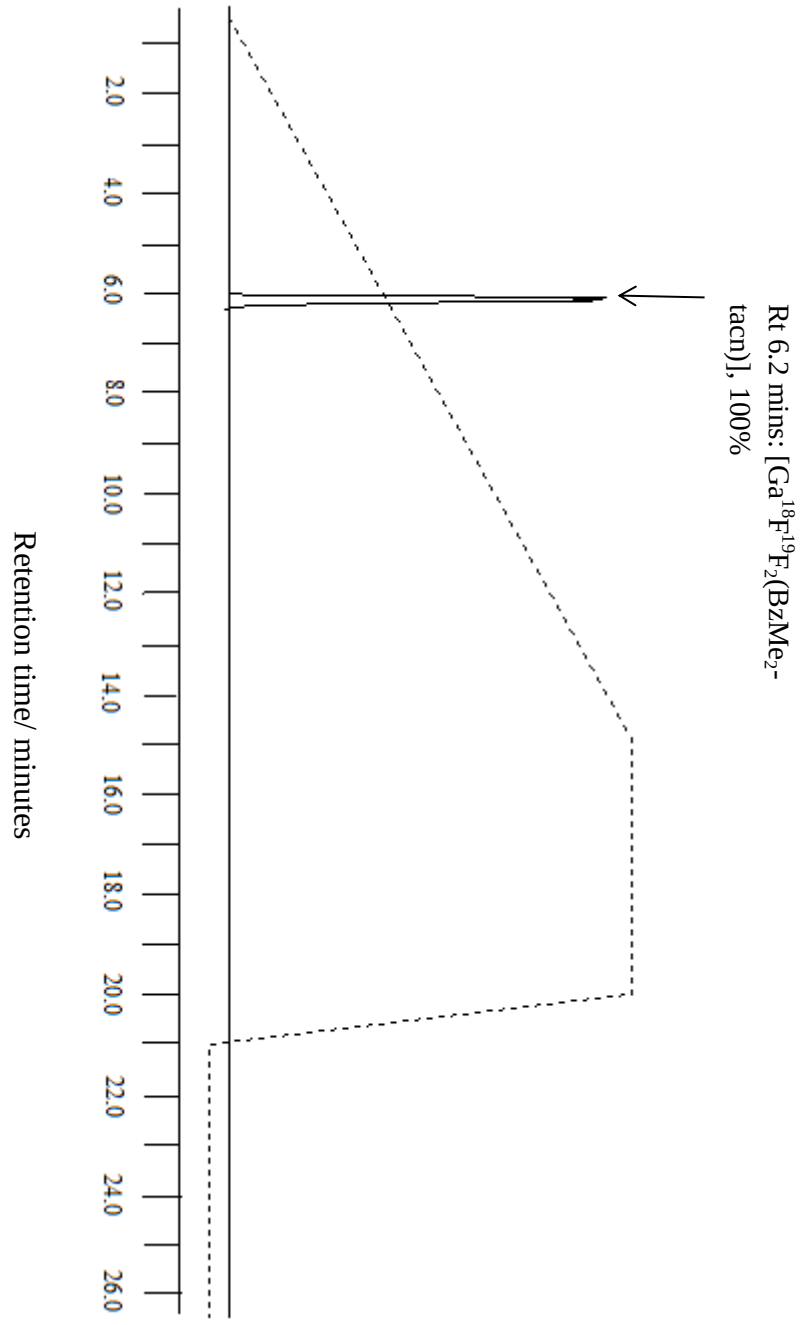

Figure 3.12: Analytical HPLC radio trace of the purified species formed in the labelling of $[GaCl_3(BzMe_2\text{-tacn})]$ with $^{18}F/K^{19}F$. Peak: Rt 6.2 mins. RCP = 100%.

To aid in unambiguously identifying whether the radiolabelled compound had formed, positive ion electrospray (ESI^+ MS) was used. ESI^+ MS analysis (MeCN/NH_4OAc mob phase) of the purified species post elution from the analytical HPLC gave an *m/z* and isotope pattern consistent with the species $\{[GaF_3(BzMe_2\text{-tacn})] + NH_4\}^+$ (*m/z* = 391; 100%) (Figures 3.13 and 3.14). The presence of associated $[NH_4]^+$ in these species was also confirmed from independent mass spectrometry experiments on the pure preformed $[GaF_3(BzMe_2\text{-tacn})]$ complex with and without added cation (see Chapter 5). Thus, introduction of one molar equivalent of $[NH_4][PF_6]$ leads to the appearance of a strong peak at *m/z* = 391.

This behaviour is attributed to the presence of the highly electronegative *facial* GaF_3 fragment which can form electrostatic and/or H-bonding interactions with the hard $[NH_4]^+$ cation introduced during the labelling experiments and HPLC analysis similar to the strong F····H–OH interactions to the associated water molecules observed crystallographically. There is also literature precedent for this behaviour in alkaline earth or lanthanide complexes of AsF_3 such as $[Ca(AsF_3)(AsF_6)_2]$, in which the pyramidal AsF_3 molecule behaves as a Lewis base, bonding to the metal cation via bridging fluorides (with further interactions between Ca^{2+} and the $[AsF_6]^-$ anions).[25-27] These unusual interactions are discussed further in Chapter 5.1.3.

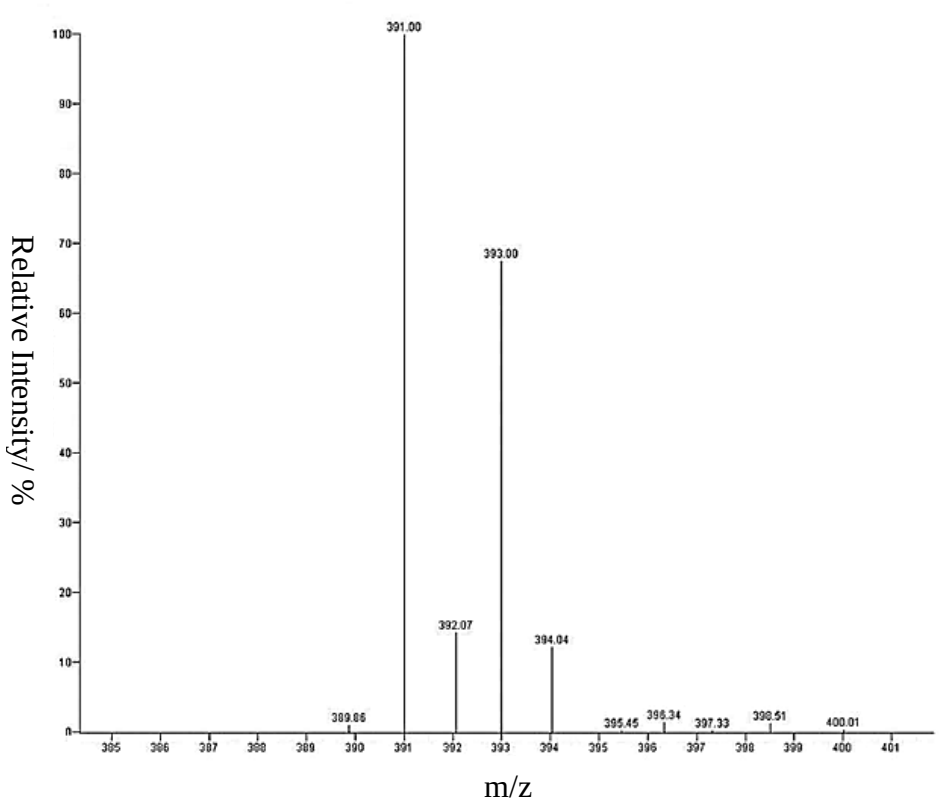

Figure 3.13: ESI^+ mass spectrum of $[GaF_3(BzMe_2\text{-tacn})] + NH_4]^+$ taken from radiolabelling reaction. Mobile phase = NH_4OAc/MeCN.

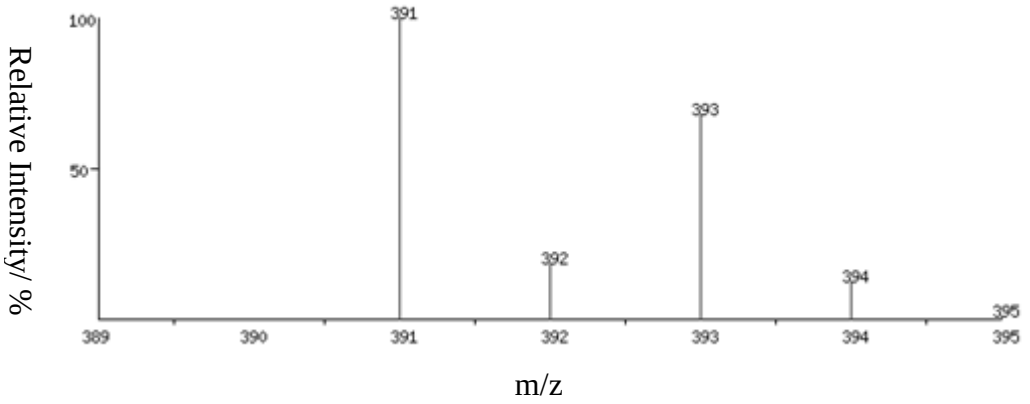

Figure 3.14: The predicted isotope pattern for $[GaF_3(BzMe_2\text{-tacn})] + NH_4]^+$.

A key experiment in the development of these compounds for imaging applications is the demonstration of the complexes stability in a formulation akin to physiological conditions. This is accomplished by formulating the purified product in a solvent regime in which the pH is buffered to 7.0 –7.5. Phosphate buffered saline (PBS) is the compound of choice in non-clinical development. The purified radio product was dried under vacuum (to remove the remaining MeCN) and treated with phosphate buffered saline (PBS) and ethanol, giving a formulation of 10% ethanol with pH 7.5. Subsequent analysis by analytical HPLC confirmed that the species was stable under these conditions for at least two hours. Figures 3.15 and 3.16 show the radiochemical purity (RCP) of the purified product remained high over this period (98–99% RCP). This shows that the radiolabelled complex is stable under physiological conditions and that the Ga-^{18}F in the complex is strongly bound.

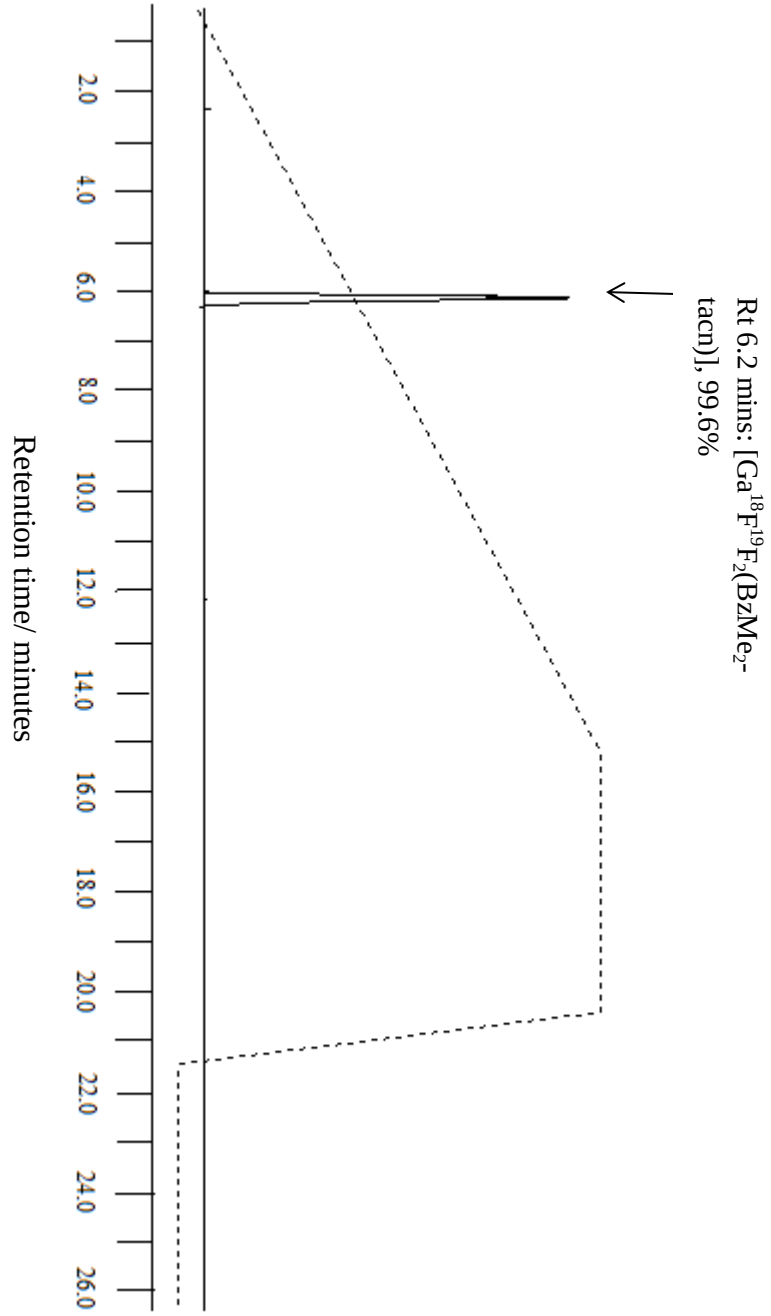

Figure 3.15: Analytical HPLC radio trace of [$Ga^{18}F^{19}F_2$($BzMe_2$-tacn)] formulated in PBS:EtOH (90:10) at t = 0. Peak: Rt 6.2 mins. RCP = 99.6%.

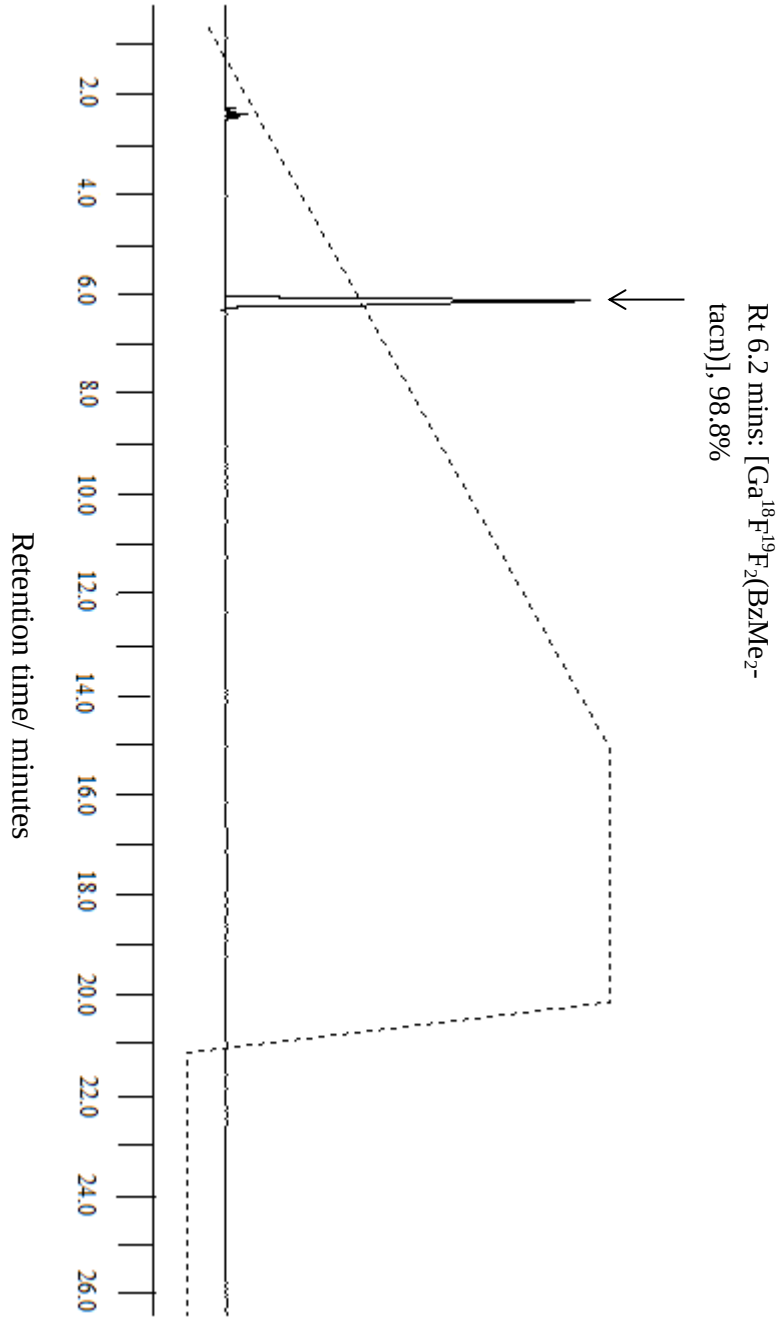

Figure 3.16: Analytical HPLC radio trace of [$Ga^{18}F^{19}F_2$($BzMe_2$-tacn)] formulated in PBS:EtOH (90:10) at t = 120 min. Peak: Rt 6.1 mins. RCP = 98.8%.

The stability of the labelled complex under physiological conditions was unexpected but a very positive result in terms of potential future labelling applications. The *facial* coordination of the three fluoride ligands may have left the metal centre exposed to attack from competing ions from the PBS solution. This implies that the Lewis acidic gallium centre is effectively able to bind the fluoride ligands even under strongly competing conditions. The use of the *facial* trifluoride moiety is a departure from the aluminium based ^{18}F agents developed recently by McBride and Jeong, in which only one site is available to bind the fluoride ligand.[28, 29]

3.3 Comparison of Work to Other Related Compounds

The work discussed within this chapter represents a completely different approach and in some areas a very significant improvement on the work pioneered by McBride *et al.* and others. The use of a well-defined preformed complex to perform the halide exchange reaction to access ^{18}F containing complexes allows more clarity on the speciation in solution to be sought. This shows the value of a coordination chemistry approach to the synthesis of ^{18}F labelled complexes *via* M-F chelation. While McBride and others show negligible incorporation of ^{18}F into the aluminium chelate at room temperature, the gallium complex may be labelled at room temperature with acceptable ^{18}F incorporation (30%). While the incorporation of ^{18}F is not as high as observed by McBride and others which shows > 95% incorporation when heated to 115 °C, the gallium complex [$Ga^{18}F^{19}F_2$($BzMe_2$-tacn)] discussed above may allow the labelling of temperature sensitive biomolecules. The need to exchange three chlorides for three fluorides required the need for KF as a carrier agent. The benzyl substituent on the $BzMe_2$-tacn ligand may be used as a tether in which a biomolecule could be attached to the chelate.

3.4 Conclusions and Future Work

The novel fluoride complexes [MF_3(Me_3-tacn)] (M = Ga, In) were synthesised *via* a chloride/fluoride exchange reaction using the NR_4F salt (R = Bu, Me) at room temperature. The halide exchange reaction was accomplished rapidly in the gallium system (5-10 minutes) while significantly slower in the indium system (45–60 minutes). The reaction does not occur in the aluminium system; no reaction occurs at room temperature, while heating results in the liberation of the ligand and the formation of the $[AlF_4]^-$ anion.

The difficulty in removing the NR_4Cl salt by-product from the reaction, and the preference in using an aqueous source of fluoride in any potential radiochemical reaction, resulted in the use of aqueous KF as the source of fluoride ligand in the exchange reaction. The complexes [MF_3(Me_3-tacn)] (M = Al, Ga, In) were successfully synthesised *via* a halide exchange reaction using aqueous KF at room temperature. The halide exchange reaction

proceeds rapidly in the gallium and aluminium systems, but slower in the indium system. The KCl by-product was more conveniently removed from the reaction mixture. Based upon this success, the novel complexes $[MF_3(BzMe_2\text{-tacn})]$ (M = Al, Ga, In) were synthesised *via* halide exchange of the chloride analogue using aqueous KF. The complexes were synthesised in good yield and fully characterised. The crystal structures of $[GaF_3(BzMe_2\text{-tacn})]\cdot 2H_2O$ and $[InF_3(BzMe_2\text{-tacn})]\cdot H_2O$ were obtained. The complexes display extensive H-bonding, forming supramolecular assemblies based upon F····O and O····O interactions.

The use of the aqueous salt $Ga(NO_3)_3\cdot 9H_2O$ as a potential route towards ^{18}F labelled compounds was investigated. The model complex $[GaF_3(Me_3\text{-tacn})]$ was synthesised using $Ga(NO_3)_3\cdot 9H_2O$ under aqueous conditions at room temperature. The formation of the complex was tracked using ^{71}Ga NMR spectroscopy. This presents an exciting alternative route towards ^{18}F labelled metal chelates, and may provide a more viable future route towards metal chelates with peptide functionality.

The complex $[GaCl_3(BzMe_2\text{-tacn})]$ was successfully radio-fluorinated with $K^{19}F/^{18}F$ at room temperature to form the complex $[Ga^{18}F^{19}F_2(BzMe_2\text{-tacn})]$. The complex is formed with 30% incorporation of ^{18}F into the complex. The compound was purified by HPLC and is shown to be stable under simulated physiological conditions (PBS, pH 7.5) for at least two hours – indicating that compounds of this type might be suitable for use *in vivo*. The compound was identified using ESI^+ mass spectrometry, which highlighted a potentially interesting property of the highly electronegative face of the metal trifluoride in the complexes. This property is discussed in more depth in Chapter 4. The radiolabelled compound is formed at room temperature, presenting the prospect of being able to use this chelate design to label temperature sensitive biomolecules, opening up a greater range of potential peptide based PET imaging agents. The work discussed here highlights the utility of the halide exchange approach – clean, rapid fluorination may be achieved from a defined precursor complex.

The unexpected success of the approach discussed, particularly the radiofluorination reaction, and the high stability of the labelled compound under simulated physiological conditions suggests that complexes of the form $[MF_3(R_3\text{-tacn})]$ might have real prospects of being used as agents in PET imaging. A potential future development to this chelate type is to attach a peptide to the benzyl substituent on the $BzMe_2$-tacn ligand. This would produce a 'bioactive' chelate which would present a more 'realistic' example to a potential PET imaging agent. Model peptide such as the human epidermal growth factor receptor (human epidermal growth factor receptor 2, HER2) peptide might be an effective choice as a 'bioactive' molecule in which to conduct the chemistry discussed above.[30]

The work conducted using the aqueous salt $Ga(NO_3)_3{\cdot}9H_2O$ as an alternative, more hydrolytically stable source of labile Ga(III) may be explored further, particularly with a peptide conjugated chelate, where sub milligram quantities of the gallium salt would be required.
The purification of the labelled complex $[Ga^{18}F^{19}F_2(BzMe_2\text{-tacn})]$ was performed using time consuming preparative HPLC, which uses a large volume of solvent. A future step might be to investigate methods of purification using a solid phase extraction (SPE) cartridge such as a hydrophilic lipophilic branched (HLB) cartridge. This would raise the prospect of being able to provide compounds of this type in kit form for clinical use.

3.5 Experimental

For full details of experimental methods and techniques see Appendix 1. The complexes $[MCl_3(RMe_2\text{-tacn})]$ (M = Al, Ga, In, R = Bz, Me) were synthesised as described in Chapter 2. NBu_4F (Sigma) was provided as a 1.0 $moldm^{-3}$ solution in thf and used as supplied under a dry N_2 atmosphere. NMe_4F (Sigma) was azeotropically distilled in benzene and dried under high vacuum at 150 ^oC.[3] The sample was stored and handled in the dry N_2 atmosphere of the glove box. $Ga(NO_3)_3{\cdot}9H_2O$ (Sigma) was used as supplied.

$[AlF_3(Me_3\text{-tacn})]{\cdot}3H_2O$:

A solution of KF (0.058 g, 0.99 mmol) in water (2 mL) was added to a suspension of $[AlCl_3(Me_3\text{-tacn})]$ (0.100 g, 0.33 mmol) in MeCN (5 mL) at room temperature. A white precipitate formed initially which redissolved into solution after a few minutes. The volatiles were removed *in vacuo*. The white solid was washed with 10 mL MeCN. The particulates were removed by filtration and the filtrate concentrated in vacuum. The product was precipitated as a white solid with Et_2O. Yield 0.06 g, 73%. Required for $C_9H_{27}N_3AlF_3O_3$: C, 34.95; H, 8.80; N, 13.58. Found: C, 34.60; H, 8.89; N, 14.66%. IR (Nujol, ν/cm^{-1}) 633, 613, 604 (Al-F). ^1H NMR (CD_3CN, 298 K) δ = 2.84-2.76 (m [6H] tacn-CH_2), 2.72-2.65 (m [6H] tacn-CH_2), 2.55 (s [9H] CH_3). ^{19}F NMR (CD_3CN, 298 K) δ = -176.1 (s). ^{27}Al NMR (CD_3CN, 298 K) δ = 19.0 (s).

$[GaF_3(Me_3\text{-tacn})]{\cdot}H_2O$

Method 1: A suspension of $[GaCl_3(Me_3\text{-tacn})]$ (0.050 g, 0.15 mmol) in 5 mL anhydrous MeCN was treated with KF (0.026 g, 0.45 mmol) in 2 mL H_2O. The resulting colourless solution was stirred at room temperature for 30 minutes. The volatiles were removed *in vacuo*. The white solid was washed with 10 mL MeCN and the undissolved particulates removed by filtration. The filtrate was concentrated under high vacuum giving a white solid. Yield 0.042 g, 90%. Anal. Required for $C_9H_{23}F_3GaN_3O$: C, 30.7; H, 7.7; N, 11.9. Found: C, 30.6; H, 6.9; N, 11.0%.

IR (Nujol, ν/cm^{-1}) 530, 492 (Ga-F). ^{1}H NMR (CD_3CN, 298 K) δ = 2.91-2.74 (m [6H], tacn-CH_2), 2.67 (m [9H], CH_3), 2.59-2.64 (m [6H] tacn-CH_2). $^{19}F\{^{1}H\}$ NMR (CD_3CN, 298 K) δ = -181.2 (br, qt). ^{71}Ga NMR (CD_3CN, 298 K) δ = 42.0 (qt), J_{Ga-F} 490Hz.

Method 2: [$GaCl_3$(Me_3-tacn)] (0.05 g, 0.15 mmol) was suspended in 5 mL anhydrous MeCN. The suspension was treated with NMe_4F (0.042 g, 0.45 mmol) and stirred at room temperature for one hour. The NMe_4Cl by-product was removed by filtration. The resulting colourless filtrate was concentrated *in vacuo* and treated with anhydrous Et_2O, resulting a white precipitate which was collected by filtration and dried *in vacuo.* Yield 0.037 g, 74%. Spectroscopy as for method 1.

Method 3: A suspension of [$GaCl_3$(Me_3-tacn)] (0.100 g, 0.30 mmol) was suspended in 5 mL anhydrous MeCN. NBu_4F (0.9 mL, 0.90 mmol) was added drop wise. This resulted in the rapid dissolution of the chloride precursor. The colourless solution was stirred at room temperature for one hour. The volatiles were removed *in vacuo* to give a pale yellow gum. The gum was dissolved in a minimum volume of MeCN (*ca.* 3 mL) and the solution exposed to air. Crystals of the target compound formed over time. These were isolated by filtration and dried under high vacuum. Yield 0.017 g, 28%. Spectroscopy as for method 1.

Method 4: $Ga(NO_3)_3{\cdot}9H_2O$ (0.100 g, 0.24 mmol) was dissolved in 5 mL H_2O. The colourless solution was treated with Me_3-tacn (0.041 g, 0.24 mmol). The pale yellow solution was stirred at room temperature for one hour. The solution was treated with KF (0.041 g, 0.72 mmol) and stirred for a further 30 minutes. The volatiles were removed *in vacuo* to give a very pale yellow solid. This was washed with 10 mL MeCN. The insoluble particulates were removed by filtration and the MeCN solvent removed *in vacuo.* Pale yellow solid. Yield 0.089 g, 74%. Spectroscopy as for Method 1.

[InF_3(Me_3-tacn)]· H_2O

Method 1: As for [GaF_3(Me_3-tacn)] method 1 using [$InCl_3$(Me_3-tacn)] (0.060 g, 0.17 mmol) and KF (0.029 g, 0.51 mmol). White solid. Yield 0.044 g, 76%. Anal. Required for $C_9H_{23}F_3InN_3O$: C, 29.9; H, 6.4; N, 11.6. Found: C, 29.9; H, 6.1; N, 11.5%. IR (Nujol, ν/cm^{-1}) 478, 462, 443 (In-F) cm^{-1}. ^{1}H NMR (CD_3CN, 298 K) δ = 3.17 (m, br [6H] tacn-CH_2), 3.00 (m, br [9H] CH_3), 2.72 (m, br [6H] tacn-CH_2). $^{19}F\{^{1}H\}$ NMR (CD_3CN, 298 K) δ = -215 (br, m), $W_{1/2}$ = 1100 Hz. (273K) δ -215 (br, m), $W_{1/2}$ = 900 Hz. (223K) δ -213 (br, m), $W_{1/2}$ = 1600 Hz. ^{115}In NMR (87 MHz, CD_3CN, 298 K) δ = 67.3 (qt), J_{In-F} 598 +/- 5 Hz.

Method 2: As for [GaF_3(Me_3-tacn)] method 2 using [$InCl_3$(Me_3-tacn)] (0.060 g, 0.17 mmol) and NMe_4F (0.047 g, 0.51 mmol). White solid. Yield 0.044 g, 76%. Spectroscopy as for method 1.

Method 3: As for [GaF_3(Me_3-tacn)] method 3 using [$InCl_3$(Me_3-tacn)] (0.214 g, 0.54 mmol) and NBu_4F (1.63 mL, 1.63 mmol). White-yellow solid. Yield 0.075 g, 35%. Spectroscopy as for method 1.

[AlF_3(BzMe_2-tacn)]·H_2O

Method as for [AlF_3(Me_3-tacn)] using [$AlCl_3$(BzMe_2-tacn)] (0.050 g, 0.130 mmol) and KF (0.023 g, 0.39 mmol). White solid. 0.035 g, 82%. IR (Nujol, ν/cm^{-1}) 3392 br (OH), 1665 (H_2O), 1639 (Bz aromatic CC), 635, 601 [Al–F]. ^{1}H NMR (CD_3CN, 298 K): δ = 7.62 (m, [5H], ArH), 4.26 (s, [2H], Ar-CH_2), 3.01 (m, [4H], tacn-CH_2), 2.89 (m, [4H], tacn-CH_2), 2.85 (s, [6H], CH_3), 2.74 (m, [4H], tacn-CH_2), 1.53 (br s, H_2O). ^{19}F{^{1}H} NMR (CD_3CN, 298 K) δ = –161.5 (F), –161.7 (2F). ^{27}Al NMR (CD_3CN, 298 K) δ = 19.8 (br s), $W_{1/2}$ 100 Hz.

[GaF_3(BzMe_2-tacn)]·2H_2O

Method as for [GaF_3(Me_3-tacn)] method 1 using [$GaCl_3$(BzMe_2-tacn)] (0.050 g, 0.10 mmol) and KF (0.017 g, 0.03 mmol). White solid. Yield 0.033 g, 70%. Required for $C_{15}H_{33}F_3GaN_3O_4$: C, 40.4; H, 8.8; N, 8.6. Found C, 40.9; H, 8.8; N, 8.6%. IR (Nujol, ν/cm^{-1}) 3390, 1654 (H_2O) 526, 515 (Ga–F).^{1}H NMR (CD_3CN, 298 K): δ = 7.30 (m, [5H], ArH), 4.73 (s, [2H], Ar-CH_2), 3.17 (m, [4H], tacn-CH_2), 2.88 (m, [4H], tacn-CH_2), 2.73 (s, [6H], CH_3), 2.36 (m, [4H], tacn-CH_2), 2.25 (s, H_2O). ^{19}F{^{1}H} NMR (CD_3CN, 298 K) δ = -172.8 (s, br). ^{71}Ga NMR (CD_3CN, 298 K) δ = 44.9 (m, br).

[InF_3(BzMe_2-tacn)]·H_2O

Method as for [GaF_3(Me_3-tacn)] method 1 using [$InCl_3$(BzMe_2-tacn)] (0.060 g, 0.10 mmol) and KF (0.017 g, 0.30 mmol). White solid. Yield 0.029 g, 69%. Required for $C_{15}H_{31}F_3InN_3O_3$: C, 38.1; H, 6.6; N, 8.9. Found C, 37.6; H, 5.2; N, 8.6%. IR (Nujol, ν/cm^{-1}) 3450 v br (H_2O), 1651 (H_2O), 481, 463 (In–F). ^{1}H NMR (CD_3CN, 298 K) δ = 7.37 (m, [5H], ArH), 4.37 (s, [2H], Ar-CH_2), 3.08 (m, [6H], CH_3), 2.91 (m, [4H], tacn-CH_2), 2.80 (m, [4H], tacn-CH_2), 2.64 (m, [4H], tacn-CH_2). ^{19}F{^{1}H} NMR (CD_3CN, 298 K) δ = -220 (s, br). ^{115}In NMR (CD_3CN, 298 K) no resonance observed.

^{18}F Radiolabelling of [$GaCl_3$(BzMe_2-tacn)]

Experiments were analysed on a Gilson 322 HPLC system with a Gilson 156 UV detector. Dionex Chromeleon 6.8 Chromatography data recording software was used to integrate the UV and radiochemical peak areas. Preparative HPLC: Luna 5µ C18(2) 100 x 10 mm (Mobile phase A = 100% water; B = 100% MeCN). Flow rate 3 mL/min. Gradient 0 to 5 min. (10% B), 5–20 min. (10–90% B), 20–25 min. (90% B), (10% B).

Analytical HPLC: Luna 5µ C18(2) 250 x 4.6 mm (Mobile Phase A = 10 mM ammonium acetate, B = 100% MeCN). Flow rate 1 mL/min. Gradient 0–15 min (10–90% B), 15–20 min (90% B), 20–21 min (90–10% B), 21–26.5 (10% B).

ESI^+ mass spectra were recorded from direct injection of the products onto a Thermo Finnigan mass spectrometer fitted with an LCQ advantage MS pump.

Procedure: In a typical experiment [$GaCl_3$($BzMe_2$-tacn)] (0.001 g, 2.36 μmol) was dissolved in a mixture of MeCN (0.5 mL) and H_2O (0.1 mL). This solution was added to 0.4 mL of an aqueous solution containing [^{18}F] KF (100 to 500 MBq) and [^{19}F] KF (7.05 μmol) and the vial was allowed to stand at room temperature for 30 to 60 minutes. The crude reaction solution was diluted with water so that approximately 10% of the solvent composition was organic. Preparative HPLC on the diluted crude reaction solution confirmed *ca.* 30% incorporation of ^{18}F into the metal complex (based upon integration of the radio peaks) after one hour. Peak 1: Rt = 2.2 mins. ($^{18}F^-$). Peak 2: Rt = 9.0 mins. (complex). The MeCN was then removed in vacuo and the product was made up with PBS and ethanol to give a ca. 10% ethanol final product (pH 7.2). Peak 2 was run through an analytical HPLC system giving a single radio and UV peak at Rt 6.2 mins. (RCP 99%).

Peak 2: ESI^+ MS (MeCN/NH_4OAc): found *m/z* = 354 [GaF_2($BzMe_2$-tacn)]$^+$; 391 [GaF_3($BzMe_2$-tacn) + NH_4]$^+$. The product is stable to chemical and radiochemical degradation for at least two hours in phosphate buffered saline and ethanol.

Table 3.2: Crystallographic data for complexes discussed in Chapter 3.[a]

Compound	**$[GaF_3(BzMe_2\text{-tacn})]\cdot 2H_2O$**	**$[InF_3(BzMe_2\text{-tacn})]\cdot 1H_2O$**
Formula	$C_{15}H_{29}F_3GaN_3O_2$	$C_{15}H_{27}F_3InN_3O_{1.20}$
M / g mol^{-1}	410.13	440.42
Temp. / K	100	100
Crystal system	Orthorombic	Monoclinic
Space group	Pbca (no. 61)	$P2_1/c$ (no. 14)
a [Å]	9.615(5)	6.7721(10)
b [Å]	13.012(5)	13.666(3)
c [Å]	29.571(5)	18.998(3)
α [deg]	90	90
β [deg]	90	96.106(10)
γ [deg]	90	90
U [Å^3]	3700 (2)	1748.2(5)
Z	8	4
μ(Mo Kα) [mm^{-1}]	1.529	1.389
F(000)	1712	898
Total reflections	17074	23249
Unique reflections	4227	4005
R_{int}	0.109	0.028
R_1 [$I_o > 2\sigma(I_o)$] [b]	0.056	0.022
R_1 [all data]	0.113	0.025
wR_2 [$I_o > 2\sigma(I_o)$] [b]	0.149	0.046
wR_2 [all data]	0.124	0.048

[a] Common items: temperature = 100 K; wavelength (Mo-K_α) = 0.71073 Å;

[b] $R_1 = \Sigma \big| \, |F_o| - |F_c| \, \big| / \Sigma |F_o|$; $wR_2 = [\Sigma w(F_o^2 - F_c^2)^2 / \Sigma w F_o^4]^{1/2}$

3.6 References

1. Sharma, R. K.; Fry, J. L., *J. Org. Chem.* **1983,** *48*, 2112-2114.
2. Sun, H.; DiMagno, S. G., *J. Am. Chem. Soc.* **2005,** *127*, 2050-2051.
3. Christe, K. O.; Wilson, W. W.; Wilson, R. D.; Bau, R.; Feng, J. A., *J. Am. Chem. Soc.* **1990,** *112*, 7619-7625.
4. Dimitrov, A.; Heidemann, D.; Kemnitz, E., *Inorg. Chem.* **2006,** *45*, 10807-10814.
5. D'Souza, C. A.; McBride, W. J.; Sharkey, R. M.; Todaro, L. J.; Goldenberg, D. M., *Bioconjugate Chem.* **2011,** *22*, 1793-1803.
6. McBride, W. J.; D'Souza, C. A.; Karacay, H.; Sharkey, R. M.; Goldenberg, D. M., *Bioconjugate Chem.* **2012,** *23*, 538-547.
7. McBride, W. J.; D'Souza, C. A.; Sharkey, R. M.; Karacay, H.; Rossi, E. A.; Chang, C.-H.; Goldenberg, D. M., *Bioconjugate Chem.* **2010,** *21*, 1331-1340.
8. McBride, W. J.; Goldenberg, D. M.; Sharkey, R. M., *J. Nucl. Med* **2014,** *55*, 1043-1054.
9. McBride, W. J.; Sharkey, R. M.; Karacay, H.; D'Souza, C. A.; Rossi, E. A.; Laverman, P.; Chang, C.-H.; Boerman, O. C.; Goldenberg, D. M., *J. Nucl. Med.* **2009,** *50*, 991-998.
10. Herron, N.; Thorn, D. L.; Harlow, R. L.; Davidson, F., *J. Am. Chem. Soc.* **1993,** *115*, 3028-3029.
11. Shannon, R. D., *Acta Cryst., Sect. A.* **1976,** *A32*, 751-767.
12. Fuoss, R. M., *J. Am. Chem. Soc.* **1958,** *80*, 5059-5061.
13. Garrison, J. M.; Crumbliss, A. L., *Inorg. Chem.* **1987,** *26*, 3660-3664.
14. Secco, F.; Venturini, M., *Inorg. Chem.* **1975,** *14*, 1978-1981.
15. Lo, S. T. D.; Swaddle, T. W., *Inorg. Chem.* **1975,** *14*, 1878-1881.
16. Jin, X.; Qian, Z.; Lu, B.; Bi, S., *Dalton Trans* **2011,** *40*, 567-572.
17. Smith, G. E.; Sladen, H. L.; Biagini, S. C. G.; Blower, P. J., *Dalton Trans* **2011,** *40*, 6196-6205.
18. Plankey, B. J.; Patterson, H. H., *Inorg. Chem.* **1989,** *28*, 4331-4333.
19. Goldenberg, D. M.; Sharkey, R. M.; McBride, W. J.; Boerman, O. C., *J. Nucl. Med.* **2013,** *54*, 1170-1173.
20. Luo, Y.-R., *Handbook of Chemical Bond Energies*. CRC Press: 2007.
21. Mason., J., *Multinuclear NMR*. Plenum Press: 1987; Vol. 1.
22. http://www.fda.gov/downloads/drugs/guidancecomplianceregulatoryinformation/guidances/ucm291573.pdf.
23. Weyhermüller, T.; Wieghardt, K., *Chem. Commun.* **1998**, 557-558.
24. Carty, A. J.; Tuck, D. G., *Prog. Inorg. Chem.* **1975,** *19*, 245-337.
25. Tramšek, M.; Zemva, B., *J. Fluorine Chem.* **2006,** *127*, 1275-1284.
26. Tramšek, M.; Benkič, P.; Turičnik, A.; Tavčar, G.; Žemva, B., *J. Fluorine Chem.* **2002,** *114*, 143-148.

27. Tramšek, M.; Žemva, B., *J. Fluorine Chem.* **2004,** *125*, 1919-1924.
28. Laverman, P.; McBride, W. J.; Sharkey, R. M.; Goldenberg, D. M.; Boerman, O. C., *J. Labelled Compd. Radiopharm.* **2014,** *57*, 219-223.
29. Shetty, D.; Choi, S. Y.; Jeong, J. M.; Lee, J. Y.; Hoigebazar, L.; Lee, Y.-S.; Lee, D. S.; Chung, J.-K.; Lee, M. C.; Chung, Y. K., *Chem. Commun.* **2011,** *47*, 9732-9734.
30. Glaser, M.; Iveson, P.; Hoppmann, S.; Indrevoll, B.; Wilson, A.; Arukwe, J.; Danikas, A.; Bhalla, R.; Hiscock, D., *J. Nucl. Med.* **2013,** *54*, 1981-1988.

Chapter 4

Synthesis, Characterisation and Radiolabelling of Gallium Chelates with Carboxylate Functionality

4.1 Introduction

The dicarboxylate pendant arm macrocycle 1,4,7-triazacyclononane-1,4-dicarboxylate (NODA) is a ligand used ubiquitously throughout the area of medical imaging. It has seen use in a number of metal chelate based imaging agents.[1-4]

Having shown in Chapter 3 that the method of halide exchange from a well-defined metal chloride precursor may be accomplished successfully under radiochemical conditions, this class of ligand was sought as a route to further improve the labelling reactions using Group 13 metal halide complexes.

The rationale behind this particular chelate design is derived from certain requirements which were identified in the labelling reactions with the neutral R_3-tacn complexes discussed in Chapters 2 and 3.

The anionic pendant arms on the macrocycle result in a pentadentate N_3O_2 donor set. The pentadentate ligand provides both a macrocyclic and chelate effect to promote robust coordination to a metal centre, resulting in kinetically inert complexes. The formation of a salt by-product should provide a further driving force for coordination.

The pentadentate coordination will mean that on a suitably sized metal, such as the Group 13 metals aluminium, gallium and indium, which depending on the ligand donor atom type, may adopt six-coordinate octahedral coordination modes, a single site will be available for halide coordination.[5] This should allow for 'cleaner' halide exchange, and raises the possibility of performing any potential radio chemical experiments without the need for a non ^{18}F containing carrier agent.

The benzyl substituent provides the same spectroscopic and future post synthetic modification role as described in Chapter 2.[6]

The 1-benzyl-1,4,7-triazacyclononane-4,7-dicarboxylate dilithium salt (Li_2L) was developed by Wieghardt *et al.* as a pentadentate ligand in the coordination chemistry of Fe(III) complexes containing chloro, azido and oxo ligands (Figure 4.1).[7]

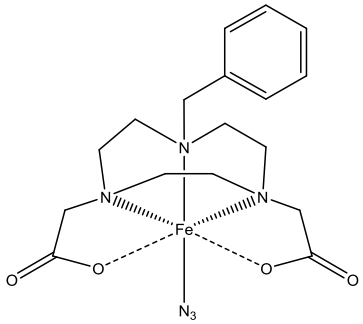

Figure 4.1: The Fe(III) azido complex synthesised be Wieghardt *et al.* using the benzyl-dicarboxylate tacn ligand motif.

The ligand 1-benzyl-1,4,7-triazacyclononane-4,7-dicarboxylic acid ($H_2L{\cdot}HCl$) has already been employed by Jeong *et al.*[8] using a modified method of the work pioneered by McBride *et al.*[6] They found that the Al-^{18}F complex was formed in high radiochemical yield when the ligand $H_2L{\cdot}HCl$ was heated with $AlCl_3{\cdot}6H_2O$ in the presence of $Na^{18}F$ in NaOAc pH 4. A crystal structure of the Al-F chelate was obtained by recrystallisation of a an H_2O/EtOH solution of the HPLC purified complex (Figure 4.2).[8] The structure depicts a distorted octahedral Al(III) centre with the pentadentate tacn ligand coordinated through 3 N-donor atoms from the tacn ring and 2 O-donor atoms from the carboxylate groups. The coordination sphere is completed by a terminal fluoride ligand. The complex crystallises as a dihydrate, which displays extensive H-bonding to the carbonyl groups on the carboxylate pendant arms. The aromatic pendant arm does not show any pi-stacking, suggesting the packing is dominated by the H-bonding interactions.

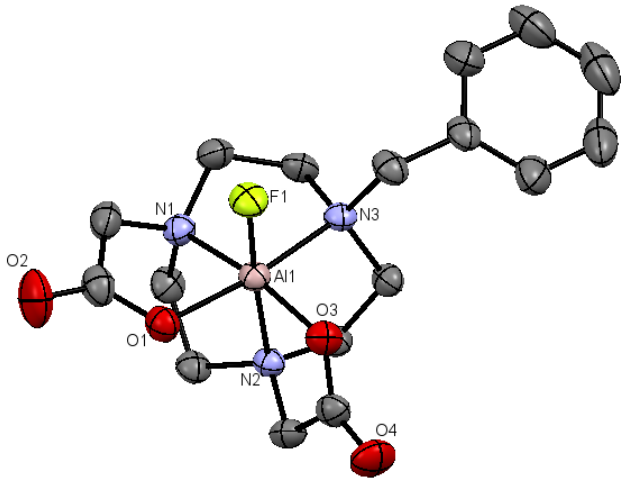

Figure 4.2: Crystal structure of $[AlF(Bz(CH_2CO_2)_2\text{-tacn})]{\cdot}2H_2O$ obtained by Jeong et al.[8] H-atoms and lattice water molecules are omitted for clarity. Image redrawn from CCDC 813724.

McBride has found the NODA based chelates to be the ligand framework of choice in his pioneering Al-^{18}F work,[9-11] of particular interest in the context of the work presented in this chapter is the use of a methylphenylacetic acid (MPAA) pendant group[12]. A crystal structure of the Al-F containing complex was obtained by recrystallization of the complex from H_2O/MeOH (Figure 4.3). Like the corresponding compound isolated by Jeong, the structure depicts a distorted Al(III) centre with the ligand acting as a pentadentate donor towards the metal centre. The coordination sphere is completed by a terminal fluoride ligand. The complex crystallises as a dihydrate, which displays extensive H-bonding not only to the carbonyl groups on the carboxylate pendant arms, but also the hydroxide group on the MPAA pendant arm to create an extensive H-bonded network. The aromatic groups display slipped pi-stacking, likely a consequence of the requirement to accommodate the MPAA pendant group.

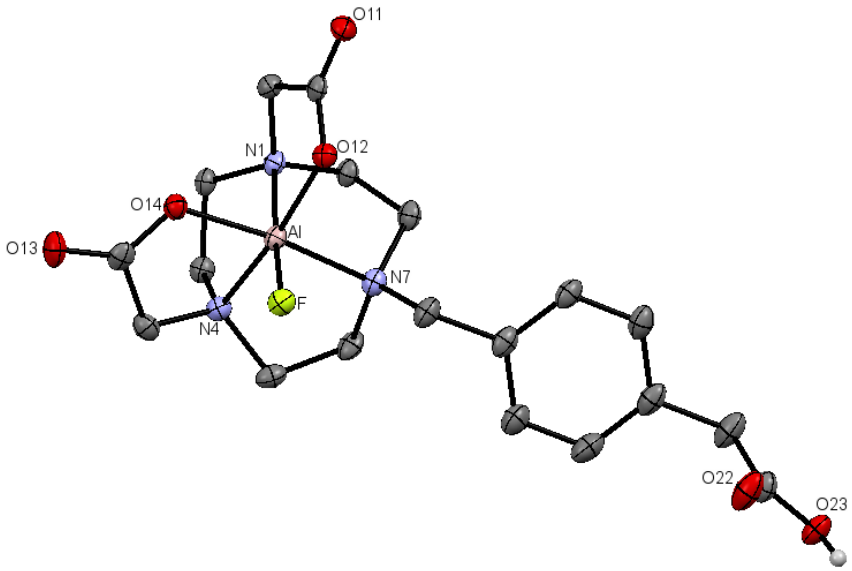

Figure 4.3: Crystal structure of [AlF(MPPA(CH_2CO_2)$_2$-tacn)]·2H_2O obtained by McBride *et al*.[6] H-atoms on the tacn ligand and lattice water molecules are omitted for clarity. Image redrawn from CCDC 859830.

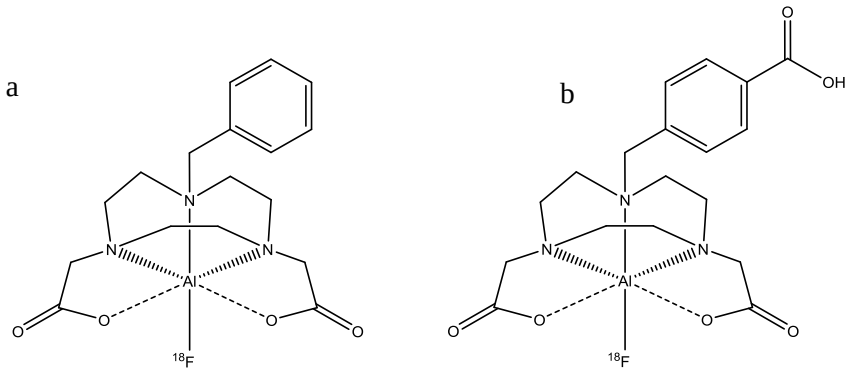

Figure 4.4: Representations of the Al-^{18}F complexes utilised by Jeong (a) and McBride (b) based upon the benzyl-dicarboxylate tacn systems.[6, 8]

The Al-^{18}F complexes synthesised by both groups were found to be stable when formulated in PBS (phosphate buffered saline, pH = 7.4) or HSA (human serum albumin, pH = 7.5).

While aluminium is the metal favoured by McBride and Jeong, the work with the neutral R_3-tacn chelates hinted that gallium offers a number of potential advantages over the aluminium analogue. These include the stability of the pre-formed gallium chelate and the ability to perform radiolabelling experiments at room temperature.

Therefore a route to synthesise and characterise a well-defined, stable '[GaX(L)]' chelate which could then be ^{18}F radiolabelled under mild conditions to the corresponding [Ga^{18}F(L)] complex was sought.

This chapter discusses the preparation and radiolabelling of a preformed gallium chloride chelate complex using the anionic ligand 1-benzyl-1,4,7-triazacyclononane-4,7-dicarboxylate (L) on a nano molar scale under aqueous conditions. The [GaCl(L)] precursor was synthesised via reaction of the ligand $H_2L{\cdot}HCl$ with the stable aqueous salt $Ga(NO_3)_3{\cdot}9H_2O$. The complex [GaF(L)] was synthesised under hydrothermal conditions using Li_2L and $GaF_3{\cdot}3H_2O$. The details of the synthesis and characterisation of the complexes is described and the relative stability of them is discussed.

The halide exchange was performed on a preparative scale under aqueous conditions at room temperature and with heating. The details of the exchange reactions are shown, and the conclusions drawn from this informed us of the conditions required for the subsequent radiolabelling reactions.

The radiolabelling reactions are described and the attempts to purify, characterise and understand the stability of the resulting labelled species [Ga^{18}F(L)] is discussed and placed into context in comparison to the related aluminium containing complexes utilised by Jeong and McBride. Future development paths for this ligand framework are also shown.

4.2 Results and Discussion

4.2.1 Ligand synthesis

The ligand system employed in this chapter was the functionalised tacn ligand 1-benzyl-1,4,7-triazacyclononane-4,7-dicarboxylate ($Bz(CH_2CO_2)_2$-tacn, L). The ligand was synthesised as both the carboxylic acid ($H_2L{\cdot}HCl$)[8] and the dilithium salt (Li_2L), as shown in Figure 4.5.[7, 13]

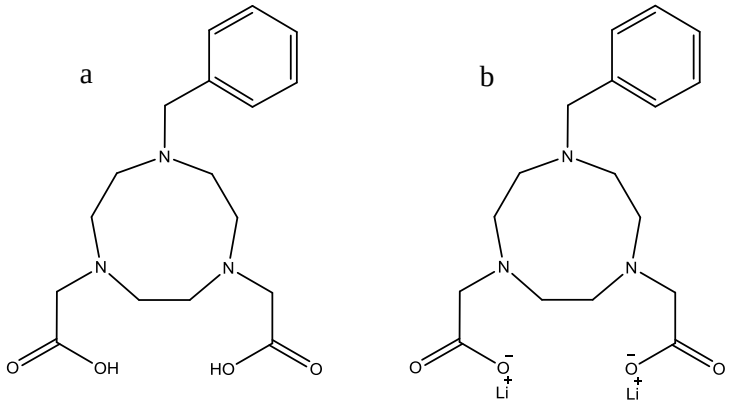

Figure 4.5: The ligands employed in this work, H_2L (a) and Li_2L (b).

The ligands were synthesised in a moderate yield (61 %) from the tacn free base over five steps (Figure 4.6). The synthesis proceeds through a selective protection of two of the tacn amines using the BOC protecting group. This allows the addition of the benzyl group into the free position. Following deprotection and esterification of the remaining tacn amine positions, a simple ester hydrolysis reaction affords the carboxylate functionalised ligand as air stable solids. The carboxylic acid was synthesised as an HCl salt, as the hydrolysis step was performed in an excess of HCl. The presence of the chloride would become of importance as the work progressed.

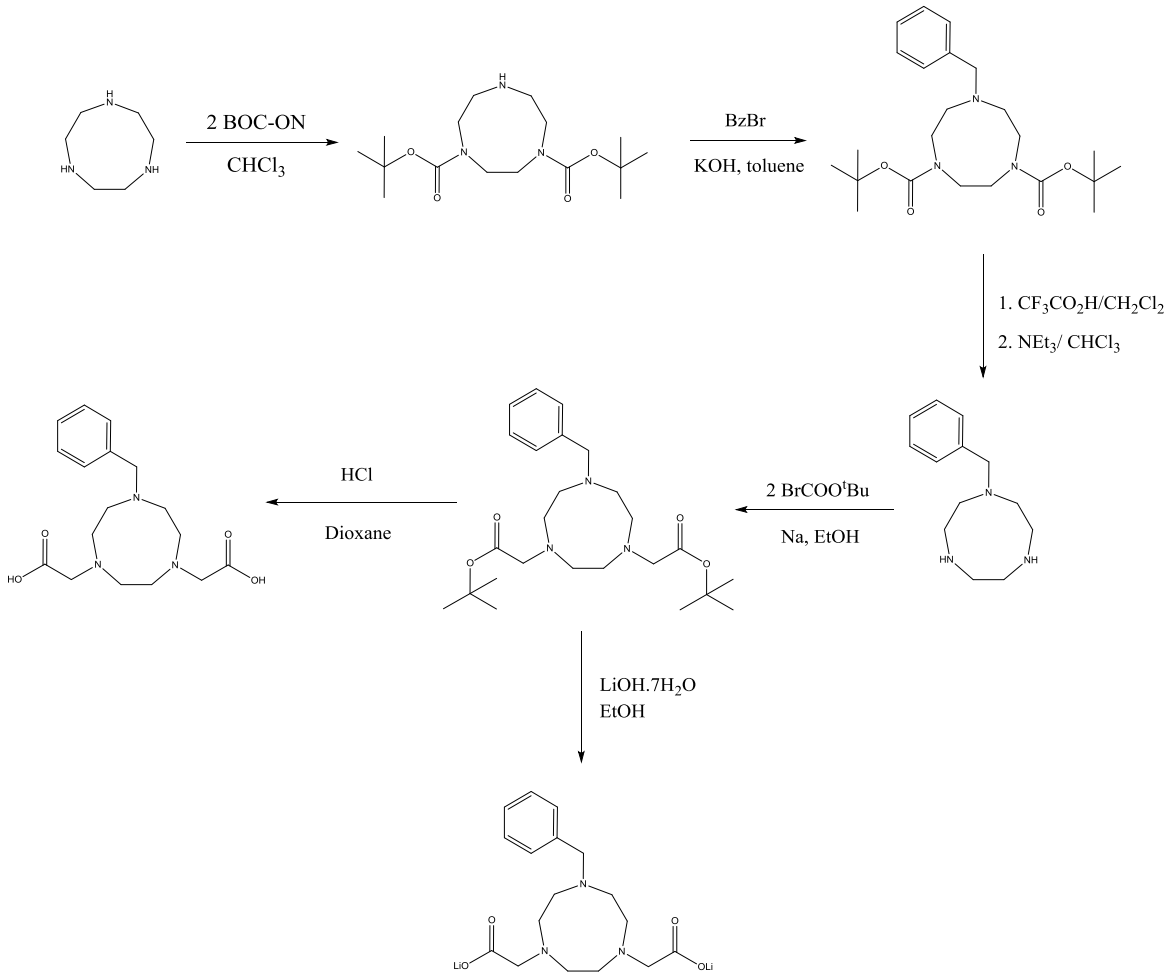

Figure 4.6: Synthetic scheme towards the ligands $H_2L{\cdot}HCl$ and Li_2L.

4.2.2 Synthesis of [GaCl(L)]

The success of the room temperature halide exchange reaction of the preformed [$MCl_3(R_3$-tacn)] complexes in aqueous solution prompted further work to determine whether the same general method could be employed with the dicarboxylate pendant arm ligand.

Preparation of the precursor complex was initially undertaken *via* reaction of the moisture sensitive solid $GaCl_3$ in anhydrous MeCN with a solution of the lithium salt Li_2L in anhydrous MeOH yielding a yellow-orange crude solid which was very poorly soluble in common solvents (H_2O, MeOH, MeCN). The LiCl formed, while providing the driving force for complexation, proved very difficult to remove from the crude reaction mixture. Furthermore, the use of $GaCl_3$, which is both very readily hydrolysed and reactive, as the source of the Ga–Cl unit in the product was undesirable considering the goal to be able to create and radio-label sub 1 milligram quantities of the pre-formed complex for imaging.

An alternative source of Ga(III) was sought which would be better suited for use in aqueous solution. The commercially available salt $Ga(NO_3)_3 \cdot xH_2O$ was identified as a potentially suitable precursor. The salt has been identified as a nona-hydrate in the solid state[14] and exists as the labile $[Ga(OH_2)_6][NO_3]_3$ in aqueous solution.

Reaction of $Ga(NO_3)_3 \cdot 9H_2O$ with one molar equivalent of $H_2L \cdot HCl$ on a preparative scale in aqueous solution gives a yellow solid after work up. The solid was recrystallised from $MeCN/Et_2O$ to remove 'inorganic' impurities. The chelation reaction is slow at room temperature in concentrated solution (*ca.* 12 h), but proceeds significantly faster at 85 °C. The reaction may also be performed in refluxing MeOH, from which the desired product precipitates as a pale yellow/white solid upon rapid ice cooling. It is stable for many months in the solid state, and the ^1H NMR spectrum (D_2O) is unchanged after four weeks in solution. The complex is soluble in H_2O, MeCN and is poorly soluble in chlorocarbons.

Spectroscopic data was consistent with the formulation [GaCl(L)]. The ^1H NMR spectrum (in D_2O) of the [GaCl(L)] is significantly shifted and more complex than that of the $H_2L \cdot HCl$. The benzylic protons are split into an AB quartet ($^2J_{HH}$ = 13.7 Hz) indicating the tacn-dicarboxylate ligand is locked by N_3O_2 coordination, leading to diastereotopic inequivalence of the CH_2 protons in the benzyl groups. The tacn CH_2 protons also appear as second order multiplets (Figure 4.7). While attempts were made to collect a ^{71}Ga NMR spectrum, the low symmetry of the complex, coupled with the quadrupolar nature of the ^{71}Ga centre meant that the resonances were too broad, and therefore no peak was observed.[15]

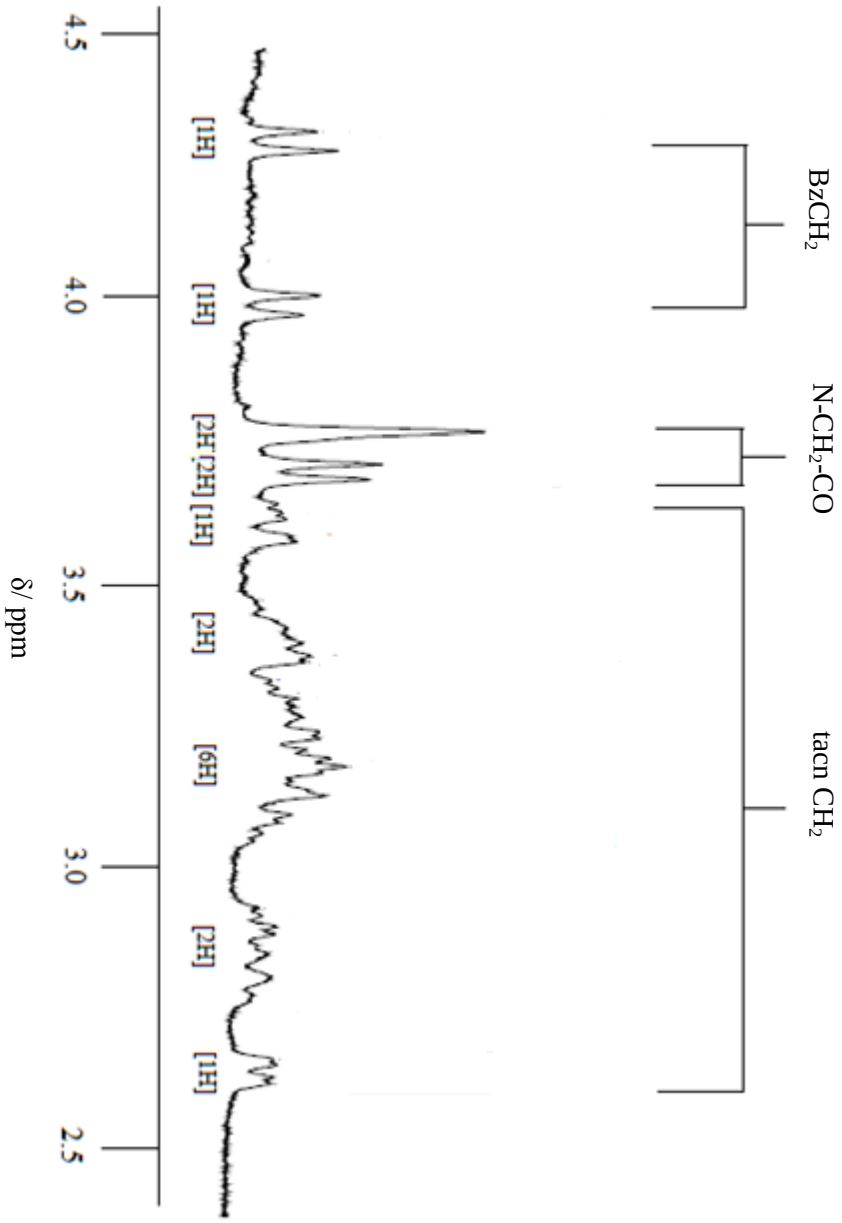

Figure 4.7: Expanded ^{1}H NMR spectrum of the tacn ligand environment in [GaCl(L)] depicting the complex tacn proton environments and the benzyl AB quartet derived from the coordination of the ligand to the metal centre. Aromatic groups are not displayed

ESI^{+} mass spectrometry gave a parent cation at *m/z* = 402.1 (100%), with an associated $^{69/71}$Ga isotope pattern, corresponding to the monocation, $[Ga(L)]^{+}$.

The infra-red spectrum showed the expected carboxylate CO bands of the ligand were shifted to low frequency by *ca.* 50 cm^{-1} *cf.* $H_2L{\cdot}HCl$ itself. The spectrum also showed a Ga−Cl stretching vibration (375 cm^{-1}) and evidence for H-bonded water (ν(OH) = 3750, δ(HOH) = 1648 cm^{-1}). On the basis of these data it was concluded that the $[NO_3]^{-}$ groups from the

$Ga(NO_3)_3 \cdot 9H_2O$ precursor were not retained in the product, being replaced by the two carboxylate pendant arms of the macrocycle and one chloride ligand, the latter derived from the $H_2L \cdot HCl$, in the distorted octahedral complex.

The proposed formulation $[GaCl(L)] \cdot 2H_2O$ was confirmed by elemental analysis. This was further confirmed *via* an X-ray crystal structure determination on a very weakly diffracting crystal obtained by slow evaporation from an MeCN solution of $[GaCl(L)] \cdot 2H_2O$ (Figure 4.8).

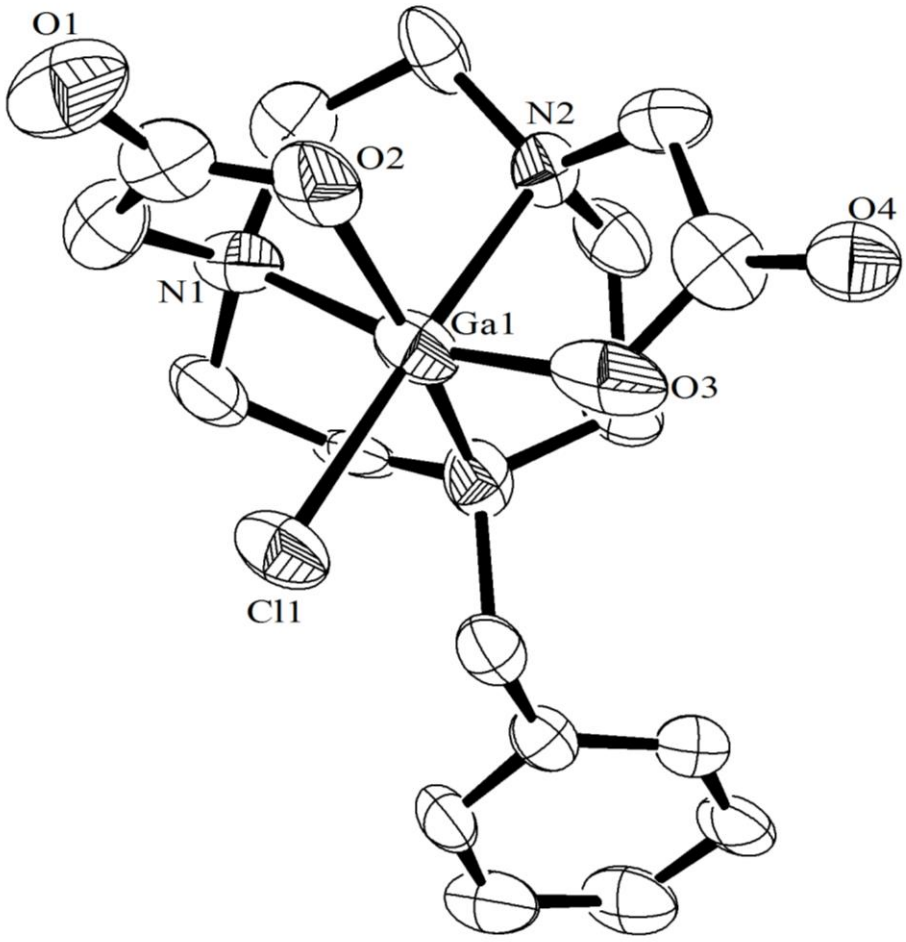

Figure 4.8: ORTEP representation of the crystal structure of $[GaCl(L)] \cdot 2H_2O$ with atom numbering scheme. H-atoms and lattice waters are omitted for clarity. Ellipsoids drawn at 50% probability level. Ga1−Cl1 2.266(4), Ga1−O2 1.888(13), Ga1−O4 2.010(11), Ga1−N1 2.122(11), Ga1−N2 2.094(13), Ga1−N3 2.147(13) Å.

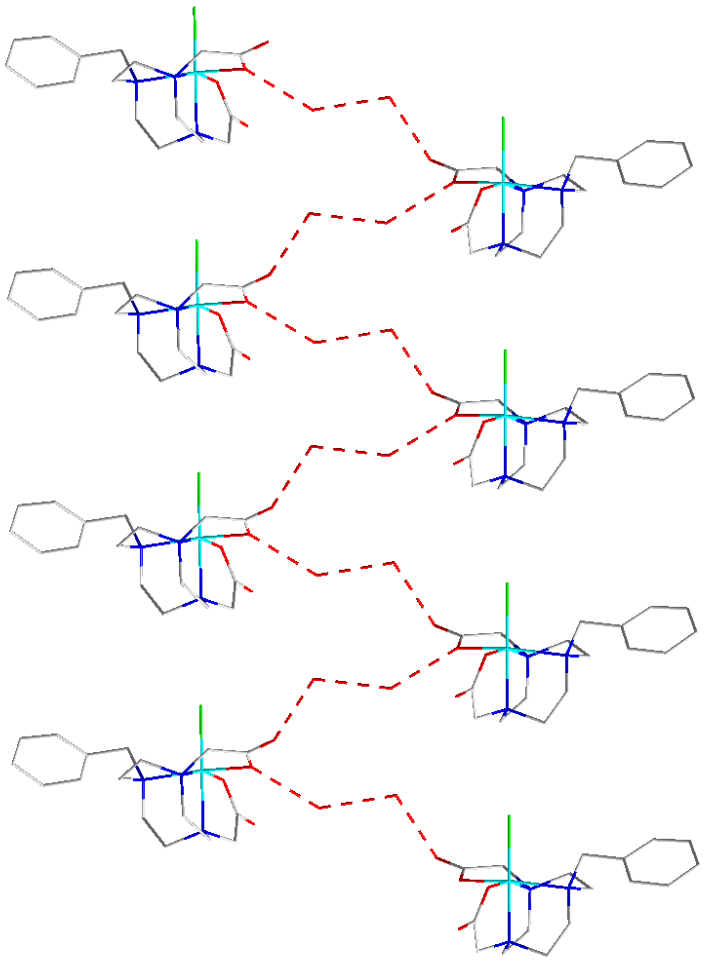

Figure 4.9: Diagram showing a portion of the extended H-bonded structure of [GaCl(L)].2H_2O viewed down the *a*-axis. The H-atoms associated with the lattice H_2O molecules were not located in the difference map, but inferred from the O····O distances. CO····O 2.811(7), O····O 2.855(7), O····OC 2.888(8) Å. Colour key: turquoise = Ga, green = Cl, blue = N, red = O, grey = C.

The structure of [GaCl(L)]·2H_2O shows a distorted octahedral coordination environment at gallium through pentadentate coordination of L^{2-} *via* its N_3O_2 donor set and one chloride ligand. The complex crystallises as a dihydrate, with one of the lattice H_2O molecules H-bonded to the O atoms of the carboxylate CO groups (Figure 4.9). This contrasts with the F····H–OH interactions observed in the [MF_3(R_3-tacn)]·xH_2O (M = Al, Ga, In), Chapter 2.[16] This is also markedly different from the complexes [MCl_3(R_3-tacn)] which all crystallised as molecular entities with no solvent molecules crystallised in the lattice. Repeated attempts to gain better quality crystals and hence improved structural data on the dihydrate complex were unsuccessful. However recystallisation of the complex from MeCN/Et_2O over a period of several weeks

yielded much better quality crystals of the acetonitrile solvated complex [GaCl(L)]·MeCN (Figure 4.10).

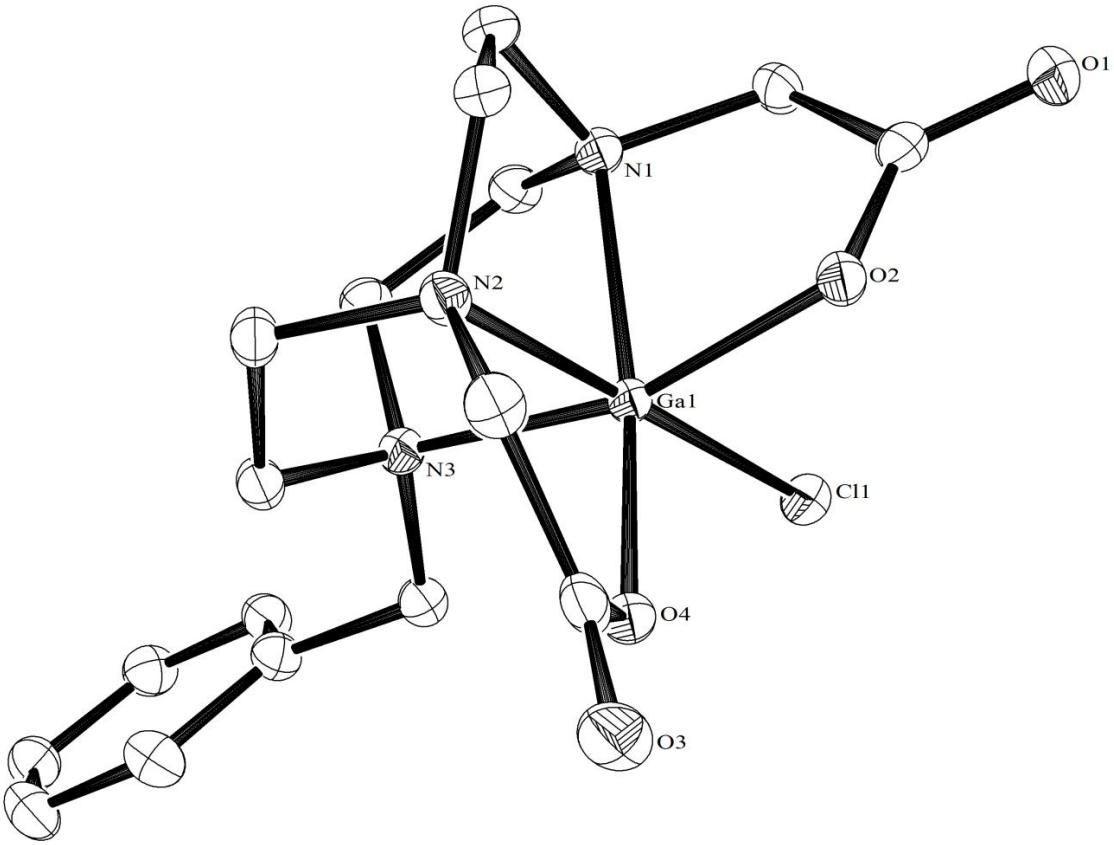

Figure 4.10: ORTEP representation of the crystal structure of [GaCl(L)]·MeCN. Solvated MeCN molecule and protons are omitted for clarity. Ellipsoids are drawn at 50% probability level. Ga1−Cl1 2.2792(4), Ga1−O2 1.9824(13), Ga1−O4 1.9139(12), Ga1−N1 2.0970(15), Ga1−N2 2.1222(15), Ga1−N3 2.1243(15) Å.

The MeCN solvated Ga-chelate is essentially unchanged compared to the dihydrate with d(Ga-Cl) 2.279 (4) Å in the acetonitrile solvate *vs.* d(Ga-Cl) 2.266(4) Å in the dihydrate. The d(Ga-O) bond lengths in the acetonitrile solvate are more symmetrical, both being *ca.* 1.95 Å in length. This is likely a reflection of the better refinement of the bond lengths in the acetonitrile complex, but is perhaps an indication that the H-bonding of the water molecules to the ligand carboxylate groups in the dihydrate has an effect on the Ga-O bond length. In comparison to the dihydrate, the lattice acetonitrile molecules do not interact with the Ga complex.

It was initially surprising to observe the formation of the chloride complex since it was expected that a nitrate complex would form. However, in aqueous solution, the gallium nitrate precursor is significantly dissociated. This allows coordination of the chloride ion from the ligand hydrochloride salt, which in conjunction with the pentadentate tacn ligand, completes the coordination sphere around the gallium centre.

The solvated [GaCl(L)] complex could be synthesised and stored for many weeks before use. No degradation was observed over a period of several weeks in both the solid state and in aqueous solution, suggesting this type of precursor complex could be a robust scaffold for labelling applications.

4.2.3 Hydrothermal synthesis of [GaF(L)]

Before the Cl/F halide exchange reaction was attempted on [GaCl(L)], a method to obtain the corresponding Ga−F complex as a model compound to provide a well-defined spectroscopic fingerprint in preparation for the exchange studies was developed. Given the success of hydrothermal synthesis in the previous work on neutral tacn chelates (Chapter 2), a similar method was employed.[16] This method has a number of advantages over traditional solution phase chemistry as the route is clean, relatively high yielding, and in the case of this system, the precipitation of LiF provides a driving force towards the complexation. Reaction of $GaF_3 \cdot 3H_2O$ with Li_2L (to ensure exclusion of Cl^-) under hydrothermal conditions (180 ^oC, 15-18 hours) results in the formation of the complex $[GaF(L)] \cdot 2H_2O$ as a yellow solid after work up.

The ^1H NMR spectrum of the product shows a complex pattern consistent with ligand coordination. The spectrum again depicts the benzyl protons split into an AB quartet ($^2J_{HH}$ 13.5 Hz), indicating ligand coordination. The CH_2 groups of the carboxylate groups are also split into two distinct environments, although the signals are too broad to define the multiplicity and coupling constants. The CH_2 tacn proton environments give a complex second order pattern, consistent with proton inequivalency through metal coordination, and coupling to the quadrupolar gallium centre. The pattern shows small chemical shift differences from the chloride analogue, [GaCl(L)], and significant differences from the spectrum of the fee Li_2L salt spectrum. The $^{19}F\{^1H\}$ NMR spectrum reveals a single resonance at δ −184.2, consistent with the Ga−F containing compounds discussed in Chapters 2 and 3. The peak positions are very similar to the neutral [GaF_3(RMe_2-tacn)] complexes, although the low symmetry of the [GaF(L)] complex leads to a high efg, meaning that couplings to the gallium are not observed.[16] The ESI^+ mass spectrum of the compounds again show *m/z* = 402.1 (100%), with the expected isotope pattern for $[Ga(L)]^+$. The IR spectrum shows a single, broad Ga−F stretching band (ν 568 cm^{-1}). Evidence for H-bonded water was also found from the IR spectrum (ν (OH) = 3420 cm^{-1}, δ (HOH) = 1643 cm^{-1}).

Slow evaporation of water from the hydrothermal reaction solution gave small crystals suitable for single crystal X-ray diffraction (Figure 4.11).

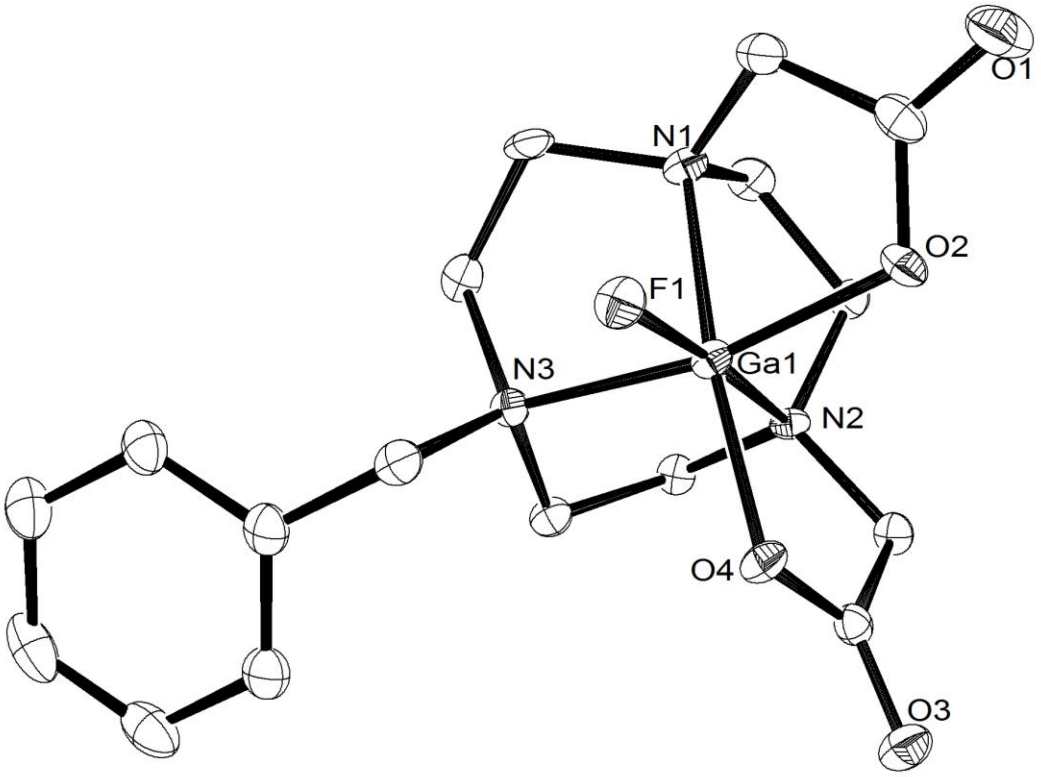

Figure 4.11: ORTEP representation of the crystal structure of $[GaF(L)]\cdot 2H_2O$. H-atoms and lattice H_2O molecules excluded for clarity. Ellipsoids are drawn at 50% probability level. Ga1−F1 1.821(2), Ga1−O4 1.940(3), Ga1−O2 1.980(3), Ga1−N1 2.082(4), Ga1−N2 2.111(3), Ga1−N3 2.146(3) Å.

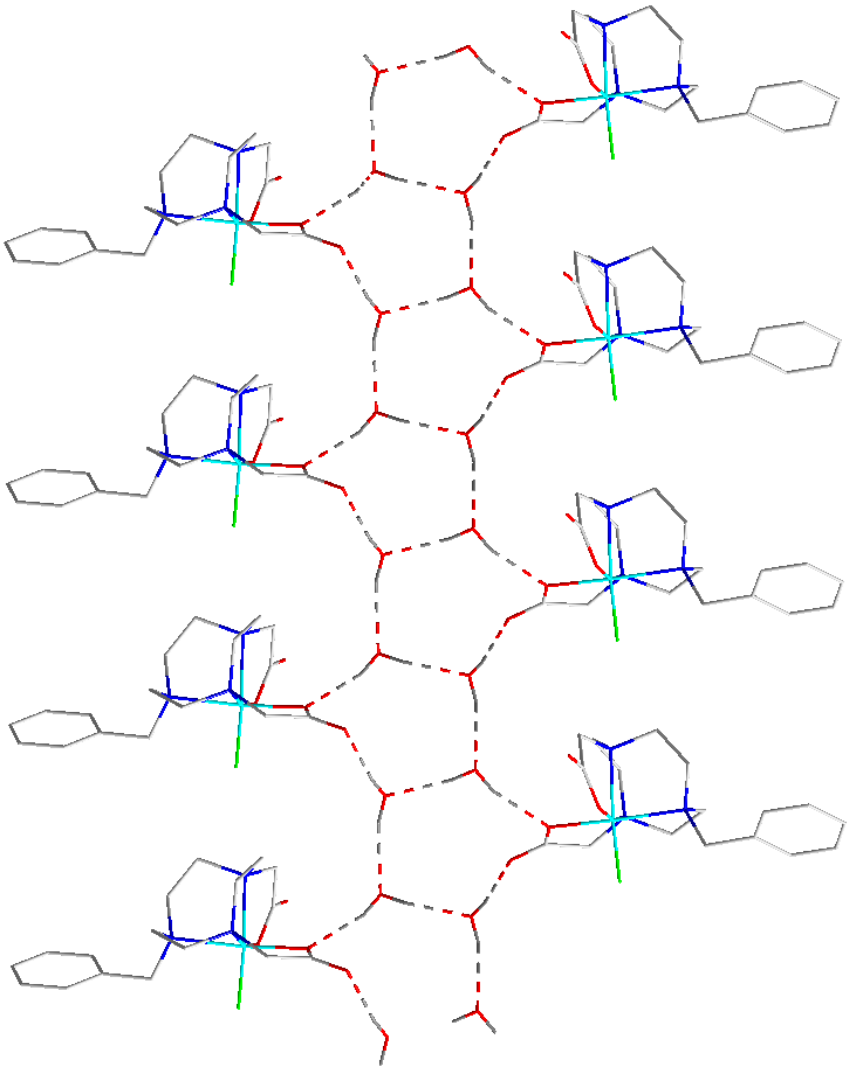

Figure 4.12: Diagram showing a portion of the extended structure of [GaF(L)]·2H_2O viewed down the *a*-axis. H-atoms on the metal complex are omitted for clarity. CO····O 2.853(2), O····O 2.783(2), O····O 2.948(2) Å. Colour key: turquoise = Ga, green = F, blue = N, red = O, grey = C.

X-Ray structural characterisation confirmed the expected distorted octahedral coordination at gallium, through a pentadentate L^{2-} ligand and one terminal F^- ligand. The Ga−F bond length is found to be 1.821(2) Å, one of the shortest Ga−F bonds observed crystallographically, and even slightly shorter than d(Ga−F) in [GaF_3(Me_3-tacn)]·4H_2O (1.851(3), 1.858(3), 1.881(3) Å), although the latter exhibits extensive F····H–OH hydrogen-bonding to lattice water which may influence the Ga−F bond lengths in this complex (Figure 4.12).

The [GaF(L)] complex crystallises as a dihydrate, analogous to the aluminium complex.[8] Comparison with the analogous Al−F complex, $[AlF(L)]\cdot 2H_2O$ shows d(Al–F) = 1.7090(14) Å, leading to a difference in d(M−F) of 0.11 Å.[8] This is larger than would be expected based on the difference in covalent radii from Al^{3+} (1.18 Å) to Ga^{3+} (1.26 Å).[17] Similarly, the difference between d(Al−O) and d(Ga−O) is *ca*. 0.10 Å. Comparison of the M−N bond lengths shows d(Ga−N) lie in the range 2.082(4) to 2.146(3) Å, while d(Al−N) lie between 2.0497(18) and 2.1125(18) Å, i.e. there is a smaller effect on the M−N distances between the aluminium and gallium complexes.

Like the [GaCl(L)] analogue, the [GaF(L)] complex crystallises as a dihydrate; although they are isostructural, they are not isomorphous due to differences in the H-bonding arrangement. In the fluoride complex both lattice waters are involved in H-bonding.

The fluoride complex is stable in the solid state and for several weeks in aqueous solution (in which the pH is measured to be ~4) and in other acidic media. Addition of KOH (aq) to an aqueous solution of the [GaF(L)] complex to bring the solution to pH 7, leads to release of F^- within 5-10 minutes. This is confirmed by the loss of the $^{19}F\{^1H\}$ resonance observed for the complex and the growth of a resonance due to F^- ($\delta = -123.7$).

The synthesis and full characterisation of the fluoride complex directly provided a strong spectroscopic fingerprint with which to analyse the halide exchange reactions.

4.2.4 Cl/F Halide exchange on a preparative scale

Reaction of $[GaCl(L)]\cdot 2H_2O$ in aqueous MeCN with one molar equivalent of $KF_{(aq)}$ leads to complete conversion to the corresponding fluoride complex.

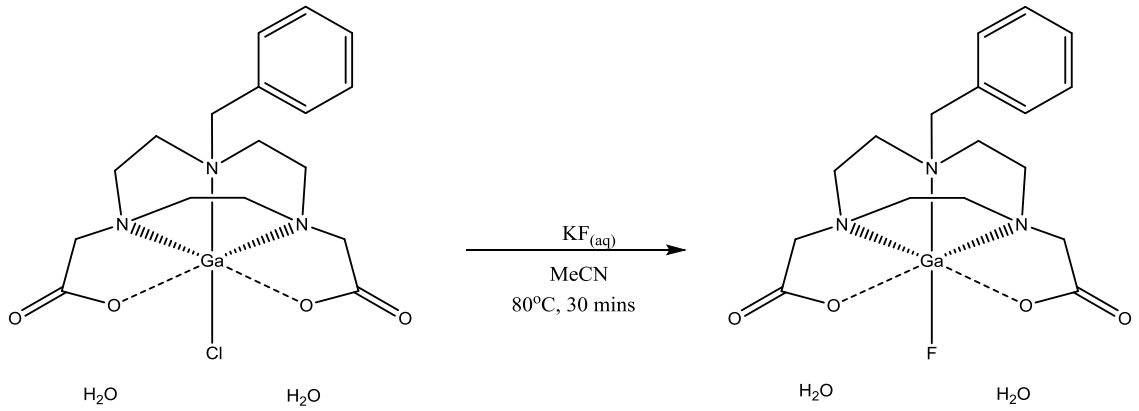

Figure 4.13: Scheme describing the halide exchange reaction of [GaCl(L)].

Complete exchange is achieved after *ca.* three hours at room temperature, but is achieved significantly more quickly (*ca*. 45 minutes.) if heated to 80 ºC. Spectroscopic analysis of the resulting product matched that observed for [GaF(L)] synthesised hydrothermally. The Cl/F halide exchange may also be performed in buffered NaOAc solution (pH 4).

The requirement for heating the reaction to accelerate the halide exchange is in contrast to the neutral R_3-tacn chelates discussed in Chapter 3.[16] Under appropriate solvent conditions, the neutral chloride precursors [MCl_3(RMe_2-tacn)] were rapidly fluorinated (particularly for Al and Ga) at room temperature. This suggests that the driving force for M-F bond formation may be higher in the neutral systems. In the complex [GaCl(L)], d(Ga-Cl) is 2.28 Å (to 2 d.p), while the average d(Ga-Cl) in the neutral tacn based complex [$GaCl_3$(Me_3-tacn)] is 2.32 Å. This slightly shorter Ga-Cl bond in [GaCl(L)] may indicate a stronger interaction with the metal centre, perhaps due to the lower steric demands of the ligand, and thus a slightly larger driving force is required to displace the chloride in the system discussed here. However the requirement to heat this class of compound in order to form the fluoride chelate is shown in the work of both McBride and Jeong.[6, 8] In their work, it is required to heat to 115 ^{o}C in order to form the Al-^{18}F complex. The lower temperature required to fluorinate the corresponding gallium complex demonstrates a slight improvement on the current methods employed by McBride and others.

Having demonstrated the ability to successfully perform the halide exchange reaction under aqueous conditions, it was considered necessary to establish the possibility of performing the exchange reaction using NR_4F under anhydrous conditions.

In addition to fluorination *via* halide exchange, it was shown that the fluoride complex [GaF(L)] could be accessed *via* a 'one pot' route akin to the method developed by McBride and Jeong[6, 8]. Addition of $KF_{(aq)}$ and $Li_2L_{(aq)}$ simultaneously to powdered $GaCl_3$ at room temperature gives the desired complex [GaF(L)] in high yield after work up. This was confirmed through comparison with the spectroscopy acquired for the complex synthesised hydrothermally. This was a rather unexpected result since it suggests that the chelation and fluorination reaction was faster than any competing hydrolysis reaction. It is likely that the combination of the macrocyclic and chelate effect, and the formation of a strong Ga-F bond drives the reaction and prevents any competing hydrolysis.

While demonstrating the ability to form the fluoride complex in a single step, the use of the moisture sensitive precursor $GaCl_3$ was viewed as being disadvantageous, especially when working on the sub milligram quantities required for labelling applications. An alternative method was therefore developed using $Ga(NO_3)_3{\cdot}9H_2O$. Combination of the gallium salt with either $H_2L{\cdot}HCl$ or Li_2L and $KF_{(aq)}$ in aqueous media results in the desired complex [GaF(L)] in high yield. In addition, one can perform the reaction under pH controlled conditions using NaOAc buffer at pH 4. This method closely mimics the McBride method in which they use water soluble $AlCl_3{\cdot}6H_2O$ as the source of Al(III) but utilises the more convenient $Ga(NO_3){\cdot}9H_2O$ starting material.

4.2.5 ^{18}F Radiolabelling

Having demonstrated the ability to successfully perform halide exchange on the pre-formed [GaCl(L)] complex on a preparative scale using $^{19}F^-$, the corresponding radiofluorination reaction was attempted using the pre-formed complex (Figure 4.14).

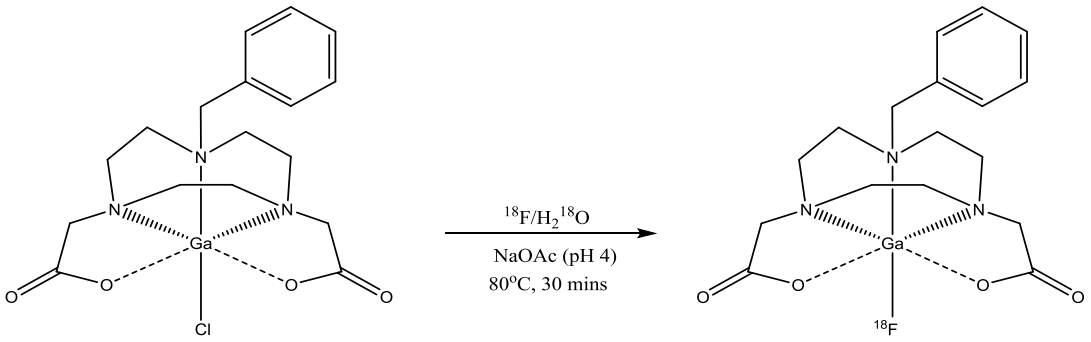

Figure 4.14: Synthetic route towards [Ga^{18}F(L)].

Carrier free $^{18}F/^{18}OH_2$ (500−1000 MBq) was added to 0.1 mg of [GaCl(L)]·2H_2O precursor (210 nmol) dissolved in NaOAc buffer (pH 4) and reacted at room temperature for 30 minutes. HPLC analysis of the crude reaction mixture showed a radio peak at Rt 6−6.2 minutes corresponding to [Ga^{18}F(L)] Integration of the radio peak indicated *ca*. 30% incorporation of ^{18}F into the gallium complex at room temperature after 30 minutes (Figure 4.15). Heating the reaction solution to 80 ºC for 30 minutes led to a significant increase in the incorporation to 65-70% (Figure 4.16).

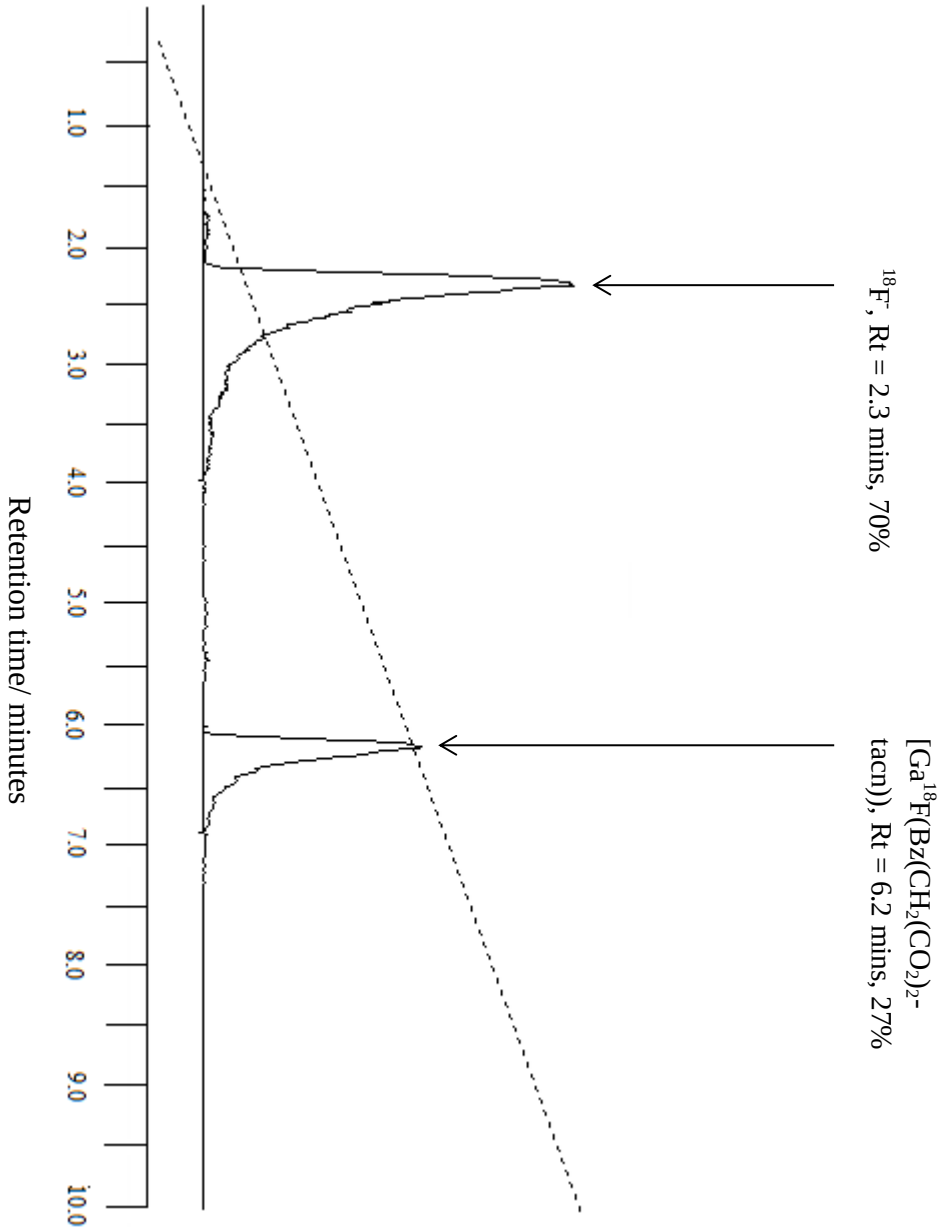

Figure 4.15: HPLC radiochemical trace of the crude reaction mixture from the reaction of [GaCl(L)]·2H_2O with $^{18}F/^{18}OH_2$ in NaOAc (pH 4), stirred at room temperature for 30 minutes. Rt 2.4 mins. (70%) $^{18}F^-$, Rt 6.2 mins. (27%) [Ga^{18}F(L)].

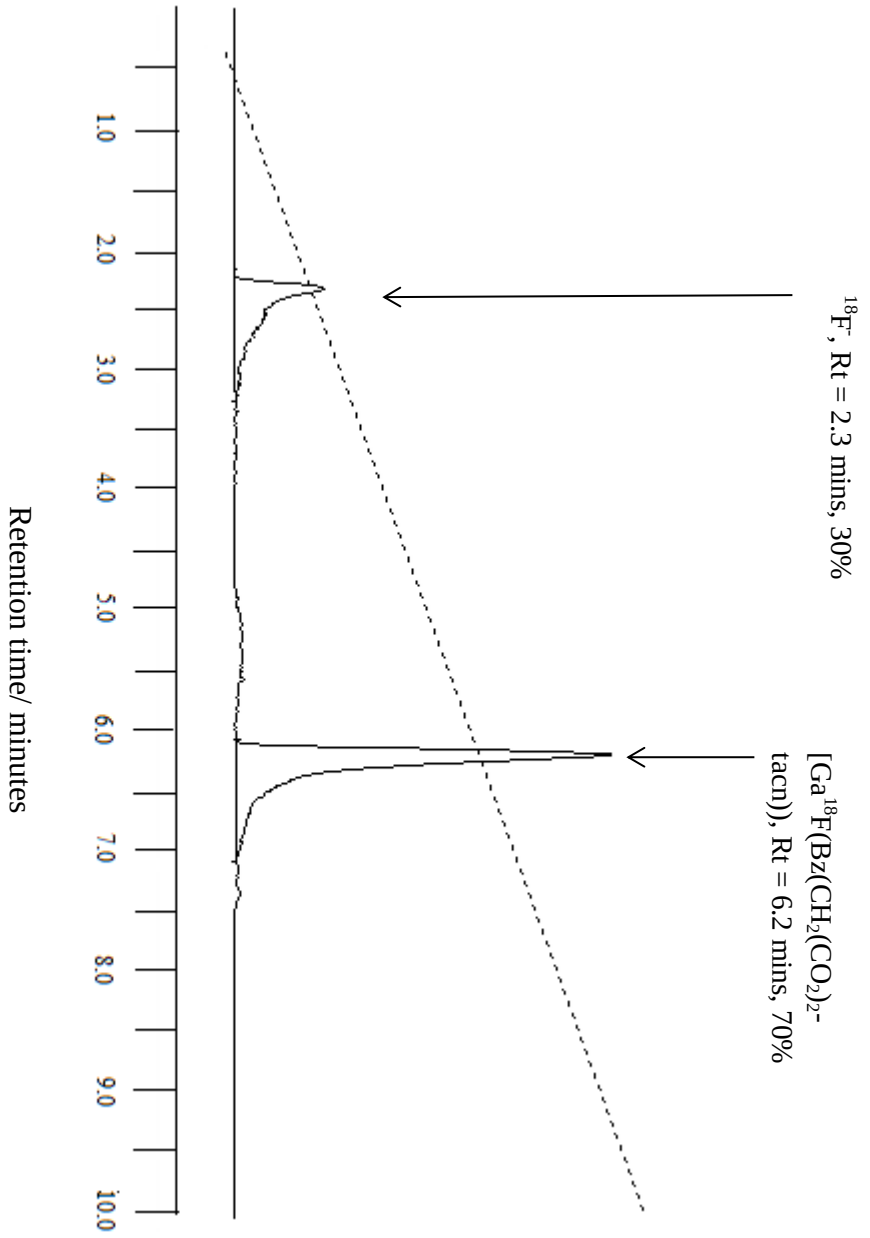

Figure 4.16: HPLC radiochemical trace of the crude reaction mixture from the reaction of [GaCl(L)]·2H_2O with $^{18}F/^{18}OH_2$ in NaOAC (pH 4), heated to 80 °C for 30 minutes. Rt 2.3 mins. (30%) $^{18}F^-$, Rt 6.2 mins. (70%) [Ga^{18}F(L)].

The observations made on a 'radiochemical' nanomolar scale mimic those observed on a preparative scale, i.e. labelling occurs slowly at room temperature but increases upon modest heating. While 30% incorporation at room temperature may not be viewed as a particularly high yield, this represents a significant increase on the corresponding aluminium systems, which show negligible incorporation at room temperature. Thus this opens up the prospect of being able to use this metal-ligand architecture as a scaffold in which temperature sensitive biomolecules may be radiolabelled under mild conditions.

As was the case with the neutral [$GaCl_3$($BzMe_2$-tacn)] complexes, the UV peak was only weakly observable in the HPLC. The signal was too weak to conclusively prove that the ^{18}F containing species also contained the UV-active chromophore on the ligand.

To confirm the species formed in the labelling reaction was the desired compound, a portion of the crude reaction mixture was eluted down an analytical HPLC system. The 'product' peak was 'cut' and the solution collected was analysed by positive ion electrospray mass spectrometry. As with the model compound, the parent ion was not observed, however, peaks attributed to the monocations, $[GaL]^+$ (*m/z* 402.1) and $[\{GaF(L)\}_2 + H_3O]^+$ (*m/z* 863.2) were observed (Figure 4.17and Figure 4.19).

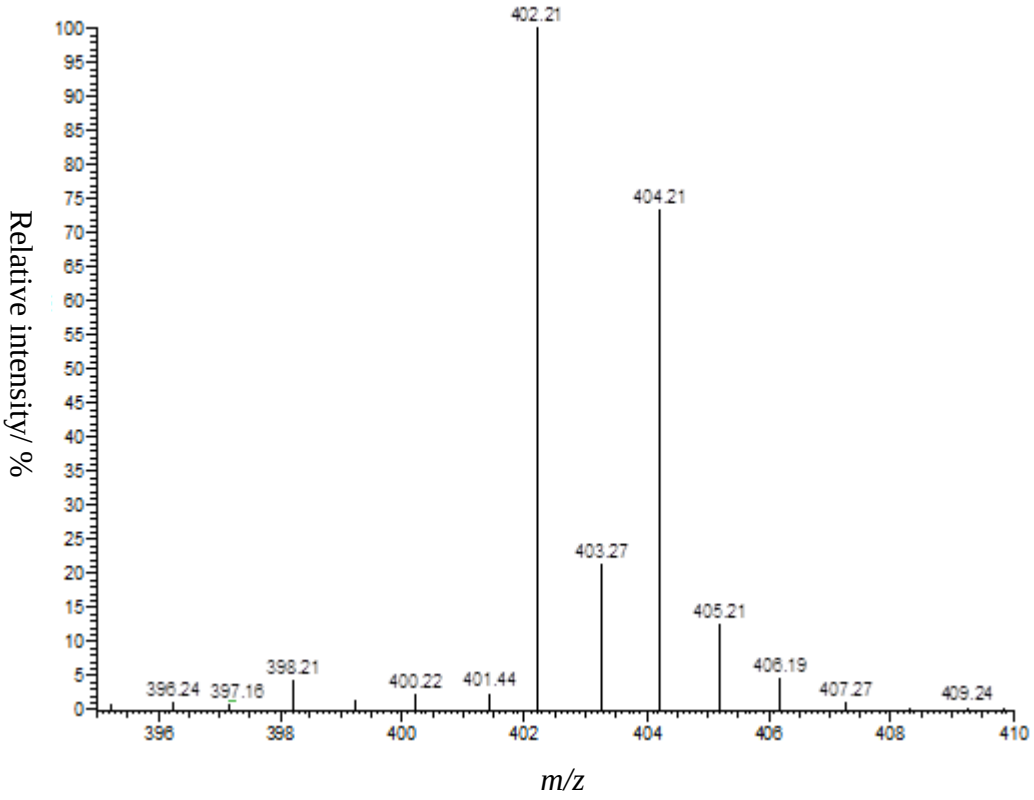

Figure 4.17: ESI^+ mass spectrum and isotope pattern for $[Ga(L)]^+$ *m/z* = 402.2 (100%).

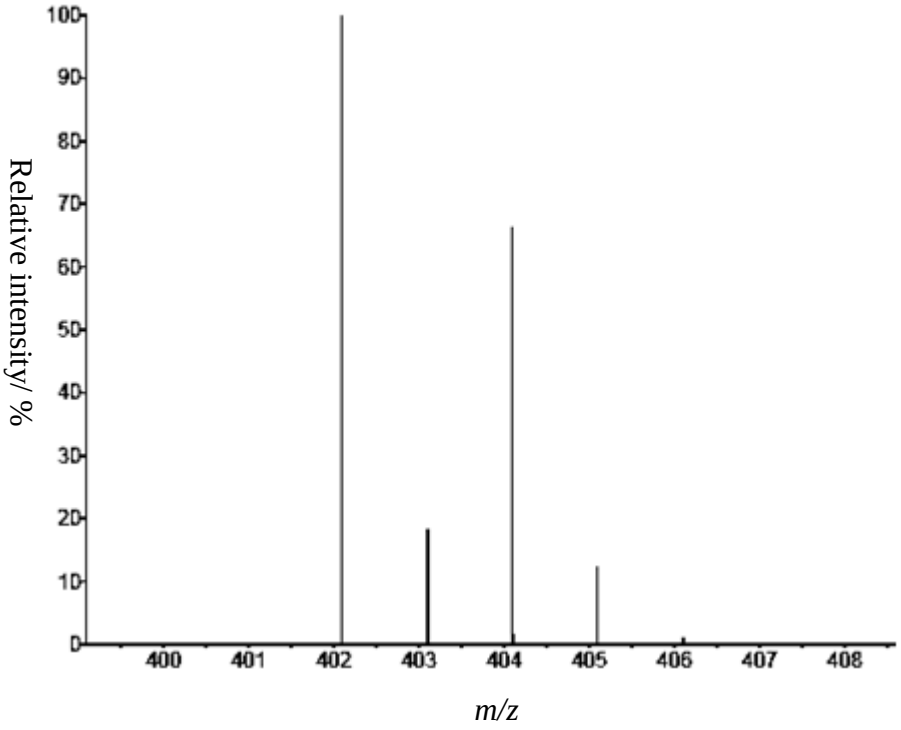

Figure 4.18: Predicted peak position and isotope pattern for the species $[Ga(L)]^+$.

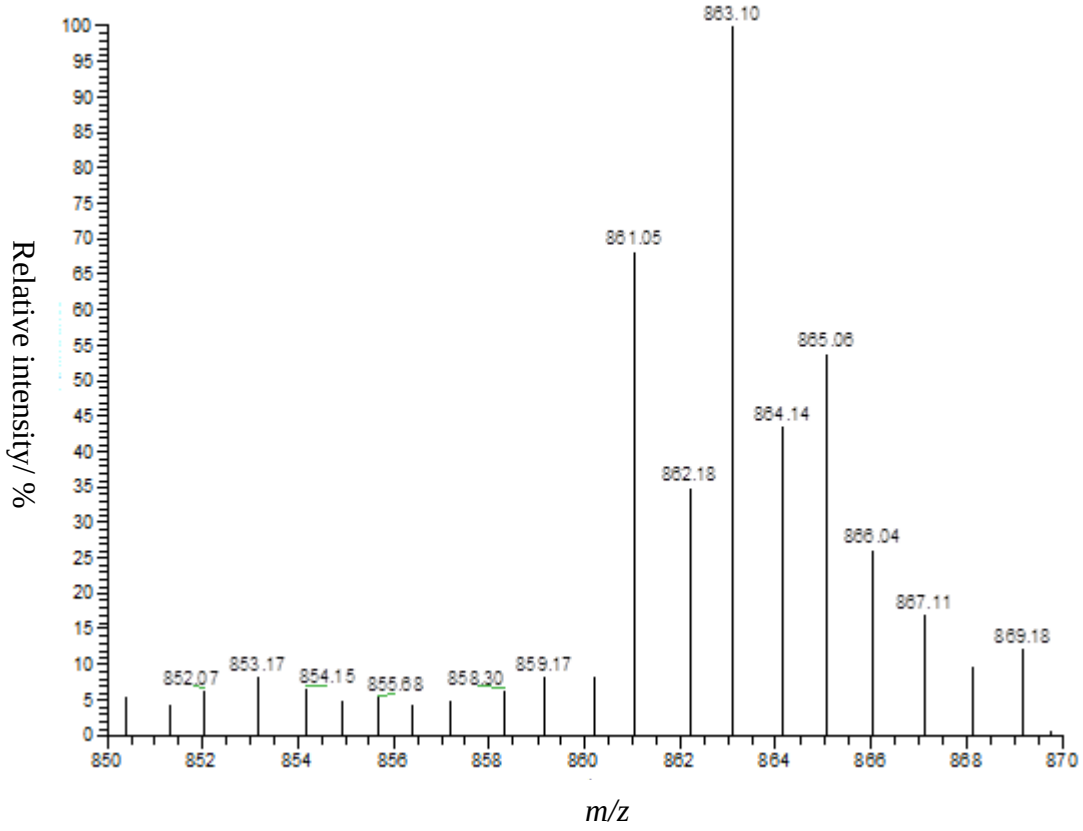

Figure 4.19: ESI^+ mass spectrum and isotope pattern for $[\{GaF(L)\}_2+H_3O]^+$ *m/z* 863.1 (100%).

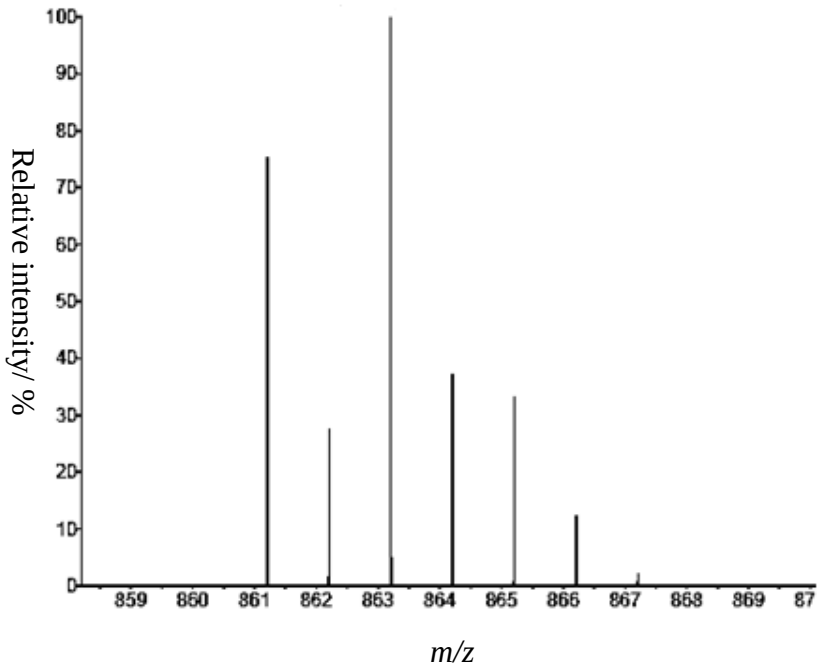

Figure 4.20: Predicted peak position and isotope pattern for the species $[\{GaF(L)\}_2+H_3O]^+$.

This, in conjunction with the radio trace from the HPLC confirmed the formation of the target Ga-F complex, [$Ga^{18}F(L)$].

An important requirement for any potential radiopharmaceutical based on this compound type is the ability to purify and isolate the radiolabelled species *via* a solid phase extraction (SPE) purification method. The crude ^{18}F labelled compound was purified by trapping it on an HLB (hydrophilic lipophilic branched) cartridge and eluted with EtOH/H_2O. This purification process is very efficient, giving radioactive concentrations (RACs) of up to 100 MBq/mL. This represents an improvement on the neutral complex [$Ga^{18}F^{19}F_2(BzMe_2\text{-tacn})$], which was purified by preparative HPLC. The purified species was formulated into a number of solvent and pH regimes (Figures 4.21 – 4.23).

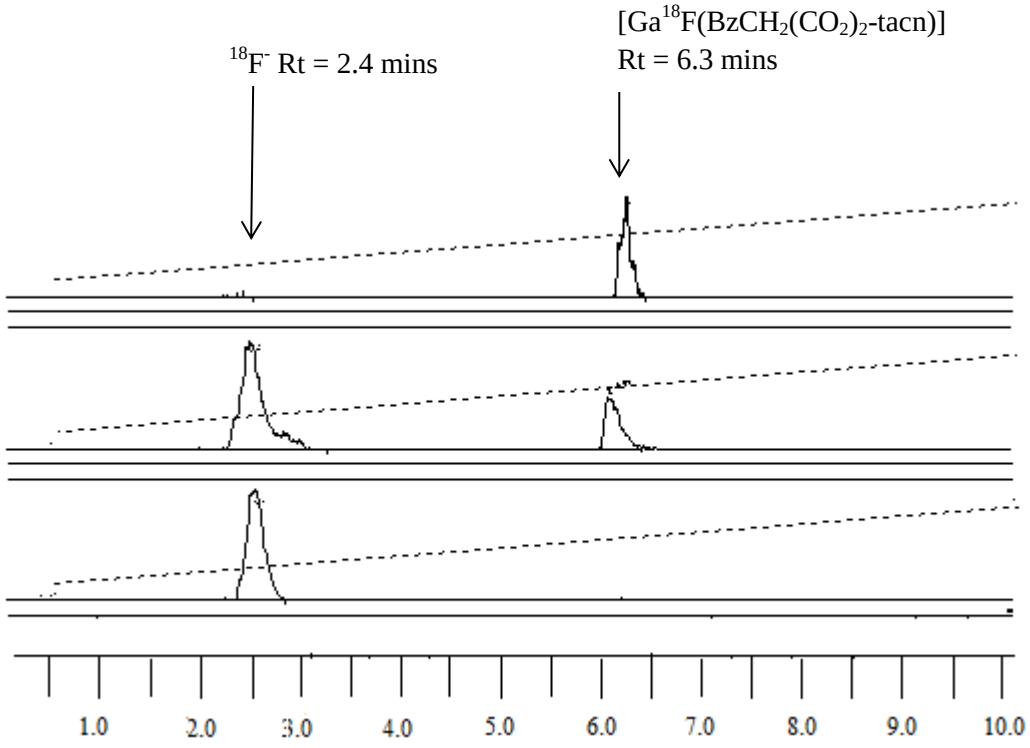

Figure 4.21: Overlay of the HPLC radio trace of the purified product formulated in 10% EtOH/PBS (pH 7.4) at t = 'zero' (top), t = 45 mins (middle) and t = 120 mins (bottom). Radiochemical purity (RCP) of [$Ga^{18}F(L)$] = 98% (top), 45% (middle), 0% (bottom).

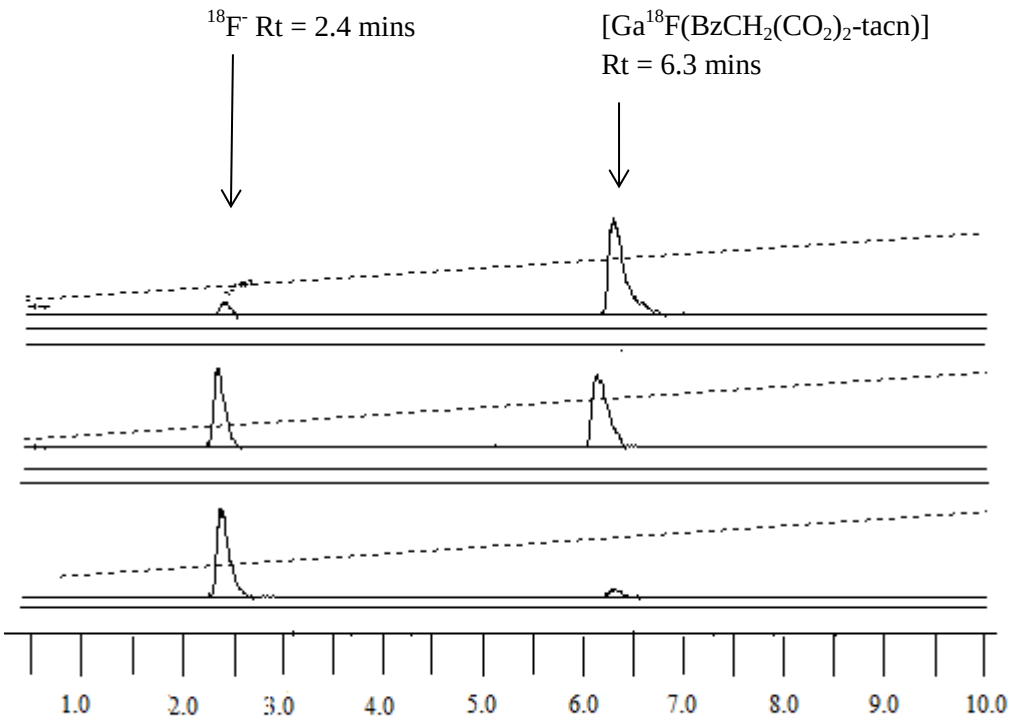

Figure 4.22: Overlay of the HPLC radio trace of the purified product formulated in 10% EtOH/HSA (pH 7.5) at t = 'zero' (top), t = 30 mins (middle) and t = 90 mins (bottom). RCP of [Ga^{18}F(L)] = 93% (top), 57% (middle), 7% (bottom).

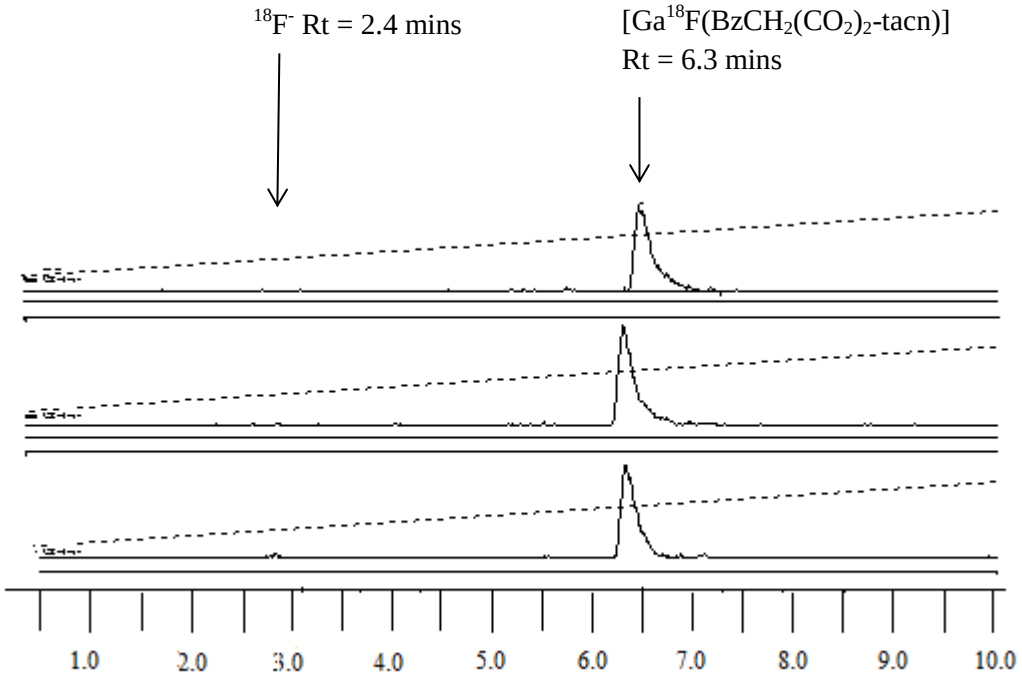

Figure 4.23: Overlay of the HPLC radio trace of the purified product formulated in 10% EtOH/NaOAc (pH 6) at t = 20 mins (top), t = 45 mins (middle) and t = 90 mins (bottom). RCP of [Ga^{18}F(L)] = 99% (top), 99% (middle), 96% (bottom).

Formulation (pH)#	**RCP/% (time/ mins)***			
EtOH/PBS (7.5)	98 (0)	40 (30)	25 (45)	2 (120)
HSA (7.4)	93 (0)	57 (30)	7 (90)	
EtOH/H_2O (7)	91 (0)	76 (30)	34 (120)	0 (180)
EtOH/10mM NH_4OAc (7)	90 (0)	49 (30)	9 (45)	4 (90)
EtOH/NaOAc (6)	99 (20)	99 (45)	96 (90)	-
EtOH/NaOAc (5)	99 (45)	99 (90)	99 (180)	-
EtOH/NaOAc (4)	99 (0)	99 (90)	99 (120)	99 (240)

Table 4.1: Table depicting % RCP of specific formulations as a function of time. # EtOH volume equated to approximately. 10% of total formulation volume (e.g. 0.1 mL EtOH in 1 mL formulated product). * RCP estimated from integration of radiochemical peaks in HPLC chromatograph.

The purified product is very stable in acidic media – the RCP of the purified product remained at 99% over a period of at least four hours. However as the pH was adjusted towards neutral pH, the purified compound rapidly hydrolysed, liberating free ^{18}F-fluoride.

Unlike the Al-^{18}F complexes developed by McBride[6] and Jeong[8] which proved stable under neutral pH conditions, it appears the gallium analogue was sensitive to pH. This is

consistent with the observation that the non-active [GaF(L)] complex is unstable in aqueous KOH at pH 7. These data suggest that the stability is strongly pH dependant, although the presence of competing ions in the PBS and HSA formulations may also play a role.

The trend in stability with pH can be replicated on a preparative scale. Dissolution of a portion of the pre-prepared [GaF(L)] complex (synthesised via chloride/fluoride halide exchange) in PBS/D_2O and subsequent analysis by $^{19}F\{^1H\}$ NMR spectroscopy showed the liberation of fluoride anion (-122 ppm), and a subsequent loss in intensity of the resonance corresponding to the metal complex (-176 ppm) at pH 7.5 It is notable that the [GaF_3($BzMe_2$-tacn)] is stable for several hours (with no evidence of defluorination) in PBS, both on a tracer scale concentration (micromolar) and on a preparative scale (mmol), and hence, it is clear that neither the Ga-F bonds nor the Ga-N(tacn) bonds are inherently unstable at pH 7.5 (Chapter 3.2.6).[16] Therefore, it is likely that the pH dependent instability of [GaF(L)] is associated primarily with the Ga-O (carboxylate) bonds, with subsequent loss of F. It is known from previous work on F/H_2O exchange on Al(III) complexes[18, 19] that small changes in the steric environment can change the substitution mechanism (e.g., from D to I), hence, the steric and/or electronic changes at Ga(III) caused by the different donor sets in [GaF(L)] compared with [GaF_3(R_3-tacn)] may be the basis for the observed instability of the former at pH 7.5. Because Ga(III) is less Lewis acidic than Al(III),[20-22] the introduction of the Ga-O (carboxylate) bonds in [GaF(L)] may lead to initial cleavage of the Ga-O bond at pH 7.5 (e.g., by H_2O or an anion present in the formulation), destabilising the Ga(III) coordination sphere to cause the observed decomposition. Hence, the experimental observations from this study suggest that modifications to the macrocyclic pendant groups either, for example, by increasing the steric bulk at the carboxylate functions, or by changing the carboxylate functions to other anionic donor groups could be important, leading to improved stability of M-^{18}F complexes.

4.3 Comparison with related systems

The work described demonstrates advancement in the field of metal chelate based agents as a source of ^{18}F containing imaging agents. However it is important to put it into context in relation to other related systems.

4.3.1 Comparison to neutral trifluoride R_3-tacn systems

In relation to the neutral R_3-tacn chelates described in Chapters 2 and 3, this system presents a number of improvements, but also highlights that the neutral R_3-tacn systems discussed in Chapters 2 and 3 may offer additional advantages.

The neutral R_3-tacn complexes may be labelled at room temperature giving a moderate incorporation of 30-40%. This compares favourably to the dicarboxylate tacn complexes

discussed above. However, while ^{18}F-incorporation in the [GaCl(L)] system increases significantly on heating (70-80%), there is no change in incorporation in the neutral R_3-tacn systems upon heating. This could be a result of the need to exchange three fluoride ligands, and the requirement to add K^{19}F as a carrier agent in the latter. The carboxylate systems are also readily labelled under carrier free conditions, greatly simplifying the synthetic procedure.

A further improvement in the carboxylate systems is the ability to label in 100% aqueous media. This makes the SPE purification simpler as there is no requirement to dilute the crude reaction mixture into large volumes of water in order to lower the percentage of organic solvent present (high percentages of organic solvent result in poor yields from the purification step). The neutral R_3-tacn systems are labelled in a predominantly organic (MeCN) solvent system. This therefore requires a 'dilution' step before the compound is purified.

However, a key advantage of the neutral trifluoride complexes is their stability at neutral pH. The trifluoride shows no decomposition after formulation into an EtOH/PBS solvent system at pH 7.5. This is a significant improvement on the carboxylate systems, which while very stable at pH 6, begins to decompose when formulated into an EtOH/PBS solution at pH 7.5.

4.3.2 Comparison to 'Al-F' systems developed by McBride and Jeong

The work of McBride and Jeong with this class of ligand indicates that their synthetic method requires more forcing conditions (higher temperatures).[6,8] The gallium analogue showed up to 30% incorporation of ^{18}F at room temperature after 30 minutes of reaction, increasing to *ca.* 70% after heating to 80 ^{o}C for 30 minutes. This could indicate the gallium system could be used to label heat or temperature sensitive biomolecules. However, despite requiring more forcing conditions, the Al analogue shows higher incorporation (*ca.* 95%), although this experiment was not investigated with the Ga equivalent.

McBride and Jeong have shown that the Al systems are stable at neutral pH (shown to be stable in HSA and PBS), however, [Ga^{18}F(L)] begins to decompose under these conditions. This may suggest that for the carboxylate-tacn ligand, the higher Lewis acidic Al(III) is more manifested towards the anionic groups in [AlF(L)]. It appears that there's a subtle 'tipping point' between the aluminium and gallium systems which results in the lower stability of the gallium chelate at neutral pH. However, modification of the ligand backbone may help increase the stability of the gallium systems.

4.4 Conclusions and Future Work

This work describes a method for the preparation of $[GaCl(L)]\cdot 2H_2O$, containing Ga(III) in a distorted octahedral environment provided by the pentadentate L^{2-} ligand and one Cl^- (derived from $H_2L\cdot HCl$), using the commercially available and easy-to-handle $Ga(NO_3)_3\cdot 9H_2O$ as a convenient source of Ga(III) in water. The corresponding fluoride complex, $[GaF(L)]\cdot 2H_2O$ has been synthesised by a hydrothermal route to provide crystallographic and spectroscopic data, and also on a bulk scale by Cl/F exchange from $[GaCl(L)]\cdot 2H_2O$ with $K^{19}F$ in water, as a model for the radio-fluorination reaction.

Direct radiofluorination at nano-molar concentration by treatment of this pre-formed $[GaCl(L)]\cdot 2H_2O$ with carrier-free $^{18}F^-$ in water at pH 4.5 (NaOAc) with heating to 80 °C for 30 mins. has also been demonstrated, yielding $[Ga^{18}F(L)]$ with 65–70% $^{18}F^-$ incorporation. The crude product is readily purified using an SPE cartridge, and shows excellent radiochemical stability at pH 6 (10% EtOH/NaOAc). In contrast, defluorination is observed over a period of 15 minutes–one hour when $[Ga^{18}F(L)]$ is formulated in PBS and HSA (pH 7.5 and 7.4, respectively). This instability at high pH is attributed to the presence of the carboxylate groups in L^{2-}, and demonstrates subtle differences in the behaviour of Ga(III) *vs*. Al(III) in this chemistry; the higher Lewis acidity of Al(III) is more manifested towards the anionic ligand groups in [AlF(L)]. This is in accord with structural data which show that the M–O and M–F bond distances are longer (by ~0.1 Å) for Ga over Al, while the M–N bond distances are more similar. The subtle influence of the precise metal-ligand coordination on the complex stability with pH observed in this work is important in guiding refinement of the design of new metal complex based imaging agents.

A potential future development to this chelate type is to attach a peptide to the benzyl substituent on the tacn ligand, which would produce a 'bioactive' chelate. Recent work from GE Healthcare has used this ligand scaffold in which a human epidermal growth factor receptor 2 (HER2) peptide was attached and its radiolabelling efficacy measured using a number of labelling methods.[23] Perhaps this peptide might be an effective choice as a 'bioactive' molecule in which to conduct the chemistry discussed above.

The purification of the radiolabelled complex $[Ga^{18}F(L)]$ was performed manually (i.e. the HLB cartridge purification was undertaken in an enclosure with no automation). Therefore a further potential future work stream is to develop an automated method on a GE FASTlab system which would allow labelling to be performed on a much higher activity (GBq scale) and would then lead to the real prospect of providing the pre-formed chelate in kit form and with a simple automated procedure.

The use of the air stable, aqueous Ga(III) salt $Ga(NO_3)_3 \cdot 9H_2O$ removes the requirement to use the moisture sensitive $GaCl_3$. This allows for much greater ease of handling on a nano-molar scale required to conjugate chelates with peptides attached (e.g. in the form of stock solutions). The use of gallium nitrate as an aqueous, stable source of Ga(III) in other radiopharmaceutical applications could be investigated, for example as a carrier agent in the synthesis of ^{68}Ga radiopharmaceuticals for PET imaging. The fundamental coordination chemistry of gallium nitrate could be investigated with a range of ligand types.

The N_3O_2 donor set of the tacn dicarboxylate ligand may favour coordination to oxophilic metal centres. The oxophilic Group 3 metals such as scandium and yttrium may provide a more robust metal centre for this ligand type.

4.5 Experimental

For general experimental methods see Appendix 1. Reactions were performed in standard lab glassware where appropriate. Water was freshly distilled before use. All other solvents used were of HPLC grade quality. $Ga(NO_3)_3 \cdot 9H_2O$ and $GaF_3 \cdot 3H_2O$ were obtained from Aldrich and used as received.

Synthesis of 4-carboxymethyl-7-benzyl-1,4,7-triazacyclononan-1-yl acetic acid lithium salt (Li_2L)

1,4,7-Triazacyclononane-1,4-dicarboxylic acid di-*tert*-butyl ester: A solution of 1,4,7-triazacyclonoanae (2.00 g, 0.016 mol) in 200 mL $CHCl_3$ was treated with 6 mL of Et_3N. A solution of 2-(boc-oxymino)-2-phenylacetonitrile (7.88 g, 0.032 mmol) in 50 mL $CHCl_3$ was added drop wise over 30 minutes to the rapidly stirring solution. The solution was stirred for a further 2 hours and was then concentrated under reduced pressure. The yellow residue was dissolved into 200 mL EtOAc before being successively washed with 4% $NaHCO_3$ (200 mL), $NaCl_{(aq)}$ (200 mL) and 10% citric acid (3 x 200 mL). Treatment with the citric acid moved the desired compound into the aqueous phase. The pH of the aqueous extracts was adjusted to pH 11 with the slow addition of NaOH. The turbid solution was extracted with 3 x 150 mL of $CHCl_3$. The organic phase was dried over $MgSO_4$, filtered and concentrated under reduced pressure to give a yellow oil. Yield 4.00 g, 77%. ^1H NMR ($CDCl_3$, 298 K) δ = 1.45 (s, [18H], ^tBu CH_3), 2.88-2.86 (m, [4H], tacn CH_2), 3.24-3.19 (m, [4H], tacn CH_2), 3.44-3.39 (m, [4H], tacn CH_2). $^{13}C\{^1H\}$ NMR ($CDCl_3$, 298 K) δ = 28.8 (^tBu CH_3), 47.9, 48.5, 48.8, 49.1, 50.2, 50.9, 51.1, 51.9, 52.8, 53.0 (tacn CH_2), 78.2, 79.8 (^tBu C), 156.2 (CO). ESI^+ MS (MeCN) *m/z* 329.0 (100%) $[M + H]^+$.

1-Benzyl-1,4,7-triazacyclononane-4,7-dicarboxylic acid di-*tert*-butyl ester: A solution of 1,4,7-triazacyclononane-1,4-dicarboxylic acid di-tert-butyl ester (2.91 g, 0.012 mol) in 30 mL toluene was treated with KOH (2.03 g, 0.037 mol). A solution of benzyl bromide (2.14 g, 0.013

mol) in 20 mL toluene was added drop wise over 10 minutes. The reaction mixture was heated to 70 °C for 24 hours. The reaction mixture was filtered to remove the salt by-product. The solution was dried over $MgSO_4$ and concentrated under reduced pressure to give the compound as a yellow oil. Yield 3.45 g, 80%. ^{1}H NMR ($CDCl_3$, 298 K) δ = 1.45 (s, [9H], ^{t}Bu CH_3), 1.52 (s, [9H], ^{t}Bu CH_3), 2.69-2.77 (m, [4H], tacn CH_2), 3.32-3.18 (m, [4H], tacn CH_2), 3.54-3.50 (m, [4H], tacn CH_2), 3.67 (s, [2H], $BzCH_2$), 7.20 (m, [1H], ArCH), 7.25 (m, [2H], ArCH), 7.31 (m, [2H], ArCH). ^{13}C{^{1}H} NMR ($CDCl_3$, 298 K) δ = 28.5 (^{t}Bu CH_3), 47.3, 47.6, 48.0, 48.2, 49.6, 49.8, (tacn CH_2), 79.7 (^{t}Bu C), 125.3, 126.9, 128.2, 129.0, 130.0, 131.5 (Ar CH), 137.9 ($BzCH_2$), 155.7 (CO). ESI$^+$ MS (MeCN) *m/z* 420 (100%) $[M + H]^+$.

4-Benzyl-1,4,7-triazacyclononane-1,4,7-ium bis(trifluoroacetate): A solution of 50% CF_3CO_2H/CH_2Cl_2 was added drop wise to a solution of 1-benzyl-1,4,7-triazacyclononane-4,7-dicarboxylic acid di-*tert*-butyl ester (2.56 g, 0.006 mol) in 15 mL CH_2Cl_2 at 0 °C. The solution was stirred at 0 °C for 3 hours. The solution was concentrated under reduced pressure and Et_2O was added to the yellow residue. The solvent was removed *in vacuo* to remove any trace CF_3COOH. This was repeated three times. The resulting yellow powder was washed with Et_2O/hexane (1:1, 200 mL) several times and dried under vacuum. Yield 2.20 g, 60%. ^{1}H NMR (CD_3OD, 298 K) δ = 2.99 (m, [4H], tacn CH_2), 3.18 (m, [4H], tacn CH_2), 3.62 (br s, [4H], tacn CH_2), 3.86 (s, [2H], $BzCH_2$), 7.40 (m, [5H], ArCH). ^{13}C{^{1}H} NMR (CD_3OD, 298 K) δ = 43.6, 45.1, 60.7 (tacn CH_2), 129.3, 129.9, 131.3 (ArCH), 137.2 ($BzCH_2$). ESI$^+$ MS (CD_3OD) *m/z* 220.3 (100%) $[M + H]^+$.

1-Benzyl-1,4,7-triazacyclononane: 4-Benzyl-1,4,7-triazacyclononane-1,4,7-ium bis(trifluoroacetate (2.10 g, 5.91 mmol) was dissolved in 75 mL $CHCl_3$ and cooled to 0 °C. Et_3N (5 mL) was added drop wise and the resulting solution stirred at 0 °C for 2 hours. The solution was washed with 3 x 200 mL saturated NaCl solution. The pale yellow organic phase was dried over $MgSO_4$, filtered and the solvent removed under reduced pressure to give the compound as an orange oil. Yield 1.26 g, 94%. ^{1}H NMR ($CDCl_3$, 298 K) δ = 2.67 (br m, [8H], tacn CH_2), 2.82 (br s, [4H], tacn CH_2), 3.73 (s, [2H], $BzCH_2$), 7.33 (m, [5H], ArCH). ^{13}C{^{1}H} δ = 43.6, 45.1, 60.7 (tacn CH_2), 129.3, 129.9, 131.4 (ArCH), 137.2 ($BzCH_2$). ESI$^+$ MS (MeOH) *m/z* 220.3 (100%) $[M + H]^+$.

4-Benzyl-7-ethoxycarbonylmethyl-1,4,7-triazacyclononane-1-yl-acetic acid ethyl ester: 1-Benzyl-1,4,7-triazacyclononane (1.22 g, 5.58 mmol) was dissolved in 20 mL anhydrous EtOH. A solution of ethyl bromoacetate (1.86 g, 11.16 mmol) in 10 mL anhydrous EtOH was added and the solution stirred. The solution was cooled to 0 °C and a solution of Na metal (0.26 g, 11.16 mmol) in 15 mL anhydrous EtOH was added drop wise. The resulting solution was stirred at 0 °C for 1 hour. A pale yellow suspension had formed. The solvent was removed *in vacuo* and the residue taken up into 30 mL of toluene, upon which the NaBr salt precipitated. The mixture

was stirred at room temperature for 2 hours in order to precipitate all of the salt by-product. The mixture was filtered and the solvent removed under reduced pressure. The intense yellow oil was washed with 20 mL 1:1 hexane/Et_2O and further dried under vacuum. Yield 1.70 g, 78%. ^{1}H NMR ($CDCl_3$, 298 K) δ = 1.27 (t, [6H], $EtCH_3$), 2.87-2.78 (m, [8H], tacn CH_2), 2.97 (br s, [4H], tacn CH_2), 3.41 (s, [4H], N-CH_2-COO), 3.68 (s, [2H], $BzCH_2$), 4.15 (quintet, [4H], $EtCH_2$), 7.34 (m, [5H], ArCH). ESI^+ MS (MeOH) *m/z* 392.1 (100%) $[M + H]^+$.

4-Carboxymethyl-7-benzyl-1,4,7-triazacyclononan-1-yl acetic acid lithium salt: 4-Benzyl-7-ethoxycarbonylmethyl-1,4,7-triazacyclononane-1-yl-acetic acid ethyl ester (1.65 g, 4.22 mmol) was dissolved in 20 mL EtOH. Lithium hydroxide hydrate (0.25 g, 6.00 mmol) was added and the solution heated to 70 °C for 25 hours. The solution was filtered and the solution removed *in vacuo* giving a yellow powder, which was washed with Et_2O and further dried *in vacuo.* Yield 1.05 g, 85%. ^{1}H NMR (D_2O, 298 K) δ = 2.22 (br m, [2H], tacn CH_2), 2.49 (m, [4H], tacn CH_2), 2.69 (br m, [6H], tacn CH_2), 3.07 (d, [2H], N-CH_2-CO), 3.73 (s, [2H], $BzCH_2$), 7.22 (m, [1H], ArCH), 7.27 (m, [2H], ArCH), 7.38 (m, [5H], Ar CH). $^{13}C\{^1H\}$ NMR (D_2O, 298 K) 52.5 (N-CH_2-CO), 53.8, 54.2, 63.7 (tacn CH_2), 129.3, 129.5, 131.6 (ArCH), 138.2 ($BzCH_2$), 181.0 (CO).

Synthesis of 1-benzyl-1,4,7-triazacyclonoane-4,7-dicarboxylic acid hydrochloride (H_2L·HCl)

The synthesis of H_2L·HCl was accomplished as described for Li_2L, however the final ester hydrolysis step was performed with HCl/dioxane to yield the dicarboxylic acid ligand as a hydrochloride salt. Yield 1.25 g, 90%. ^{1}H NMR (D_2O, 298 K) δ = 3.12-3.08 (m, [2H], tacn CH_2), 3.19 (s, [4H], tacn CH_2), 3.48 (m, [2H], tacn CH_2), 3.59 (br m, [4H], tacn CH_2), 3.72 (d, [4H], N-CH_2-CO), 4.50 (s, [2H], $BzCH_2$), 7.51 (br s, [3H], Ar CH), 7.55 (br s, [2H], Ar CH). $^{13}C\{^1H\}$ NMR (D_2O, 298 K) δ = 27.3 (N-CH_2-CO), 50.3, 50.6, 52.8, 56.7 (tacn CH_2), 129.5, 130.7, 130.9 (Ar CH), 136.8 ($BzCH_2$), 174.0 (CO).

[GaCl(L)]·2H_2O

A solution of H_2L·HCl (0.111 g, 0.332 mmol) in 3 mL freshly distilled H_2O was added dropwise to a solution of $Ga(NO_3)_3$·9H_2O in 3 mL H_2O. The yellow solution was heated to 85 °C for two hours. The solution was then cooled to room temperature and the volatiles were removed under high vacuum with gentle heating (~40 °C). The resulting yellow solid was washed with MeCN and the solution was filtered to remove undissolved particulates, before concentrating this to *ca.* 50% volume *in vacuo.* Treatment of the solution with diethyl ether precipitated a yellow-orange solid which was isolated by filtration and dried under high vacuum. Orange solid. Yield: 0.032 g, 21%. Required for $C_{17}H_{27}ClGaN_3O_6$; C; 43.02, H; 5.73, N; 8.85. Found: C; 42.80, H; 5.55, N; 8.77%. IR (Nujol, ν/cm^{-1}) 3619 (H_2O), 1749, 1641 (CO), 376 (Ga–Cl). ^{1}H NMR (D_2O, 298 K)

δ = 2.71−2.67 (m, [1H], tacn CH_2), 2.99–2.81 (m, [2H], tacn CH_2), 3.38–3.10 (m, [6H], tacn CH_2), 3.49–3.42 (m, [2H], tacn CH_2), 3.69–3.63 (m, [2H], tacn CH_2), 3.76–3.74 (d, [2H], $^2J_{HH}$ 10.5 Hz, N-CH_2CO_2), 3.82 (br s, [2H], N-CH_2CO_2), 4.06–4.02 (d, [1H], $^2J_{HH}$ 13.7 Hz, BzCH_2), 4.34–4.31 (d, [1H], $^2J_{HH}$ 13.8 Hz, BzCH_2), 7.48 (s, [5H], ArCH). $^{13}C\{^1H\}$ NMR (D_2O, 298 K) δ = 45.8, 51.5, 51.8, 52.4, 52.7, 53.4, 60.4, 62.0, 128.8, 132.2, 149.2, 175.4. ESI^+ MS (MeCN): *m/z* = 402.1 (100%) $[GaL]^+$. Weakly diffracting crystals of [GaCl(L)]·$2H_2O$ were grown from slow evaporation of a MeCN solution of the complex. Better quality crystals of the MeCN solvate [GaCl(L)]·MeCN were obtained from slow diffusion of ether into an acetonitrile solution of the complex.

[GaF(L)]·$2H_2O$

Method 1: $GaF_3·3H_2O$ (0.052 g, 0.288 mmol) and Li_2L (0.100 g, 0.288 mmol) were added to 7 mL freshly distilled H_2O. The mixture was transferred into a Teflon cup. The cup was placed into a stainless steel acid digestion bomb. The reaction was heated to 180 ºC for 18 h. The vessel was cooled gradually to room temperature. The grey LiF by-product was removed by filtration, leaving a yellow solution. Removal of the volatiles *in vacuo* gave a light brown solid which was washed with hexane and dried under high vacuum. Brown solid. Yield: 0.072 g, 54%. IR (Nujol, ν/cm-1) 3420 (H_2O), 1665, 1650 (C=O), 568 (Ga−F).^{1}H NMR (CD_3OD, 298 K) δ = 2.66 (m, [2H], tacn CH_2), 2.73 (s, [2H], tacn CH_2), 2.84 (br s, [2H], tacn CH_2), 3.15−2.99 (br m, [6H], tacn CH_2), 3.73−3.64 (m, [4H], N-CH_2CO_2), 4.14−3.95 (d, [1H], $^2J_{HH}$ 14.0 Hz, Bz CH_2), 4.70−4.46 (d, [1H], $^2J_{HH}$ 13.9 Hz, Bz CH_2), 7.45 (m, [5H], Ar CH). $^{19}F\{^1H\}$ NMR (CD_3OD, 298 K) δ = −184.6 (br s). ESI^+ MS (MeOH): *m/z* 402.1 (100%) $[GaL]^+$. Slow evaporation of the reaction solution produced large yellow crystals suitable for single crystal X-ray diffraction.

Method 2: A solution of KF (0.006 g, 0.095 mmol) in 3 mL H_2O was added drop wise to a solution of [GaCl(L)] (0.040 g, 0.095 mmol) in 3 mL H_2O. The yellow solution was stirred at room temperature for 90 minutes. The volatiles were removed under high vacuum with gentle heating (~ 40 ºC). The yellow solid was washed with MeOH. The solution was filtered to remove insoluble particulates. Removal of the volatiles *in vacuo* gave the product as a yellow solid. Yield 0.017 g, 60%. Spectroscopic data as for method 1.

Method 3: $Ga(NO_3)_3·9H_2O$ (0.030 g, 0.072 mmol), $H_2L·HCl$ (0.024 g, 0.072 mmol), and KF (0.004 g, 0.072 mmol) were added to 5 mL freshly distilled H_2O. The resulting yellow solution was stirred at room temperature for 90 minutes. The volatiles were removed under high vacuum with gentle heating (~ 40 ºC). The yellow solid was washed with MeOH. The insoluble particulates were removed by filtration and the solution concentrated *in vacuo* to give the complex as a yellow solid. Yield: 0.016 g, 58%. Spectroscopic data as for method 1.

Method 4: As described for method 3, but using $Ga(NO_3)_3 \cdot 9H_2O$ (0.025 g, 0.060 mmol), Li_2L (0.021 g, 0.060 mmol), and KF (0.003 g, 0.060 mmol). Yellow solid. Yield: 0.012 g, 44%. Spectroscopic data as for method 1.

Method 5: A solution of KF (0.005 g, 0.086 mmol) in 1 mL H_2O and Li_2L (0.033 g, 0.086 mmol) in 5 mL H_2O was added simultaneously to powdered $GaCl_3$ (0.015 g, 0.086 mmol). Addition of the aqueous solutions resulted in an exothermic reaction and the formation of an orange solution. The mixture was stirred at room temperature for 90 mins. over which time the solution darkened. The volatiles were removed under high vacuum with gentle heating (~ 40 ^oC). The yellow-orange solid was washed with MeOH. The insoluble particulates were removed by filtration and the solution concentrated *in vacuo* to give the desired complex as a yellow solid. Yellow solid. Yield: 0.026 g, 50%. Spectroscopic data as for method 1.

Radiolabelling Experiments

Experiments were analysed on a Gilson 322 HPLC system with a Gilson 156 UV detector. Dionex Chromeleon 6.8 Chromatography data recording software was used to integrate the UV and radiochemical peak areas. Analytical HPLC: Luna 5μ C18(2) 250 x 4.6 mm (Mobile Phase A = 10 mM ammonium acetate, B = 100% MeCN). Flow rate 1 mL/min. Gradient 0–15 min (10–90% B), 15–20 min (90% B), 20–21 min (90–10% B), 21–26.5 min (10% B). Product purification was accomplished using a Waters HLB SPE cartridge (WAT0942260) pre-conditioned with 5 mL EtOH and 10 mL H_2O.

ESI^+ mass spectra were recorded from direct injection of the products onto a Thermo Finnigan mass spectrometer fitted with an LCQ advantage MS pump.

NaOAc Buffer solutions were prepared *via* combination of the appropriate volumes of 2 mM NaOAc and 2 mM HOAc.

^{18}F Radiolabelling of [GaCl(L)]·2H_2O

$[GaCl(L)] \cdot 2H_2O$ (0.1 mg, 210 nmol) was dissolved into 0.4 mL of NaOAc buffer (pH 4) and added to ^{18}F (500-1000 MBq) in 0.1 mL NaOAc buffer (pH 4). The solution was stirred rapidly for 30 mins. at 80 ^oC. A 100 μL sample of the reaction mixture was removed and made up to 1 mL in H_2O. 100 μL of this solution was injected onto an RP HPLC system. Peak 1: Rt = 2.5 mins ($^{18}F^-$) 30-35%, 5.9–6.5 mins (product) 65-70% incorporation.

HLB Purification of [Ga^{18}F(L)]

The crude reaction mixture was diluted into 10 mL NaOAc buffer, loaded onto a pre-conditioned HLB cartridge and washed with 3 x 1 mL H_2O. The product was eluted with 2 x 0.2 mL 1:1 EtOH:H_2O. Cartridge purification gave *ca.* 50% yield of desired compound in up to 100 MBq/mL radioactive concentration.

Stability Studies

The HLB purified product was formulated into a number of solvent compositions of various pH so that the total formulated volume was 1 mL. 100 μL aliquots of the formulated product were removed and diluted further prior to injection on to the analytical HPLC.

***In situ* 'one pot' labelling reaction to form [Ga^{18}F(L)]**

$Ga(NO_3)_3 \cdot 9H_2O$ (1 mg in 0.5 mL NaOAc (pH 4), 2.40 μmol) and Li_2L (0.5 mg in 0.5 mL NaOAc (pH 4), 2.40 nmol) was added to $^{18}F/H_2{}^{18}O$ (300–500 MBq). The mixture was heated to 80 ºC for 30 mins. with vigorous stirring. The solution was cooled to room temperature. A 100 μL sample of the reaction mixture was removed and made up to 1 mL in NaOAc. 100 μL of this solution was injected onto an RP HPLC system. Peak 1: Rt = 2.5 mins ($^{18}F^-$) 10%, 3.1 mins (unidentified F^- salt) 10%, 6.0 mins. (product) 80%. The crude reaction mixture was purified by HLB cartridge purification.

X-Ray Crystallography

Crystals were obtained as described above. Details of the crystallographic data collection and refinement are in Table 1. *Rigaku AFC12* goniometer equipped with an enhanced sensitivity (HG) *Saturn724+* detector mounted at the window of an *FR-E+ SuperBright* molybdenum rotating anode generator (λ_1 = 0.71073 Å) with VHF *Varimax* optics (70 μm focus). Cell determination, data collection, data reduction, cell refinement and absorption correction: CrystalClear-SM Expert 2.0 r7. Structure solution and refinement were routine using WinGX and software packages within except for $[GaCl(L)] \cdot 2H_2O$ for which only very small, weakly diffracting crystals were obtained despite numerous recrystallization attempts. This species is isostrucutral with $[GaF(L)] \cdot 2H_2O$ and also with $[AlF(L)] \cdot 2H_2O$ hence, although the structure determination has high residuals, the geometry around the Ga atom is not in doubt.

Table 4.2: Selected crystallographic data.[a] L = $Bz(CH_2CO_2)_2$-tacn

Compound	**[GaCl(L)]·2H$_2$O**	**[GaCl(L)]·MeCN**	**[GaF(L)]·2H$_2$O**
Formula	$C_{17}H_{27}ClGaN_3O_6$	$C_{19}H_{26}ClGaN_4O_4$	$C_{17}H_{27}FGaN_3O_6$
M / g mol^{-1}	474.59	479.61	458.14
Temp. / K	100(2)	100(2)	100(2)
Crystal system	Monoclinic	Monoclinic	Monoclinic
Space group	$P2_1/c$ (14)	$P2_1/n$ (14)	$P2_1/c$ (14)
a [Å]	18.648(7)	12.018(2)	19.883(3)
b [Å]	8.132(3)	13.032(2)	7.1449(7)
c [Å]	13.197(5)	13.230(2)	13.8880(15)
α [deg]	90	90	90
β [deg]	101.328(12)	102.373(2)	106.465(8)
γ [deg]	90	90	90
U [Å^3]	1962.2(13)	2024.0(6)	1892.1(4)
Z	4	4	4
μ(Mo Kα) [mm^{-1}]	1.579	1.526	1.505
F(000)	984	992	952
Total reflections	9388	10274	12106
Unique reflections	4438	4626	4303
R_{int}	0.221	0.029	0.089
R_1 [$I_o > 2\sigma(I_o)$] [b]	0.141	0.030	0.067
R_1 [all data]	0.293	0.037	0.0907
wR_2 [$I_o > 2\sigma(I_o)$] [b]	0.322	0.077	0.144
wR_2 [all data]	0.412	0.080	0.155

[a] Common items: temperature = 100 K; wavelength (Mo-K_α) = 0.71073 Å;

[b] $R_1 = \Sigma \big| \, |F_o| - |F_c| \, \big| / \Sigma |F_o|$; $wR_2 = [\Sigma w(F_o^2 - F_c^2)^2 / \Sigma w F_o^4]^{1/2}$

4.6 References

1. Simecek, J.; Schulz, M.; Notni, J.; Plutnar, J.; Kubicek, V.; Havlickova, J.; Hermann, P., *Inorg. Chem* **2012,** *51*, 577-590.
2. Sun, Y.; Cutler, C. S.; Martell, A. E.; Welch, M. J., *Tetrahedron* **1999,** *55*, 5733-5740.
3. Craig, A. S.; Parker, D.; Adams, H.; Bailey, N. A., *J. Chem. Soc., Chem. Commun.* **1989**, 1793-1794.
4. Singh, A. N.; Liu, W.; Hao, G.; Kumar, A.; Gupta, A.; Oez, O. K.; Hsieh, J.-T.; Sun, X., *Bioconjugate Chem.* **2011,** *22*, 1650-1662.
5. Aldridge, S.; Downs, A., *The Group 13 Metals, Aluminium, Gallium, Indium and Thallium: Chemical Patterns and Paculiarities*. Wiley: Chichester, 2011.
6. D'Souza, C. A.; McBride, W. J.; Sharkey, R. M.; Todaro, L. J.; Goldenberg, D. M., *Bioconjugate Chem.* **2011,** *22*, 1793-1803.
7. Song, Y.-F.; Berry, J. F.; Bill, E.; Bothe, E.; Weyhermüller, T.; Wieghardt, K., *Inorg. Chem.* **2007,** *46*, 2208-2219.
8. Shetty, D.; Choi, S. Y.; Jeong, J. M.; Lee, J. Y.; Hoigebazar, L.; Lee, Y.-S.; Lee, D. S.; Chung, J.-K.; Lee, M. C.; Chung, Y. K., *Chem. Commun.* **2011,** *47*, 9732-9734.
9. Goldenberg, D. M.; Sharkey, R. M.; McBride, W. J.; Boerman, O. C., *J. Nucl. Med.* **2013,** *54*, 1170-1173.
10. McBride, W. J.; D'Souza, C. A.; Goldenberg, D. M. Methods and compositions for F-18 labeling of proteins, peptides and other molecules. US20090246130A1, 2009.
11. McBride, W. J.; Sharkey, R. M.; Goldenberg, D. M., *EJNMMI Res.* **2013,** *3*, 36/1-36/11.
12. D'Souza, C. A.; McBride, W. J.; Sharkey, R. M.; Todaro, L. J.; Goldenberg, D. M., *Bioconjugate Chem.* **2011,** *22*, 1793-1803.
13. Kimura, S.; Bill, E.; Bothe, E.; Weyhermüller, T.; Wieghardt, K., *J. Am. Chem. Soc.* **2001,** *123*, 6025-6039.
14. Carty, A. J.; Tuck, D. G., *Prog. Inorg. Chem.* **1975,** *19*, 245-337.
15. Mason., J., *Multinuclear NMR*. Plenum Press: 1987; Vol. 1.
16. Bhalla, R.; Darby, C.; Levason, W.; Luthra, S. K.; McRobbie, G.; Reid, G.; Sanderson, G.; Zhang, W., *Chem. Sci.* **2014,** *5*, 381-391.
17. Shannon, R. D., *Acta Crystallogr., Sect. A* **1976,** *A32*, 751-767.
18. Secco, F.; Venturini, M., *Inorg. Chem.* **1975,** *14*, 1978-1981.
19. Bodor, A.; Tóth, I.; Bányai, I.; Szabó, Z.; Hefter, G. T., *Inorg. Chem.* **2000,** *39*, 2530-2537.
20. Kazakov, I. V.; Bodensteiner, M.; Timoshkin, A. Y., *Acta Crystallogr., Sect. C.* **2014,** *70*, 312-314.
21. Burt, J.; Levason, W.; Light, M. E.; Reid, G., *Dalton Trans.* **2014,** *43*, 14600-14611.

22. Timoshkin, A. Y.; Bodensteiner, M.; Sevastianova, T. N.; Lisovenko, A. S.; Davydova, E. I.; Scheer, M.; Grassl, C.; Butlak, A. V., *Inorg. Chem.* **2012,** *51*, 11602-11611.
23. Glaser, M.; Iveson, P.; Hoppmann, S.; Indrevoll, B.; Wilson, A.; Arukwe, J.; Danikas, A.; Bhalla, R.; Hiscock, D., *J. Nucl. Med.* **2013,** *54*, 1981-1988.

Chapter 5

H-bonding and Secondary Coordination of Neutral Trifluoride Complexes to Metal cations; Synthesis, Characterisation and Structural Trends

5.1 Introduction

A key contribution to the identification of the radio-labelled compound $[Ga^{18}F^{19}F_2(BzMe_2\text{-tacn})]$ discussed in Chapter 3 was based on the evidence observed in the ESI mass spectrum of the purified labelled compound (Chapter 3.2.5). The dominant species was identified as the monocation $\{[GaF_3(BzMe_2\text{-tacn})] + NH_4\}^+$, the ammonium cation arising from the NH_4OAc mobile phase used in the HPLC purification of the radiolabelled complex. It was proposed that the interaction arose from the highly electronegative face of the *fac*-trifluoride complex which formed an H-bonding interaction with the positively charged ammonium cation. The role of the ammonium cation was vital in being able to identify the radiolabelled compound; the neutral molecular gallium complex is not readily protonated and so requires the association of the ammonium cation to be observed with positive ion electrospray mass spectrometry. This observation raised the possibility of being able to utilise the electron rich *fac*-GaF_3 core to form similar interactions with a series of other cations, and to identify this both under the soft ionisation technique of electrospray mass spectrometry and in the solid state by single crystal X-ray diffraction, provided the correct salt is chosen. This chapter describes an investigation probing these unusual interactions. Suitable cations were identified through a series of mass spectrometry experiments, which showed that monocations of the alkali metals and organic molecules such as ammonium were more favoured than any di- or tri-cations of the alkaline earth and early transition metals. Once screened by ESI^+ MS, attempts were made to crystallise interesting new assemblies. The crystal structures are described and discussed in detail, especially in the context of potential new metalloligand building blocks. Attempts to observe the H-bonding interactions between the GaF_3 unit and ammonium based cations to the metal fluoride complexes in the solution phase using ^1H NMR spectroscopy are also shown.

5.1.1 Metalloligand

A metalloligand is broadly defined as the smallest building block that allows the construction of a more complex architecture; often a supramolecular structure.[1] In order to extend into new and interesting architectures, a metalloligand offers functional groups that allow its transition from a molecular species to a supramolecular assembly. In this context, hydrogen bond or coordination bond sensitive groups are the ideal synthons because of their propensity to self-assemble into highly ordered structures. In the case of the complexes

discussed in this chapter, the *fac*-trifluoride moiety in the complexes [MF_3(RMe_2-tacn)] offers a region of high electronegativity, which may allow weakly electrostatic or dative interactions, and act as a strong H-bond acceptor. The strong H-bonding ability of the metal trifluoride complexes has already been demonstrated by the supramolecular assemblies formed *via* H-bonding of the complex to the co-crystallised water molecules (see Chapter 2.3.1).[2]

A metalloligand also offers binding sites to coordinate a secondary metal ion, which facilitates the placing of two metals in close proximity to one another. This thus allows the construction of heterometallic networks which might otherwise be synthetically challenging.

There are numerous examples of ligand frameworks used towards potential metalloligands, a selection of neutral ligands are depicted in Figure 5.1.

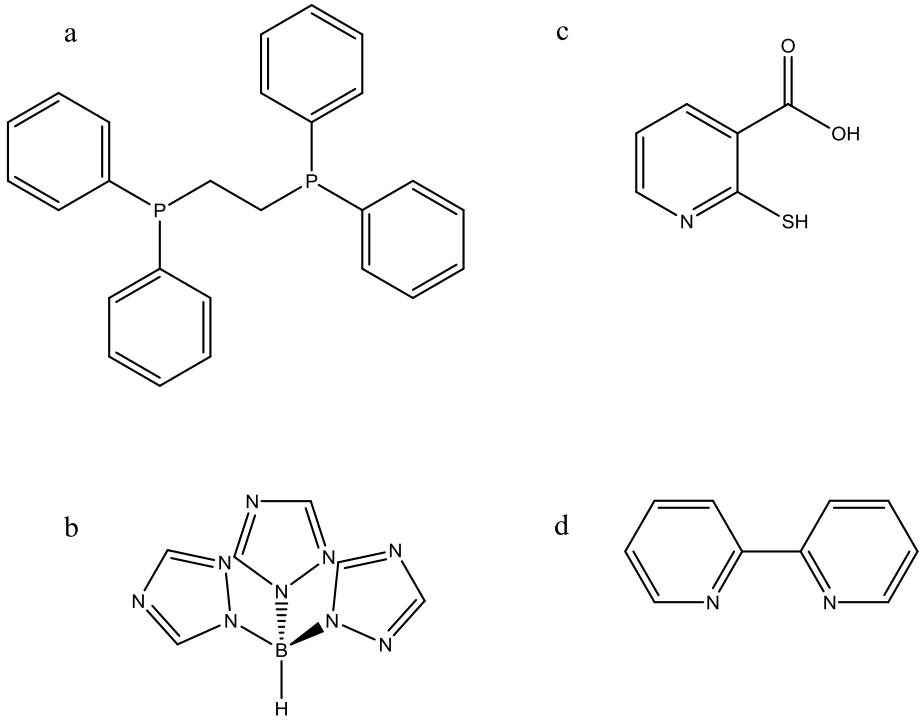

Figure 5.1: Selected example of neutral ligand frameworks from which metalloligands have been prepared. a = 1,2-bis(diphenylphosphino)ethane[3], b = hydrotris(1,2,4-pyrazolyl)borate[4], c = 2-mercaptonicotine acid[5], d = 2,2′-bipyridine[6].

Reaction of 1,2-bis(diphenylphosphino)ethane (dppe, a) with $AuCl_2$ gives the phosphine bridged complex [Au_2Cl_2(dppe)] which through further reaction with a chiral penicillaminate $_D$-Hpen and $Co(OAc)_2{\cdot}4H_2O$ gives the $Au^I_4Co^{III}_2$ hexanuclear complex [Au_4Co_2(dppe)$_2$($_D$-pen)$_4$][ClO_4]. The crystal structure showed that the cations and anions aggregated separately leading to distinct supramolecular assemblies.[3]

Hydrotris(1,2,4-pyrazolyl)borate (Tt, b) was shown to react with $Co(OAc)_2 \cdot 4H_2O$ to form the paramagnetic complex $[Co(Tt)_2]$. This complex has shown its utility in the preparation of multifunctional magnetic metal organic frameworks.[4]

2-Mercaptonicotine acid (c) has been utilised in the assembly of 3d-4d heterometallic coordination polymers under mild conditions [5] and 2,2′-bipyridine (d) has formed complexes with ruthenium, which can act as a metalloligand for asymmetric catalysis.[6]

5.1.2 Metal fluorides as functional building blocks

It is likely that the use of metal fluorides as potential building blocks has had limited study due to the generally poor solubility of neutral metal fluoride complexes in common organic solvents.[7] Until recently, the coordination of functional metal fluoride species to form interesting assemblies was limited to the studies by Tramsek and co-workers on the binary p-block fluorides XeF_2 and AsF_3 and their ability to coordinate *via* F to Ln^{3+} and alkaline earth dications.[8, 9] Examples include the complex $[Ca(AsF_3)](AsF_6)_2$ the first alkaline earth metal cation coordinated to AsF_3, in which the AsF_3 'ligand' bridges two metal centres (Figure 5.2).[10]

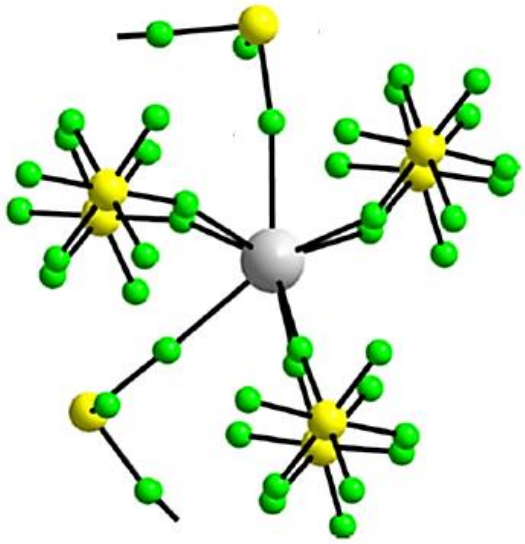

Figure 5.2: Image showing the coordination sphere of Ca(II) in $[Ca(AsF_3)](AsF_6)_2$.[10] Colour key: silver = Ca, green = F, yellow = As. Image redrawn from CCDC 413965.

The formation of this complex occurs under rather forcing conditions. Not only does it require the use of anhydrous HF and AsF_5 as a solvent, it also requires heating at 393 K for 14 days.[11]

Examples of XeF_2 coordination are demonstrated through reaction of $Mg(AsF_6)_2$ with an excess of XeF_2 and anhydrous HF over several days at room temperature to give the unusual complex $[Mg(XeF_2)_n](AsF_6)_2$ n = 2, 4, the first example of XeF_2 coordinated to an alkaline earth metal cation (Figure 5.3).[12]

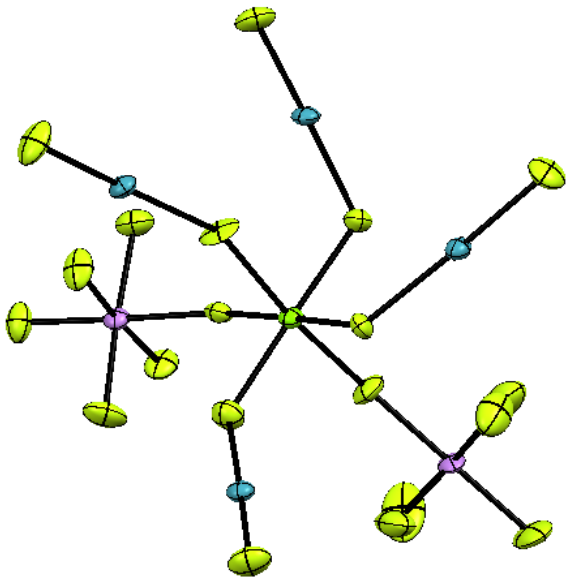

Figure 5.3: Crystal structure of $[Mg(XeF_2)_4](AsF_6)_2$.[12] Colour key: green = Mg, yellow = F, blue = Xe, pink = As. Image redrawn from CCDC 060421.

The structure shows a six-coordinate magnesium centre with contribution to the coordination sphere provided by four fluorides from XeF_2 and two fluorides from the $[AsF_6]^-$. The two coordinated $[AsF_6]^-$ anions are coordinated in a *cis*-arrangement.

Werner *et al.* described the synthesis and crystal structures of a number of caesium triorganofluorometalates *via* reaction of two molar equivalents of CsF with $MMes_3$ (M = Ga, In, mes = mesityl) in anhydrous MeCN.[13] Cooling of the reaction mixture yielded crystals of the unusual complexes $[\{Cs(MeCN)_2\}\{Mes_3MF\}]_2 \cdot 2MeCN$ (Figure 5.4).[13] The structure shows a centrosymmetric dimer in which two $GaMes_3$ units coordinate to two CsF molecules to form a Cs_2F_2 rhombus core. The coordination sphere around each Cs^+ centre is completed by two MeCN molecules, and an η^3-arene interaction of one of the mesityl groups to form a 7-coordinate Cs centre. The gallium complex is tetrahedral in which d(Ga-F) was measured to be 1.904(5) Å, approximately 0.04 Å longer than the mean Ga-F bond lengths in the complex $[GaF_3(Me_3\text{-tacn})] \cdot 4H_2O$ prepared in Chapter 2.3.3 (mean d(Ga-F) = 1.866(3) Å). This elongated Ga-F bond length is probably due to the sterically bulky mesityl groups coordinated to the gallium centre.

The η^3-arene coordination to the mesityl group to the caesium centre results in the caesium sequestering the MeCN solvent to complete the coordination sphere.

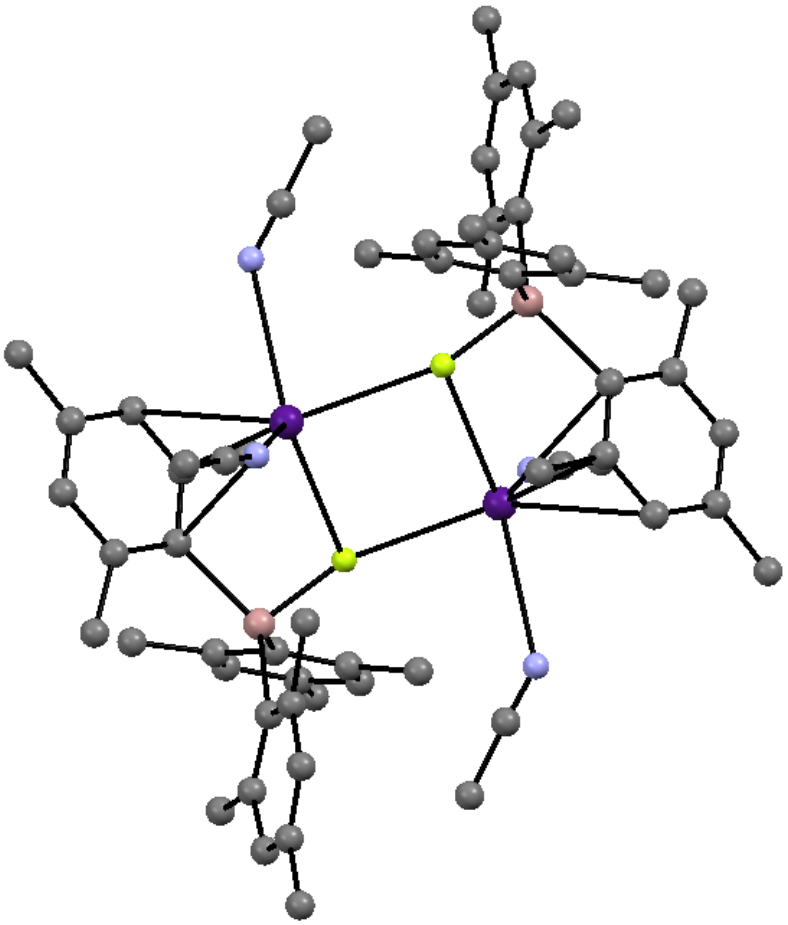

Figure 5.4: The crystal structure of $[\{Cs(MeCN)_2\}\{Mes_3GaF\}]_2 \cdot 2MeCN$.[13] H-atoms and solvent molecules are omitted for clarity. η^3 interaction of the mesityl group towards the Cs centre is shown. Colour key: pale pink = Ga, purple = Cs, yellow = F, blue = N, grey = C.

Reaction of two molar equivalents of CsF with $Ga(Bz)_3$ in anhydrous MeCN leads to the formation of $[Cs\{(Bz)_3GaF\}]_2 \cdot 2MeCN$, where the aryl groups fold over to form an η^6 interaction with the caesium ion (Figure 5.5).

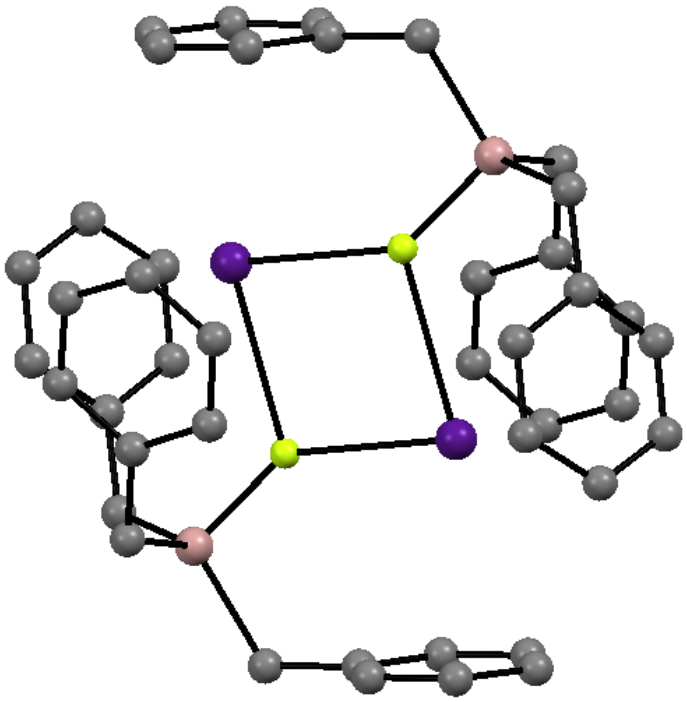

Figure 5.5: Crystal structure of $[Cs\{(Bz)_3GaF\}]_2 \cdot 2MeCN$.[13] H-atoms and solvent molecules are omitted for clarity. The η^6 arene interactions are omitted for clarity. Colour key: pale pink = Ga, purple = Cs, yellow = F, blue = N, grey = C.

The centrosymmetric dimer contains the same Cs_2F_2 rhombus core as the $[\{Cs(MeCN)_2\}\{Mes_3GaF\}]_2 \cdot 2MeCN$ structure however, unlike the $[\{Cs(MeCN)_2\}\{Mes_3GaF\}]_2 \cdot 2MeCN$ complex, in which the MeCN solvent is coordinated to the caesium ion in order to complete the coordination sphere, there is no coordinated solvent. This is due to the three η^6 interactions from the aromatic rings. The Ga-F bond length in $[Cs\{(Bz)_3GaF\}]_2 \cdot 2MeCN$ was found to be 1.860(2) Å which is 0.04 Å shorter than the $[\{Cs(MeCN)_2\}\{Mes_3GaF\}]_2 \cdot 2MeCN$ complex. This work demonstrated that complex structures may be obtained from the reaction of suitable metal fluoride salts with a neutral gallium containing complex.

Work by Weyhermüller *et al.* published shortly before the work discussed in this chapter showed the utility of fluoride-bridged bimetallic clusters of the form $\{Gd^{III}_3M^{III}_2\}$ (M= Fe, Cr, Ga) as potential molecular magnetic refrigerants.[14]

The complexes $[MF_3(Me_3\text{-tacn})] \cdot 4H_2O$ (M = Fe, Ga) were synthesised by refluxing FeF_3 and $GaF_3 \cdot 3H_2O$ with Me_3-tacn in DMF, in contrast to the hydrothermal synthesis applied previously in this thesis. Gentle mixing of $[MF_3(Me_3\text{-tacn})] \cdot 4H_2O$ (M = Fe, Cr, Ga) with

$Gd(NO_3)_3{\cdot}5H_2O$ in acetonitrile leads to crystals of the unusual complexes $[\{MF_3(Me_3\text{-tacn})\}_2Gd_3F_2(NO_3)_7(H_2O)(MeCN)]{\cdot}4MeCN$ (Figure 5.6).

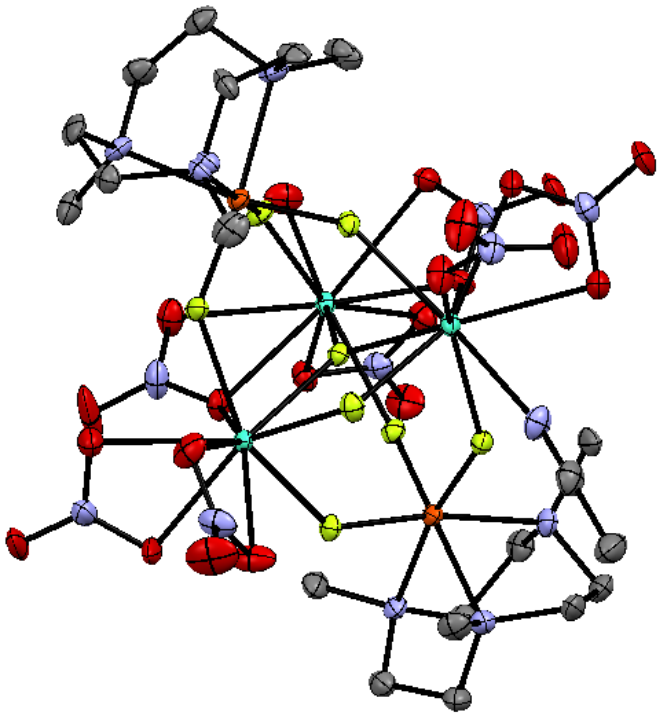

Figure 5.6: Structure of $[\{FeF_3(Me_3\text{-tacn})\}_2Gd_3F_2(NO_3)_7(H_2O)(MeCN)]{\cdot}4MeCN$. H-atoms and solvated MeCN molecules omitted for clarity. The fluoride ligands from the $[FeF_3(Me_3\text{-tacn})]$ act as ligands towards the gadolinium centre, forming a Fe-F-Gd unit. Colour key: turquoise = Gd, orange = Fe, green = F, blue = N, red = O, grey = C. The chromium and gallium analogues are isomorphous. Image redrawn from CCDC 961241.

The crystal structures show two $[MF_3(Me_3\text{-tacn})]$ complexes acting as metalloligands to three gadolinium centres. A single fluoride ligand from the $[MF_3(Me_3\text{-tacn})]$ coordinates to each Gd(III) centre forming a M-F-Gd-F-M fragment (Figure 5.7).

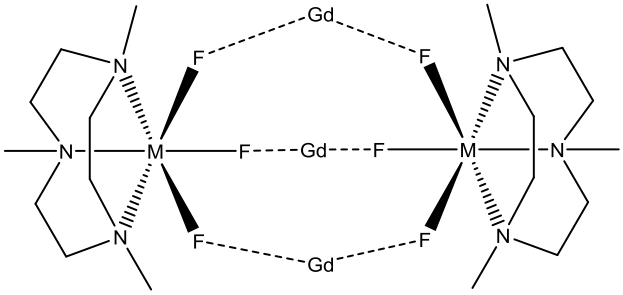

Figure 5.7: Schematic showing the coordination of the $[MF_3(Me_3\text{-tacn})]$ to the Gd(III) centres in the complexes $[\{MF_3(Me_3\text{-tacn})\}_2Gd_3F_2(NO_3)_7(H_2O)(MeCN)]{\cdot}4MeCN$. The full coordination environment around the gadolinium is not shown. Bond lengths and angles not drawn to scale.

The capping *fac*-[$MF_3(Me_3tacn)$] units impose an approximately isosceles {Gd_3} triangle. Two edges consist of η_1:η_2 :μ_2-bridging nitrate ions and one edge consists of a μ_2-fluoride (Figure 5.7). Additionally, the centre furnishes a single μ_3-fluoride bridge close to the {Gd_3} plane. This results in the three Gd(III) centres adopting a 9-coordinate tricapped trigonal prismatic geometry. The Gd-F bond lengths derived from the fluoride ligands in the [$MF_3(Me_3$-tacn)] complex for the gallium example fall within the range of 2.264(3) - 2.330(3) Å. These fall within the sum of the ionic radii of Gd^{3+} and F^- (1.247 and 1.19 Å respectively). The Ga-F distances in the cluster lie in the range of 1.867(4) – 1.891(3) Å. This shows a small 0.02 Å increase from the molecular complex reported in Chapter 2.2.3 (d(Ga-F) = 1.846(3)-1.865(3) Å).

A surprising element in the formation of these structures is that the formation of the fluoride bridged bimetallic clusters is preferred over precipitation of the insoluble polymeric GdF_3.

The chromium and iron analogues were found to have large magnetic entropy changes due to the weak interactions and the lightweight ligand sphere. This work in particular has demonstrated the potential utility of the complexes [$MF_3(RMe_2$-tacn)] in the formation of interesting supramolecular assemblies and provided the metal centres are suitable, have been shown to have potential utility in molecular magnetic refrigerants.

5.2 Results and Discussion

5.2.1 Mass spectrometry experiments

In order to further investigate the unusual behaviour observed in the mass spectrometry from the ^{18}F radiolabelling work (Chapter 3.2.6), ESI mass spectrometry was used to investigate the speciation of the pre-formed neutral trifluoride complexes [$MF_3(RMe_2$-tacn)] (M = Al, Ga, R= Bz, Me) with a variety of cations on a preparative scale.[15]

The preformed neutral complexes [$GaF_3(RMe_2$-tacn)] R = Bz, Me, were reacted in a 1:1 molar ratio with various metal and organic cations in 5:1 MeCN:H_2O. This solvent mixture mimics the solvent composition used in the radiolabelling of the neutral chelates. An aliquot of the solution was taken and further diluted with aqueous MeCN and the ESI^+ mass spectrum recorded.

ESI^+ MS of the solution formed by addition of NH_4PF_6 to the neutral complex [$GaF_3(BzMe_2$-tacn)] gives the expected species {[$GaF_3(BzMe_2$-tacn)] + NH_4}$^+$ confirming the observations from the labelling experiments (Figures 5.8 and 5.9).

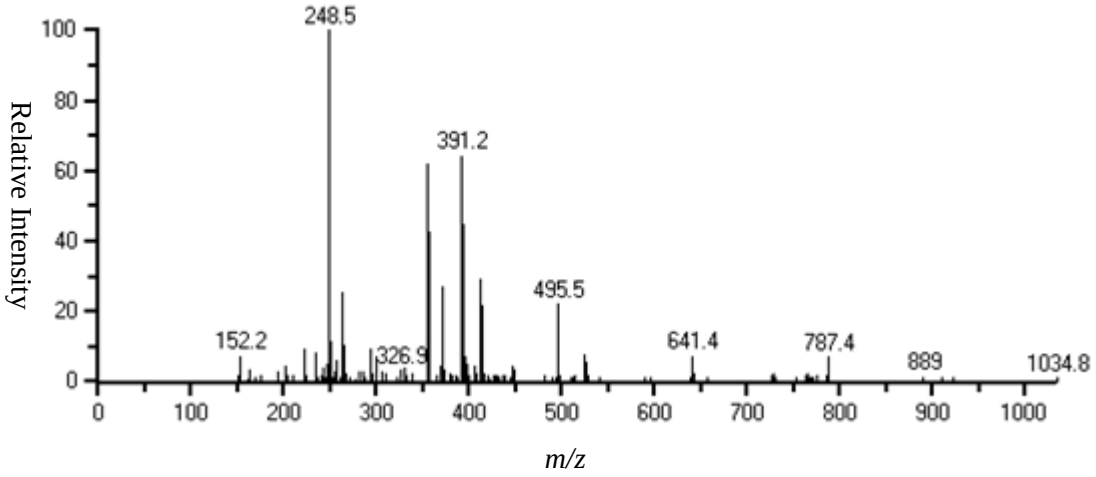

Figure 5.8: ESI^+ mass spectrum from the reaction of $[GaF_3(BzMe_2\text{-tacn})]$ with NH_4PF_6. *m/z* = 391.2 (63%) $\{[GaF_3(BzMe_2\text{-tacn})] + NH_4\}^+$.

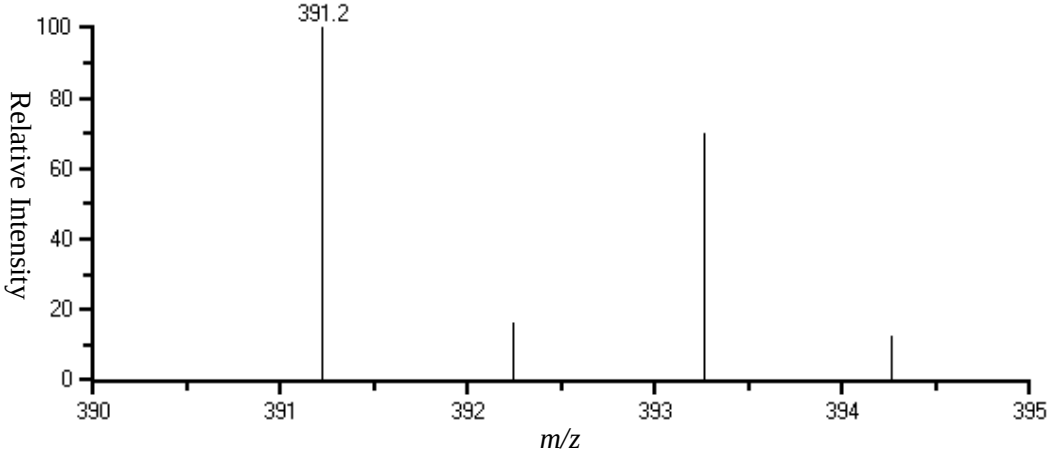

Figure 5.9: Expansion of the peak at *m/z* = 319.2 confirming the correct isotope pattern for $\{[GaF_3(BzMe_2\text{-tacn}] + NH_4\}^+$.

Gallium has two stable isotopes, ^{69}Ga and ^{71}Ga,[16] in a ratio of approximately 3:2. This is reflected in the isotope pattern of the gallium containing compounds mass spectrum, where the peak at 100% intensity is complimented by a peak two mass units higher at about 66% intensity.

Due to the more readily available hydrated complex $[GaF_3(Me_3\text{-tacn})]\cdot 4H_2O$, which was expected to provide a greater range of species, the vast majority of the mass spectrum experiments were performed with the complex $[GaF_3(Me_3\text{-tacn})]$. Combination of $[GaF_3(Me_3\text{-tacn})]$ with a variety of Group 1 salts give the correct *m/z* and isotope pattern consistent with $\{[GaF_3(Me_3\text{-tacn})] + M\}^+$, M = Li, Na, K, Rb, Cs.

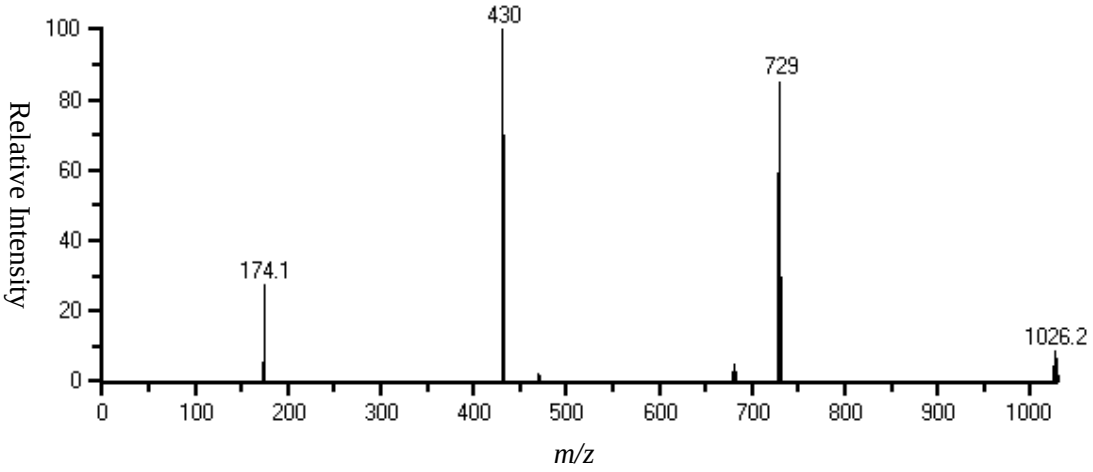

Figure 5.10: ESI^+ mass spectrum from the reaction of $[GaF_3(Me_3\text{-tacn})]$ with Cs_2CO_3. m/z = 174.1 (28%) $\{Me_3\text{-tacn} + H\}^+$, 430 (100%) $\{[GaF_3(Me_3\text{-tacn})] + Cs\}^+$, 729 (84%) $\{[GaF_3(Me_3\text{-tacn})]_2 + Cs\}^+$, 1026 (9%) $\{[GaF_3(Me_3\text{-tacn})]_3 + Cs\}^+$.

In addition, some mass spectra gave evidence for the dimeric and trimeric monocations $\{[GaF_3(Me_3\text{-tacn})]_x+M\}^+$ x = 2, 3 (Figure 5.11 and 5.12). This indicates that under the mass spectroscopy conditions utilised, the metal cation could bind up to three gallium fluoride metalloligands.

The observation of these species was unexpected. The high affinity of the alkali metal cations for water is well known, therefore one would expect the alkali metal to preferentially bind to water under the aqueous conditions in the mass spectrometer injection system.[17] The mass spectrometry data therefore shows the driving force required for the alkali metal to associate to the MF_3 face is even lower than that required to bind to water.

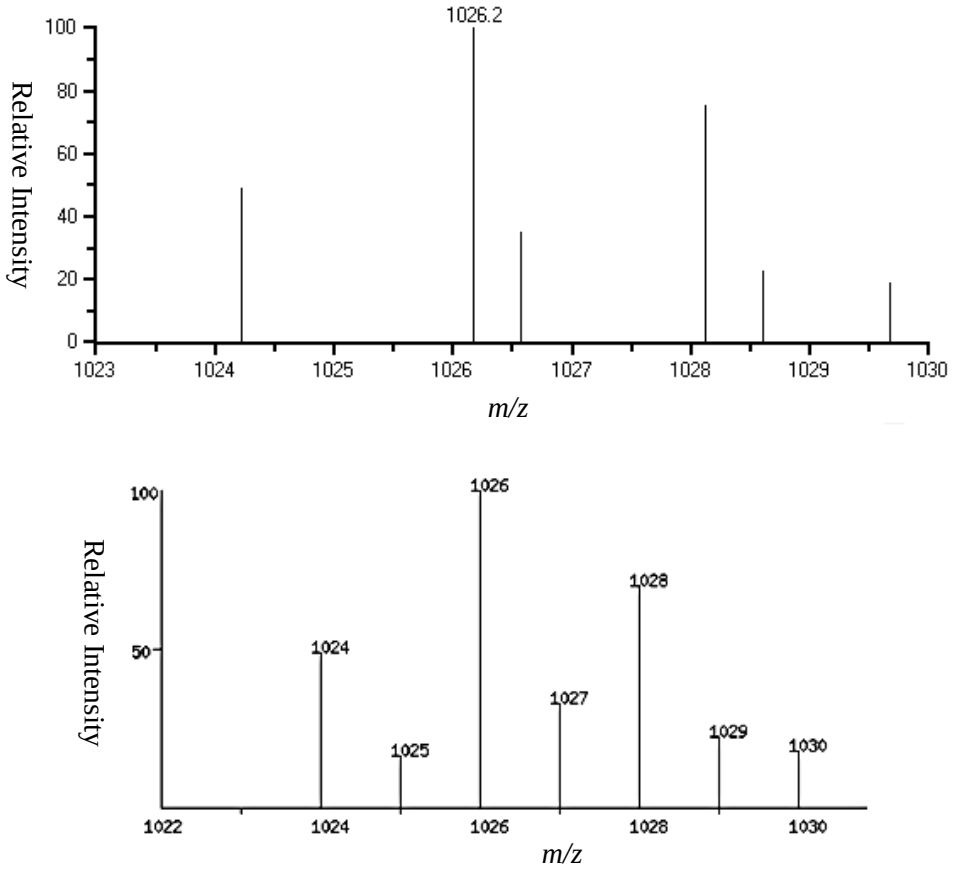

Figure 5.11: The expanded ESI$^+$ mass spectrum for $\{[GaF_3(Me_3\text{-tacn})]_3 + Cs\}^+$ (above) and the predicted isotope pattern for the species (below).

Salt	***m/z* {[GaF_3(Me_3-tacn)] + M}$^+$ (relative intensity)**	***m/z* {[GaF_3(Me_3-tacn)]$_2$ + M}$^+$ (relative intensity)**	***m/z* {[GaF_3(Me_3-tacn)]$_3$ + M}$^+$ (relative intensity)**
NH_4PF_6	315 (100%)	614 (7%)	n.o.
$NaBF_4$	320 (100%)	619 (75%)	916 (30%)
KPF_6	336 (100%)	635 (60%)	n.o.
$RbNO_3$	384 (100%)	681 (78%)	n.o.
$CsCO_3$	430 (100%)	729 (82%)	1026 (17%)

Table 5.1: Table describing the m/z and relative intensity of the species formed via reaction of [GaF_3(Me_3-tacn)] with a variety of monocations, (n.o. = not observed).

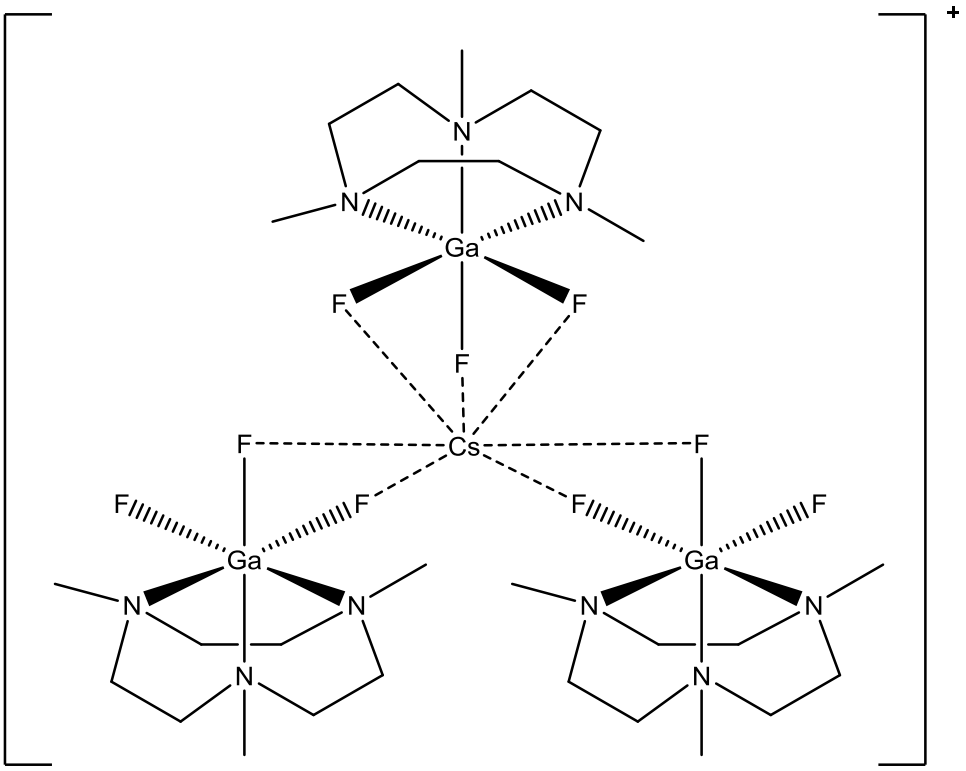

Figure 5.12: Diagram of the proposed cation $\{[GaF_3(Me_3\text{-tacn})]_3 + Cs\}^+$ observed by mass spectrometry. *m/z* = 1026 (17%). Solvent water molecules may also be coordinated to the large Cs^+ ion leading to 8 or 9-coordinate species.

The data shows that with monocationic salts of the alkali metals and ammonium there is an affinity for binding of the neutral trifluoride complex to the cation under the conditions utilised in the mass spectrometry technique.

An extension of the organic monocations involved the use of the imidazolium based 1-methyl-3-ethyl-imidizolium (EMIM) cation (Figure 5.13).

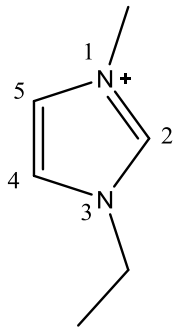

Figure 5.13: 1-methyl-3-ethyl-imidizolium organic cation used in the mass spectrometry experiments.

The proton in the 2-position of the imidazolium ring is particularly acidic (pKa 14.52 for free imidazole[18]), resulting in strong H-bond donor capability, hence giving the possibility of the

cation associating to the metal complex in a similar fashion as the ammonium cation discussed above and in Chapter 3.2.6.[19]

The [EMIM][BF_4] salt was combined with [GaF_3(Me_3-tacn)] and the mass spectrum was recorded. Evidence for the formation of the associated ion {[GaF_3(Me_3-tacn)] + EMIM}$^+$ was observed. However, the relative proportion of the cation (based upon the relative intensity) was significantly lower than the sodium associated species (also observed in the same mass spectrum). It is assumed that the gallium complex preferentially interacts with the sodium cations present in the mass spectrometer rather than the strongly H-bonding organic cation (Figure 5.14).

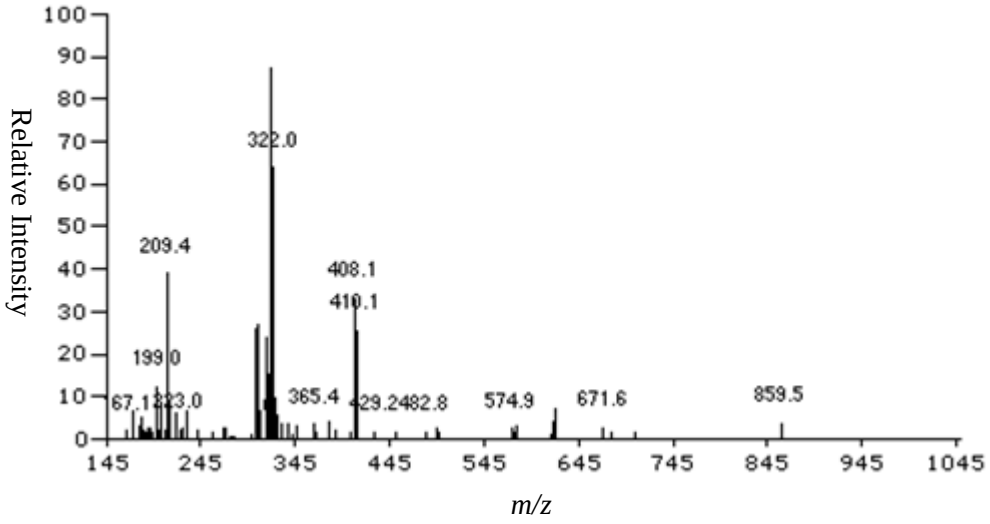

Figure 5.14: ESI$^+$ mass spectrum from the reaction of [GaF_3(Me_3-tacn)] with [EMIM][BF_4]. *m/z* = 322 (88%) {[GaF_3(Me_3-tacn)] + Na}$^+$, 408 (33%) {[GaF_3(Me_3-tacn)] + EMIM}$^+$.

Attempts were made to observe similar species in the mass spectrum using the Group two and three salts such as $CaCO_3$ and $Sc(NO_3)_3$. However no identifiable species were observed. While the vast majority of the mass spectrometry experiments were performed with the gallium complexes, and thus are discussed in most depth here, the corresponding aluminium-fluoride complex [AlF_3(Me_3-tacn)] also formed similar species as described for the gallium analogue. Examples include reaction of [AlF_3(Me_3-tacn)] with NH_4PF_6 which gives a mass spectrum consistent with the species {[AlF_3(Me_3-tacn)] + NH_4}$^+$ (m/z = 273.3 (100%) (Figure 5.15).

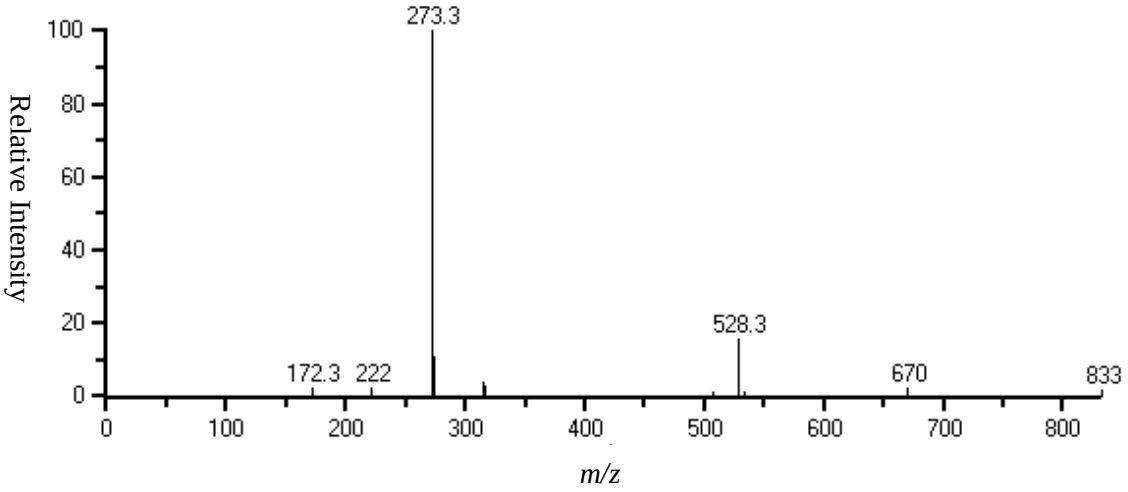

Figure 5.15: ESI^+ mass spectrum from the reaction of $[AlF_3(Me_3\text{-tacn})]$ with NH_4PF_6. m/z = 273.3 (100%) $\{[AlF_3(Me_3\text{-tacn})] + NH_4\}^+$, 528.3 (18%) $\{[AlF_3(Me_3\text{-tacn})]_2 + NH_4\}^+$.

This shows that the effect of the metal centre in the metal fluoride complex has no influence on the type of species observed in the mass spectrum.

5.2.2 Solid state structures of cation associated supramolecular structures

Having demonstrated the ability to form the cation associated complexes of the form $\{[GaF_3(RMe_2\text{-tacn})] + M\}^+$ using the soft ionisation technique of electrospray mass spectrometry, the ability to form these complexes in the solid state was investigated. As ESI^+ mass spectrometry does not take into account the anion, hence the solid state structures could potentially demonstrate some unusual coordination chemistry of traditionally 'non-coordinating' anions.[20, 21]

Despite repeated attempts, crystallisation of complexes using $[GaF_3(Me_3\text{-tacn})]\cdot 4H_2O$ proved unsuccessful, instead the constituent components crystallising separately (as confirmed from unit cell determinations from crystals grown from the reaction vial). The $[GaF_3(Me_3\text{-tacn})]$ is heavily hydrated in the solid state, forming extensive F···H-O and O···H-O H-bonding interactions.[2] It is presumed that the high degree of hydration prevented the formation of the desired complexes in the solid state. It is likely that the crystallisation conditions would need to be modified to drive the formation of the extended structures with $[GaF_3(Me_3\text{-tacn})]$. The corresponding $[GaF_3(BzMe_2\text{-tacn})]\cdot 2H_2O$ complex was used which crystallised out the complexes discussed more readily. Reaction of $[GaF_3(BzMe_2\text{-tacn})]$ with one molar equivalent of the appropriate salt (e.g. $LiBF_4$, $NaBF_4$, KPF_6, and NH_4PF_6) in 5:1 MeCN:H_2O yielded colourless solutions which were allowed to slowly evaporate at room temperature.[15, 22] In some

cases an amorphous white solid formed. However, in other cases large crystals suitable for single crystal X-ray diffraction were obtained.

Combination of $[GaF_3(BzMe_2\text{-tacn})]$ with $LiBF_4$ in aqueous MeCN furnished a small number of crystals suitable for single crystal X-ray diffraction. Structural analysis indicated the formation of the very unusual centrosymmetric dimer $[\{GaF_3(BzMe_2\text{-tacn})\}_2Li_2(OH_2)_2(BF_4)_2]\cdot H_2O$ (compound **1)** (Figure 5.16).

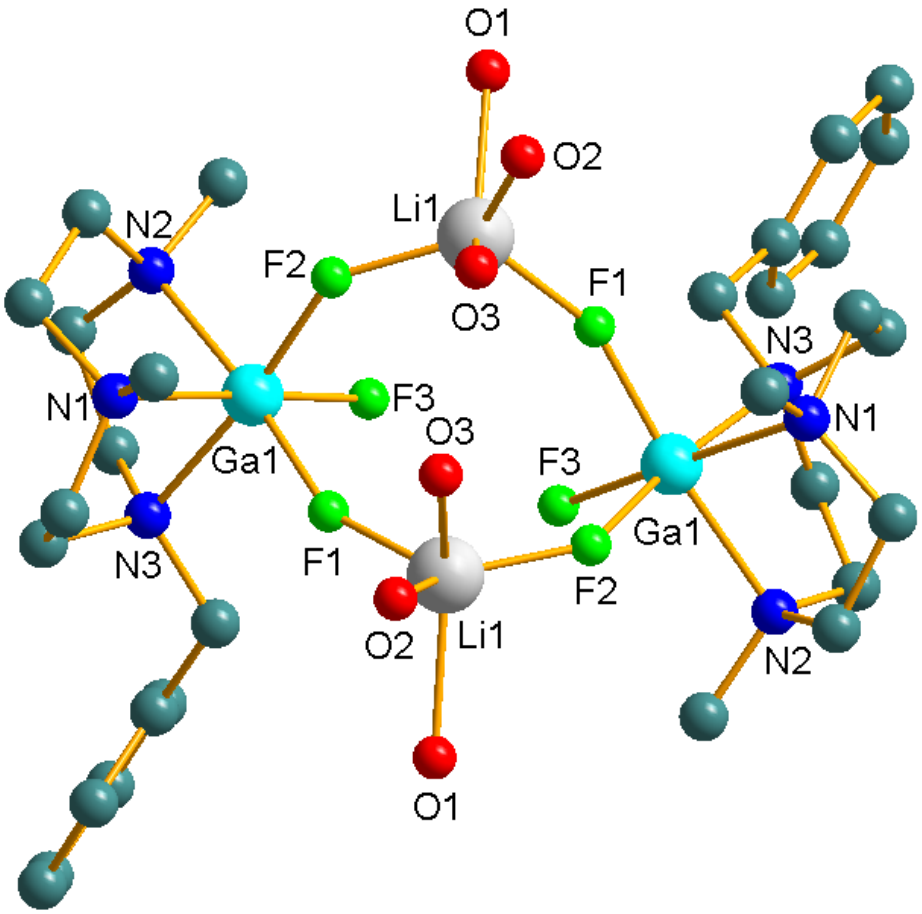

Figure 5.16: View of the asymmetric unit of the crystal structure of $[\{GaF_3(BzMe_2\text{-tacn})\}_2Li_2(OH_2)_2(BF_4)_2]\cdot H_2O$ (compound **1)**. H-atoms, isolated solvent water molecule and non-coordinating $[BF_4]^-$ anions are omitted for clarity. Ga1-F1 1.852(1), Ga1-F2 1.859(1), Ga1-F3 1.937(1), Li1-F1 1.830(6), L1-F2a 1.755(5), Li1-O1 2.113(7), Li1-O2 1.898(7), Li1-O3 2.263(8) Å. Symmetry codes: -x, y, -z + 1/2. O2 and O3 are half occupied.

Compound **1** crystallises in the monoclinic space group C_2/c with two $[GaF_3(BzMe_2\text{-tacn})]$ complexes bridged by two symmetry related 4-coordinate tetrahedral lithium cations. Each lithium is coordinated by two μ^1-bridging fluoride ligands from one $[GaF_3(BzMe_2\text{-tacn})]$ unit (κ^2) and two coordinated water ligands – one water ligand is disordered over two positions,

hence the position of O2/O3 cannot be confirmed unambiguously. Unlike the structures discussed later in this chapter, the $[BF_4]^-$ anion does not contribute to the coordination sphere around the lithium centre, probably due to the high hydrophilicity of the lithium ion. The non-coordinating $[BF_4]^-$ anion is very disordered, as might be expected for a discrete tetrahedral anion. The structure is heavily disordered partly due to the requirement to collect the crystallographic data at room temperature.

The Ga-F bond lengths for the fluoride ligands coordinated to the lithium ion are measured to be 1.852(1) – 1.859(1) Å, which are not too dissimilar to the Ga-F bond lengths in the complex $[GaF_3(BzMe_2\text{-tacn})]\cdot 2H_2O$, which has been shown to H-bond to the waters of crystallisation (Chapter 3.2.4). However the d(Ga1-F3) is significantly longer in the complex above (1.937(1) Å). This might be due to the absence of any H-bonding or dative interaction to this particular fluoride ligand, and is perhaps a reflection of the true Ga-F bond length in the neutral complexes $[GaF_3(RMe_2\text{-tacn})]$ (R = Bz, Me) in the absence of any H-bonding interactions. The Li-F bond lengths (1.755(5) – 1.830(6) Å) are well within the sum of the ionic radii of Li^+ and F^- (0.73 and 1.19 Å respectively), indicating strong interactions.[22] The Ga-N bond lengths (2.105(2) – 2.134(1) Å) are little different from the hydrated $[GaF_3(BzMe_2\text{-tacn})]\cdot 2H_2O$ prepared in Chapter 3.2.4, indicating that coordination of the GaF_3 moiety to the lithium ion has little effect on the macrocyclic coordination.

While it is likely that the structure forms a supramolecular assembly based upon H-bonding interactions between the coordinated water molecules and the co-crystallised water molecules, due to the large amount of disorder in both the coordinated water ligands and the solvated water molecule, the H-bonding interactions could not be satisfactorily identified and the extended structure determined.

Due to the very small quantity of material isolated, the only other characterisation data obtained was an ESI^+ mass spectrum which showed the presence of the lithium associated cation $\{[GaF_3(BzMe_2\text{-tacn})] + Li\}^+$ at *m/z* 380.4 (100%). The crystal structure establishes the ability of the complex $[GaF_3(BzMe_2\text{-tacn})]$ to act as a metalloligand towards the small Li^+ cation promoting the formation of an unusual dimeric assembly. This characteristic of $[GaF_3(BzMe_2\text{-tacn})]$ was therefore investigated in greater depth with the sodium and potassium cations.

Reaction of $[GaF_3(BzMe_2\text{-tacn})]$ with $NaBF_4$, gave the non-centrosymmetric dimeric compound $[\{GaF_3(BzMe_2\text{-tacn})\}_2Na_2(BF_4)_2]$ (Compound **2**).

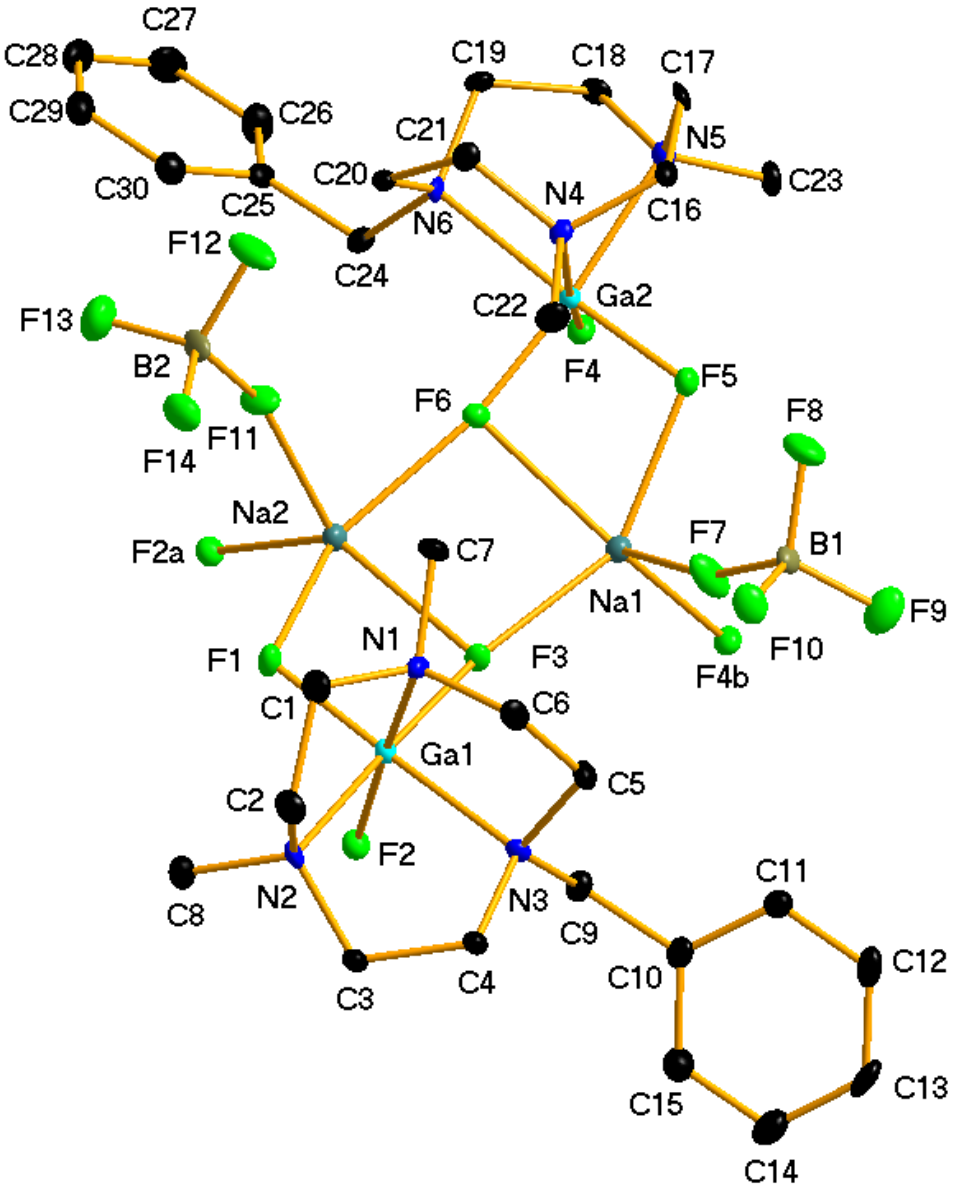

Figure 5.17: View of the asymmetric unit of [{$GaF_3(BzMe_2$-tacn)}$_2Na_2(BF_4)_2$] (Compound **2)** including the symmetry related atoms F2a and F4b that complete the coordination environment at Na1 and Na2 with associated numbering scheme. H atoms are omitted for clarity. Ellipsoids drawn at 50% probability level. Ga1–F1 1.842(2), Ga1–F2 1.848(2), Ga1–F3 1.902(2), Ga2–F5 1.834(2), Ga2–F4 1.849(2), Ga2–F6 1.896(2), Na1–F4b 2.210(3), Na1–F5 2.241(3), Na1–F7 2.254(3), Na1–F3 2.377(2), Na1–F6 2.426(3), Na2–F2a 2.200(3), Na2–F1 2.229(2), Na2 F11 2.264(3), Na2–F6 2.355(3), Na2–F3 2.421(3), F7–B1 1.399(5), F8–B1 1.378(5), F9–B1 1.385(5), F10–B1 1.403(5), F11–B2 1.412(5), F12–B2 1.394(5), F13–B2 1.381(6), F14–B2 1.386(5) Å. Symmetry codes: a = 2–x, 1–y, –z; b = 1–x, 1–y, –z.

a

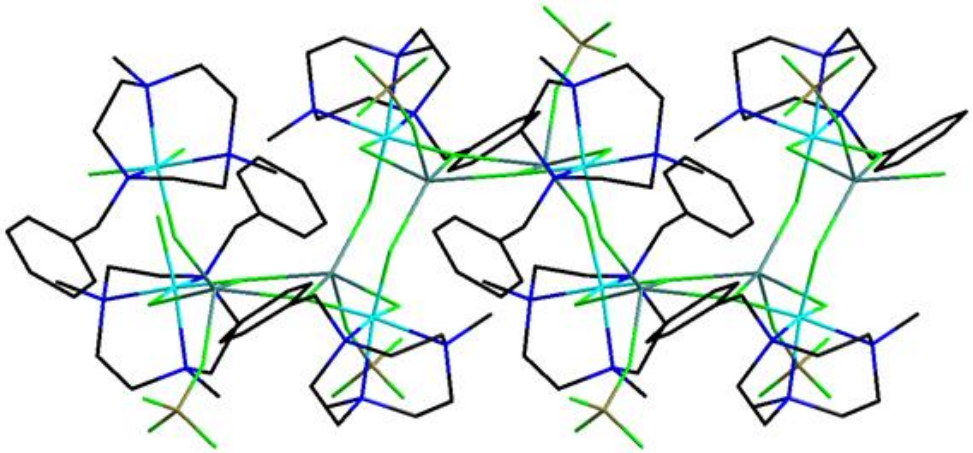

b

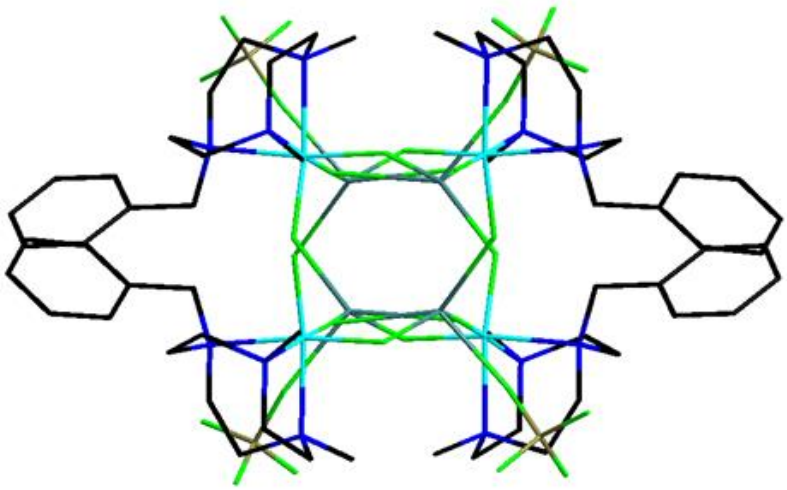

Figure 5.18: View down the *c*-axis (a) and the *a*-axis (b) of the extended structure of Compound **2**. Colour key: turquoise = Ga, teal = Na, brown = B, green = F, blue = N, black = C.

The complex crystallises in the monoclinic space group $P2_1/c$ with two [GaF_3($BzMe_2$-tacn)] moieties and two $NaBF_4$ units in the asymmetric unit. Figure 5.17 shows two [GaF_3($BzMe_2$-tacn)] moieties bridged by two five-coordinate, distorted square based pyramidal (τ = 0.21 (Na1), 0.23 (Na2)) sodium cations.[23] Each sodium ion is coordinated through two μ^2-bridging fluoride ligands from one [GaF_3($BzMe_2$-tacn)] unit (κ^2), one fluoride from a (κ^1) BF_4^- ion, and a single μ^3-bridging fluoride from each of two further distinct (symmetry-related) gallium moieties. This leads to an extended 1D zig-zag chain structure (Figure 5.18). The μ^3-F atoms form a Na_2F_2 rhombus at the core (Figure 5.19).

The Na–F bond distances involving the GaF_3 unit are slightly longer for the F atoms which are both bound to the sodium ions (i.e. the μ^3-F atoms F3 and F6) than for the μ^2-F atoms

(F1 and F5). The d(Ga-F) for F1 and F5 are little different from those observed in $[GaF_3(BzMe_2\text{-tacn})]\cdot 2H_2O$ (see Chapter 3.2.4 for more crystallographic information), where the F atoms are involved in H-bonding with the co-crystallised H_2O molecule. The Na–F distances lie in the ranges 2.210(3)–2.426(3) Å (Na1) and 2.200(3)–2.421(3) Å (Na2). These mostly lie within the sum of the ionic radii for Na^+ and F^- (1.16 and 1.19 Å respectively)[22] derived from crystalline NaF. In contrast to compound **1** and despite the hydrophilicity of the Na^+ cations, no crystallised water is present in the crystal structure of compound **2**. This was a rather unexpected observation, although the high affinity of sodium for fluoride ions likely drives this preferential interaction. A further unexpected observation was the role of the $[BF_4]^-$ ion. Traditionally seen as a non-coordinating anion, the $[BF_4]$ ion plays a key role in completing the coordination sphere around the sodium ion, although an elongated Na-F bond length of 2.254(3) Å suggests a weak interaction. The coordination of the $[BF_4]^-$ anion to the sodium centre locks it in position, thus removing any positional disorder that is often associated with crystallised discrete $[BF_4]^-$ anions. The Ga-N bond lengths are not significantly affected by the alkali metal cation coordination in compound **2**. This was expected as the $BzMe_2$-tacn moiety takes no part in the alkali metal coordination.

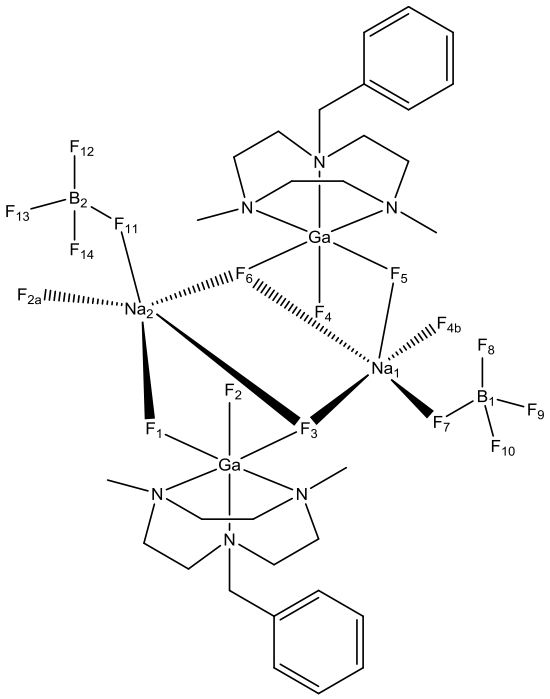

Figure 5.19: Diagram showing the coordination sphere of the sodium cations in Compound **2** with respect to the $[GaF_3(BzMe_2\text{-tacn})]$ complex and $[BF_4]^-$ anions. The Na_2F_2 rhombus core is shown. Bond lengths and angles not drawn to scale.

Figure 5.19 shows that only two of the fluoride ligands from the $[GaF_3(BzMe_2\text{-tacn})]$ complex are coordinated to each sodium centre. This is in contrast to the potassium containing compound discussed below, in which all three fluoride ligands partake in bonding to the alkali

metal. This is consistent with the smaller Na^+ ion (1.16 Å) which has lower coordination numbers than the larger K^+ ion (1.65 Å).[22]

Infra-red spectroscopy of the bulk solid supported the formulation observed crystallographically. The Ga-F bands associated with the GaF_3 unit (a_1 + e, 520, 515 cm^{-1}) displayed small shifts compared to the hydrated [GaF_3($BzMe_2$-tacn)] (526, 514 cm^{-1}). The BF_4 stretching bands associated with the $NaBF_4$ had broadened and split, likely due to the breaking of the local symmetry around the BF_4. The infra-red spectrum of the bulk solid showed the presence of solvent water (3656, 3435 ν br (ν O-H), 1640 br (δ H-O-H), which was supported by the microanalytical measurements which indicated the compound exists as a tri-hydrate in the bulk. ESI^+ mass spectrometry of Compound **2** showed the expected cation {[GaF_3($BzMe_2$-tacn)] + Na}$^+$. Attempts were made to characterise the complex in the solution phase (D_2O solution) with ^1H, $^{19}F\{^1H\}$, ^{23}Na and ^{71}Ga NMR spectroscopy. However it was found that the resonances are not significantly different from those of the constituents in water. The resonances in the ^1H, $^{19}F\{^1H\}$ and ^{71}Ga NMR spectra were consistent with the hydrated [GaF_3($BzMe_2$-tacn)]·$2H_2O$ complex obtained in the halide exchange reactions discussed in Chapter 3.2.4. The ^{23}Na NMR spectrum showed a single resonance at 0 ppm. This indicates that Compound **2** is completely dissociated in water, typical of very labile alkali metal complexes.

Reaction of [GaF_3($BzMe_2$-tacn)] with KPF_6 in aqueous MeCN yielded crystals of the very unusual centrosymmetric dimer [{GaF_3($BzMe_2$-tacn)}$_2$$K_2$($OH_2$)$_4$($PF_6$)$_2$]·$H_2O$ (Compound **3**).

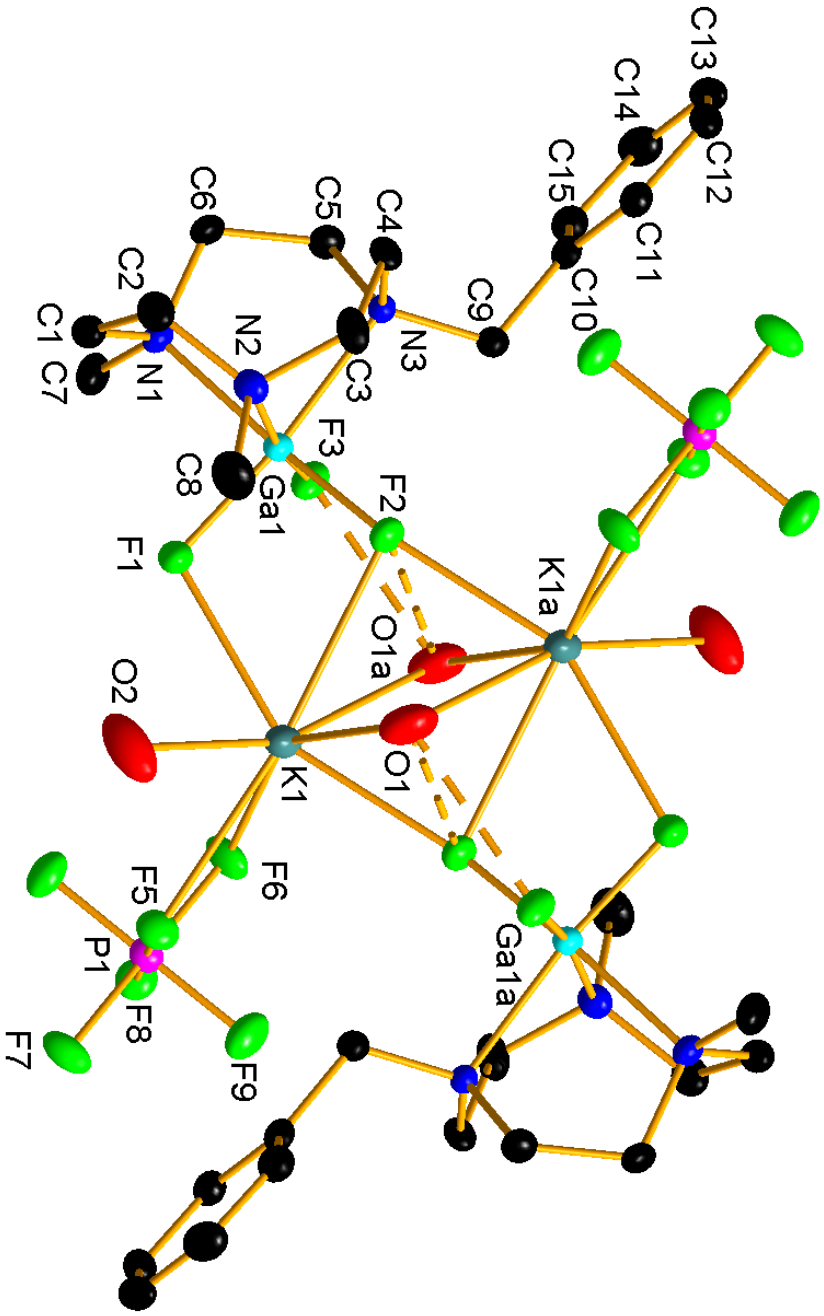

Figure 5.20: View of the structure of the centrosymmetric 'Ga_2K_2' species present in $[\{GaF_3(BzMe_2\text{-tacn})\}_2K_2(OH_2)_4(PF_6)_2]\cdot H_2O$ (Compound **3**) with associated numbering scheme. Dashed bonds indicate H-bonding contacts. H atoms associated with the macrocycle are omitted for clarity (H atoms on the water were not located in the difference map – see Experimental). Ellipsoids drawn at 50% probability level. Ga1–F2 1.8382(18), Ga1–F1 1.871(2), Ga1–F3 1.873(2), K1a–F2 2.577(2), K1–F1 2.649(2), K1–F5 2.867(2), K1–O2 2.866(3), K1–F2 2.882(2), K1–O1 2.902(3), K1–F6 2.929(2), K1–O1a 2.940(3), P1–F7 1.588(2), P1–F4

1.590(2), P1–F6 1.597(2), P1–F9 1.600(2), P1–F8 1.600(2), P1–F5 1.609(2), F2–K1 2.577(2) Å . Symmetry operation: a = 2–x, 1–y, –z.

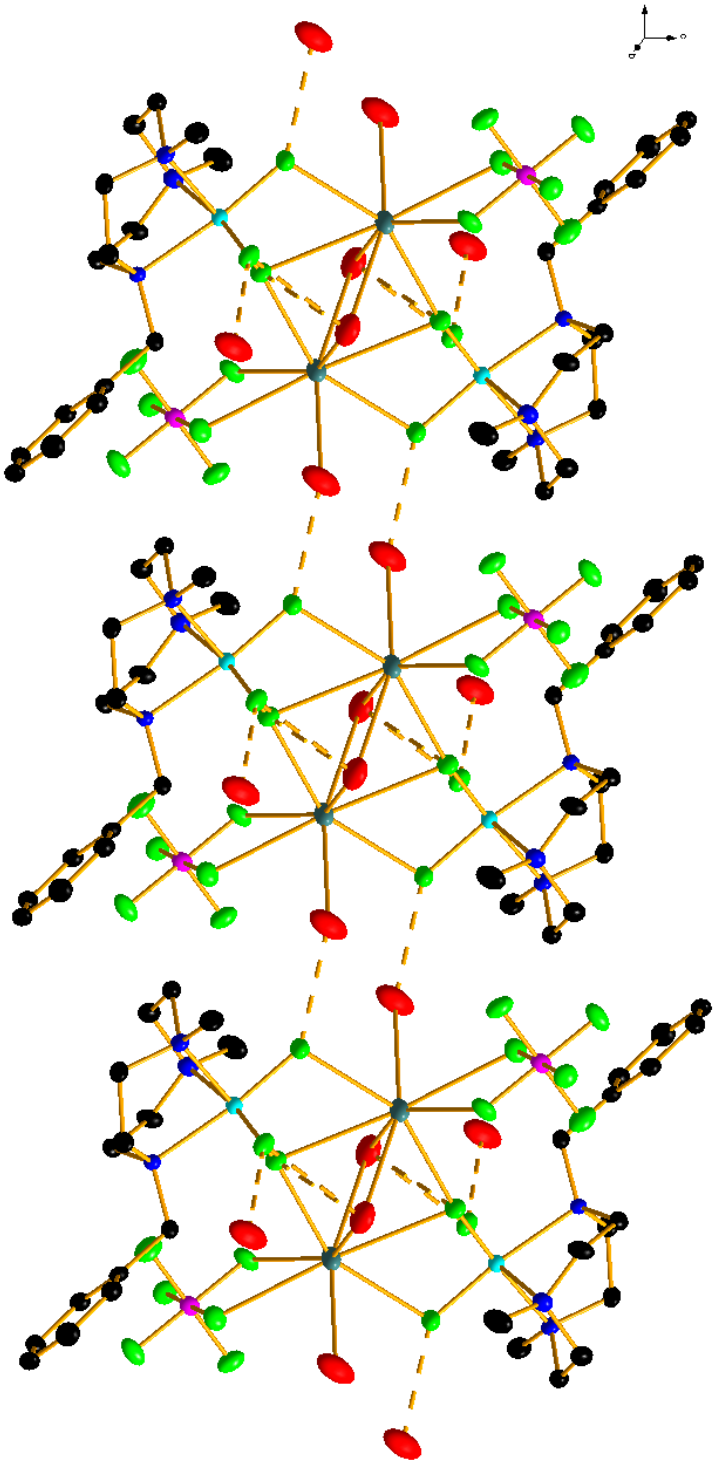

Figure 5.21: A portion of the extended structure of $[\{GaF_3(BzMe_2\text{-tacn})\}_2K_2(OH_2)_4(PF_6)_2]\cdot H_2O$ viewed down the *c*-axis. Solvent H_2O molecules are excluded for clarity. Colour key: turquoise = Ga, teal = K, pink = P, green = F, blue = N, black = C.

Compound **3** crystallises in the triclinic space group *P*–1 with one half of a centrosymmetric tetranuclear entity in the asymmetric unit. The structure also confirms coordination of the K^+ to [GaF_3($BzMe_2$-tacn)] through the fluorides (Figure 5.20). The structure is based upon eight-coordinate K^+, coordinated to two F atoms from one [GaF_3($BzMe_2$-tacn)] moiety (one of which is μ^2, and the other μ^3), one μ^3-F from the second [GaF_3($BzMe_2$-tacn)] unit, one terminal and two bridging OH_2 ligands. The coordination environment at each K^+ ion is completed by a κ^2-coordinated $[PF_6]^-$ ion. This tetranuclear (Ga_2K_2) species shows intramolecular H-bonding interactions between the bridging OH_2 ligands and two fluoride ligands of the gallium species (O1····F2 2.893(3), O1····F3 2.762(3) Å). In addition, further intermolecular H-bonding is evident between the terminal OH_2 ligands and a fluoride ligand from an adjacent 'Ga_2K_2' unit (O2····F1 2.740(4) Å), resulting in a 1D chain polymer motif (Figure 5.21). This gives a strongly H-bonded supramolecular assembly. The solvent water molecule also forms a Ga–F····H–OH hydrogen bond (O3····F3 2.729(4) Å). The K–F distances lie in the range 2.577(2) to 2.929(2) Å, comparable with the sum of the ionic radii of K^+ (1.65 Å for eight coordination) and F^- (1.19 Å).[22] Like Compound **2**, Compound **3** shows no differences in the Ga-N bond lengths involving the $BzMe_2$-tacn residue.

Compared to Compound **2**, Compound **3** does show residual water coordinating to the alkali metal cation which was not unexpected. The larger potassium ion favours higher (seven-nine) coordination numbers,[24, 25] therefore to complete the coordination sphere, the potassium sequesters water molecules from the reaction solvent. However, the presence of the coordinated waters results in the interesting assembly based upon the intermolecular H-bonding interactions (Figure 5.21). The coordination of the $[PF_6]^-$ anion locks its confirmation meaning no positional disorder is observed in the crystal structure.

The infra-red spectrum of the bulk material formed aided in confirming the formulation derived crystallographically. The spectrum showed the $[PF_6]^-$ stretching band shifts to 845 cm^{-1} and broadens significantly from the KPF_6 salt (ν PF_6 = 891 cm^{-1}). The coordination of the $[PF_6]^-$ anion to the metal centre is the likely reason for the change in stretching frequency in the infra-red spectrum. Microanalysis of the bulk material is also consistent with the formula identified crystallographically, as is the ESI^+ mass spectrum.

The three structures described above have demonstrated two distinct assemblies based upon the one [GaF_3($BzMe_2$-tacn)] complex. Compound **2** displays an extended structure based upon metal coordination (of an adjacent fluoride to the sodium centre), while Compounds **1** and **3** forms an extended structure based upon H-bonding interactions.

Reaction of NH_4PF_6 with [GaF_3($BzMe_2$-tacn)] in a glass vial also yielded crystals, although in comparison to the two compounds discussed above the quality of the crystals was

poor. However the data quality was sufficient to identify the unexpected mixed Na^+/NH_4^+ coordinated chain polymer $[\{GaF_3(BzMe_2\text{-tacn})\}_2Na(NH_4)(PF_6)_2]$, Compound **4**.

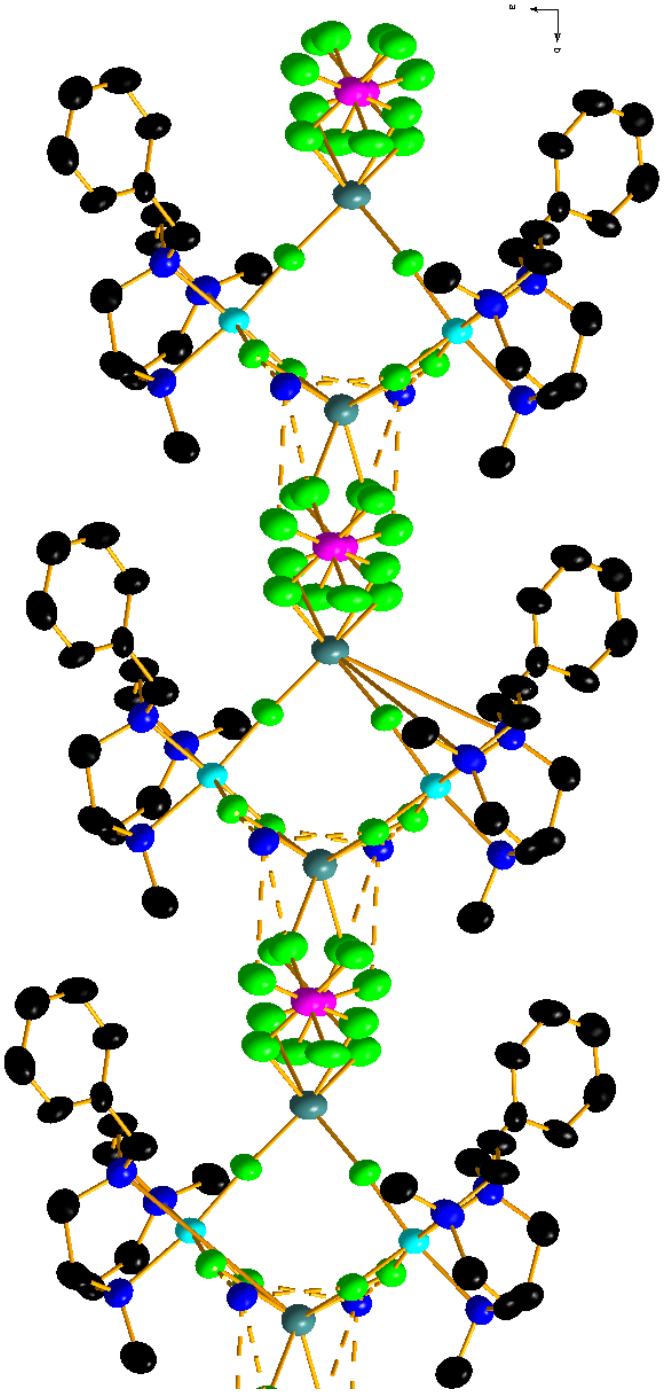

Figure 5.22: View of a portion of the polymeric structure formed by $[\{GaF_3(BzMe_2\text{-tacn})\}_2Na(NH_4)(PF_6)_2]$ (Compound **4**) viewed down the *b*-axis. Ellipsoids are drawn at 50% probability level. H-atoms on the $BzMe_2$-tacn ligand are omitted for clarity; those of the NH_4^+ cation were not located (see Experimental). Colour key: turquoise = Ga, teal = Na, pink = P, green = F, blue = N, black = C.

Due to the inferior quality of the crystal, detailed comparisons of the bond lengths and angles cannot be made. However, analysis of the structure confirms the composition and reveals the key features of the coordination environment. Figure 5.22 shows that Compound **4** is a chain polymer with two alternating types of six coordinate Na^+ ions, both with F_6 coordination; one type involving two κ^2-[GaF_3($BzMe_2$-tacn)] units and two κ^1-[PF_6]$^-$ anions, the second involving two κ^1-[GaF_3($BzMe_2$-tacn)] units and two κ^2-[PF_6]$^-$ anions (Figure 5.23). Interestingly, the [NH_4]$^+$ cation also form significant F····H-N hydrogen bonding interactions with adjacent fluorine's both from [GaF_3($BzMe_2$-tacn)] and from [PF_6]$^-$ anions.

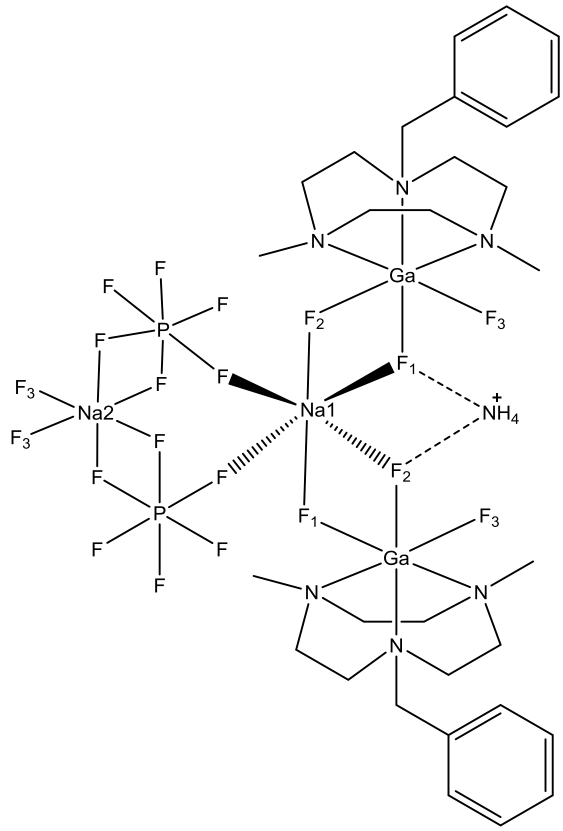

Figure 5.23: Line drawing illustrating the coordination environment at Na^+ and the F····HNH_3^+ hydrogen bonding interactions in Compound **4**. Bond lengths and angles are not drawn to scale.

While surprising to observe the sodium cation in the structure, it is likely that it was leached from the glassware, with the formation of a Na-F interaction coordinated to the GaF_3 moiety providing the driving force. ESI$^+$ mass spectrometry of the sample showed both the sodium and ammonium associated cation. Due to the small quantity of compound, infra-red spectroscopy could not be performed.

The observation of the ammonium cation forming H-bonding interactions with the fluorides from the [GaF_3($BzMe_2$-tacn)] complexes helps support the observations in the ESI$^+$ mass spectrum of the radiolabelled complex [$Ga^{18}F^{19}F_2$($BzMe_2$-tacn)] (Chapter 3.2.6), and indicates that this was indeed the interaction seen. This has thus created a new interesting way

in which compounds, particularly ones which have *facial* trifluoride moieties could be identified and analysed with mass spectrometry.

Compound **4** has shown that assemblies based upon [GaF_3($BzMe_2$-tacn)] may be formed via both metal coordination and H-bonding interactions. This implies that the complex [GaF_3($BzMe_2$-tacn)] has the potential to form many assemblies depending upon the metal salt it is combined with; the examples above show that choice of both cation and anion are important considerations in the formation of supramolecular assemblies with this metalloligand.

Given the work discussed in Chapter 3, gallium was the favoured metal system in which to study these compound types. Attempts were not made to isolate crystals of the corresponding [MF_3($BzMe_2$-tacn)] (M = Al, In) complexes, although there is no reason to assume that the same type of complexes would not form. Despite repeated recrystallisation attempts, examples of these supramolecular assemblies with the heavier alkali metals rubidium ($RbNO_3$) and caesium ($CsBF_4$ – used instead of Cs_2CO_3 due to the non-competitive $[BF_4]^-$ ion) were not obtained. This was also the case for the organic EMIM cation. Attempts to form complexes with [EMIM][BF_4] repeatedly crystallised the two constituents. EMIM is an excellent H-bond acceptor, which suggests that complexes based upon significant H-bonding interactions should be accessible. It is likely that the crystallisation conditions need to be modified to help drive the interaction to occur in the solid state.

5.2.3 ^{1}H NMR study of H-bonding interactions

Both mass spectrometry and single crystal X-ray diffraction have shown that alkali metal and organic cations can interact with the strongly electronegative trifluoride face of the complexes [GaF_3(RMe_2-tacn)]. It was therefore of interest to investigate whether H-bonding interactions could be observed and measured in the solution phase. ^{1}H NMR spectroscopy was used to probe the interactions. It was proposed that addition of one equivalent of the metal complex [GaF_3($BzMe_2$-tacn)] to a soluble ammonium salt might result in a chemical shift of the ammonium cation in the ^{1}H NMR spectrum in response to the H-bonding interaction. The salt identified as suitable was triethylammonium acetate [$HNEt_3$][OAc]. This viscous liquid is soluble in a variety of solvents and the ethyl groups of the triethylammonium salt are readily identified in the ^{1}H NMR spectrum, and do not overlap with the resonances associated with the metal complex. The salt is readily accessed through combination of equimolar quantities of triethylamine and acetic acid. The ^{1}H NMR spectrum of the salt was as expected, with a triplet at 1.57 ppm and a quartet at 3.27 ppm. One molar equivalent of [GaF_3(Me_3-tacn)] was added to the solution and the spectrum recollected. While the resonances corresponding to the metal complex appeared, no change in the chemical shift of the triethylammonium salt was observed. This shows that in this case there was no observable interaction between the [GaF_3(Me_3-tacn)]

complex and the ammonium salt. Given that Compound **2** dissociated in aqueous conditions (demonstrated by multinuclear NMR spectroscopy), it is unlikely that the H-bonding interactions would be strong enough to overcome the solvation energy. If the molecular complex could be isolated as a solid, solid state magic angle spinning (MAS) NMR could be used to quantify the H-bonding interactions by measuring the difference in the chemical shift of the $[HNEt_3]^+$ cation between the associated compound and free $[HNEt_3][OAc]$.

5.3 Conclusions and Further Work

The work discussed in this chapter has described a novel and unusual new use for neutral trifluoride complexes. It has been shown that complexes of the form $[GaF_3(RMe_2\text{-tacn})]$ can function as very effective F-donor metalloligands towards alkali metal cations in water. The mass spectrometry experiments showed that complexes of the form $\{[GaF_3(RMe_2\text{-tacn})] + M\}^+$ (M = alkali metals, NH_4, EMIM) could be formed under the predominantly aqueous conditions employed. The observation of these cationic species was quite unexpected with the alkali metal cations due to their high affinity for water. The use of the ammonium cation and the subsequent observations helped confirm the species seen in the mass spectrum of the radiolabelled complex discussed in Chapter 3.2.6. The alkali metal cations were able to bind up to three of the $[GaF_3(Me_3\text{-tacn})]$ complexes to give the interesting $\{[GaF_3(Me_3\text{-tacn})]_x + M\}^+$ x = 2,3 monocation. Reaction of $[GaF_3(Me_3\text{-tacn})]$ with the Group 2 and 3 cations did not show the cation associated species.

Reaction of $[GaF_3(BzMe_2\text{-tacn})]$ with alkali metal salts ($LiBF_4$, $NaBF_4$, KPF_6) in aqueous MeCN gave a series of highly unusual and distinct structural types. $[\{GaF_3(BzMe_2\text{-tacn})\}_2Li_2(OH_2)_2(BF_4)_2]\cdot H_2O$ (Compound **1**) crystallises as a centrosymmetric dimer with two four-coordinate lithium ions interacting with two $[GaF_3(BzMe_2\text{-tacn})]$ complexes to form an Li_2F_2 core. The coordination sphere around the lithium ion is completed by coordinated water molecules rather than from any other fluoride containing species such as the $[BF_4]^-$ ion. $[\{GaF_3(BzMe_2\text{-tacn})\}_2Na_2(BF_4)_2]$ (Compound **2**) crystallises as a dimeric species with two six-coordinate sodium ions interacting with two of the metal fluoride complexes giving an Na_2F_2 core. Interaction of the sodium ions with a symmetry related MF_3 complex results in a 1D zig zag polymer chain. $[\{GaF_3(BzMe_2\text{-tacn})\}_2K_2(OH_2)_4(PF_6)_2]\cdot H_2O$ (Compound **3**) crystallises with an 8-coordinate potassium ion, with contributions from the metal fluoride complex, the $[PF_6]^-$ anion and also from water molecules. The coordinated water molecules partake in both inter- and intra-molecular H-bonding interactions. This gives an extended supramolecular assembly based upon O····F interactions.

The highly unusual mixed cation complex $[\{GaF_3(BzMe_2\text{-tacn})\}_2Na(NH_4)(PF_6)_2]$ (Compound **4**) was synthesised via reaction of $[GaF_3(BzMe_2\text{-tacn})]$ with NH_4PF_6. It is likely

that the sodium ion was sequestered from the glassware used to grow the crystals. The reaction was also attempted in PTFE vessels in order to exclude any source of sodium ion. However despite several attempts, crystals suitable for single crystal X-ray diffraction could not be obtained. Of particular interest in Compound **4** was the H-bonding of the ammonium cation to the metal fluoride complex, further providing evidence for this interaction occurring in the radiolabelling experiments in Chapter 3.2.6.

Attempts were made to investigate whether the H-bonded interaction of the ammonium cation with the [GaF_3($BzMe_2$-tacn)] complex observed in both the solid state (Compound **4**) could be seen in the solution phase utilising ^{1}H NMR spectroscopy. However the interactions are not strong enough and so no change in the ^{1}H NMR spectrum was observed. This would imply that the complexes are extensively dissociated in solution.

The work in this chapter provides a solid grounding in which these interactions can be explored in more detail, with rational design and careful choice of cation. The work discussed above utilises the highly electronegative face of a *fac*-MF_3 complex. It would be interesting to investigate whether the complexes *mer*-[MF_3(terpy)]·$3H_2O$ discussed in Chapter 6 would be able to form similar interactions. The *mer*-isomer places the fluoride atoms further apart, which diffuses the electronegativity across the complex. This would determine whether the compounds discussed above arise because of the highly electronegative face, or whether it's the consequence of the strong donating power of the fluoride ligand.

As mentioned, attempts were made to crystallise complexes with the EMIM cation but suitable crystallisation conditions were not found. Work could be focussed on improving the synthetic method to gain the $EMIM^+$ associated complexes in the solid state.[26] Of particular interest in regards to PET imaging applications, and indeed MRI contrast agents would be to investigate whether H-bonding groups could be incorporated into the ligand framework to create an intramolecular H-bonded system. This would help stabilise the metal-fluoride bond in the chelate and would likely make the labelled compound more stable under physiological conditions. Such H-bonding groups may include amines, amides, pyrroles or indeed imidazole containing functional groups. The use of amide functionalised tacn based ligands scaffolds towards H-bond stabilised chelates is discussed in more detail in Chapter 7.

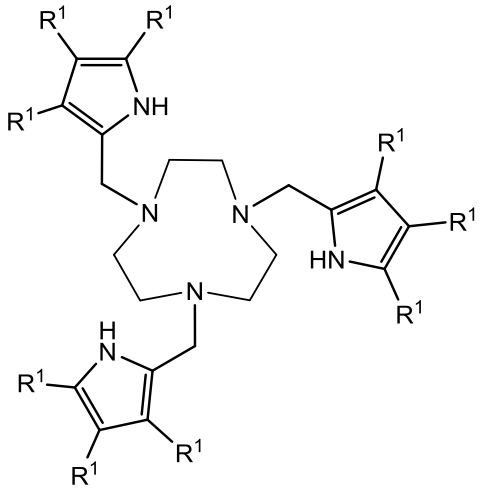

Figure 5.24: Pyrrole functionalised tacn chelate; a proposed ligand scaffold to investigate intramolecular H-bonding interactions to stabilise an M-F bond.

5.4 Experimental

For general experimental techniques see Appendix 1. The $[GaF_3(BzMe_2\text{-tacn})]$ and $[GaF_3(Me_3\text{-tacn})]$ were prepared as hydrates by the reported method.[2] Alkali metal and ammonium salts were used as supplied. Freshly distilled water and chromatography grade MeCN (undistilled) were used in all reactions. *In situ* ESI^+ MS data were obtained using a VG Biotech Platform with $[MF_3(BzMe_2\text{-tacn})]$ or $[MF_3(Me_3\text{-tacn})]$ and the appropriate alkali metal salt or ammonium salt dissolved in water in a 1:1 molar ratio.

$[\{GaF_3(BzMe_2\text{-tacn})\}_2Li_2(OH_2)_2(BF_4)_2]\cdot H_2O$ (1)

$[GaF_3(BzMe_2\text{-tacn})]$ (0.010 g, 0.026 mmol) dissolved in 0.5 mL MeCN was added to $LiBF_4$ (0.002 g, 0.026 mmol) in 0.1 mL H_2O. The solutions were gently mixed and the reactions solution left to evaporate slowly at room temperature. A small number of crystals suitable for single crystal X-ray diffraction were identified from amongst the amorphous solid. Yield 0.010 g, 86%. ESI^+ MS (MeCN/H_2O): *m/z* 380.4 (100%) $[GaF_3(BzMe_2\text{-tacn}) + Li]^+$.

$[\{GaF_3(BzMe_2\text{-tacn})\}_2Na_2(BF_4)_2]$ (2)

$[GaF_3(BzMe_2\text{-tacn})]\cdot 2H_2O$ (0.010 g, 0.026 mmol) dissolved in 0.5 mL MeCN was added to $NaBF_4$ (0.003 g, 0.026 mmol) in 0.1 mL H_2O. The solutions were mixed and the reaction solution was left to evaporate slowly at room temperature, resulting in the formation of large colourless crystals suitable for single crystal X-ray diffraction. Yield: 0.012 g, 92%. Required for $C_{30}H_{56}B_2F_{14}Ga_2N_6Na_2O_3$: C: 33.5, H: 5.8, N: 7.8. Found; C: 33.7, H: 4.8, N: 7.7%. IR (Nujol, ν/cm^{-1}) 3656, 3435 v br (ν O-H), 1640 br (δ OH_2), 1500 w (C-H aromatic), 1073 vs br, 1024 sh (ν BF_4^-), 536 m (δ BF_4^-), 520 m, 514 sh (Ga-F). ESI^+ MS (MeCN/H_2O): *m/z* 396.1

(100%) $[GaF_3(BzMe_2\text{-tacn}) + Na]^+$, 771.2 (30%) $[\{GaF_3(BzMe_2\text{-tacn})\}_2 + Na]^+$. ^1H and ^{71}Ga NMR: spectra unchanged from $[GaF_3(BzMe_2\text{-tacn})]$. ^{1} $^{19}F\{^1H\}$ NMR: δ = −150.58, −150.63 (BF_4^-), −172.41 (br, $[GaF_3(BzMe_2\text{-tacn})]$). ^{23}Na NMR: δ = 0.0 (Na^+ in water).

$[\{GaF_3(BzMe_2\text{-tacn})\}_2K_2(OH_2)_4(PF_6)_2]\cdot H_2O$ (3)

Method as above using $[GaF_3(BzMe_2\text{-tacn})]\cdot 2H_2O$ (0.010 g, 0.026 mmol) and KPF_6 (0.005 g, 0.026 mmol). Colourless crystals. Yield: 0.014 g, 97%. Required for $C_{30}H_{60}F_{18}Ga_2K_2O_5N_6P_2$: C, 29.9; H, 5.0; N, 7.0. Found: C, 30.0; H, 4.9; N, 7.1%. IR (Nujol, ν/cm^{-1}) 3656, 3435 ν br (ν O-H), 1631 br (δ OH_2), 1500 w (C-H aromatic), 845 vs br (ν PF_6^-), 558 s (δ PF_6^-), 527 m br (Ga-F). ESI^+ MS (MeCN/H_2O): *m/z* 412.1 (100%) $[GaF_3(BzMe_2\text{-tacn}) + K]^+$, 771.2 (20%) $[\{GaF_3(BzMe_2\text{-tacn})\}_2 + K]^+$.

$[\{GaF_3(BzMe_2\text{-tacn})\}_2Na(NH_4)(PF_6)_2]$ (4)

Method as above using $[GaF_3(BzMe_2\text{-tacn})]\cdot 2H_2O$ (0.010 g, 0.026 mmol) and NH_4PF_6 (0.002 g, 0.026 mmol). White solid, including a few very small, weakly diffracting needle-like crystals. Yield 0.011 g. ESI^+ MS (MeCN/H_2O): *m/z* 391.1 (100%) $[GaF_3(BzMe_2\text{-tacn}) + NH_4\}^+$, 396.1 (18%) $[GaF_3(BzMe_2\text{-tacn}) + Na]^+$.

Crystals of compounds **1**-**4** were obtained by slow evaporation of aqueous solutions of $[GaF_3(BzMe_2\text{-tacn})]$ containing 1 mol. equiv. of $LiBF_4$, $NaBF_4$, KPF_6 or NH_4PF_6 in a glass vial. Diffractometer: *Rigaku AFC12* goniometer equipped with an enhanced sensitivity (HG) *Saturn724+* detector mounted at the window of an *FR-E+ SuperBright* molybdenum rotating anode generator (λ_1 = 0.71073 Å) with VHF *Varimax* optics (70 or 100 μm focus). Cell determination, data collection, data reduction, cell refinement and absorption correction: CrystalClear-SM Expert 2.0 r7. Structure solution and refinement were carried out using WinGX and software packages within. H atoms attached to C atoms were placed in geometrically assigned positions, with C-H distances of 0.95 Å (CH), 0.98 Å (CH_3) or 0.99 Å (CH_2) and refined using a riding model, with $U_{iso}(H) = 1.2U_{eq}(C)$ (CH, CH_2) or $1.5U_{eq}(C)$ (CH_3). For Compound **3** the difference map contains peaks that approximately correspond to possible hydrogen positions, however, it was not possible to refine these into a mutually consistent arrangement. The hydrogen atoms for both the coordinated and isolated water molecules have therefore been omitted from the refined model but are included in the formula and derived parameters.

Due to instrumentation issues, the crystallographic data for Compound **1** was collected at room temperature. While the data quality was sufficient to identify the coordination

environment and bond lengths, the thermal motion of the atoms and thus the size of the thermal ellipsoids are large. The structure shows significant disorder in both the coordinated and solvated water molecules, thus location of isolated H-atoms on the water molecules from the difference map was not possible. However, while the H-atoms are not included in the refinement, they're included in the structural formulae. The coordinated water molecules O2/O3 are disordered over two positions. Therefore unambiguous assignment of the Li-O bond distances is not possible.

The crystals of [{GaF_3($BzMe_2$-tacn)}$_2$Na(NH_4)(PF_6)$_2$] (Compound **4**) were very small and poorly diffracting, leading to very weak diffraction data and no significant reflections beyond 40^o (even with increased exposure times). This weak, low resolution data has affected the final quality of the refinement and associated statistics; however, the structure is clearly defined (although detailed comparisons of bond lengths are not justified). The H atoms associated with the NH_4^+ cation were not convincingly located in the difference map, and given the data quality, these were excluded from the refinement, although the N4····F(1) 2.728, N(4)····F(2) 2.769 Å distances are well within the normal H-bonding range. Thus, while the structure determination for this compound serves to confirm the connectivities, close analysis and comparison of geometric parameters must be treated with caution.

Table 5.2: Crystallographic data for the compounds discussed in this chapter (L = $BzMe_2tacn$).[a]

Compound	**$[\{GaF_3(L)\}_2Li_2(OH_2)_2(BF_4)_2]\cdot H_2O$ (1)**	**$[\{GaF_3(L)\}_2Na_2(BF_4)_2]$ (2)**
Formula	$C_{30}H_{50}B_2F_{14}Ga_2Li_2O_6$	$C_{30}H_{50}B_2F_{14}Ga_2N_6Na_2$
M/g mol^{-1}	947.6	967.80
Crystal system	Monoclinic	Monoclinic
Space group (No.)	C2/c (15)	$P2_1/c$ (14)
a/Å	30.611(9)	10.967(2)
b/Å	10.015(2)	15.793(3)
c/Å	17.186(5)	22.313(3)
α/°	90	90
β/°	117.656(5)	90.057(6)
γ/°	90	90
U/Å^3	4667(2)	3864.8(11)
Z	8	4
μ(Mo-Kα) /mm^{-1}	0.7105	1.517
F(000)	2164	1968
Total reflections	4576	16094
Unique reflections	3935	8511
R_{int}	0.0631	0.049
R_1[b] [$I_o > 2\sigma(I_o)$]	0.0671	0.052
R_1 (all data)	0.0913	0.085
wR_2[b] [$I_o > 2\sigma(I_o)$]	0.1955	0.090
wR_2 (all data)	0.2119	0.098

[a] Common items: temperature = 100 K; wavelength (Mo-K_α) = 0.71073 Å;

[b] $R_1 = \Sigma \big| |F_o| - |F_c| \big| / \Sigma |F_o|$; $wR_2 = [\Sigma w(F_o^2 - F_c^2)^2 / \Sigma w F_o^4]^{1/2}$

Table 5.3: Crystallographic data for the compounds discussed in this chapter (L = $BzMe_2tacn$).[a]

Compound	**$[\{GaF_3(L)\}_2K_2(OH_2)_4(PF_6)_2]\cdot H_2O$ (3)**	**$[\{GaF_3(L)\}Na(NH_4)(PF_6)_2]$ (4)**
Formula	$C_{30}H_{62}F_{18}Ga_2K_2N_6O_6P_2$	$C_{15}H_{29}F_{15}GaN_4NaP_2$
M/g mol^{-1}	1224.43	705.07
Crystal system	Triclinic	Monoclinic
Space group (No.)	*P*-1 (2)	*C*2/*c* (15)
a/Å	9.5708(10)	31.23(2)
b/Å	10.2233(10)	10.037(5)
c/Å	13.1728(10)	18.142(12)
α/°	95.498(7)	90
β/°	91.765(7)	116.85(2)
γ/°	112.970(8)	90
U/Å^3	1177.96(19)	5073(6)
Z	1	8
μ(Mo-Kα) /mm^{-1}	1.506	1.353
F(000)	624	2832
Total reflections	8591	19561
Unique reflections	4590	4978
R_{int}	0.053	0.232
R_1 [$I_o > 2\sigma(I_o)$] [b]	0.055	0.119
R_1 (all data)	0.085	0.248
wR_2 [$I_o > 2\sigma(I_o)$] [b]	0.108	0.274
wR_2 (all data)	0.122	0.360

[a] Common items: temperature = 100 K; wavelength (Mo-K_α) = 0.71073 Å;

[b] $R_1 = \Sigma \big| |F_o| - |F_c| \big| / \Sigma |F_o|$; $wR_2 = [\Sigma w(F_o^2 - F_c^2)^2 / \Sigma w F_o^4]^{1/2}$

5.5 References

1. Kumar, G.; Gupta, R., *Chem. Soc. Rev.* **2013,** *42*, 9403-9453.
2. Bhalla, R.; Darby, C.; Levason, W.; Luthra, S. K.; McRobbie, G.; Reid, G.; Sanderson, G.; Zhang, W., *Chem. Sci.* **2014,** *5*, 381-391.
3. Lee, R.; Igashira-Kamiyama, A.; Motoyoshi, H.; Konno, T., *CrystEngComm.* **2012,** *14*, 1936-1938.
4. Ryu, D. W.; Lee, W. R.; Lee, J. W.; Yoon, J. H.; Kim, H. C.; Koh, E. K.; Hong, C. S., *Chem. Commun.* **2010,** *46*, 8779-8781.
5. Sun, D.; Wang, D.-F.; Han, X.-G.; Zhang, N.; Huang, R.-B.; Zheng, L.-S., *Chem. Commun.* **2011,** *47*, 746-748.
6. Hamelin, O.; Rimboud, M.; Pecaut, J.; Fontecave, M., *Inorg. Chem.* **2007,** *46*, 5354-5360.
7. Benjamin, S. L.; Levason, W.; Reid, G., *Chem. Soc. Rev.* **2013,** *42*, 1460-1499.
8. Tramsek, M.; Zemva, B., *J. Fluorine Chem.* **2006,** *127*, 1275-1284.
9. Hope, E. G., *Coord. Chem. Rev.* **2013,** *257*, 902-909.
10. Tramšek, M.; Žemva, B., *J. Fluorine Chem.* **2004,** *125*, 1919-1924.
11. Tramšek, M.; Benkič, P.; Turičnik, A.; Tavčar, G.; Žemva, B., *J. Fluorine Chem.* **2002,** *114*, 143-148.
12. Tramsek, M.; Benkic, P.; Zemva, B., *Inorg. Chem.* **2004,** *43*, 699-703.
13. Werner, B.; Kräuter, T.; Neumüller, B., *Organometallics* **1996,** *15*, 3746-3751.
14. Pedersen, K. S.; Lorusso, G.; Morales, J. J.; Weyhermüeller, T.; Piligkos, S.; Singh, S. K.; Larsen, D.; Schau-Magnussen, M.; Rajaraman, G.; Evangelisti, M.; Bendix, J., *Angew. Chem., Int. Ed.* **2014,** *53*, 2394-2397.
15. Bhalla, R.; Levason, W.; Luthra, S. K.; McRobbie, G.; Reid, G.; Sanderson, G.; Zhang, W., *Chem. Commun.* **2014,** *50*, 12673-12675.
16. Aldridge, S.; Downs, A., *The Group 13 Metals, Aluminium, Gallium, Indium and Thallium: Chemical Patterns and Paculiarities*. Wiley: Chichester, 2011.
17. Hanusa.T.P, *Comprehensive Coordination Chemistry II*. Elsevier: Oxford, 2004; Vol. 3.
18. Walba, H.; Isensee, R. W., *J. Org. Chem.* **1961,** *26*, 2789-2791.
19. Bartlett, P. N.; Cummings, C. Y.; Levason, W.; Pugh, D.; Reid, G., *Chem. - Eur. J.* **2014,** *20*, 5019-5027.
20. Krossing, I.; Raabe, I., *Chem. - Eur. J.* **2004,** *10*, 5017-5030.
21. Strauss, S. H., *Chem. Rev.* **1993,** *93*, 927-942.
22. Shannon, R. D., *Acta Crystallogr., Sect. A* **1976,** *A32*, 751-767.
23. Addison, A. W.; Rao, T. N.; Reedijk, J.; Van Rijn, J.; Verschoor, G. C., *J. Chem. Soc., Dalton Trans.* **1984**, 1349-1356.
24. Bellemin-Laponnaz, S.; Dagorne, S., *Chem. Rev.* **2014,** *114*, 8747-8774.

25. Hill, M. S., *Annu. Rep. Prog. Chem., Sect. A: Inorg. Chem.* **2009,** *105*, 55-74.
26. Thaning, M. J.; Olsson, A.; Bhalla, R.; Morisson-Iveson, V.; Iveson, P. B. Preparation of bis 2H-imidazole-2-thione chelating agents as ligands for radiopharmaceutical in vivo imaging. WO2014096191A1, 2014.

Chapter 6

Hydrothermal Synthesis and Characterisation of Group 13 Metal Fluoride Complexes with Di- and Triimines

6.1 Introduction

The very insoluble metal halides MF_3, M = Al, Ga, In have shown to have limited coordination chemistry under mild synthetic conditions.[1] The small, hard electronegative fluoride ligands significantly influence the electronic environment at the metal centre, and hence the binding of other ligands. The hydrates, $MF_3 \cdot 3H_2O$, are more reactive, but have poor solubility in organic solvents or water.[1] Two structural forms of $AlF_3 \cdot 3H_2O$ are known, the α-form with discrete $[AlF_3(OH_2)_3]$ molecules, and the β-form which is a polymer, $[\{AlF_2(OH_2)_2(\mu\text{-}F)\}_n] \cdot nH_2O$.[2] The structure of $GaF_3 \cdot 3H_2O$ is unclear, but $InF_3 \cdot 3H_2O$ is also a fluoride bridged polymer.[3] Therefore entry into the coordination chemistry of these materials cannot be achieved under mild conditions.[4] The significant H-bonded networks created through interaction of both the coordinated water and fluorides mean that there is a large energetic cost associated with breaking the lattice. This has so far limited a detailed investigation into the chemistry of the Group 13 metal fluorides.[5]

There are limited examples in which the Group 13 trifluorides have been used directly to form metal fluoro complexes with neutral ligands under conventional reaction conditions. These include *mer*-$[GaF_3(pyridine)_3]$, synthesised through prolonged stirring (> 15 hours) of the proposed synthon $[GaF_3(thf)_3]$ (suggested to form from prolonged refluxing of $GaF_3 \cdot 3H_2O$ in anhydrous thf) in a large excess of pyridine.[6] Removal of insoluble particulates followed by slow diffusion of pentane into the solution afforded the *tris*-pyridine adduct. As discussed in Chapter 1.8, Wieghardt *et al.* utilised $GaF_3 \cdot 3H_2O$ in the synthesis of the unusual complex $[GaF_3\{1,4,7\text{-tris(2-amino-3,5-di-butylbenzyl)-1,4,7-triazacyclononane}\}]$ via refluxing in EtOH (Chapter 1.6).[7]

Reaction of $InF_3 \cdot 3H_2O$ with 2,2′-bipyridine (bipy) or 1,10′-phenanthroline (phen) (L–L) in aqueous HF forms the distorted octahedral species $[InF_3(L\text{–}L)(H_2O)]$ (Figure 6.1).[8, 9]

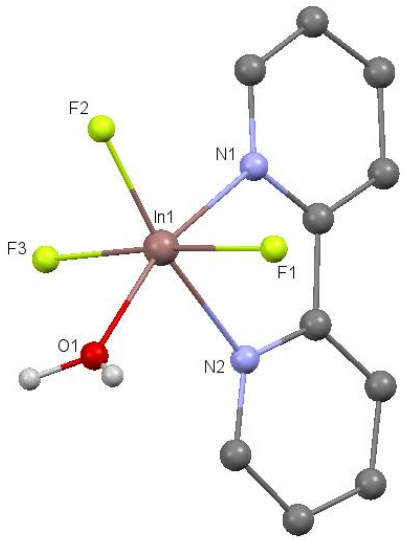

Figure 6.1: Crystal structure of $[InF_3(bipy)(H_2O)]\cdot 2H_2O$.[8] The hydrogen atoms on the bipy ligand and lattice water molecules are omitted for clarity. Image redrawn from CCDC 141279.

Under more forcing conditions, reaction of AlN or InN and NH_4F in supercritical ammonia (400 ^oC, 2.2 K bar) forms $[AlF_3(NH_3)_2]$ and $[InF_2(NH_2)(NH_3)]$ respectively.[10] All the examples highlighted above require rather forcing conditions and are often low yielding.

The work discussed in Chapter 2, in which hydrothermal synthesis was used to successfully form the aza-macrocyclic complexes $[MF_3(Me_3\text{-tacn})]\cdot xH_2O$, M = Al, Ga, In, directly through combination of the relevant metal fluoride hydrate with ligand, highlighted the relative lack of relevant coordination chemistry of the Group 13 metal fluorides, particularly with N-donor ligands. Given the successful formation of the complexes $[MF_3(RMe_2\text{-tacn})]\cdot xH_2O$ under hydrothermal conditions, the method was explored further using a number of N-donor ligands, focusing specifically on the rigid imine donors.

The rigid imine donors 2,2′-bipyridine (bipy), 1,10′-phenanthroline (phen) and 2,2′,6,2″-terpyridine (terpy) are ubiquitous ligands in coordination chemistry, capable of forming complexes with a huge variety of elements across the periodic table. Their air and moisture stability, coupled with their commercial availability and low cost, make them a very popular class of ligand. Within metal fluoride chemistry, previous work by Levason *et al.* has shown their utility in forming complexes with metal fluorides in unusual oxidation states; the hard nitrogen donors are able to coordinate to the small, hard metal fluoride centres. Examples include the vanadium(V) oxo-fluoride complexes $[VOF_3(phen)]$ and $[VOF_3(bipy)]$ synthesised from reaction of ligand with the soluble synthon $[VOF_3(MeCN)_2]$.[11] The rigidity of the aromatic backbone allows the ligands to be exposed to harsh synthetic conditions without decomposition.

The acyclic ligand N,N,N′,N′,N″-pentamethyldiethylenetriamine (pmdta) was also investigated. As an open chain equivalent of the 1,4,7-triazacyclononane (tacn) ligands utilised in Chapters 2 and 4, it may offer useful comparisons with the complexes synthesised in the earlier chapters.

6.2 Results and Discussion

6.2.1 General hydrothermal synthesis method

Combination of the appropriate metal fluoride hydrate and ligand in freshly distilled water, followed by heating at 180 °C under hydrothermal conditions yields coloured solutions upon cooling. Any unreacted material or by-products are conveniently removed by filtration. Subsequent removal of the reaction solvent under high vacuum gave the desired complexes as coloured solids (Figure 6.2). The air stable complexes are soluble in water and methanol solutions, but are very poorly soluble in chlorocarbons.

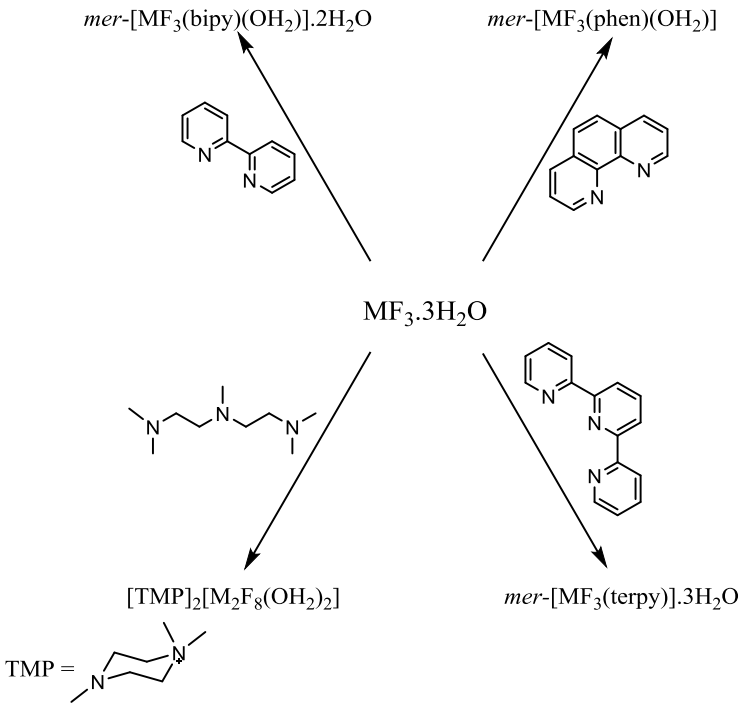

Figure 6.2: Scheme describing the hydrothermal reactions (180 °C, 15 hours) discussed in this chapter. M = Al, Ga, In.

6.2.2 Reaction of $MF_3{\cdot}3H_2O$ with terpyridine

Reaction of $MF_3{\cdot}3H_2O$ with the tridentate terpy ligand gives the pale orange distorted octahedral complexes $[MF_3(terpy)]{\cdot}3H_2O$ in high yield. Slow evaporation of the reaction solution from the reaction of $AlF_3{\cdot}3H_2O$ with terpy yielded high quality crystals suitable for single crystal X-ray diffraction.

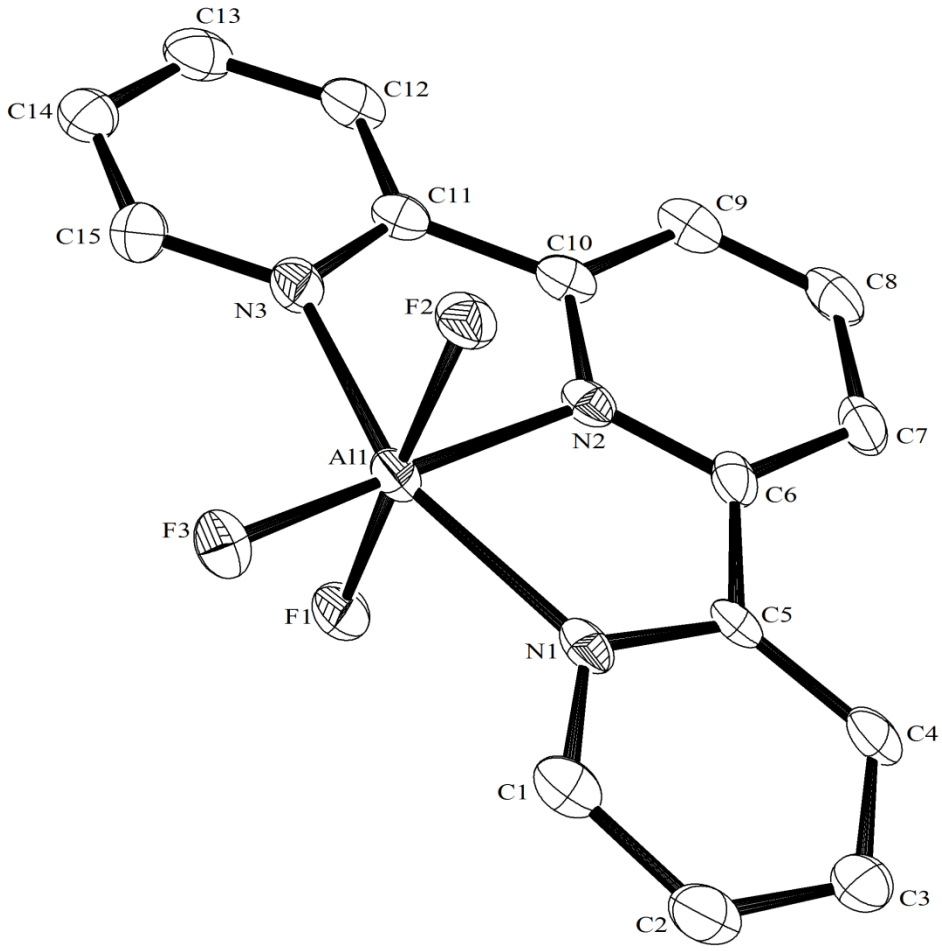

Figure 6.3: Crystal structure of $[AlF_3(terpy)]\cdot 3H_2O$. H-atoms and lattice water molecules are omitted for clarity. Ellipsoids drawn at 50% probability level. Al1-F1 1.761(2), Al1-F2 1.762(2), Al1-F3 1.737(2), Al1-N1 2.057(3), Al1-N2 2.010(3), Al1-N3 2.059(3) Å. F1-Al1-F3 92.55(12), F2-Al1-F3 91.08(11), F1-Al1-F2 176.34(13), N1-Al1-N2 77.58(13), N2-Al1-N3 78.17(13), N1-Al1-N3 155.73(13)°.

The structure of $[AlF_3(terpy)]\cdot 3H_2O$ (Figure 6.3) shows a distorted octahedral geometry about the aluminium. The terpy ligand coordinates as the *mer*-isomer as it is too rigid to adopt a *fac*-geometry. The distortions in the octahedral geometry are largely due to the rigid terpy ligand which results in N–Al–N angles significantly less than 90°/180° (*ca*. 78°/155°) , whereas the F–Al–F and (*cis*) F–Al–N angles are close to expectation for an octahedron. The Al–F bond lengths are very similar to those observed in *fac*-$[AlF_3(Me_3\text{-tacn})]\cdot 4H_2O$ discussed in Chapter 2.2.3, although the Al–N are shorter by ~0.05 Å.

The complex is heavily hydrated, leading to extensive H-bonding interactions based upon F····O (2.694(2) - 2.754(2) Å) and O····O (2.738(1) – 2.744(1) Å). This is well within the range

of the 3.0 Å mean donor-acceptor distances between secondary structure elements.[12] An H-bond of distance between 2.5 and 3.2 Å may be described as being moderately strong and mostly electrostatic in nature.[12] These interactions give rise to an extended 1D-polymeric supramolecular assembly (Figure 6.4). These assemblies are very similar to those observed for the neutral [MF_3(RMe_2-tacn)] complexes discussed in Chapters 2.3.2 and 3.2.4.

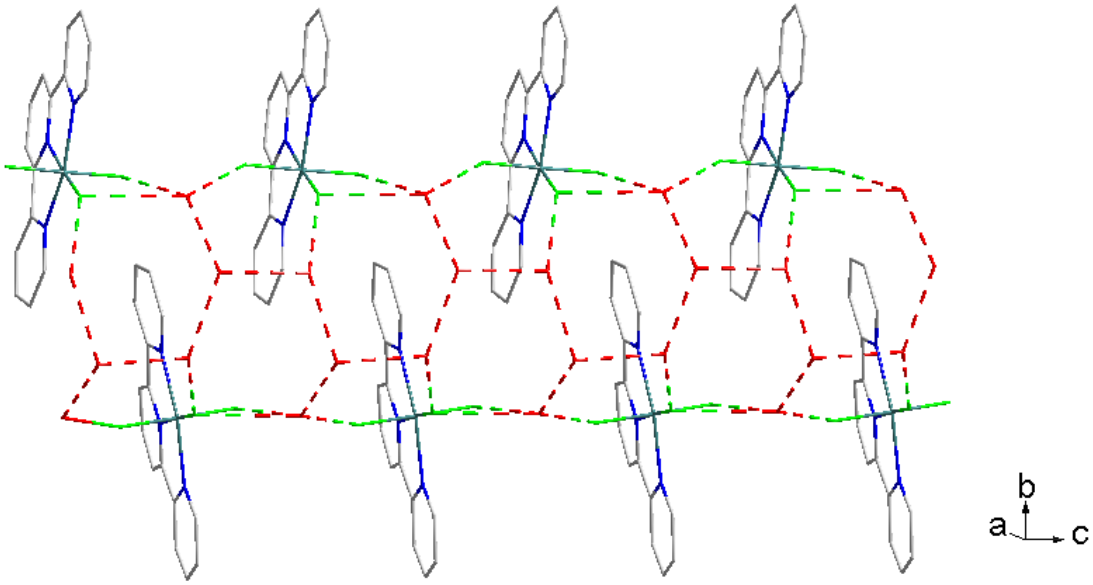

Figure 6.4: A portion of the extended structure of the complex [AlF_3(terpy)]·3H_2O viewed down the *b*-axis showing the extended supramolecular assembly formed from the H-bonding interactions of the fluoride ligands and the lattice water molecules. Colour code: teal = Al, green = F, blue = N, red = O, grey = C.

The complex also displays parallel displaced π-stacking interactions in the solid state as shown in Figure 6.5 (π-stacking distance = 3.734, 3.676 Å).

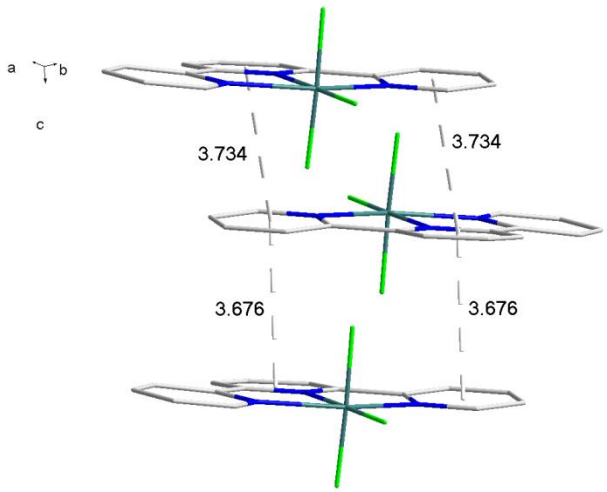

Figure 6.5: π-stacking interactions in the complex [AlF_3(terpy)]·3H_2O. Lattice water molecules are omitted for clarity. Colour code: teal = Al, green = F, blue = N, grey = C.

Spectroscopic analysis of the bulk solid supported the formulation derived crystallographically. The infra-red spectrum showed strong, broad features due to the (υ(OH) = 3370 cm^{-1} and δ(HOH) = 1640 cm^{-1}) modes of the water and three υ(MF) stretches at 656, 631, 620 cm^{-1}, as expected for a *mer*-trifluoride with C_{2V} symmetry (theory $2a_1 + b_1$). The ^1H NMR spectrum in CD_3OD shows six distinct, sharp multiplet resonances corresponding to the terpy ligand at room temperature. A broad resonance for the water in the complex (4.87 ppm) was also observed. The presence of six sharp, distinct terpy resonances in the ^1H NMR spectrum shows that the ligand coordination is static, i.e. there is no ligand dissociation in solution. The $^{19}F\{^1H\}$ NMR spectrum showed two resonances in a ratio of 2:1 due to the ratio of F_{transF} and F_{transN} in the complex. The spectrum displays doublet and triplet $^2J_{FF}$ couplings of 23 Hz (Figure 6.6). This arises through the coupling of the F_{trans} to the F_{cis} and *vice versa*.

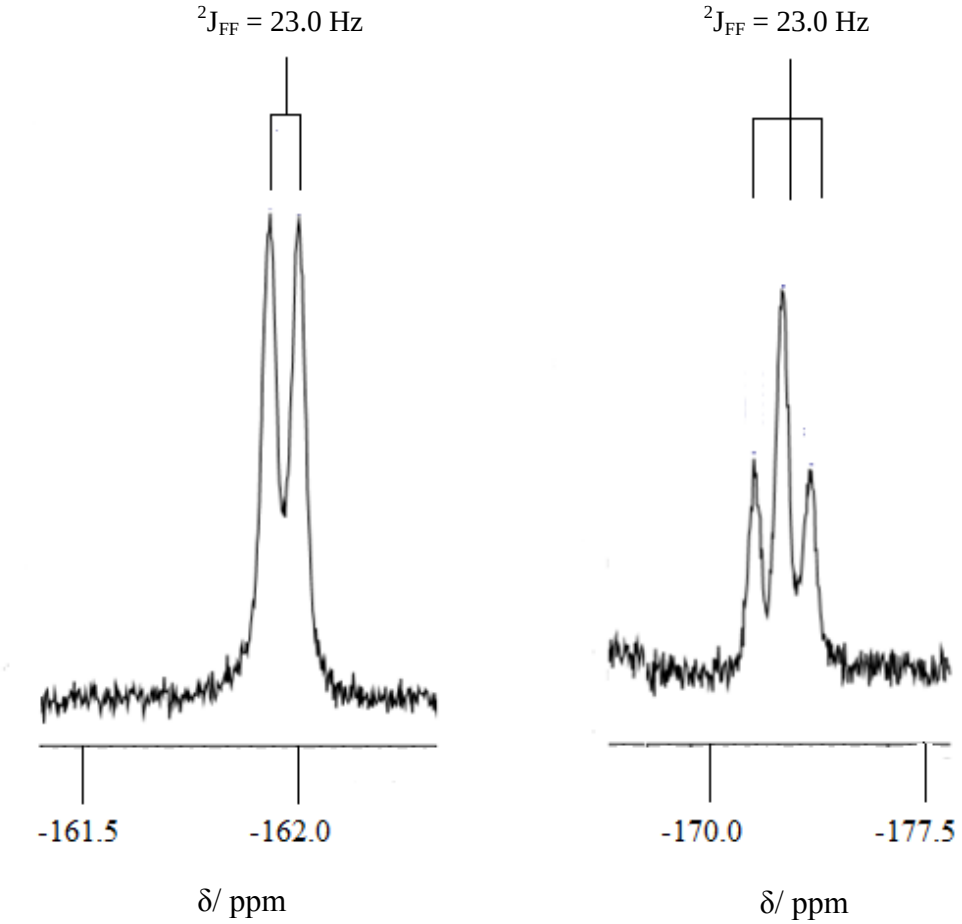

Figure 6.6: Expanded $^{19}F\{^1H\}$ NMR spectrum of $[AlF_3(terpy)]\cdot 3H_2O$ showing FF coupling. δ = -162.3 ppm J_{FF} 23.0 Hz, *trans* F, δ =-172.7 J_{FF} 23.0 Hz, *cis* F.

The observation of multiplets in the $^{19}F\{^{1}H\}$ NMR spectrum further indicates that the $[AlF_3(terpy)]$ complex is static in the solution phase. Despite the complex being quite low symmetry, it was possible to observe a signal in the ^{27}Al NMR spectrum, giving a single resonance at 16.7 ppm. The resonance was a broad singlet which showed no aluminium fluorine coupling even on cooling the solution. It is likely that the presence of the significant H-bonding H_2O/ MeOH molecules broadens the resonances sufficiently to prevent coupling from being observed. However, the position of the resonance is in the range expected for six-coordinate aluminium, as evidenced by the complex $[AlF_3(Me_3\text{-tacn})]\cdot 4H_2O$ which displays a single resonance at 19 ppm in the ^{27}Al NMR spectrum.[13] Despite repeated attempts, the elemental analysis always showed large deviations from the expected value for C, although H and N values were consistent with the proposed formulation. This might therefore indicate a combustion problem during the analysis, since the crystal structure and the spectroscopic data confirmed the identity of the complex.

The corresponding gallium complex $[GaF_3(terpy)]\cdot 3H_2O$ also crystallises as a trihydrate in the solid state (Figure 6.7), although they are not isostructural.

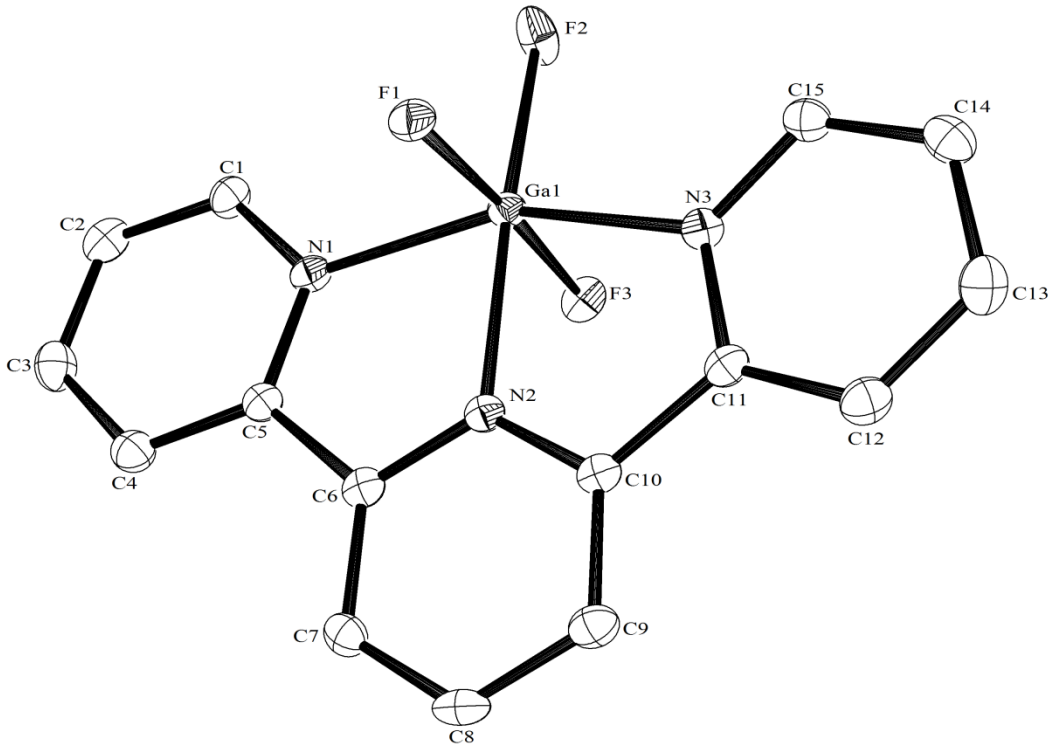

Figure 6.7: Crystal structure of the complex $[GaF_3(terpy)]\cdot 3H_2O$. H-atoms and lattice water molecules are excluded for clarity. Ellipsoids drawn at 50% probability level. Ga1–F1 1.8781(17), Ga1-F2 1.8780(16), Ga1-F3 1.8895(17), Ga1-N1 2.082(2), Ga1-N2 2.045(2), Ga1-N3 2.093(2) Å. F1-Ga1-F2 92.12(7), F2-Ga1-F3 90.60(7), F1-Ga1-F3 176.29(7), N1-Ga1-N2 77.21(8), N2-Ga1-N3 77.26(9), N1-Ga1-N3 154.28(8)°.

The structure of $[GaF_3(terpy)]\cdot 3H_2O$ shows a distorted octahedral environment around the gallium centre. Like the aluminium analogue the distortions in the octahedral geometry arise from the rigid terpy ligand which results in N-Ga-N angles significantly less than 90°/180°, although the difference in N-Ga-N from N-Al-N between the two complexes is negligible. The Ga–F distances are very similar to those found in $[GaF_3(Me_3\text{-tacn})]\cdot 4H_2O$ (2.3.2). The Ga-N distances also appear to be very similar in comparison to the heavier halide analogue $[MX_3(terpy)]$ (X = Cl, Br),[14] although the extensive H-bonding in the fluoride complex is absent in the structures of the heavier halides.

Comparison of M-F in the $[MF_3(terpy)]\cdot 3H_2O$ shows a large difference (0.116 – 0.153 Å) between the d(Al-F) and d(Ga-F). This is significantly larger than the *ca.* 0.07 Å difference in the ionic radius between Al^{3+} and Ga^{3+}.[15, 16] The limited number of structurally characterised complexes of the trifluorides restricts detailed comparisons, but it seems that the metal-donor bond length may be very sensitive to the electronegativity of the donor atom, with little difference between Al–N and Ga–N with heavier donor ligands and halides,[17] but significant differences in the M–F bond lengths. The effects of solvent molecules and the hydrogen bonding thereof also complicates the interpretation of small differences in metal-donor bond lengths, but it would seem likely that these may be a significant factor in the extensively hydrogen bonded $[MF_3(terpy)]\cdot 3H_2O$ fluoride complexes.

The complex $[GaF_3(terpy)]\cdot 3H_2O$ packs differently to the corresponding $[AlF_3(terpy)]\cdot 3H_2O$ complex in the solid state (Figure 6.8) – where alternating dimers at 90° to one another are seen in the extended structure. This difference results in an even greater degree of H-bonding interactions between the coordinated fluoride ligands and the lattice water molecules leading to a 2D sheet assembly:

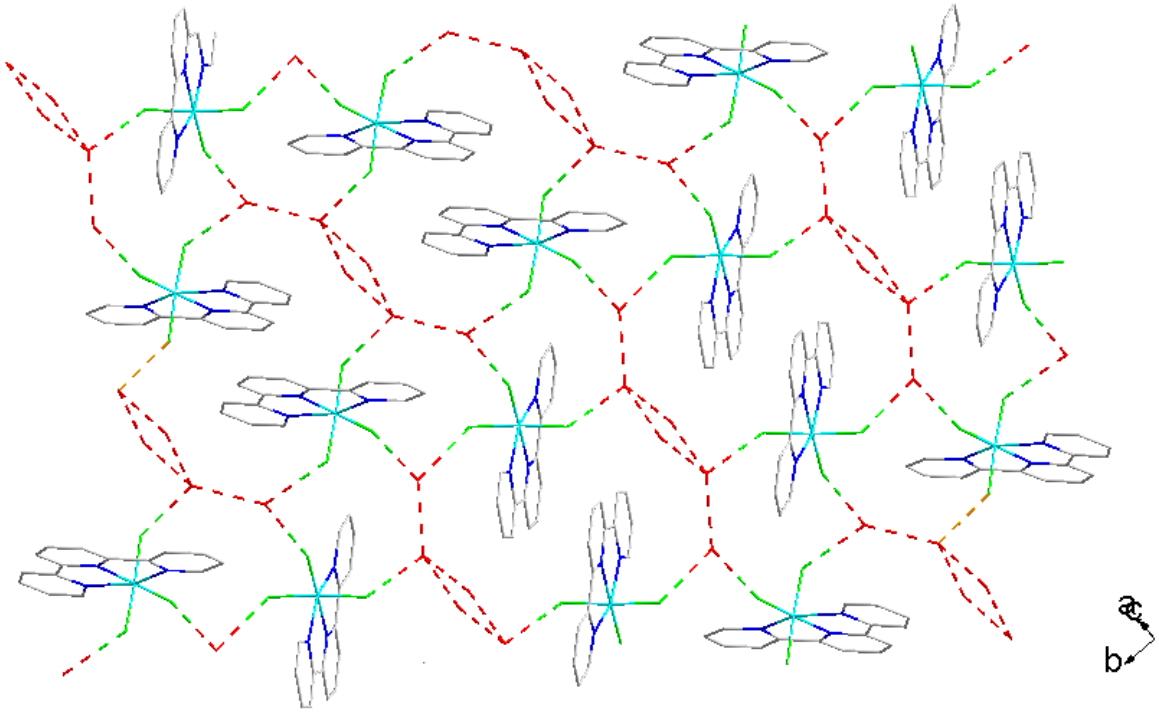

Figure 6.8: A portion of the extended structure of $[GaF_3(terpy)]\cdot 3H_2O$ viewed down the *a*-axis showing the extended supramolecular assembly formed from the H-bonding interactions of the fluoride ligands and the lattice water molecules. Colour code: teal = Ga, green = F, blue = N, red = O, grey = C. F1····O2 2.645(3), F2····O3 2.970(1), F3····O3 2.831(1), O2····O1 2.811(2), O2····O3 2.790(3) Å.

The $[GaF_3(terpy)]\cdot 3H_2O$ complexes are also associated *via* π-stacking interactions (3.57 and 3.62 Å) in the solid state as shown in Figure 6.9.

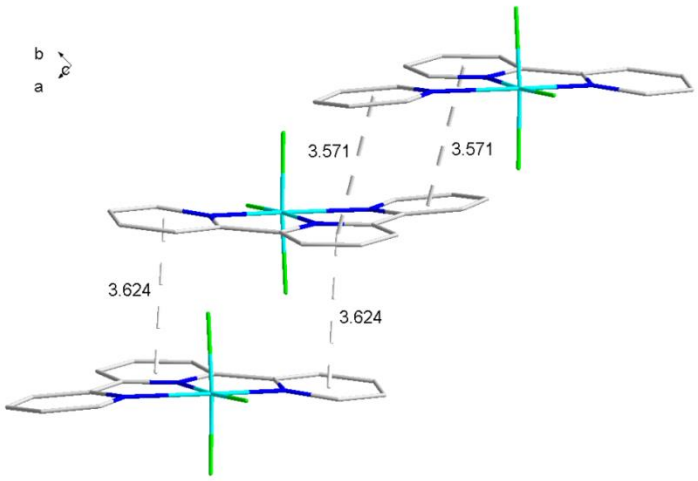

Figure 6.9: View of $[GaF_3(terpy)]\cdot 3H_2O$ showing the π-stacking interactions. Lattice water molecules are omitted for clarity. Colour code: turquoise = Ga, green = F, blue = N, grey = C.

Comparison of the π-stacking distances in the two $[MF_3(terpy)]\cdot 3H_2O$ complexes shows some small differences, specifically that the stacking distances in $[GaF_3(terpy)]\cdot 3H_2O$ are shorter than those of the aluminium analogue. This is a consequence of the different way in which the two complexes pack in the solid state. Given that the π-stacking distances are long (> 3.5 Å) and therefore can be inferred as being weak, it is likely that the packing in the complexes is dominated by the H-bonding interactions.[18]

The infra-red spectrum of the complex $[GaF_3(terpy)]\cdot 3H_2O$ contained all the features expected for the complex – namely the ν(O-H) (3407 cm^{-1}) and δ(H-O-H) (1644 cm^{-1}) modes of the water and three ν (M-F) 548, 504, 490 cm^{-1} stretches, as expected for a *mer*-trifluoride with C_{2V} symmetry. The ^{1}H NMR spectrum of the complex displays six broad resonances corresponding to the terpy ligand shifted by *ca.* 0.5 ppm from the free ligand resonances, and a broad singlet at 4.73 ppm corresponding to the water in the complex. Cooling of a CD_3OD solution of the complex gives a sharpening of the terpy proton resonances. This suggests that at room temperature the gallium complex is slightly labile in solution. The $^{19}F\{^{1}H\}$ NMR spectrum showed two resonances with a ratio of 2:1 due to the ratio of $F_{trans F}$ and $F_{trans N}$. Unlike the aluminium analogue, the couplings on the gallium complex could not be resolved even upon cooling to -90 °C; instead the signals remained as two broad singlets. This may be due to a combination of the labile nature of the complex and the fast quadrupolar relaxation of the $^{69/71}Ga$ nuclei. The fast quadrupolar relaxation is also the reason for the complex not being observed in the ^{71}Ga NMR spectrum. The *mer*-isomer is low symmetry and therefore has a significant efg at the ^{71}Ga nucleus, resulting in fast relaxation and broad resonances. Elemental analysis confirmed the expected formulation, $[GaF_3(terpy)]\cdot 3H_2O$.

The $[InF_3(terpy)]\cdot 3H_2O$ analogue was also prepared. Despite several attempts, crystals of suitable quality to perform single crystal X-ray analysis were not obtained. However, other spectroscopic data confirmed the proposed formula. The three In-F bands at 476, 427 and 406 cm^{-1} are consistent with the *mer*-isomer and with the trend that the frequency of the stretching bands falls with increasing mass of the metal centre. Like the $[GaF_3(terpy)]\cdot 3H_2O$ analogue, the ^{1}H NMR spectrum of the complex in CD_3OD gave six very broad resonances corresponding to the coordinated terpy ligand. The $^{19}F\{^{1}H\}$ NMR spectrum also showed two broad signals in a ratio of 2:1 arising from the $F_{trans F}$ and $F_{trans N}$, but again the couplings in the $^{19}F\{^{1}H\}$ NMR spectrum could not be resolved. Upon cooling the sample, precipitation of the complex occurred, showing that the $[InF_3(terpy)]\cdot 3H_2O$ complex is less soluble than the aluminium and gallium analogues. A resonance in the ^{115}In NMR spectrum was not observed due to the fast quadrupolar relaxation of the indium centre. Confirmation was provided by elemental analysis, which were consistent with the proposed formulation.

The synthesis and full characterisation of the neutral trifluoride complexes $[MF_3(terpy)]\cdot 3H_2O$ has added several new examples of rare Group 13 metal fluoride complexes and will hopefully aid in gaining a fuller understanding of the coordination chemistry of these trifluorides, which it is envisioned may contribute to advancing the design of the next generation of ^{18}F imaging agents.

6.2.3 Synthesis of $[GaF_3(terpy)]$ *via* halide exchange and attempted radiolabelling

Halide exchange reactions

Based upon the success of the halide exchange method described in Chapters 2 and 4, attempts to access the trifluoride complex $[GaF_3(terpy)]\cdot 3H_2O$ by a chloride/fluoride exchange reaction was investigated. The gallium complex $[GaCl_3(terpy)]$ was identified as a suitable candidate based upon the rapid and successful radiolabelling reactions of the gallium complexes in Chapters 3 and 4.

As a potential scaffold for radiolabelling applications, terpy has a number of advantages compared to the tacn-based scaffolds discussed in Chapters 2, 3 and 4. The ligand is commercially available and moderately inexpensive. This is in contrast to the tacn ligands discussed which require multiple synthetic steps before use. Furthermore, terpy can be easily functionalised in the 4-position, allowing the addition of peptides or bioactive groups to the ligand scaffold. In addition, terpy is rigid and pre-organised for chelation, which results in rapid complexation kinetics. If successful, the *mer*-isomer formed when coordinated may give subtle changes to the nature of the M-^{18}F bond and alter its stability under physiological conditions.

In an attempt to mimic the chemistry which worked so successfully with the neutral tacn complexes, $[MX_3(RMe_2\text{-tacn})]$ discussed in Chapters 2 and 3, the complex, $[GaCl_3(terpy)]$ was synthesised. The synthesis involved the reaction of $GaCl_3$ with terpy in anhydrous CH_2Cl_2.[14] The complex matched spectroscopically with the literature data.[14] The complex is isolated in very high yield and with little purification required. While solution phase spectroscopic data could be gained, the solubility of the complex in weakly polar, non-competitive donor solvents such as CH_2Cl_2 and MeCN was poor. The complex is soluble in more strongly donating solvents such as DMSO and DMF, but ^1H NMR spectroscopic analysis indicates that the terpy ligand is readily liberated, shown by the presence of 'free' ligand in the spectrum. This is similar behaviour to that observed with the neutral $[MCl_3(RMe_2\text{-tacn})]$ complexes, which rapidly decomposed in strong donor solvents (Chapter 2.2.2).

The halide exchange reactions were then studied, using the spectroscopic fingerprint acquired for $[GaF_3(terpy)]\cdot 3H_2O$ synthesised hydrothermally. The hydrolytically unstable $[MCl_3(Me_3\text{-tacn})]$ complexes discussed in Chapters 2.1.2 and 3.2.1 were shown to successfully

convert to the corresponding [MF_3(Me_3-tacn)] in the presence of $KF_{(aq)}$ at room temperature. Therefore the chloride/fluoride exchange reaction of [$GaCl_3$(terpy)] using KF under aqueous conditions was investigated. The method involved fully dissolving the [$GaCl_3$(terpy)] precursor in a mixed MeCN:H_2O solvent in a ratio of 5:1. Three molar equivalents of $KF_{(aq)}$ dissolved in a minimum volume of H_2O were added and followed by stirring of the reaction mixture at room temperature for one hour. The course of the reaction was monitored *in situ* using ^1H and $^{19}F\{^1H\}$ NMR spectroscopy. The ^1H NMR spectrum gave a pattern in the correct region and with the correct integrals corresponding to the terpy ligand. However, the pattern and peak positions were different from both the chloride starting material and the expected fluoride product. The $^{19}F\{^1H\}$ NMR spectrum recorded in D_2O showed a sharp singlet at -122.2 ppm corresponding to free fluoride ion in water.

In an effort to promote the halide exchange reaction, the mixture was heated to 80 ^oC for 45 minutes. The ^1H and $^{19}F\{^1H\}$ NMR spectrum of the product formed matched that observed in the room temperature reaction. This therefore made it clear that the halide exchange had not succeeded. However, the change in the ^1H NMR spectrum indicated that the chloride complex had undergone a chemical change. In order to determine what this was the chloride precursor was dissolved in the same mixed MeCN/H_2O solvent regime used in the failed halide exchange reaction. The ^1H NMR spectrum of this solution matched that observed in the failed fluorination reaction. This indicates that hydrolysis of the complex had occurred leading to decomposition. The hydrolysis appears to be rapid, having occurred in *ca.* 10 minutes between dissolution and the collection of the ^1H NMR spectrum, and completely converts the chloride complex, as the NMR spectrum was unchanged over the next three hours.

The appearance of the spectrum, and the relative chemical shifts did not match those of the free ligand. The hydrolysis pathway was proposed to proceed *via* liberation of the terpy ligand which was most likely protonated. The formation of the stable tetrahedral $[GaCl_4]^-$ anion may have provided a driving force.

This was confirmed by treatment of a solution of free terpy ligand in CD_3CN with 1.0 $moldm^{-3}$ HCl in water to form [H-terpy][Cl]. The ^1H NMR spectrum of the protonated ligand salt matched the peak positions and integrals for the spectrum acquired from the failed halide exchange reaction.

As the halide exchange reaction did not proceed as expected using $KF_{(aq)}$, the fluorination was investigated under anhydrous conditions using the fluoride salts NBu_4F in anhydrous THF and [K(2.2.2-crypt)]F in anhydrous MeCN.

Treatment of a suspension of [$GaCl_3$(terpy)] in MeCN with three molar equivalents of NBu_4F results in the full dissolution of the precursor complex. The mixture was stirred at room temperature for one hour. Spectroscopic analysis of the product obtained from removal of the

volatiles *in vacuo* matched that gained for the hydrothermal reaction, corresponding to $[GaF_3(terpy)]\cdot 3H_2O$. The infra-red spectrum showed the formation of three Ga-F stretching bands at 548, 504 and 490 cm^{-1} and the loss of the Ga-Cl bands at 267 and 254 cm^{-1} of the precursor complex. The ^{1}H and $^{19}F\{^{1}H\}$ NMR spectra were also consistent with the expected trifluoride complex discussed in Chapter 6.2.1. As was the case for the $[MF_3(Me_3\text{-tacn})]$ complexes discussed in Chapter 3.2.2, removal of the NBu_4Cl salt by-product proved challenging. However, recrystallisation from CH_2Cl_2/hexane in air provided crystals of the desired complex (confirmed from unit cell determinations on several crystals).

While being able to demonstrate the potential utility of this compound type in radiolabelling applications, the use of the NR_4F to carry ^{18}F in organic media is not an FDA approved agent for radiofluorination reactions.[19] A preferable agent in which ^{18}F may be administered is the use of the potassium-cryptand fluoride [K(2·2·2-crypt)]. As discussed in 1.1, this method provides an organic soluble source of fluoride ion. [K(2·2·2-crypt)]F is readily synthesised from reaction of a solution of 2·2·2-crypt in MeCN with aqueous KF, followed by removal of the volatiles under high vacuum. The resulting solid was dissolved in anhydrous MeCN, providing a stock solution of [K(2·2·2-crypt)]F. Reaction of $[GaCl_3(terpy)]$ with three molar equivalents of [K(2·2·2-crypt)]F in anhydrous MeCN at room temperature results in the dissolution of the precursor complex and leads to complete conversion to the corresponding $[GaF_3(terpy)]$ complex as evidenced from the spectroscopy. The reaction is complete within 60 minutes. This is an important consideration in regards to the potential radiolabelling reactions discussed below. It was also shown that the complex could be accessed even with heating to 80 °C in MeCN, confirming the Ga species is thermally stable under these conditions. This raises the prospect of performing any potential radiofluorination reactions both manually and using an automated synthesiser. The outcome of these experiments demonstrated that the trifluoride complex $[GaF_3(terpy)]$ could be accessed *via* chloride/fluoride exchange from the well-defined precursor $[GaCl_3(terpy)]$ under mild conditions. This provides an exciting alternative ligand framework in which the formation of ^{18}F labelled metal chelates for imaging applications could be studied.

Attempted ^{18}F Radiolabelling of [$GaCl_3$(terpy)]

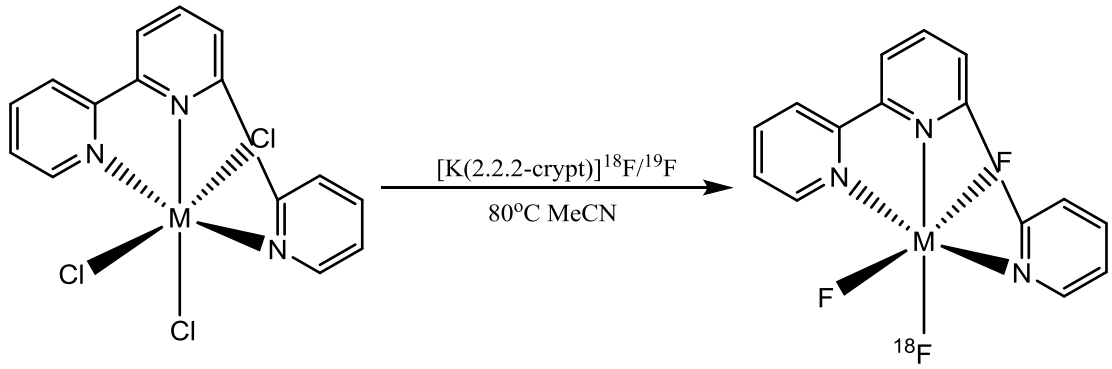

Figure 6.10: Scheme showing the proposed synthetic route towards ^{18}F labelled gallium terpy complexes.

Based upon the success of the chloride/fluoride exchange on a preparative scale, the ^{18}F radiolabelling was attempted to form the complex [Ga^{18}F$^{19}F_2$(terpy)] (Figure 6.10). Based upon the halide exchange studies performed on a preparative scale it was of importance to exclude moisture from the reaction mixture. This therefore required the use of anhydrous MeCN solvent and the rigorous azeotropic drying of the aqueous $^{18}F^-$ solution produced from the cyclotron.

The radiolabelling reaction was performed on a 1 mg (2.44 μmol) scale of the metal chloride chelate. The aqueous $^{18}F^-$ solution was treated with an aqueous solution of K^{19}F (0.99 eq) and stirred. A stoichiometric solution of 2.2.2-cryptand in anhydrous MeCN solution was added. The [K(2.2.2-crypt)]^{18}F^{19}F mixture was azeotropically dried with heating under a strong flow of N_2 gas three times. This gave a sample of [K(2.2.2-crypt)]^{18}F^{19}F. This was dissolved in 0.5 mL anhydrous MeCN and added to a fine suspension of [$GaCl_3$(terpy)] in 0.5 mL MeCN. While on a preparative scale the precursor complex dissolved upon addition of the fluoride source, on a radiochemical scale the precursor did not appear to dissolve. Upon heating to 80 °C for 20 minutes the [$GaCl_3$(terpy)] complex partially went into solution. However analysis of the crude reaction mixture by HPLC showed the only radioactive peak corresponded to unreacted $^{18}F^-$. This proved the case after several different reactions in which the solvent composition, reaction methodology and conditions were changed, e.g. using anhydrous MeOH as the reaction solvent and heating the reaction to 110 °C in both anhydrous MeCN and MeOH. Attempts were also made to prepare the ^{18}F containing complex using an automated GE FASTlab synthesiser. At no point was there any evidence for the successful formation of the radiolabelled complex [Ga^{18}F$^{19}F_2$(terpy)] based upon HPLC analysis. HLB purification of the crude reaction mixture as described in Chapter 4.2.6 was also attempted but the radioactivity that was loaded onto the cartridge was eluted off in the water wash; indicating that the only radioactive species was unreacted $^{18}F^-$.

Possible reasons for the failure to successfully form the radiolabelled complex are:

i) The poor solubility of the [$GaCl_3$(terpy)] precursor complex in non-aqueous media meant that the reaction could not proceed as expected.

ii) Rapid hydrolysis of the [$GaCl_3$(terpy)] precursor from trace water during the synthetic process (particularly from the ^{18}F solution produced in the cyclotron) prevented the halide exchange reaction from proceeding.

Based upon these results, the terpy ligand framework appears to be much inferior to the tacn based precursors described in Chapters 3 and 4.

Synthesis and Characterisation of [$GaCl_3$(^{t}Bu_3-terpy)]

Due to the poor solubility of [$GaCl_3$(terpy)], thought to be a key contributor to the inability to perform the halide exchange reaction with $^{18}F^-$, the corresponding complex of 4,4′,4″-tris-t-butyl,-2,2′6′,2″-terpyridine (Figure 6.11), [$GaCl_3$(^{t}Bu_3-terpy)], was prepared. It was thought that the bulky alkyl groups would aid in the solubility of the complex in organic media. Reaction of $GaCl_3$ with ^{t}Bu_3-terpy in anhydrous CH_2Cl_2 precipitated the complex as a white solid.

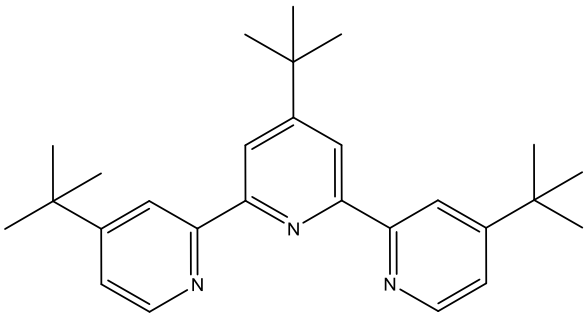

Figure 6.11: Structure of 4,4′,4″-tris-t-butyl,-2,2′6′,2″-terpyridine (^{t}Bu-terpy).

Surprisingly the complex proved very poorly soluble in organic media. This therefore precluded an investigation into the halide exchange reaction and subsequent attempts to radiolabel the complex.

The infra-red spectrum of the complex showed only two distinct Ga-Cl bands at 357 and 327 cm^{-1}. Group theory predicts that for the proposed *mer*-isomer with C_{2V} symmetry there would be three IR-active bands ($2a_1$ + b_1). However the bulky ^{t}Bu-substituents on the terpyridine ligands may drop the symmetry of the complex. The ^{1}H NMR spectrum recorded in CD_3CN of the poorly soluble complex shows a strong similarity to the [$GaCl_3$(terpy)] complex; a *ca.* 0.5 ppm shift in the terpyridine proton environments, and a small shift in the ^{t}Bu proton environments compared to the free ligand. Elemental analysis of the sample confirmed formation of the complex as a CH_2Cl_2 solvate. Unexpectedly, crystals grown from the filtrate from one synthesis were found to be of [$GaCl_2$(^{t}Bu_3-terpy)][$GaCl_4$]·CH_2Cl_2, containing an

unusual five-coordinate gallium cation (Figure 6.12). This minor by-product probably results from the presence of a small excess of $GaCl_3$ in the synthesis, which abstracts a chloride from the neutral species to form the stable $[GaCl_4]^-$ anion.

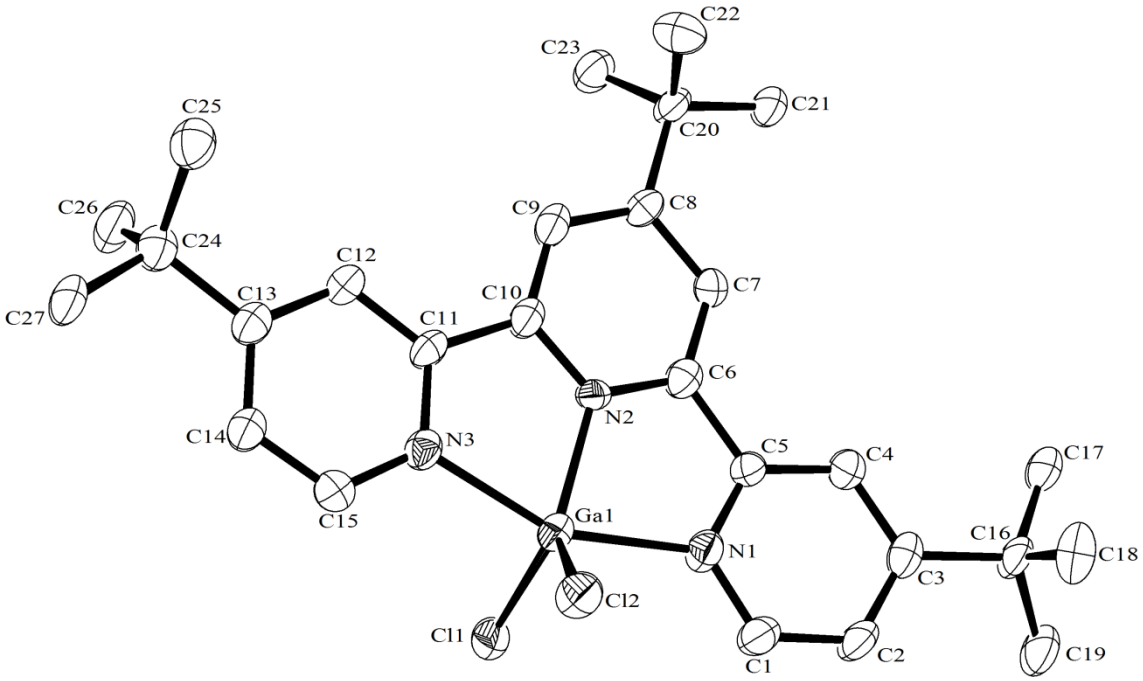

Figure 6.12: Crystal structure of the cation in $[GaCl_2(^tBu_3\text{-terpy})][GaCl_4]\cdot CH_2Cl_2$. H-atoms are excluded for clarity. Ellipsoids drawn at 50% probability level. Ga1-N1 2.092(5), Ga1-N2 1.995(5), Ga1-N3 2.066(5), Ga1-Cl1 2.195(2), Ga1-Cl2 2.169(2) Å. N2-Ga1-N3 77.9(2), N1-Ga1-N2 77.3(2), N1-Ga1-N3 155.1(2), N2-Ga1-Cl2 125.68(18), N3-Ga1-Cl2 97.76(17), N1-Ga1-Cl2 95.78(17), N2-Ga1-Cl1 120.20(18), N3-Ga1-Cl1 96.80(16), N1-Ga1-Cl1 96.56(18), Cl1-Ga1-Cl2 114.10(8)°.

The cation adopts a distorted trigonal bipyramidal geometry with apical N-donor atoms. The coordination sphere is distorted by the steric constraints of the $^tBu_3$-terpy (N3–Ga1–N1 = 155.1(2)°). Comparisons of the bond lengths between $[GaCl_2(^tBu_3\text{-terpy})]^+$ and $[GaCl_3(terpy)]$ reported previously by Kazakov *et al*,[14] as expected, show shorter bonds in the five-coordinate cation (Ga–Cl = 2.169(2), 2.195(2), Ga–N = 1.995(5)–2.092(5) Å) compared to the six-coordinate neutral complex (Ga–Cl = 2.2511(5) –2.4118(6), Ga–N = 2.0412(5)–2.1024(15) Å) in keeping with the release of steric strain on the metal centre. Due to the poor solubility of the complex the chloride/fluoride exchange reaction was not investigated.

6.2.4 Reaction of $MF_3 \cdot 3H_2O$ with 2,2′-bipyridine and 1,10′-phenanthroline

In order to provide comparisons with the tridentate terpy ligand complexes, and to provide further examples of complexes of the Group 13 fluorides with neutral ligands, the chemistry with the bidentate imine donors bipy and phen were investigated. Hydrothermal synthesis was shown to be a very suitable route to obtain the complexes $[MF_3(bipy)(OH_2)] \cdot 2H_2O$ and $[MF_3(phen)(OH_2)]$ (M = Al, Ga). The structures of $[InF_3(bipy)(OH_2)] \cdot 2H_2O$ and $[InF_3(phen)(OH_2)]$ have already been characterised crystallographically but with little other spectroscopic data.[8, 9] These complexes were therefore also synthesised hydrothermally and full characterisation obtained.

$[MF_3(bipy)(OH_2)] \cdot 2H_2O$

Reaction of $AlF_3 \cdot 3H_2O$ with 2,2′-bipy gives the solvated complex $[AlF_3(bipy)(OH_2)] \cdot 2H_2O$ in high yield as a pale pink solid. The infra-red spectrum of the material formed via removal of the reaction solvent showed two Al-F stretches at 610 (br) and 590 (sh) cm^{-1}. Group theory for a C_S point group would predict three infra-red active bands ($2a_1 + a_2$), but the broad band may have two overlapping signals. The infra-red spectrum also gave evidence of water in the complex with ν(O-H) and δ (H-O-H) bands present at 3422 and 1689 cm^{-1}. The ^1H NMR spectrum showed eight distinct resonances with sharp multiplets corresponding to the bipy protons. The bipy proton environments displayed a *ca.* 0.5 ppm shift due to metal coordination. A broad singlet corresponding to the water was also observed. The observation of eight distinct bipy proton environments, with resolved multiplicities, indicates that the bipy ligand coordinates *trans* to a fluoride and to a water ligand and hence the pyridyl rings are inequivalent. The $^{19}F\{^1H\}$ spectrum of $[AlF_3(bipy)(OH_2)] \cdot 2H_2O$ at room temperature in CD_3OD depicts a broad singlet at -172.0 ppm. Upon cooling the resonance splits to give two sharper resonances at -162.3 and -176.4 ppm in a ratio of 1:2 corresponding to F_{trans} and F_{cis} respectively. However, unlike $[AlF_3(terpy)] \cdot 3H_2O$, in which $^2J_{FF}$ coupling could be seen in the $^{19}F\{^1H\}$ NMR spectrum, no coupling was observed for $[AlF_3(bipy)(OH_2)] \cdot 2H_2O$.

Slow evaporation of an aliquot of the reaction solution furnished crystals suitable for single crystal X-ray diffraction.

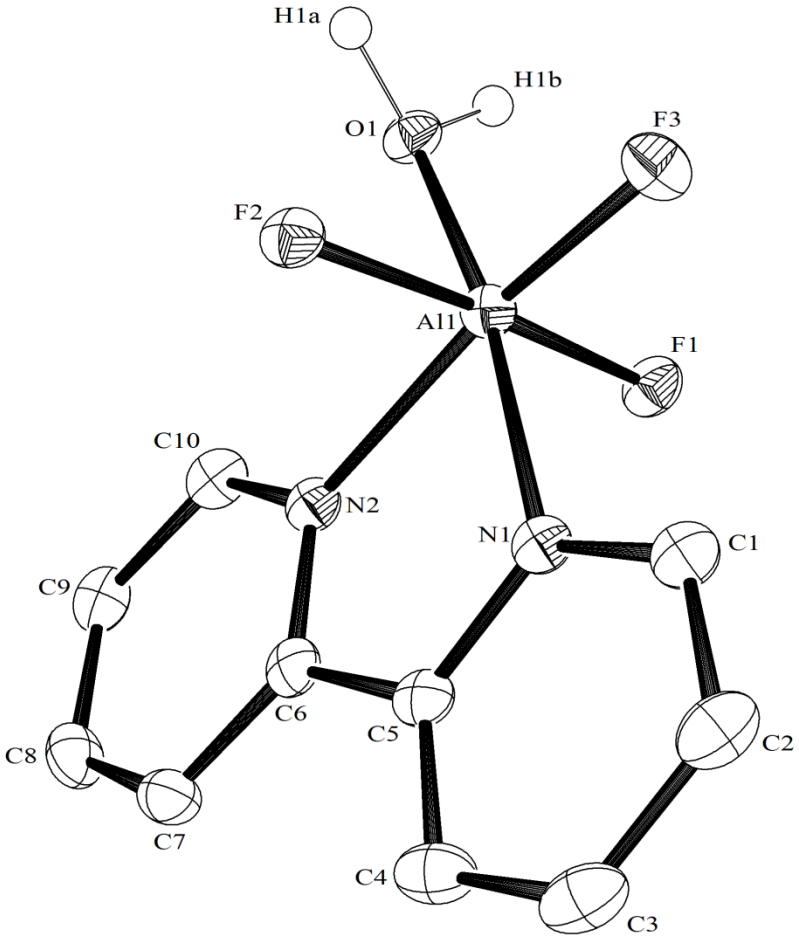

Figure 6.13: Crystal structure of $[AlF_3(bipy)(OH_2)]\cdot 2H_2O$. H-atoms on the bipy ligand and lattice water molecules are omitted for clarity. Ellipsoids drawn at 50% probability level. Al1-F1 1.786(2), Al1-F2 1.781(2), Al1-F3 1.743(2), Al1-O1 1.900(2), Al1-N1 2.050(3), Al1-N2 2.072(3) Å. F2-Al1-F3 93.35(11), F1-Al1-F3 92.22(11), F3-Al1-O1 97.24(10), F2-Al1-O1 88.30(11), F1-Al1-O1 89.16(11), F3-Al1-N1 92.19(10), F2-Al1-N1 90.08(10), F1-Al1-N1 91.55(10), F2-Al1-N2 86.50(11), F1-Al1-N2 88.32(11), O1-Al1-N2 92.39(11), N1-Al1-N2 78.18(11)°.

The structure (Figure 6.13) shows a six-coordinate, distorted octahedral Al(III) centre with the trifluoride ligands adopting a *mer*-arrangement, in which the neutral bipy ligand lies *trans* to coordinated OH_2/F ligands. Like the other hydrated complexes discussed throughout this work, $[AlF_3(bipy)(OH_2)]\cdot 2H_2O$ extensively H-bonds to the lattice water molecules forming an extended H-bonded assembly based upon F····H-O and O····H-O interactions. Each metal complex H-bonds to the molecule adjacent to it, forming an H-bonded 1D chain polymer in the solid state (Figure 6.14).

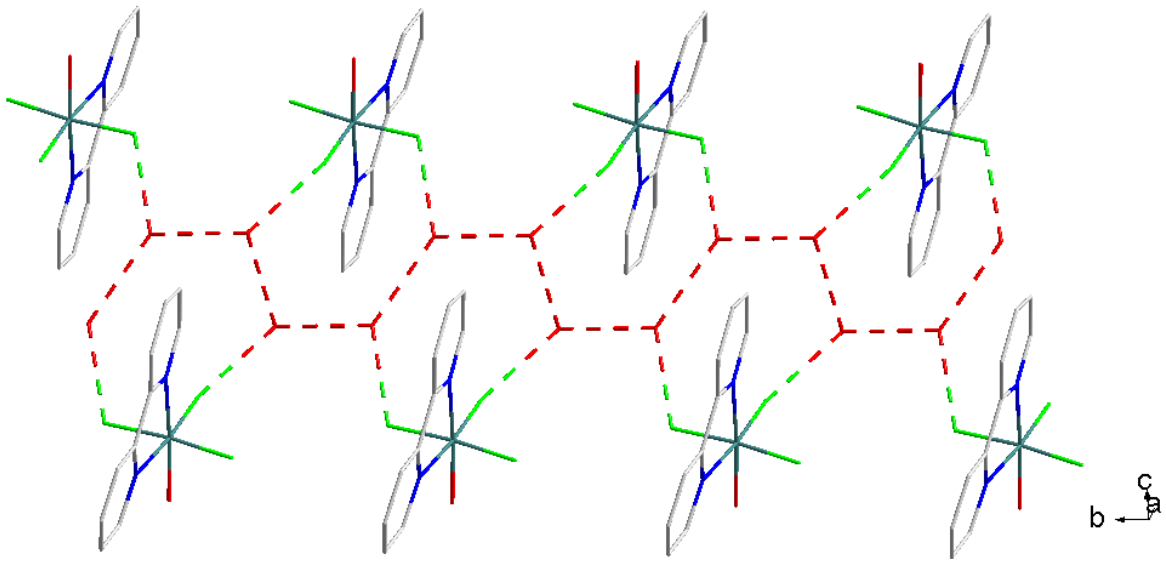

Figure 6.14: A portion of the extended structure of $[AlF_3(bipy)(OH_2)]\cdot 2H_2O$ viewed down the *b*-axis showing the H-bonded interactions between the complex and lattice water molecules. F1····O1 2.594(4), F2····O1 2.562(3), F1····O2 2.787(2), F3····O2 2.678(3) Å.

Figure 6.15 shows that the complexes are also associated in the solid state by π-stacking interactions (3.730 and 3.805 Å).

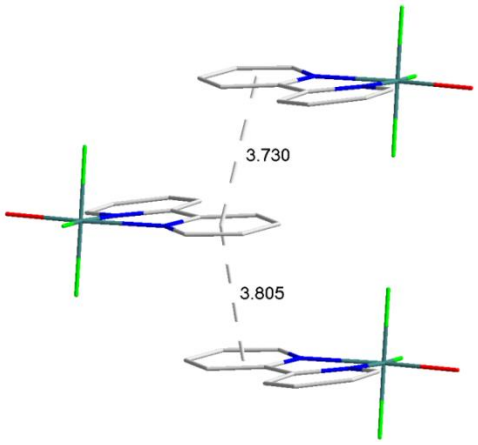

Figure 6.15: π-stacking arrangement in $[AlF_3(bipy)(OH_2)]\cdot 2H_2O$. Lattice water molecules are omitted for clarity.

The corresponding gallium complex $[GaF_3(bipy)(OH_2)]\cdot 2H_2O$ is also readily crystallised from slow evaporation of the aqueous reaction solution at ambient temperature (Figure 6.16).

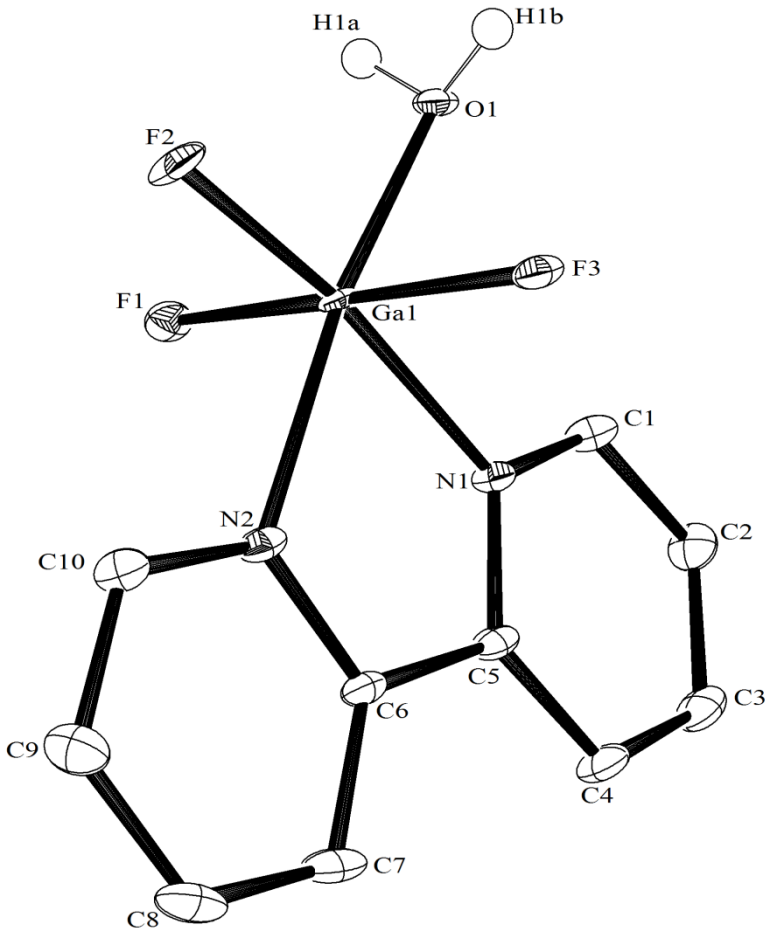

Figure 6.16: The crystal structure of $[GaF_3(bipy)(OH_2)]\cdot 2H_2O$. H-atoms on the bipy ligand and lattice water molecules are omitted for clarity. Ellipsoids are drawn at 50% probability level. Ga1-F11.8892(15), Ga1-F2 1.8442(17), Ga1-F3 1.8857(14), Ga1-O1 1.962(2), Ga1-N1 2.093(2), Ga1-N2 2.064(3) Å. F2-Ga1-F3 92.41(7), F1-Ga1-F2 90.74(7), F1-Ga1-F3 175.68(7), F2-Ga1-O1 96.70(8), F3-Ga1-O1 87.76(7), F1-Ga-O1 88.94(7), F2-Ga1-N2 92.28(9), F3-Ga1-N2 90.64(8), F1-Ga1-N2 92.19(8), F3-Ga1-N1 87.52(7), F1-Ga1-N1 89.86(7), O1-Ga1-N1 92.67(8), N2-Ga1-N1 78.35(9)°.

Like the aluminium and indium analogues, $[GaF_3(bipy)(OH_2)]\cdot 2H_2O$ adopts a distorted octahedral geometry with the trifluoride ligands adopting a *mer*-conformation.[8]

Comparison of the bond lengths in the three complexes $[MF_3(bipy)(OH_2)]\cdot 2H_2O$ (Table 6.1) demonstrates some interesting subtle trends.[8] Comparison of d(M-N) in the Al and Ga complex shows only a slight difference (*ca*. 0.02 Å). However the d(M-O) and d(M-F) distances increase significantly (0.06-0.10 Å). This implies that the more electronegative atoms feel a greater influence of the change in metal centre, as was the case with the terpy complexes discussed above in Chapter 6.2.1.

As expected the corresponding bond lengths all increase in the indium complex, but here the differences with donor type are less clear with all showing an increase of ~0.15–0.2 Å over the gallium analogue.

Complex	**d(M–F)/Å**	**d(M–N)/Å**	**d(M–O)/Å**
$[AlF_3(bipy)(OH_2)]\cdot 2H_2O$	1.786(2) 1.781(2) 1.743(2)	2.050(3) 2.072(3)	1.900(2)
$[GaF_3(bipy)(OH_2)]\cdot 2H_2O$	1.889(15) 1.844(17) 1.885(14)	2.093(2) 2.064(3)	1.962(2)
$[InF_3(bipy)(OH_2)]\cdot 2H_2O$	2.061(3) 2.007(4) 2.059(4)	2.234(4) 2.257(5)	2.114(4)

Table 6.1: Table of selected bond lengths for the complexes $[MF_3(bipy)(OH_2)]\cdot 2H_2O$.

Comparison of the structural data of $[MF_3(bipy)(OH_2)]\cdot 2H_2O$ demonstrates that the trends in the bond lengths in the Al, Ga complexes are different from those predicted on the basis of simple Lewis acidity in the gas phase.[20-22] However the effects of the lattice solvent and the H-bonding thereof should also be considered, and thus drawing a clear conclusion on the effect of the Lewis acidity of the Group 13 fluorides in these complexes should be made with caution.[14, 16, 20-22]

The effects of the electronegative ligands are less pronounced in the heavier indium analogue where the ~0.2 Å increase in the bond lengths compared to the gallium complex reflect the increased radius of the metal centre.

The $[GaF_3(bipy)(OH_2)]\cdot 2H_2O$ complex also displays extensive H-bonding interactions between the complex and the co-crystallised water molecules. The assembly formed is more extensive than the aluminium analogue as the H-bonded dimers may also interact with the adjacent dimer to form a 2D-sheet network (Figure 6.17).

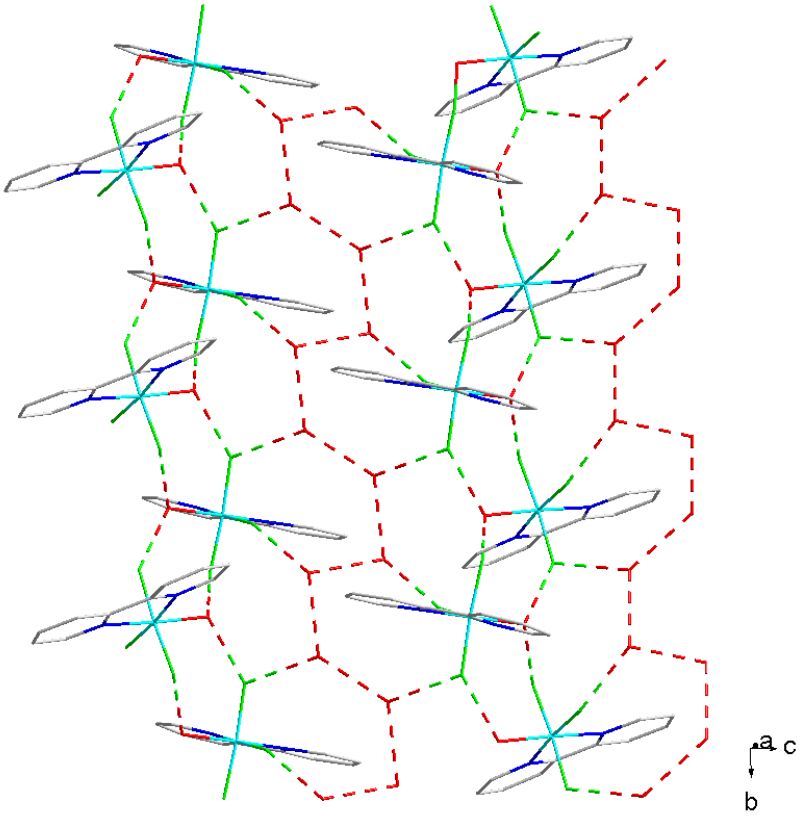

Figure 6.17: A view of the extended structure of $[GaF_3(bipy)(OH_2)]\cdot 2H_2O$ viewed down the *b*-axis showing the 2D-network formed from extensive H-bonding interactions between the complex and the co-crystallised water molecules. F2····O3 2.683(2), O3····O2 2.745(2), O3····O3 2.802(3) Å.

The complex is also associated in the solid state through π-stacking interactions (Figure 6.18).

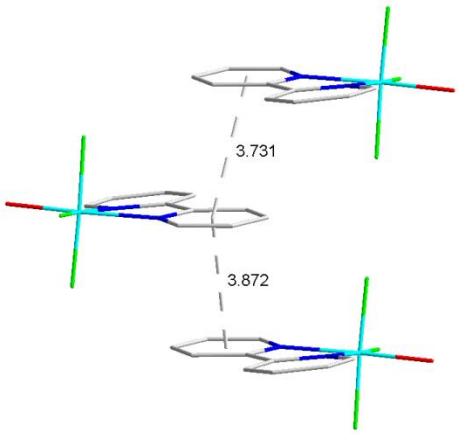

Figure 6.18: π-stacking arrangement in $[GaF_3(bipy)(OH_2)]\cdot 2H_2O$. Lattice water molecules are omitted for clarity.

Spectroscopic analysis of the crystals of $[GaF_3(bipy)(OH_2)]\cdot 2H_2O$ supported the proposed formulation. The infra-red spectrum showed two Ga-F stretches (527, 473 cm^{-1}). The ^1H NMR spectrum showed broad resonances corresponding to the bipyridine protons, associated with a 0.4 ppm coordination shift. The resonances remained broad even upon cooling to 183 K. This would suggest that the gallium complex is prone to reversible ligand dissociation – probably of the water in the solution phase. The dissociation of the coordinated water ligand likely results in a fluxional five-coordinate intermediate. This fluxional system is also observed in the $^{19}F\{^1H\}$ NMR spectrum which at room temperature depicts a broad singlet at -176.2 ppm. Upon cooling to 183 K, the resonance splits and sharpens to give two signals at -160.9 and -181.5 ppm in a ratio of 1:2, indicative of the F_{transF} and F_{cisF} environments. Even upon cooling no signal could be observed in the ^{71}Ga NMR spectrum. The fluxional gallium centre likely aids in accelerating the quadrupolar relaxation, resulting in resonances too broad to observe. Microanalysis of the solid formed in the bulk indicated that the proposed formulation was correct.

Solution phase spectroscopic analysis of $[InF_3(bipy)(OH_2)]\cdot 2H_2O$ proved more challenging. The complex decomposes in solution as shown by the $^{19}F\{^1H\}$ spectrum in which peaks ascribed to F^- (-122.1 ppm) and HF_2^- (-152.0 ppm) were observed shortly after preparing the sample. Therefore all spectroscopic data for the indium complex was obtained from fresh CD_3OD solutions of the complex. The ^1H NMR spectrum showed very broad resonances corresponding to the bipyridine protons shifted from the free ligand resonances. These resonances remained very broad even upon cooling. The $^{19}F\{^1H\}$ NMR spectrum at 295 K shows no resonance associated with the complex, however upon cooling to 183 K two new resonances appear at -152.9 and -178.1 ppm in a 1:2 ratio confirming the complex was present. The temperature dependence of the spectra is further evidence of a ligand dissociated fluxional five-coordinate intermediate, the dissociation rate increasing with decreased Lewis acid strength Al > Ga > In.

$[MF_3(phen)(OH_2)]$

These complexes were also readily accessed *via* hydrothermal synthesis. In contrast to the terpy and 2,2′-bipy complexes discussed above, crystallisation of the phen adducts proved very challenging. Crystals of the aluminium complex could not be obtained, however spectroscopic analysis confirmed the formation of the desired complex. The two Al-F bands (637, 608 cm^{-1}) are at higher frequency than those of the corresponding bipy complex. The lower frequency of the Al-F bands in the bipy complex are believed to be a reflection of the significant H-bonding in the complex. The features associated with the water ligand in the phen complex are significantly weaker than the bipy equivalent, as expected since the complex may be less hydrated in the solid state. As observed throughout this study, the ^1H and $^{19}F\{^1H\}$ NMR spectra of $[AlF_3(phen)(OH_2)]$ showed distinct sharp resonances indicating that the complex is static in

solution. In particular the $^{19}F\{^{1}H\}$ NMR spectrum depicted the distinctive 1:2 resonance pattern consistent with *mer* fluoride ligands. The $[AlF_3(phen)(OH_2)]$ also displays a broad singlet at 8.8 ppm ($W_{1/2}$ 450 Hz) ^{27}Al NMR spectrum; consistent with six coordinate octahedral aluminium.[7,13]

This proposed formulation of the phen adducts was confirmed from a crystal structure determination on crystals of the gallium analogue grown from slow evaporation of the reaction solvent at ambient temperature (Figure 6.19).

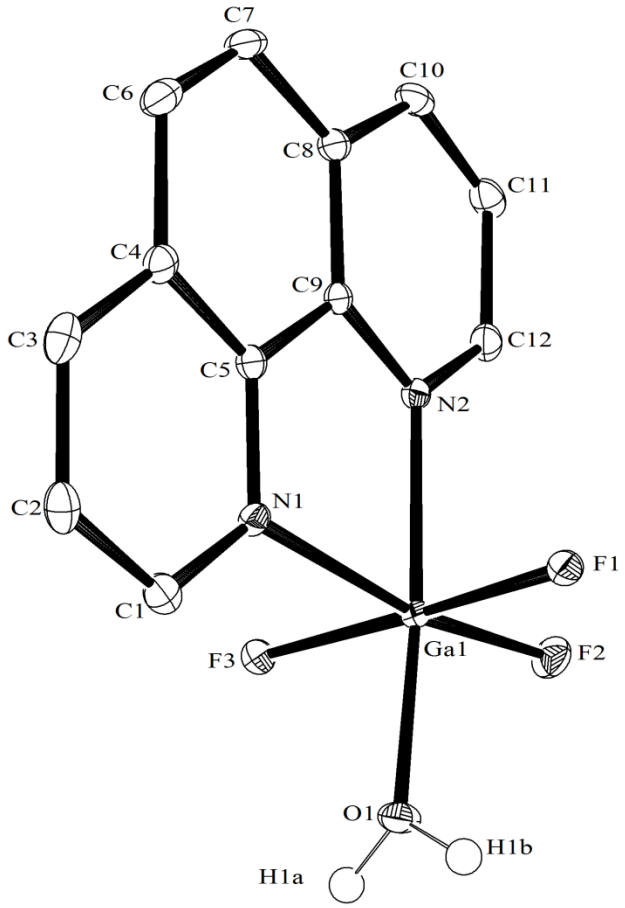

Figure 6.19: Crystal structure of $[GaF_3(phen)(OH_2)]$. H-atoms on the phen ligand are omitted for clarity. Ellipsoids are drawn at 50% probability level. Ga1-F1 1.8990(11), Ga1-F2 1.8242(12), Ga1-F3 1.8790(11), Ga1-N1 2.1250(16), Ga1-N2 2.0897(16), Ga1-O1 1.9594(14) Å. F2-Ga1-F3 95.13(5), F1-Ga1-F2 93.69(5), F2-Ga1-O1 98.11(6), F3-Ga1-O1 89.79(5), F1-Ga1-O1 86.92(5), F2-Ga1-N2 92.02(6), F3-Ga1-N2 93.11(5), F1-Ga1-N2 88.65(5), F3-Ga1-N1 87.18(6), F1-Ga1-N1 84.47(6), O1-Ga1-N1 91.54(6), N2-Ga1-N1 78.20(6)°.

The structure shows a distorted octahedral Ga(III) centre with the phen ligand coordinated *trans* to F/OH_2 with *mer*-fluorides. It is isomorphous to the heavier

[InF_3(phen)(OH_2)] analogue. As expected there is a 0.15-0.20 Å elongation in the corresponding bond lengths in the indium complex (Figures 6.20 and 6.21).

In contrast to the other imine based trifluoride complexes discussed above, the [GaF_3(phen)(OH_2)] complex crystallises as the molecular species, with no lattice solvent. Instead the complex forms F····H-O H-bonded interactions with the molecules adjacent to it, resulting in a 1D-chain.

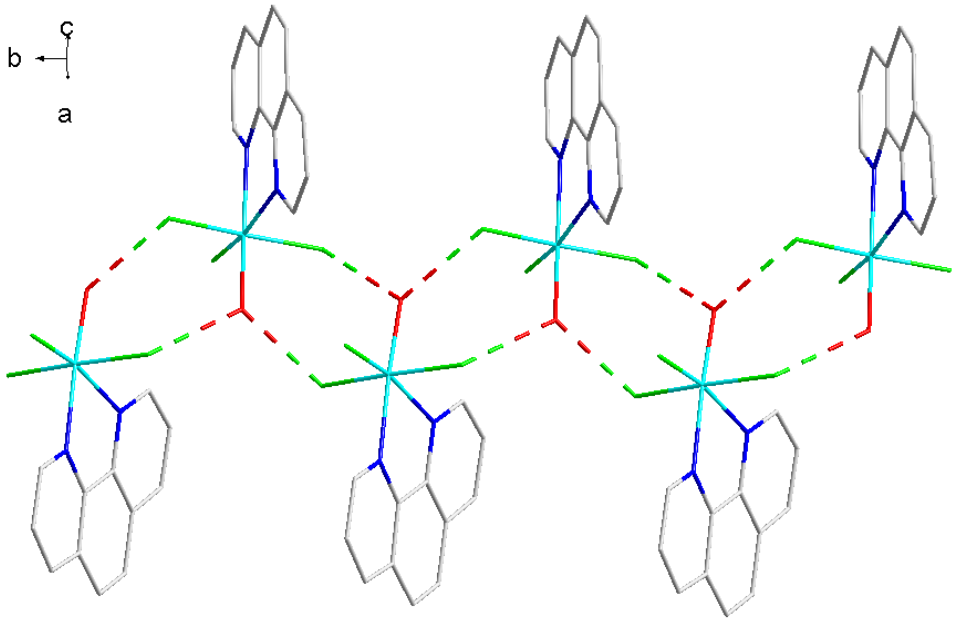

Figure 6.20: A portion of the extended structure of [GaF_3(phen)(OH_2)] viewed down the *b*-axis. It depicts a 1D-chain held by H-bonding interactions between adjacent complexes through F····O interactions. F1····O3 2.523(2), O1····F3 2.583(2) Å.

The [GaF_3(phen)(OH_2)] complex packs in the same way as the analogous [InF_3(phen)(OH_2)] complex prepared by Ilyukhin *et al.*[9] The H-bonded distances are similar in the two complexes. The F1····O3 (2.556 Å) and O1····F3 (2.499 Å) H-bonded distances in the indium analogue are similar to those in the gallium complex and may be considered strong interactions.

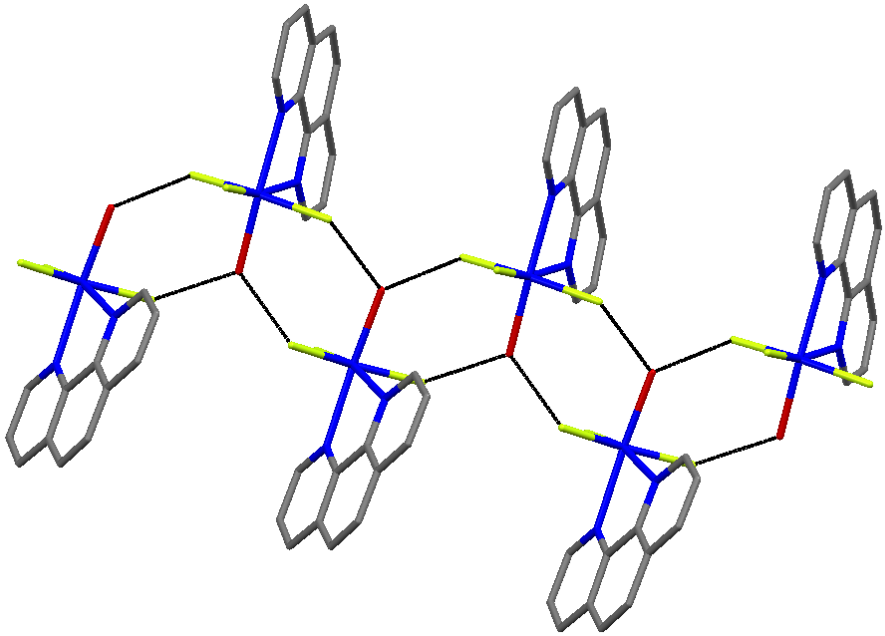

Figure 6.21: A portion of the extended structure of the complex [$InF_3(phen)(OH_2)$] synthesised by Ilyukhin *et al.* showing intermolecular H-bonding.[9] The H-bonding interactions, and thus the crystal packing is the same as the gallium analogue. Image re-drawn from original manuscript. Colour key: purple = In, blue = N, green = F, red = O, grey = C.

Figure 6.22 indicates that the [$GaF_3(phen)(OH_2)$] also shows slipped π-stacking interactions:

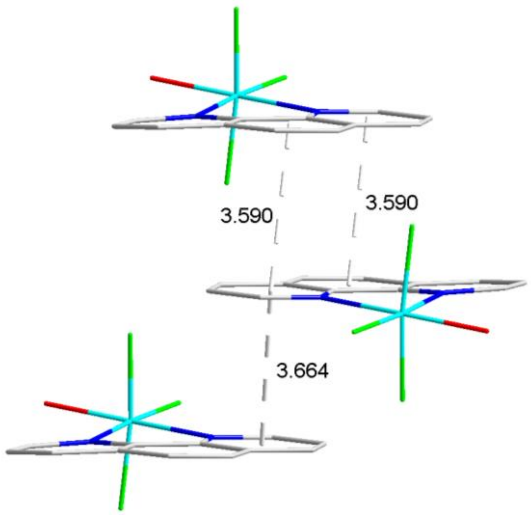

Figure 6.22: π-stacking interactions observed in [$GaF_3(phen)(OH_2)$].

The π-π interaction is shorter (*ca.* 0.2 Å) than the corresponding bipy complex, indicating that in the absence of the lattice water molecules in which to partake in H-bonding, the π-stacking interaction may be slightly stronger.

The solution phase spectroscopic trends observed as one descended the group for the bipy complexes was retained in the phen complexes; the gallium and indium complexes are dynamic in solution and hence at room temperature the resonances in the NMR spectra are shown to be broad and ill defined.

The synthesis and characterisation of the complexes $[MF_3(bipy)(OH_2)]\cdot 2H_2O$ and $[MF_3(phen)(OH_2)]$ represents a significant advancement in the coordination chemistry of the Group 13 metal fluorides and has provided several new examples of this compound type. In particular the synthesis and X-ray crystallographic determination of the structure of the Al and Ga complexes with bipy and phen has, in conjunction with the previously obtained In complexes, allowed detailed comparisons to be drawn and trends formed down the group.

6.2.5 Reaction of $MF_3\cdot 3H_2O$ with acyclic N-donor and other ligands

The complexes discussed in this chapter thus far have demonstrated the utility of the hydrothermal technique with regards to rigid, pre-organised imine ligands. It was also of interest to investigate whether the procedure could be extended to other ligand types such as acyclic N-donor ligands, crown-ethers and phosphine oxide ligands.

N,*N*,*N*′,*N*′,*N*′′-pentamethyldiethylenetriamine (pmdta) is a flexible, aliphatic acyclic triamine analogue of Me_3-tacn and terpy. Therefore its reactions with $AlF_3\cdot 3H_2O$ were investigated to provide a comparison.

Hydrothermal reaction of $AlF_3\cdot 3H_2O$ with pmdta gave a brown gum which after several MeCN washes gave a white-grey precipitate. Crystallisation of this solid by slow evaporation of a MeOH solution gave crystals of the salt $[TMP]_2[Al_2F_8(OH_2)_2]\cdot 2H_2O$ (Figure 6.23 and Figure 6.24). TMP = N,N,N′-trimethylpiperazinium.[23]

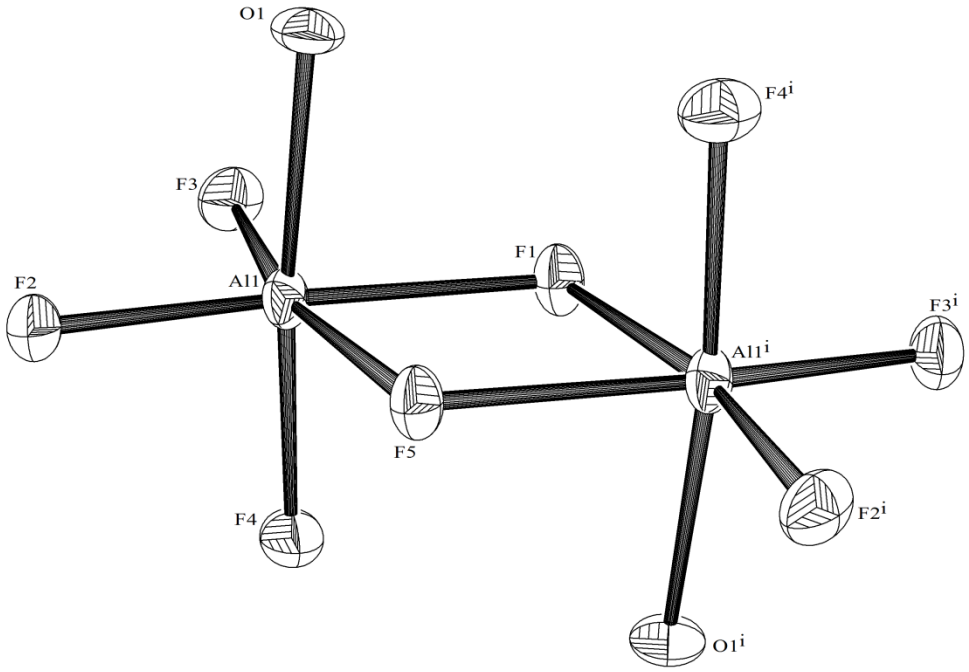

Figure 6.23: Crystal structure of the centrosymmetric $[Al_2F_8(OH_2)_2]^{2-}$ anion. H-atoms on the coordinated water ligands were not located in the difference map. Ellipsoids drawn at 50% probability level. Al1-F1 1.9048(19) , Al1-F2 1.748(2), Al1-F3 1.749(2), Al1-F4 1.778(2), Al1-F5 1.8968(19), Al1-O1 1.895(2) Å. F2-Al1-F3 99.65(11), F2-Al1-F4 93.28(10), F3-Al1-F4 93.83(10), F2-Al1-O1 90.62(10), F3-Al1-O1 90.65(10), F2-Al1-F5 92.34(10), F4-Al1-F5 88.95(8), O1-Al1-F5 85.68(8), F3-Al1-F1 91.94(10), F4-Al1-F1 88.61(8), O1-Al1-F1 86.52(8), F5-Al1-F1 75.93(10) , Al1-F5-Al1^i 104.38(13), Al1-F1-Al1^i 103.77(13)°.

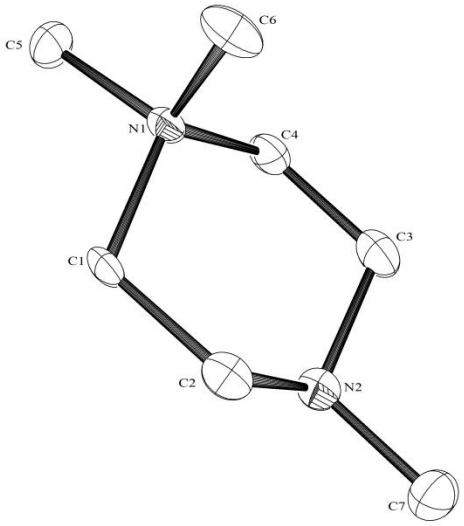

Figure 6.24: The crystal structure of the $[TMP]^+$ cation produced from hydrothermal reaction of $AlF_3{\cdot}3H_2O$ with pmdta.

The structure of the unusual $[Al_2F_8(OH_2)_2]^{2-}$ anion shows a centrosymmetric dimer based on two symmetry related octahedral Al(III) centres bridged by two fluoride ligands. The coordination sphere around the aluminium centre is completed by three terminal fluoride ligands, and a terminal coordinated water ligand. While the quality of the crystal was sufficient to gain detailed bond lengths, the hydrogen atoms on the water ligand were not located. The inference that it was an oxygen atom coordinated to the aluminium centre was based upon the difference in bond length between the other terminal ligands and comparison of the Al-F bond lengths in the corresponding $[Al_2F_{10}]^{4-}$ anion.[24, 25] In comparison to the other literature example of $[Al_2F_8(OH_2)_2]^{2-}$ the d(Al-O) in the anion discussed above was significantly shorter (1.895(2) Å) than that reported previously, d(Al-O) = 1.974(2) Å.[26] This difference could be explained by the degree of H-bonding in which the two structures partake. As expected the bridging fluoride bonds show an elongation compared to the terminal fluoride ligands.

The TMP cation is proposed to arise from the intramolecular cyclisation of the pmdta ligand with elimination of the volatile $HNMe_2$. The decomposition of pmdta to give this cationic species has been shown to occur under mild conditions,[23] so it is highly likely that the forcing conditions of the hydrothermal bomb may promote this unusual decomposition.

Solution phase structural data supports the formation of the cationic species; the ^1H NMR spectrum was significantly different from the free pmdta ligand, showing two broad resonances corresponding to the methylene CH_2 protons in the piperazine ring, accompanied by two singlets in a 2:1 ratio corresponding to the methyl groups on the nitrogen atoms. The $^{19}F\{^1H\}$ and ^{27}Al NMR spectra indicates that in the solution phase, the $[AlF_8(OH_2)_2]^{2-}$ anion dissociates giving the monoanionic $[AlF_4]^-$.[27] This implies that the anion is weakly bound and readily dissociates in the solution phase. In the solid state however, infra-red spectroscopy showed two broad bands at 616 and 569 cm^{-1} corresponding to the bridging and terminal Al-F stretching bands.

It appeared that the formation of metal fluoride complexes with the pmdta ligand could not be accomplished under hydrothermal conditions. The flexible acyclic pmdta is not pre-organised for chelation and so the entropy to form complexes is higher. The intramolecular reaction to eliminate a volatile by-product is likely to be a more favourable route. The formation of the rare fluoro-aquo-aluminate ion is unusual and probably driven by the coordinated water ligand promoting more rapid crystallisation. This work suggested that hydrothermal synthesis may have the best utility with rigid pre-organised ligands such as the imine based ligands discussed above, and the macrocyclic ligands discussed in Chapter 2.

Attempts were made to utilise hydrothermal synthesis to synthesise Group 13 metal fluoride complexes using crown ether and phosphine oxide ligands, which could provide the first evidence of the first structurally characterised neutral metal fluoride complexes with O-

donor ligands.[1, 6] Unfortunately no evidence of successful complex formation was observed. It appeared that no reaction occurred, with solution phase NMR data showing peaks corresponding to free ligand in the ^{1}H and $^{31}P\{^{1}H\}$ NMR spectra. The $^{19}F\{^{1}H\}$ showed no evidence for a 'Ga-F' containing species, often displaying no resonances at all, or a singlet corresponding to fluoride ion (δ -122 ppm). It therefore seems that under the conditions utilised, complexes of Group 13 fluorides with oxygen donors cannot be accessed. This may be due to the higher lability of O-donor ligands, and that the large excess of water present may preferentially bind to the metal centre. This also supports the evidence that careful choice of ligand architecture and donor atom type is an important consideration in these hydrothermal reactions.

6.2.6 $[Al_2F_9]^{3-}$: a rare fluoroaluminate

In addition to the formation of molecular adducts of the Group 13 fluorides, the synthesis and characterisation of novel fluoroaluminate salts with tetraalkylammonium salts was also investigated. Reaction of $AlF_3{\cdot}3H_2O$ with NMe_4F in refluxing water gave a white solid. Washing of this solid with MeCN followed by slow evaporation of the mother liquor at ambient temperature gives crystals of the highly unusual $[NMe_4]_3[Al_2F_9]$ salt, only the second cystallographically characterised example of this fluoroaluminate (Figure 6.25).[13, 28]

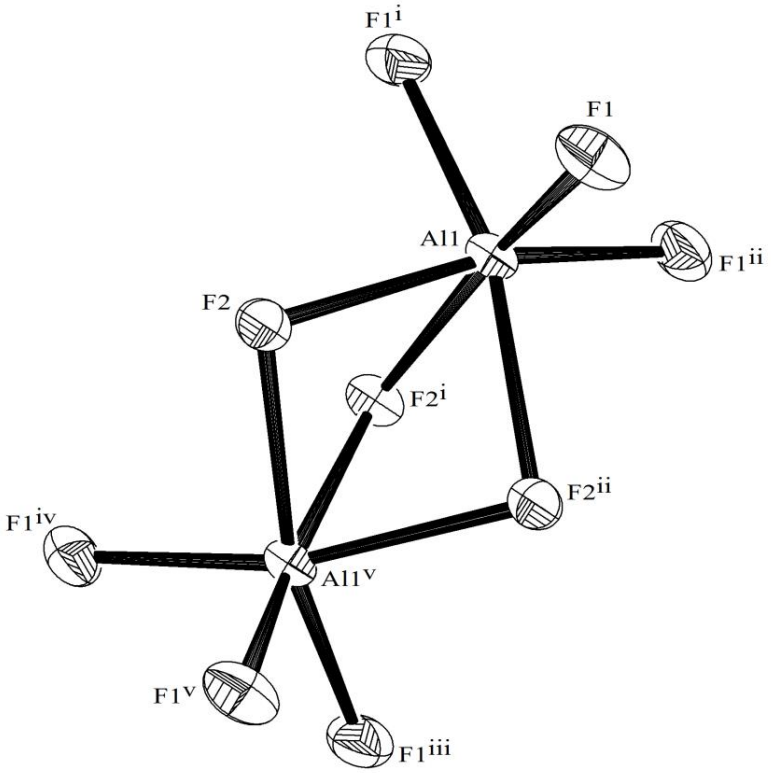

Figure 6.25: Crystal structure of the anion of $[NMe_4]_3[Al_2F_9]$. Ellipsoids are drawn at 50% probability level. Symmetry operation: a = x, y, 3/2 – z. Al1-F1 1.7389(14), Al1-F2 1.9136(14) Å. F1 Al1 F1a 96.94(6), F1 Al1 F2 91.89(6), F1-Al1-F2a 165.19(6), F2-Al1-F2a 75.63(7), Al1-F2-Al1 89.86(8)°.

The structure indicates two symmetry related distorted octahedral aluminium (III) centres bridged by three fluoride ligands. The coordination sphere is completed by three terminal fluoride ligands. The F1-Al1-F2 angles are particularly acute indicating that the species is quite sterically constrained. As expected, d(Al-F) of the bridging fluoride interactions are significantly longer than the terminal Al-F bonds, a reflection of the fluoride ligand having to coordinate with two metal centres. Infra-red spectroscopy shows a very broad signal with overlapping bands at 637 cm^{-1} corresponding to the terminal Al-F stretches, along with a sharper band at 358 cm^{-1} corresponding to the bridging Al-F-Al stretches.

While this was the dominant species formed in the solid state, the solution phase behaviour proved rather different. The complex, weakly soluble in CD_3CN gave a resonance in the ^1H NMR spectrum at δ 3.30 ppm, corresponding to the tetramethylammonium cation. The $^{19}F\{^1H\}$ NMR spectrum depicted a six line signal with lines of equal intensity at δ -194.0 ppm – consistent with $[AlF_4]^-$, but also another resonance at δ -150.1 ppm likely corresponding to fluoride ion in acetonitrile. The ^{27}Al NMR spectrum showed a singlet at 48.0 ppm

corresponding to $[AlF_4]^-$.[27] This suggests that the anion is weakly bound in the solid state and readily dissociates in solution.

While the $[Al_2F_9]^{3-}$ anion was predicted to be present in molten salts such as cryolite,[29-32] this preparation and the recently reported work by Xu *et al.* are the first crystallographically determined examples of the face sharing bioctahedral anion. Xu *et al.* obtained their crystals through slow evaporation of a solution of $[C_{18}MIm][AlF_4]$ ($C_{18}MIm^+$ = 1-methyl-3-octadecylimidazolium) in CH_2Cl_2.[28] They theorized that the formation of $[Al_2F_9]^{3-}$ was driven by the large stabilisation energy of forming a lattice structure including CH_2Cl_2, and that the polymerisation to form an infinite polymer of AlF_6 units is prevented by the large $C_{18}MIm$ cation. The crystal structure obtained in this work contained no co-solvent in the lattice, suggesting that solvent effects do not drive the formation of the anion. In addition, the cation present in the structure obtained was the small, sterically undemanding tetramethylammonium $[NMe_4]^+$ cation. This would suggest that the cation has little effect in the formation of the bridging anion.

The rationale for the formation of $[Al_2F_9]^{3-}$ rather than $[AlF_4]^-$ is likely derived from packing effects; an octahedral $[Al_2F_9]^{3-}$ unit will fill less space than two tetrahedral $[AlF_4]^-$ units, and the preference for any free fluoride to form an interaction with a metal centre rather than remain as free fluoride.

6.3 Conclusions and Future Work

The work discussed in this chapter provides an increased understanding of Group 13 metal fluoride complexes. Hydrothermal synthesis was found to be a highly successful way of accessing the complexes $[MF_3(terpy)]\cdot 3H_2O$, $[MF_3(bipy)(OH_2)]\cdot 2H_2O$ and $[MF_3(phen)(OH_2)]$ (M = Al, Ga, In) in high yield and purity from the reaction of $MF_3\cdot 3H_2O$. The stability of the trifluoride complexes contrasts with the moisture sensitivity of complexes of the Group 13 metals with heavier halides. Crystallographic studies show that all the complexes adopt *mer*-geometries with respect to the fluoride ligands, in contrast to the triaza-macrocyclic complexes discussed in Chapters 2, 3 and 4. Extensive H-bonded networks based upon F···H-O and O···H-O interactions are observed for the hydrated terpy and bipy complexes. H-bonded networks are also observed in the phen complexes based upon intermolecular F···H-O interactions. In addition to the H-bonding networks, the complexes are stabilised in the solid state by π-stacking interactions. Comparison of the M-O and M-F bond lengths in the terpy and bipy complexes show that the electronegative donor is more heavily influenced in the change of metal centre than the M-N bond lengths. However the differences in M-O and M-F bond lengths between Al

and Ga are not as expected based upon changes in the ionic radii. This indicates that the Lewis acidity trends down Group 13 may not be as clear as first thought.

The complex $[GaF_3(terpy)]\cdot 3H_2O$ was successfully accessed via a chloride/fluoride exchange reaction using NBu_4F in thf and [K(2.2.2-crypt)]F in MeCN at room temperature. The complex forms quantatively in short reaction times (1 hour). The halide exchange reaction does not occur with aqueous KF, instead liberating the ligand from the metal centre. Attempts were made to radiolabel the chloride complex to form $[Ga^{18}F^{19}F_2(terpy)]$. Despite numerous reaction attempts utilising different solvent regimes and *via* both manual and automated synthetic methods, the radiolabelled complex could not be accessed. It was concluded that the failure to radiolabel the complex was due to one of two factors; (i) the very poor solubility of the chloride precursor complex in non-aqueous media and (ii) the inability to fully dry the $^{18}F^-$ meant residual H_2O in the reaction system resulted in complex hydrolysis.

Attempts to improve the solubility of the chloride precursor utilised the bulky $^tBu_3$-terpy ligand. While the resulting chloride complex was not any more soluble, crystallisation of the reaction filtrate gave crystals of the highly unusual 5-coordinate cation $[GaCl_2(^tBu_3\text{-terpy})]^+$. Reaction of $AlF_3\cdot 3H_2O$ with the acyclic triamine pmdta under hydrothermal conditions results in decomposition of the ligand to from the trimethylpiperazinium cation $[TMP]^+$ and the unusual $[Al_2F_8(OH_2)_2]^{2-}$ anion. The formation of this species, coupled with the failed attempts to form trifluoride complexes with the O-donor crown ether and phosphine oxide ligands suggests that choice of ligand architecture and donor atom has a large influence on the success of hydrothermal synthesis.

Reaction of $AlF_3\cdot 3H_2O$ with NMe_4F in water followed by recrystallization from MeCN gives crystals of the unexpected and rare $[Al_2F_9]^{3-}$ anion. The formation of this species was unusual and unexpected considering the proposed conditions required for its formation.

The work discussed above represents a significant development of Group 13 metal fluoride complexes with neutral ligands. However, there is scope in which to further the chemistry. In regards to the key work discussed throughout this thesis, the incorporation of ^{18}F to give a new class of imaging agents, there is scope to continue the development of terpy based ligand scaffolds as potential new imaging agents. The key, based upon the work conducted in this chapter is to identify a ligand design which would improve the precursor's solubility, or to design a ligand which would allow the precursor complex to be stable under aqueous conditions (Figure 6.26).

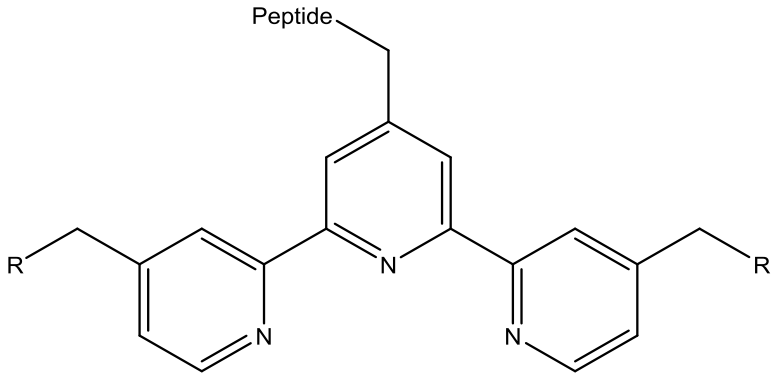

Figure 6.26: An example of a potential terpy based ligand architecture suitable for radiolabelling reactions. R = alkyl, amine, amide.

The formation of neutral trifluoride complexes with O-donor ligands would be of interest to allow comparison with the triaza-macrocyclic and imine donor complexes discussed in this volume of work. The complexes might be accessed from a preformed chloride precursor, in a similar manner to the halide exchange reactions discussed in Chapter 3.2.2.

It would be of interest to access the trifluoride complex [MF_3(pmdta)] in order to compare with the triaza-macrocyclic complexes discussed in Chapters 2 and 3. As detailed in Chapter's 1.6 and 6.1.1 some Group 13 fluoride complexes can be accessed from prolonged reflux of the constituents in alcohol. This method could be utilised as a potential route to the complex, or *via* halide exchange of a pre-formed [$GaCl_3$(pmdta)] complex.

The complexes [MF_3(terpy)] were shown to be heavily hydrated in the solid state, forming extensive H-bonded assemblies, similar to those observed in the [MF_3(RMe_2-tacn)] complexes discussed in Chapters 2 and 3. The neutral triaza-macrocyclic complexes were shown to coordinate to alkali metal and ammonium cations in the solid state (Chapter 5). It would therefore be of great interest to investigate whether the terpy complexes discussed here would be able to form similar interactions. This would aid in further understanding the nature of the trifluoride moiety in the two complexes. Is the requirement of the trifluoride to adopt a *fac*-geometry key to forming the interesting assemblies discussed in Chapter 5.2.2, or can the *mer*-geometry also form them? If indeed they are capable of coordinating to alkali metals in the solid state, the [MF_3(terpy)] complexes could lead to another new class of metalloligand.

6.4 Experimental

For general synthetic techniques see Appendix 1. The $MF_3 \cdot 3H_2O$ (M = Al, Ga or In), $GaCl_3$, 2,2′-bipyridine, 1,10′-phenanthroline, 2,2′,6′,2″-terpyridine, 4,4′,4”-tris-t-butyl,-2,2′,6′,″-terpyridine ($^tBu_3$-terpy), and N,N,N′,N′,N″-pentamethyldiethylenetriamine were obtained from Sigma-Aldrich or Alfa-Aesar and used as supplied.

$[AlF_3(terpy)] \cdot 3H_2O$

$AlF_3 \cdot 3H_2O$ (0.100 g, 0.72 mmol) was suspended in freshly distilled water (7 mL) and terpy (0.169 g, 0.72 mmol) was then added. The suspension was transferred into a Teflon container and loaded into a stainless steel high pressure vessel (Parr) and heated to 180 °C for 15 h. The vessel was then allowed to cool. A pale yellow solution had formed, a small aliquot of which was retained to grow crystals. For the remaining reaction mixture the solvent was removed *in vacuo,* yielding a pale orange solid. Yield: 0.182 g, 70%. IR (Nujol, ν/cm^{-1}): 3370 (ν O–H), 1640 (δ H–O–H) 656, 631, 620 (Al–F). ^{1}H NMR (CD_3OD, 298 K) δ = 8.90 (d, J_{HH} 8.0 Hz, [2H], ArH,) 8.76 (d, J_{HH} 8.0 Hz, [2H], ArH), 8.54 (d, J_{HH} 8.0 Hz, [2H], ArH), 8.39 (t, J_{HH} 8.0 Hz, [2H], ArH), 8.28 (t, J_{HH} 8.0 Hz, [H], ArH), 7.83 (t, J_{HH} 6.0 Hz, [2H], ArH), 4.87 (s, H_2O). ^{19}F{^{1}H} NMR (CD_3OD, 298 K) δ = −162.0 (d, $^2J_{FF}$ 23.0 Hz, [2F]), −177.3 (t, $^2J_{FF}$ 23.0 Hz, [F]). ^{27}Al NMR (CD_3OD, 298 K) δ = 16.7 (br). Slow evaporation of the reaction solvent gave crystals suitable for X-ray diffraction.

$[GaF_3(terpy)] \cdot 3H_2O$

Method 1: Method as for $[AlF_3(terpy)] \cdot 3H_2O$ using $GaF_3 \cdot 3H_2O$ (0.200 g, 1.11 mmol) and terpy (0.259 g, 1.11 mmol). Orange solid. Yield 0.366 g, 80%. Required for $C_{15}H_{17}F_3GaN_3O_3$: C, 43.5; H, 4.1; N, 10.2. Found: C, 43.3; H, 4.0; N, 10.3%. IR (Nujol, ν/cm^{-1}): 3407 (ν O–H), 1644 (δ H–O–H), 548, 504, 490 (sh) (Ga–F). ^{1}H NMR (CD_3OD, 298 K) δ = 9.04 (d, J_{HH} 8.0 Hz, [2H], ArH,) 8.80 (d, J_{HH} 8.0 Hz, [2H], ArH), 8.78 (d, J_{HH} 8.0 Hz, [2H], ArH), 8.64 (t, J_{HH} 8.0 Hz, [H], ArH), 8.49 (t, J_{HH} 8.0 Hz, [2H], ArH), 8.03 (t, J_{HH} 6.0 Hz, [2H], ArH), 4.87 (s, H_2O). ^{19}F{^{1}H} NMR (CD_3OD, 298 K) δ = −156.3 (s, [2F]), −189.7 (s, [F]); (183K) δ = −154.5 (s, [2F]), −188.9 (s, [F]). Slow evaporation of the reaction solvent gave crystals suitable for X-ray diffraction.

Method 2: A suspension of $[GaCl_3(terpy)]$ (0.06 g, 0.15 mmol) in 5 mL anhydrous MeCN was treated with 0.45 mL (0.45 mmol) of a 1.0 M solution of $[NBu_4]F$ in thf. Addition of the fluoride source resulted in the dissolution of the chloride precursor and the formation of a pale yellow solution. The mixture was stirred at room temperature for 1 h, and then the volatiles were removed *in vacuo* to yield a yellow gum. This was dissolved in a minimum volume of CH_2Cl_2 (*ca*. 2 mL) and layered with hexane. A pale yellow precipitate formed overnight. Yield 0.042 g, 67%. Spectroscopic data matched that observed for Method 1 and recrystallisation from

CH_2Cl_2/hexane yielded small crystals whose unit cell dimensions matched that of the crystals obtained *via* Method 1.

Method 3: [$GaCl_3$(terpy)] (0.020 g, 0.050 mmol) was suspended in 5 mL anhydrous MeCN. A solution of [K(2.2.2-crypt)]F (0.067 g, 0.150 mmol) in 3 mL anhydrous MeCN was added drop wise to the chloride precursor. Addition of the fluoride source resulted in the dissolution of the chloride precursor and the formation of a colourless solution. The mixture was stirred at room temperature for 1 h, then the volatiles were removed *in vacuo* to give a white solid containing both the expected fluoride complex and the [K(2.2.2-crypt)]Cl by-product. Spectroscopic data for the former matched that observed from Method 1.

Method 4: As for method 3 but the mixture was refluxed for 20 minutes. Spectroscopic data matched that observed from method 1.

[InF_3(terpy)]·3H_2O

Method as for [AlF_3(terpy]·3H_2O using InF_3·3H_2O (0.100 g, 0.44 mmol) and terpy (0.103 g, 0.44 mmol). Pale orange solid. Yield: 0.100 g, 49%. Required for $C_{15}H_{17}F_3InN_3O_3$: C, 39.2; H, 3.7; N, 9.2. Found: C, 39.4; H, 3.9; N, 9.3%. IR (Nujol, ν/cm^{-1}): 3490, 3400(ν O–H), 1654 (δ H–O–H), 476, 427, 406 (In–F). ^{1}H NMR (CD_3OD, 298 K) δ = 8.68 (m, [2H], ArH), 8.61 (d, J_{HH} 8.0 Hz, [2H], ArH), 8.39 (d, J_{HH} 8.0 Hz, [2H], ArH), 8.07–7.97 (m, [3H], ArH), 7.47 (m, [2H], ArH), 4.87 (s, H_2O). ^{19}F{^{1}H} NMR (CD_3OD, 298 K) δ = –157.8 (br s [2F]), –181.6(br s [F]); (183K): –157.5 (br s [2F]), –178.5(br s [F]).

[AlF_3(bipy)(OH_2)]·2H_2O

Method as for [AlF_3(terpy)]·3H_2O using AlF_3·3H_2O (0.200 g, 1.45 mmol) and bipy (0.226 g, 1.45 mmol). The resulting pale pink solid was washed with acetonitrile and filtered to leave a white solid which was dried *in vacuo*. Yield: 0.20 g, 47%. Required for $C_{10}H_{14}AlF_3N_2O_3$: C, 40.8; H, 4.8; N, 9.5. Found: C, 40.6; H, 4.6; N, 9.7%. IR (Nujol, ν/cm^{-1}): 3533, 3422 (ν O–H), 1689 br (δ H–O–H), 610, 590 (sh) (Al–F). ^{1}H NMR (CD_3OD, 298 K) δ = 9.04 (d, J_{HH} 4.0 Hz, [1H], ArH), 8.76 (d, J_{HH} 4.4 Hz, [1H], ArH), 8.59 (d, J_{HH} 7.6 Hz, [1H], ArH), 8.44 (d, J_{HH} 8.1 Hz, [1H], ArH), 8.33 (t, J_{HH} 7.7 Hz, [1H], ArH), 8.14 (t, J_{HH} 7.5 Hz, [1H], ArH), 7.81–7.85 (m, [1H], ArH), 7.63 (t, J_{HH} 5.9 Hz, [1H], ArH), 4.75 (s, H_2O). ^{19}F{^{1}H} NMR (CD_3OD, 298 K) δ = –172.8 (br s); (183 K): –162.3 (s, [F]), –176.4 (s, [2F]). ^{27}Al NMR (CD_3OD, 298 K) δ = 8.3 (br s, $W_{1/2}$ = 400 Hz), resonance lost on cooling < 233 K. Slow evaporation of the reaction solvent gave crystals suitable for X-ray diffraction.

[GaF_3(bipy)(OH_2)]·2H_2O

Method as for [AlF_3(terpy)]·3H_2O using GaF_3·3H_2O (0.200 g, 1.11 mmol) and bipy (0.158 g, 1.11 mmol). Pale pink solid. Yield 0.314 g, 84%. Required for $C_{10}H_{14}F_3GaN_2O_3$: C, 35.7; H, 4.1; N, 8.3. Found: C, 35.6; H, 4.1; N, 8.2%. IR (Nujol, ν/cm^{-1}): 3500, 3380 (ν O–H), 1660 br (δ H–O–H), 527, 473 (Ga–F). ^{1}H NMR (CD_3OD, 298 K) δ = 9.07 (br, [2H], ArH), 8.66 (d, J_{HH} 8 Hz, [2H], ArH), 8.37 (t, J_{HH} ~ 8 Hz, [2H], ArH), 7.89 (s, [2H], ArH); (183 K): 9.09 (s, [2H], 8.81 (br, s [2H], ArH), 8.47 (s, [2H]), 7.97 (s, [2H]), 4.75 (s, H_2O). ^{19}F{^{1}H} NMR (CD_3OD, 298 K) δ = –176.2 (br s); (183 K): –160.9 (s, [F]), –181.5 (s, [2F]). Slow evaporation of the reaction solvent gave crystals suitable for X-ray diffraction.

[InF_3(bipy)(OH_2)]·2H_2O

Method as for [AlF_3(terpy)]·3H_2O using InF_3·3H_2O (0.200 g, 0.89 mmol) and bipy (0.138 g, 0.89 mmol), yielding a pale yellow solid. Yield: 0.17 g, 50%. Required for $C_{10}H_{14}F_3InN_2O_3$: C, 31.4; H, 3.7; N, 7.3. Found: C, 31.6; H, 3.6; N, 7.4%. IR (Nujol, ν/cm^{-1}): 3422 br (ν O–H), 1655 br (δ H–O–H), 442, 428, 404 (In–F). ^{1}H NMR (CD_3OD, 298 K) δ = 8.78 (br s, [2H], ArH), 8.68 (br s, [2H], ArH), 8.45 (br s, [2H], ArH), 7.96 (br s, [2H], ArH), 4.75 (s, H_2O); (183 K): 8.99 (br, s), 8.95 (br s,), 8.66 (s), 8.52 (v br), 8.05–7.99 (m). ^{19}F{^{1}H} NMR (CD_3OD, 298 K) not observed; (183 K): δ = –152.9 (s, [F]), –178.1 (s, [2F]).

[AlF_3(phen)(OH_2)]

Method as for [AlF_3(bipy)(OH_2)]·2H_2O, but using AlF_3·3H_2O (0.200 g, 1.45 mmol) and phen (0.261 g, 1.45 mmol). White solid. Yield: 0.254 g, 62%. Required for $C_{12}H_{10}AlF_3N_2O$: C, 51.1; H, 3.6; N, 9.9. Found: C, 50.9; H, 3.4; N, 10.0%. IR (Nujol, ν/cm^{-1}): 3200br (ν O–H), 1670 (δ H–O–H), 637, 608 (Al–F). ^{1}H NMR (CD_3OD, 298 K) δ = 9.30 (d, J_{HH} 5.1 Hz, [1H], ArH), 9.17 (d, J_{HH} 3.7 Hz, [1H], ArH), 8.88 (d, J_{HH} 7.6 Hz, [1H], ArH), 8.66 (d, J_{HH} 8.8 Hz, [1H], ArH), 8.25 (s, [1H], ArH), 8.14 (m, [1H], ArH), 8.09 (s, [1H], ArH), 7.93 (m, J_{HH} 4.2 Hz, [1H], ArH), 4.75 (s, H_2O). ^{19}F{^{1}H} NMR (CD_3OD, 298 K) δ = –157.3 (br s [F]), –174.8 (s, [2F]); (183 K): δ = –162.5 (br s [F]), –177.3 (s, [2F]). ^{27}Al NMR (298 K) δ = 8.8 (br s, $W_{1/2}$ = 450 Hz).

[GaF_3(phen)(OH_2)]

Method as for [AlF_3(terpy)]·3H_2O, using GaF_3·3H_2O (0.200 g, 1.11 mmol) and phen (0.200 g, 1.11 mmol). Pale red solid. Yield 0.315 g, 79%. Required for $C_{12}H_{10}F_3GaN_2O$: C, 44.4; H, 3.1; N, 8.6. Found: C, 44.4; H, 3.1; N, 8.5%. IR (Nujol, ν/cm^{-1}): 3200 br (ν O–H), 1680 (δ H–O–H), 560, 543, 511 (Ga–F). ^{1}H NMR (CD_3OD, 298 K) δ = 9.34 (d, J_{HH} 4 Hz, [2H], ArH), 8.89 (d, J_{HH} 12.2 Hz, [2H], ArH), 8.26 (s, [2H], ArH), 8.15 (br, [2H], ArH) 4.87 (s, H_2O); (183 K): 9.34 (s), 9.02 (d), 8.94 (d), 8.33–8.21 (m). ^{19}F{^{1}H} NMR (CD_3OD, 298 K) δ = –152 (br s [F]), –176 (br,

[2F]); (183K): δ = −151.0 (br s, [F]), −184.0 (s, [2F]). Slow evaporation of the reaction solvent gave crystals suitable for X-ray diffraction.

[InF_3(phen)(OH_2)]

Method as for [AlF_3(terpy)]·3H_2O, but using InF_3·3H_2O (0.200 g, 0.89 mmol) and phen (0.161 g, 0.89 mmol). Pale orange solid. Yield: 0.16 g, 49%. Required for $C_{12}H_{10}F_3InN_2O$: C, 39.0; H, 2.7; N, 7.6. Found: C, 39.2; H, 2.8; N, 7.7%. IR (Nujol, ν/cm^{-1}): 3360 br, 3177 (ν O–H), 1660 w (δ H–O–H), 446, 422 (br), 405 (sh) (In–F). ^{1}H NMR (CD_3OD, 298 K) δ = 9.30 (br s, [1H], ArH), 9.02–8.96 (br [3H], ArH), 8.29–8.07 (br, m, [4H], ArH), 4.87 (s, H_2O); (183 K): 9.28 (s), 8.98 (s), 8.76 (s), 8.33–8.22 (m), 7.95 (m). ^{19}F{^{1}H} NMR (298 K) not observed; (183 K) δ = −157 (br, [F]), −199 (br, [2F]).

[$GaCl_3$(terpy)]

A solution of terpy (0.258 g, 1.11 mmol) in 5 mL anhydrous CH_2Cl_2 was added drop wise to a solution of $GaCl_3$ (0.195 g, 1.11 mmol) in 5 mL anhydrous CH_2Cl_2. A white precipitate formed upon addition of the ligand. The mixture was stirred at room temperature for 1 h. The product was isolated by filtration, washed with hexane and dried *in vacuo*. White solid. Yield: 0.402 g, 88%. Required for $C_{15}H_{11}Cl_3GaN_3$: C, 44.0; H, 2.7; N, 10.3. Found: C, 43.5; H, 2.6; N, 10.1%. IR (Nujol, ν/cm^{-1}): 267 (s), 254 (br), (Ga–Cl). ^{1}H NMR (CD_3CN, 298 K) δ = 9.06–9.04 (m, [2H], ArH), 8.75–8.73 (m, [3H], ArH), 8.67–8.65 (m, [2H], ArH), 8.53–8.49 (m, [2H], ArH), 8.08–8.05 (m, [2H], ArH).

[$GaCl_3$(^{t}Bu_3-terpy)]

A solution of ^{t}Bu_3-terpy (0.111 g, 0.278 mmol) in 5 mL anhydrous CH_2Cl_2 was added drop wise to a solution of $GaCl_3$ (0.025 g, 0.139 mmol) in 5 mL anhydrous CH_2Cl_2. Addition of the ligand resulted in the formation of a white precipitate. The mixture was stirred at room temperature for 1 h. The solid was isolated by filtration, washed with a further 10 mL CH_2Cl_2 and dried *in vacuo*. White solid. Yield 0.062 g, 77%. Required for $C_{27}H_{35}Cl_3GaN_3$·CH_2Cl_2: C, 50.7; H, 5.6; N, 6.3. Found: C, 50.4; H, 5.6; N, 6.5%. IR (Nujol, ν/cm^{-1}): 257 (s), 227 (s) (Ga–Cl). ^{1}H NMR (CD_3CN, 298 K) δ = 1.42 (s, [18H], ^{t}Bu), 1.44 (s, [9H], ^{t}Bu), 7.47–7.46 (br m, [2H], ArH), 8.50 (br s, [2H], ArH), 8.61–8.60 (br m, [2H], ArH), 8.77 (br s, [2H], ArH).

The same reaction was performed in a 1:1 stoichiometric ratio to give a spectroscopically identical product. However, crystals formed from the filtrate gave the ionic by-product [$GaCl_2$(^{t}Bu_3-terpy)][$GaCl_4$]·CH_2Cl_2.

$[TMP]_2[Al_2F_8(OH_2)_2]\cdot 2H_2O$

Method as for $[AlF_3(bipy)(OH_2)]\cdot 2H_2O$, but using $AlF_3\cdot 3H_2O$ (0.200 g, 1.45 mmol) and pmdta (0.3 mL, 1.45 mmol). A brown gum was obtained after removing the solvent. This was washed with MeCN, producing a white powder. Yield: 0.092 g, 12% . Required for $C_{14}H_{42}Al_2F_8N_4O_4$: C, 31.4; H, 7.8; N, 10.4. Found: C, 31.3; H, 7.8; N, 10.4%. IR (Nujol, ν/cm^{-1}): 3370 (br) (ν O–H), 1673 (δ H–O–H), 616 (br), 569 (br) (Al–F). ^{1}H NMR (CD_3CN, 298 K) δ = 4.87 (s, H_2O), 3.35 (t, J_{HH} 6.0 Hz, [4H], CH_2), 3.07 (s, [6H], Me), 2.67 (br s, [4H], CH_2CH_2), 2.32 (s, [3H], Me). $^{19}F\{^1H\}$ NMR (CD_3CN, 298 K) δ = –194.6 (6 lines $^1J_{AlF}$ = 38.0 Hz). ^{27}Al NMR (CH_3CN, 298 K) δ = 48.7 (s). Slow evaporation of the reaction solvent gave crystals suitable for X-ray diffraction.

Crystals suitable for single crystal X-ray analysis were obtained as described above. Data collections used a Rigaku AFC12 goniometer equipped with an enhanced sensitivity (HG) Saturn724+ detector mounted at the window of an FR-E+ SuperBright molybdenum (λ = 0.71073 Å) rotating anode generator with VHF Varimax optics (70 µm focus) with the crystal held at 100 K (N_2 cryostream). Structure solution and refinements were performed with either SHELX(S/L)97 or SHELX(S/L)2013[18] and were straightforward, except where detailed below. H atoms bonded to C were placed in calculated positions using the default C–H distance and refined using a riding model. In the case of $[AlF_3(bipy)(OH_2)]\cdot 2H_2O$ structure, the H-atoms on the co-crystallised water molecules were not located in the difference map. While not included in the refinement, the H-atoms are inferred from the H-bonding distances of F····O and O····O and are thus included in the formulae. The H-atoms on both the coordinated and co-crystallised water molecules could not be located in the structure of $[TMP]_2[Al_2F_8(OH_2)_2]\cdot 2H_2O$. While not included in the refinement, the H-atoms are similarly inferred and included in the formulae.

Table 6.2: Table of crystallographic data for the complexes discussed in this chapter.[a]

Compound	**$[AlF_3(terpy)]\cdot 3H_2O$**	**$[GaF_3(terpy)]\cdot 3H_2O$**	**$[AlF_3(bipy)(OH_2)]\cdot 2H_2O$**
Formula	$C_{15}H_{17}AlF_3N_3O_3$	$C_{15}H_{17}F_3GaN_3O_3$	$C_{10}H_{14}AlF_3N_2O_3$
M	371.30	414.04	294.20
Crystal system	Monoclinic	Monoclinic	Monoclinic
Space group (no.)	$P2_1/c$ (14)	$P2_1/c$ (14)	$P2_1/n$ (14)
a /Å	9.4806(9)	10.323(5)	8.976(5)
b /Å	25.104(2)	9.708(5)	7.300(5)
c /Å	7.0846(6)	16.131(5)	19.062(5)
α /°	90	90	90
β /°	104.425(7)	100.484(5)	93.331(5)
γ /°	90	90	90
U /Å^3	1633.0(3)	1589.6(12)	1246.9(11)
Z	4	4	4
μ(Mo-K$_\alpha$) /mm^{-1}	0.177	1.785	0.207
F(000)	768	840	608
Total number reflections	6803	9623	8257
Unique reflections	2163	3646	2848
R_{int}	0.0622	0.0481	0.0778
R_1 [$I > 2\sigma(I)$][b]	0.713	0.037	0.060
R_1 (all data)	0.146	0.056	0.104
wR_2 [$I > 2\sigma(I)$] [b]	0.133	0.084	0.144
wR_2 (all data)	0.172	0.089	0.168

[a] Common items: T = 100 K; wavelength (Mo-Kα) = 0.71073 Å; θ(max) = 27.5°;

[b] $R_1 = \Sigma \big| |F_o| - |F_c| \big| / \Sigma |F_o|$; $wR_2 = [\Sigma w(F_o^2 - F_c^2)^2 / \Sigma wF_o^4]^{1/2}$

Table 6.3: Table of crystallographic data for the complexes discussed in this chapter.[a]

Compound	**$[GaF_3(bipy)(OH_2)]\cdot 2H_2O$**	**$[GaF_3(phen)(OH_2)]$**	**$[GaCl_2(^tBu_3\text{-terpy})][GaCl_4]\cdot CH_2Cl_2$**
Formula	$C_{10}H_{14}F_3GaN_2O_3$	$C_{12}H_{10}F_3GaN_2O$	$C_{14}H_{18.5}Cl_4GaN_{1.5}$
M	336.95	324.94	419.32
Crystal system	Monoclinic	Monoclinic	Triclinic
Space group (no.)	$P2_1/n$ (14)	$P2_1/n$ (14)	P–1(2)
a /Å	9.056(3)	8.3906(5)	11.674(3)
b /Å	7.371(2)	7.1940(5)	12.642(4)
c /Å	18.904(6)	19.0124(13)	13.756(5)
α /°	90	90	89.137(17)
β /°	93.462(6)	100.631(3)	78.682(16)
γ /°	90	90	65.276(15)
U /Å^3	1259.6(7)	1127.93(13)	1803.1(11)
Z	4	4	4
μ(Mo-K$_\alpha$) /mm^{-1}	2.228	2.472	2.111
F(000)	680	648	848
Total number reflections	11425	12632	16476
Unique reflections	2883	2581	7870
R_{int}	0.1541	0.051	0.141
R_1 [$I > 2\sigma(I)$][b]	0.048	0.025	0.086
R_1 (all data)	0.051	0.028	0.125
wR_2 [$I > 2\sigma(I)$] [b]	0.130	0.064	0.192
wR_2 (all data)	0.132	0.066	0.211

[a] Common items: T = 100 K; wavelength (Mo-Kα) = 0.71073 Å; θ(max) = 27.5°;

[b] $R_1 = \Sigma \big| \, |F_o| - |F_c| \, \big| / \Sigma |F_o|$; $wR_2 = [\Sigma w(F_o^2 - F_c^2)^2 / \Sigma w F_o^4]^{1/2}$

Table 6.4: Table of crystallographic data for the complexes discussed in this chapter.[a]

Compound	**$[TMP]_2\,[Al_2F_8(OH_2)_2]\cdot 2H_2O$**	**$[NMe_4]_3[Al_2F_9]$**
Formula	$C_{14}H_{42}Al_2F_8N_4O_4$	$C_{12}H_{36}Al_2F_9N_3$
M	538.4	447.40
Crystal system	Monoclinic	Hexagonal
Space group (no.)	C2/c (15)	$P6_3/m$ (176)
a /Å	24.054(10)	7.997(5)
b /Å	7.558(3)	7.997(5)
c /Å	16.389(7)	18.178(7)
α /°	90	90
β /°	123.374(4)	90
γ /°	90	120
U /Å^3	2488.3(17)	1006.8(10)
Z	6	2
μ(Mo-K$_\alpha$) /mm^{-1}	0.214	0.227
F(000)	1200	472
Total number reflections	5785	4622
Unique reflections	2822	799
R_{int}	0.035	0.064
R_1 [$I > 2\sigma(I)$] [b]	0.078	0.043
R_1 (all data)	0.098	0.063
wR_2 [$I > 2\sigma(I)$] [b]	0.212	0.098
wR_2 (all data)	0.231	0.107

[a] Common items: T = 100 K; wavelength (Mo-Kα) = 0.71073 Å; θ(max) = 27.5°;

[b] $R_1 = \Sigma\,||F_o| - |F_c||\,/\,\Sigma\,|F_o|$; $wR_2 = [\Sigma w(F_o^2 - F_c^2)^2/\Sigma\, wF_o^4]^{1/2}$

6.5 References

1. Benjamin, S. L.; Levason, W.; Reid, G., *Chem. Soc. Rev.* **2013,** *42*, 1460-1499.
2. Kemnitz, E.; Gross, U.; Ruediger, S.; Scholz, G.; Heidemann, D.; Troyanov, S. I.; Morosov, I. V.; Lemee-Cailleau, M. H., *Solid State Sci.* **2006,** *8*, 1443-1452.
3. Bukovec, P.; Kaucic, V., *Inorg. Nucl. Chem. Lett.* **1978,** *14*, 79-81.
4. Aldridge, S.; Downs, A., *The Group 13 Metals, Aluminium, Gallium, Indium and Thallium: Chemical Patterns and Paculiarities*. Wiley: Chichester, 2011.
5. Bandoli, G.; Dolmella, A.; Tisato, F.; Porchia, M.; Refosco, F., *Coord. Chem. Rev.* **2009,** *253*, 56-77.
6. Petricek, S.; Demsar, A.; Bukovec, P.; Golic, L.; Brencic, J. V., *Acta Chim. Slov.* **1997,** *44*, 317-325.
7. Penkert, F. N.; Weyhermüller, T.; Wieghardt, K., *Chem. Commun.* **1998**, 557-558.
8. Ilyukhin, A. B.; Malyanik, M. A., *Zh. Neorg. Khim.,* **1999,** *44*, 1511.
9. Ilyukhin, A. B.; Malyarik, M. A., *Kristallografiia.,* **1994,** *39*, 439-445.
10. Ketchum, D. R.; Schimek, G. L.; Pennington, W. T.; Kolis, J. W., *Inorg. Chim. Acta.* **1999,** *294*, 200-206.
11. Davis, M. F.; Levason, W.; Paterson, J.; Reid, G.; Webster, M., *Eur. J. Inorg. Chem.* **2008**, 802-811.
12. George, J., *An Introduction to Hydrogen Bonding*. OUP: 1997; Vol. 1.
13. Bhalla, R.; Darby, C.; Levason, W.; Luthra, S. K.; McRobbie, G.; Reid, G.; Sanderson, G.; Zhang, W., *Chem. Sci.* **2014,** *5*, 381-391.
14. Kazakov, I. V.; Bodensteiner, M.; Timoshkin, A. Y., *Acta Crystallogr., Sect. C.* **2014,** *70*, 312-314.
15. Cordero, B.; Gomez, V.; Platero-Prats, A. E.; Reves, M.; Echeverria, J.; Cremades, E.; Barragan, F.; Alvarez, S., *Dalton Trans.* **2008**, 2832-2838.
16. Burt, J.; Levason, W.; Light, M. E.; Reid, G., *Dalton Trans.* **2014,** *43*, 14600-14611.
17. George, K.; Jura, M.; Levason, W.; Light, M. E.; Reid, G., *Dalton Trans.* **2014,** *43*, 3637-3648.
18. Martinez, C. R.; Iverson, B. L., *Chem. Sci.* **2012,** *3*, 2191-2201.
19. Karimi, F.; Laangstrom, B. In *The role of recent development of ^{18}F radiochemistry in drug development*, World Scientific Publishing Co. Pte. Ltd.: 2012; pp 111-180.
20. Timoshkin, A. Y.; Bodensteiner, M.; Sevastianova, T. N.; Lisovenko, A. S.; Davydova, E. I.; Scheer, M.; Grassl, C.; Butlak, A. V., *Inorg. Chem.* **2012,** *51*, 11602-11611.
21. Bessac, F.; Frenking, G., *Inorg. Chem.* **2006,** *45*, 6956-6964.
22. Timoshkin, A. Y.; Suvorov, A. V.; Bettinger, H. F.; Schaefer, H. F., III, *J. Am. Chem. Soc.* **1999,** *121*, 5687-5699.

23. Konarev, D. V.; Kuzmin, A. V.; Khasanov, S. S.; Lyubovskaya, R. N., *Dalton Trans.* **2013,** *42*, 9870-9876.
24. Adil, K.; Leblanc, M.; Maisonneuve, V., *Acta Crystallogr., Sect. E.* **2004,** *60*, m1379-m1381.
25. Adamczyk, B.; Troyanov, S. I.; Schneider, M.; Kemnitz, E., *Z. Anorg. Allg. Chem.* **2000,** *626*, 2543-2548.
26. Herron, N.; Harlow, R. L.; Thorn, D. L., *Inorg. Chem.* **1993,** *32*, 2985-6.
27. Herron, N.; Thorn, D. L.; Harlow, R. L.; Davidson, F., *J. Am. Chem. Soc.* **1993,** *115*, 3028-3029.
28. Xu, F.; Matsumoto, K.; Hagiwara, R., *Dalton Trans.* **2013,** *42*, 1965-1968.
29. Producing the salt, 4AlF3.6NaF, and an alloy of aluminium and silicon. GB760136, 1956.
30. Synthetic cryolite. CH520622A, 1972.
31. Abramov, G. A.; Kostyukov, A. A.; Kulakov, L. B., *Trudy Leningrad. Politekh. Inst. im. M. I. Kalinina, Elektromet. Tsvetnykh Metal.* **1957**, 45-57.
32. Craig, D. F.; Brown, J. J., Jr., *J. Am. Ceram. Soc.* **1980,** *63*, 254-61.

Chapter 7

Amide Functionalised Tacn Frameworks as Future Ligand Architectures

7.1 Introduction

The work discussed in Chapters 2.3, 3.2.3, and 4.2.3 demonstrated that the Group 13 metal fluoride complexes formed with functionalised tacn ligands showed a strong affinity to hydrogen bond to lattice water molecules in the solid state. It was postulated that these interactions, particularly in the case of the neutral R_3-tacn complexes $[MF_3(R_3\text{-tacn})]\cdot xH_2O$ (M = Al, Ga, In) helped to stabilise the M-F interaction and aid in directing the fluoride to the metal centre.[1]

Consequently, a series of functionalised tacn ligands with amide pendant arm groups were designed and synthesised. The amide pendant arms have the potential to form intramolecular H-bonded interactions with a metal fluoride fragment, if coordination of the amide to the metal centre can be avoided (Figure 7.1).

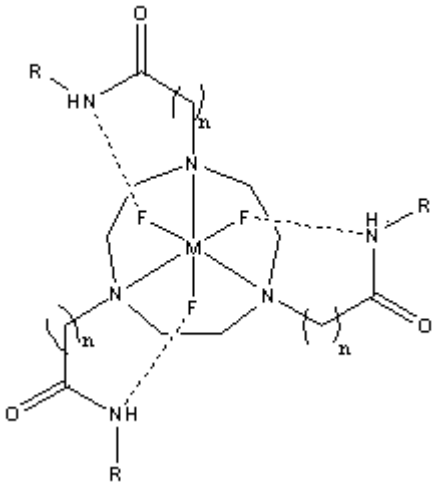

Figure 7.1: Diagram showing proposed intramolecular H-bonding interactions with amide pendant arm functionality. M = Al, Ga, In, R = alkyl, n = 1, 2.

While a wide range of N-functionalised derivatives of tacn have been synthesised including among others, carboxylates ($-CH_2CO_2H$),[2, 3] alcohols (-ROH)[4, 5] and amines ($-CH_2NR_2$)[6, 7], there is surprisingly little literature precedent for the use of amide functionalised tacn ligands. Wieghardt *et al.* have reported the synthesis of the ligands 1,4,7-tris(carbamoylmethyl)-1,4,7-triazacyclononane (TCMT) (Figure 7.2) and the N-methyl equivalent, and investigated their coordination chemistry with a number of transition metals (e.g. Ni(II), Cr(II), Cr(III)).[8]

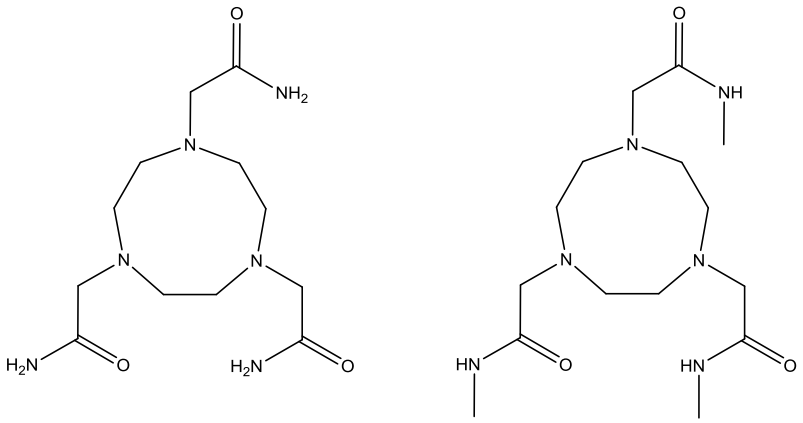

Figure 7.2: 1,4,7-tris(carbamoylmethyl)-1,4,7-triazacyclononane (left) and the methyl equivalent synthesised by Wieghardt, Amin and others.[8, 9]

It was found that overwhelmingly hexadentate coordination was observed, giving an N_3O_3 donor set, with the oxygen from the ligand amide groups coordinating to form stable 5-membered chelate rings (Figure 7.3 and 7.4).[8]

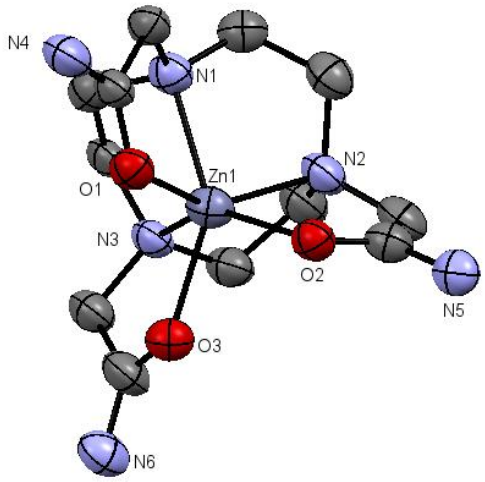

Figure 7.3: Crystal structure of the Zn(II) containing cation in the complex $[Zn((CH_2CONH_2)_3$-tacn)$][ClO_4]_2$ showing octahedral coordination around the metal centre *via* the hexadentate ligand. H-atoms and $[ClO_4]^-$ anions are omitted for clarity.[8] Image redrawn from CCDC 114020.

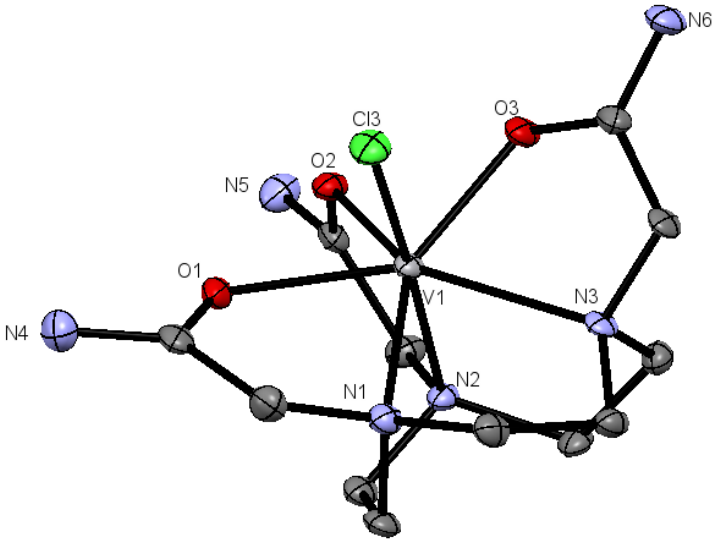

Figure 7.4: Crystal structure of the V(II) containing cation in the complex $[VCl((CH_2CONH_2)_3\text{-}tacn)][ClO_4]_2$. H-atoms and $[ClO_4]^-$ anions are omitted for clarity.[8] Image redrawn from CCDC 114019.

Interestingly, reaction of $CrCl_2$ with 1,4,7-tris(carbamoylmethyl)-1,4,7-triazacyclononane in MeOH followed by salt metathesis with $NaPF_6$ results in the deprotonation of one of the amide pendant arms, and thus coordination of one of the terminal amido groups to the metal centre to provide an N_4O_2 donor set (Figure 7.5).

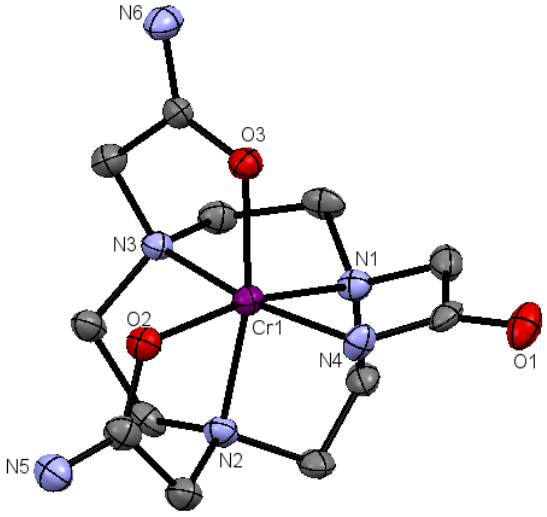

Figure 7.5: Crystal structure of the cation in $[Cr((CH_2CONH_2)_3\text{-}tacn)][PF_6][Cl]$ showing four coordinated N-donor atoms. The fourth N-donor arises through deprotonation of the amide pendant arm functionality.[8] Image redrawn from CCDC 114021.

This work indicates that control of the reaction conditions may result in differing coordination modes. Amide functionalised tacn complexes have also been prepared with Cu(II) and Zn(II) through hydrolyis of nitrile functionalised pendant arm tacn ligands.[10, 11]

Amin *et al.* demonstrated the ability to form complexes of TCMT with yttrium(III) and lutetium(III) salts as part of their interest in preparing new complexes for the hydrolytic cleavage of RNA.[9]

Potentially of more interest with regards to potential applications as ligands for ^{18}F incorporated imaging agents are the examples of tacn based frameworks in which only one or two amide pendant arms are placed onto the macrocycle (Figure 7.6).[12, 13]

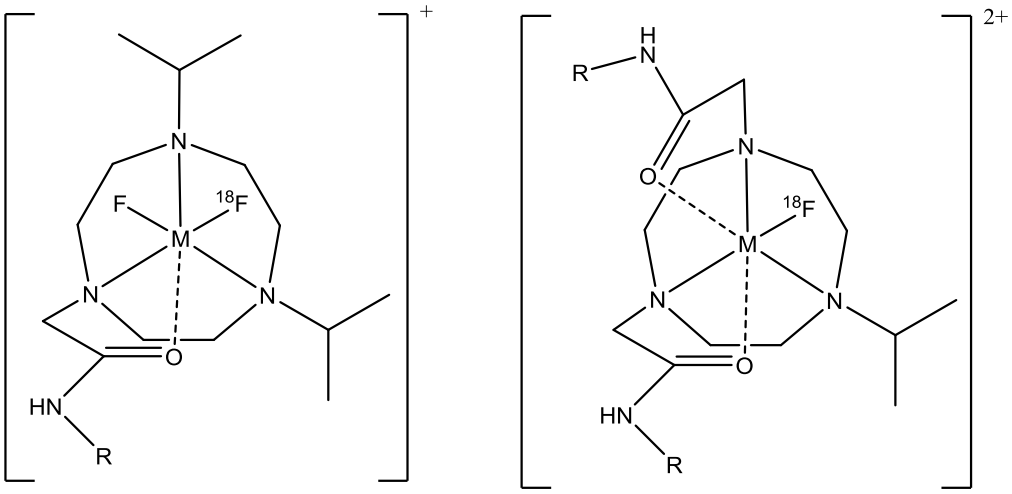

Figure 7.6: Schematic showing proposed ^{18}F labelled metal complexes with monoamide (left) and diamide (right) functionality to a trivalent metal centre (M = Al, Ga, In).

The use of mono- or di-amide pendant arms will guarantee a vacant site in which the $^{18}F^-$ may be introduced in labelling reactions, but also allows the potential H-bonded interactions to occur between the amido N-H's and the coordinated fluoride ligand.

As part of the ongoing investigation to identify suitable ligand frameworks in which $^{18}F^-$ may be incorporated into a preformed metal macrocyclic complex rapidly, at a late stage and under mild conditions, a series of aza-macrocylic ligands with varying amide pendant arm functionality were synthesised and characterised using ^1H and $^{13}C\{^1H\}$ NMR spectroscopy and ESI^+ MS. The coordination chemistry was investigated with both Group 13 ions and selected transition metal salts to establish the preferred coordination modes. Potential uses of these ligand frameworks are also discussed in the context of PET imaging applications.

7.2. Results and Discussion

7.2.1 Rationale for Ligand Design

A number of parameters needed to be considered in the design and synthesis of amide functionalised tacn based ligands for potential radiolabelling applications. These include:

i) To conveniently synthesise the ligands in high yield.

ii) The amide functionality must not be too challenging to synthesise and where possible should incorporate alkyl groups to aid solubility.

iii) Ideally, the amide carbonyl groups should not coordinate to the metal centre, thus leaving vacant coordination sites in which the $^{18}F^-$ may bind to the metal centre.

Based upon these considerations, two general ligand types were identified; one in which all three tacn N-atoms were functionalised with amide pendant arms, and one in which only a single tacn N-atom was functionalised and the other nitrogen atoms were functionalised with alkyl groups, specifically in this work the isopropyl group was selected (Figure 7.7).

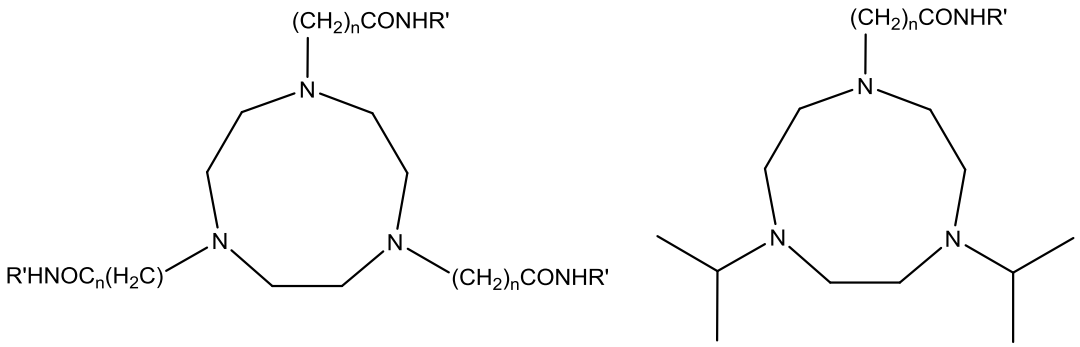

Figure 7.7: Diagram showing the two general classes of ligand discussed in this chapter. n = 1, 2, R' = ^{i}Pr, phenyl.

The ligand 1,4-isopropyl-1,4,7-triazacyclononane (^{i}Pr$_2$-tacn) was synthesised as described by Martin *et al.* in which Ts$_3$-tacn is selectively deprotected in two positions to give Ts-tacn. Alkylation using 1-bromo-2-methyl-propane introduces the ^{i}Pr functionality. Further deprotection of the remaining tosyl group gives ^{i}Pr$_2$-tacn as a brown oil in good yield (70%) (Figure 7.8).[14] This therefore leaves a single secondary amine which is available to be functionalised with a pendant arm group.

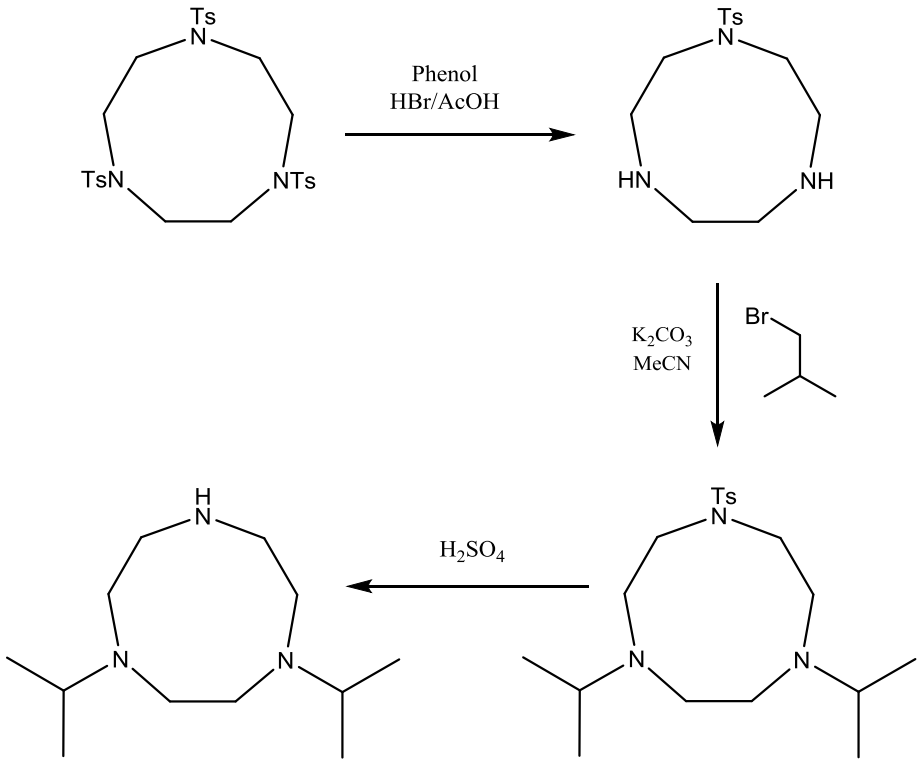

Figure 7.8: Synthesis of $^{i}Pr_2$-tacn.[14]

The amide functionalised pendant arms were further subdivided based upon the length of the pendant arm, and the group attached to the terminal N-atom of the amide (Figure 7.9).

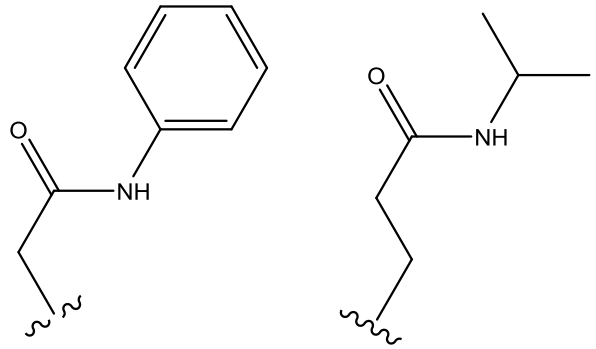

Figure 7.9: Amide pendant arms utilised in this chapter.

Of potential interest for PET imaging applications is the phenyl substituent, which, as discussed in Chapter 3.2.6, can act as a tether in which a peptide or bioactive molecule may be conjugated. The ^{i}Pr-amide substituents were selected in an effort to aid in the solubility of the resulting complexes in organic media.

Based upon these requirements a series of ligands were prepared and characterised (Figure 7.10).[15]

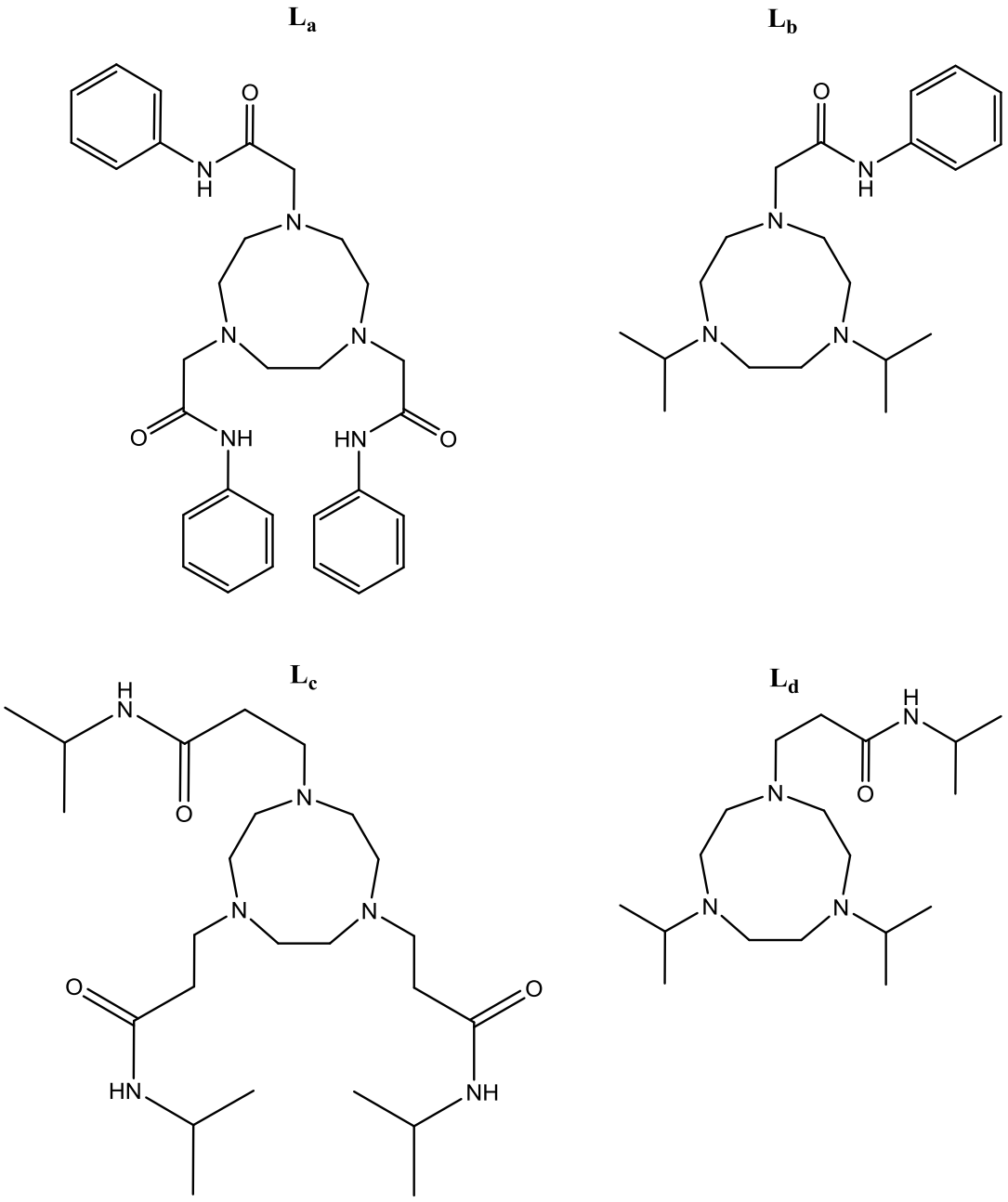

Figure 7.10: The ligands synthesised and used in this chapter.

7.2.2 Ligand synthesis and characterisation

The acidity of amine protons on the tacn ring (pKa = 10.60)[16] means that they are readily deprotonated using mild bases such as Na_2CO_3 or K_2CO_3. This allows for post synthetic modification to be performed under mild conditions, in high yield and with minimal purification.

The methylene bridged amide ligands $\mathbf{L_a}$ and $\mathbf{L_b}$ were readily accessed through reaction of the parent tacn and $^{i}Pr_2$-tacn with 2-chloro-N-phenylacetamide in the presence of an excess of K_2CO_3 (Figures 7.11 and 7.12).[8] Removal of the salts by filtration and subsequent pH

adjustment to pH 12 gave the desired compounds as a yellow solid ($\mathbf{L_a}$) or a highly viscous tan oil ($\mathbf{L_b}$).

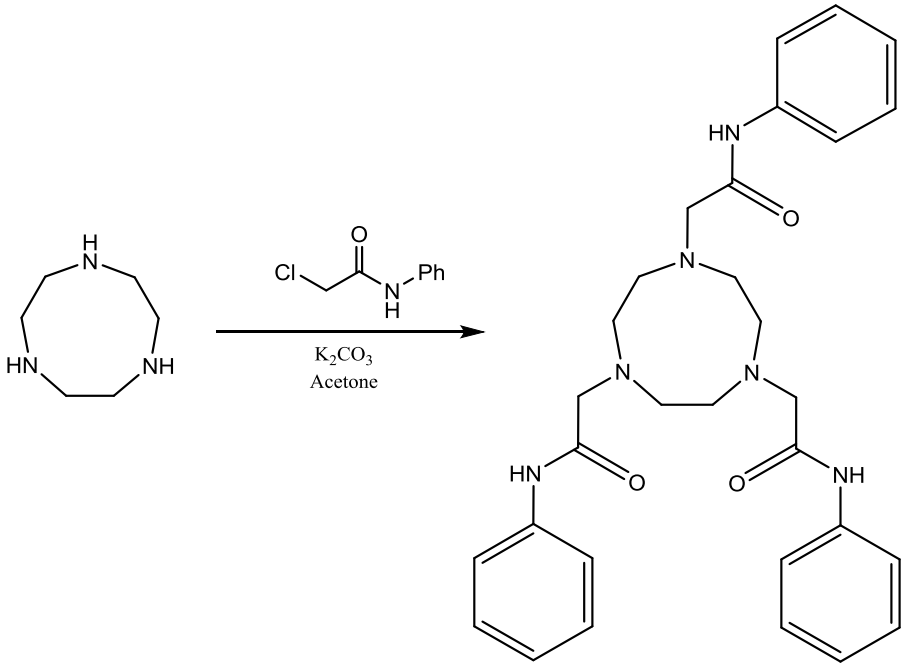

Figure 7.11: Synthesis of $(CH_2CONHPh)_3$-tacn, $\mathbf{L_a}$.

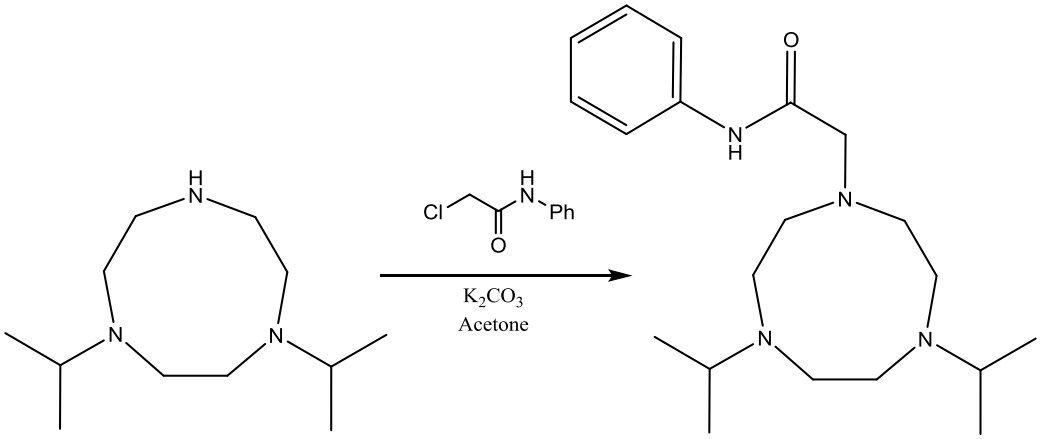

Figure 7.12: Synthesis of $^{i}Pr_2(CH_2CONHPh)$-tacn, $\mathbf{L_b}$.

The ^{1}H NMR spectrum of $\mathbf{L_a}$ showed a singlet [12H] at 2.91 ppm corresponding to the tacn CH_2 protons. This shows a 0.12 ppm shift from the parent triamine, a reflection on the effect of the pendant arm substituents. In addition, a singlet at δ = 3.66 ppm [6H] corresponding to the methylene groups in the amide pendant arm, and three resonances in the aromatic region corresponding to the phenyl group, confirm that the desired ligand had been synthesised. The ^{1}H

NMR spectrum showed no evidence for any unreacted 2-chloro-N-phenylacetamide. Further evidence of successful ligand formation was shown in the ESI^+ mass spectrum, which showed a single peak at *m/z* 529, corresponding to the monocation $[M + H]^+$. Repeated recrystallisation of $\mathbf{L_a}$ from MeCN/Et_2O gave crystals suitable for single crystal X-ray diffraction (Figure 7.13).

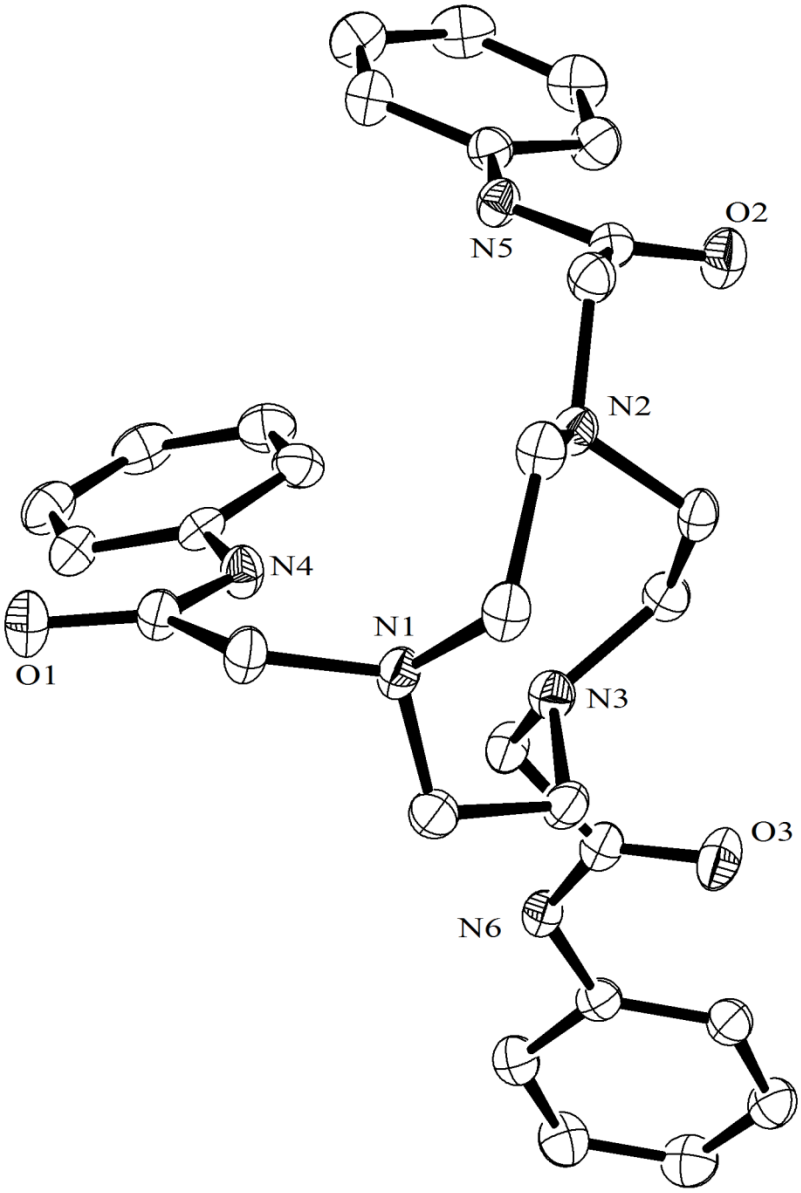

Figure 7.13: Crystal structure of $\mathbf{L_a}$·Et_2O. H-atoms and solvated Et_2O molecule are omitted for clarity. Ellipsoids are drawn at 50% probability level.

As might be expected, the pendant arms lie as far away from one another to minimise steric repulsion on the aromatic groups. The molecules are closely associated in the solid state by H-bonding interactions between the amide N-H of one ligand to the amide carbonyl in an adjacent molecule (N-H···O = 2.051(3) Å), which gives rise to an extended 3D structure.

The spectroscopic data acquired for $\mathbf{L_b}$ also supports the proposed ligand formation. The ^{1}H NMR spectrum showed a very broad singlet at δ = 2.98 ppm [12H] indicative of the tacn CH_2 groups. The broadness is presumed to arise from overlapping of the inequivalent tacn CH_2 environments. The ESI^+ mass spectrum recorded in MeCN showed two peaks, one corresponding to the doubly protonated dication $[M + 2H]^{2+}$ (*m/z*; 174.3 (100%)) and one arising from the molecular ion $[M + H]^+$ (*m/z* 347.2 (45%)). This confirmed that the ligand had been successfully prepared.

Treatment of a portion of the ligand in MeCN with 1.0 M HCl followed by evaporation of the solvent at ambient temperature gave crystals suitable for single crystal X-ray diffraction (Figure 7.14).

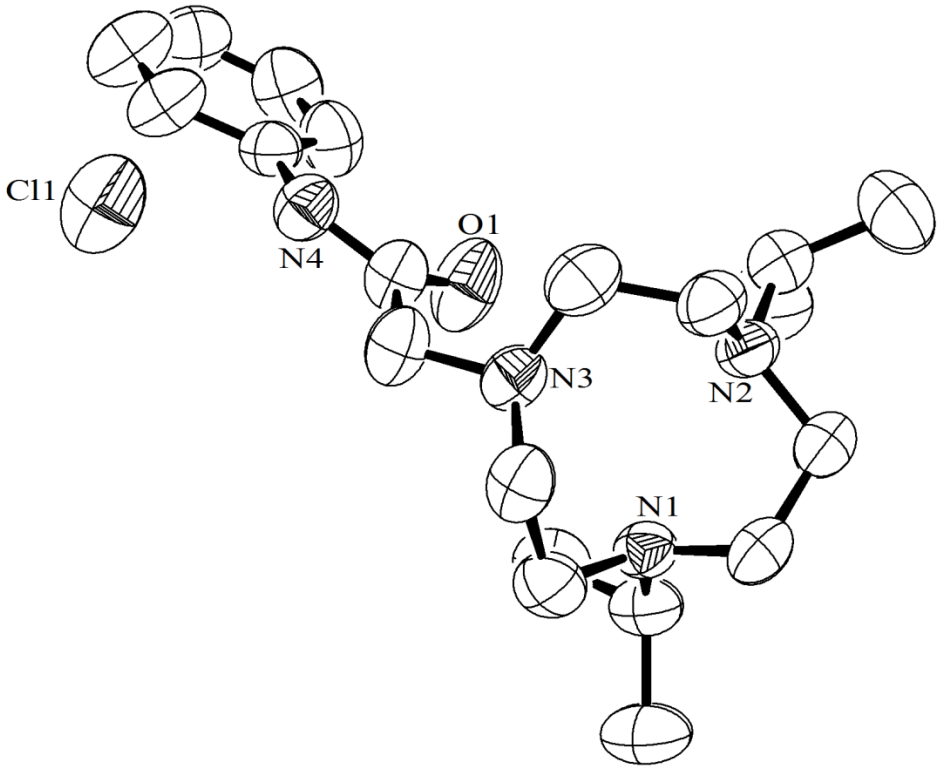

Figure 7.14: Crystal structure of $\mathbf{L_b}$·HCl·H_2O with atom numbering scheme. H-atoms and solvent water molecule are omitted for clarity. Ellipsoids are drawn at 50% probability level.

Despite the lower crystal quality and the data being collected at room temperature, the data confirms that the expected ligand had been formed. As might be expected the chloride ion is engaged in a weak H-bonding interaction with the amide N-H (N-H···Cl = 3.260 Å), as well as the lattice water molecule (O-H···Cl = 3.225 Å). This is significant in that is shows that there is potential for the amide N-H to H-bond to a coordinated fluoride ligand in a metal complex.

Initially, attempts to synthesise the dimethylene bridged amide pendant arm azamacrocycles $\mathbf{L_c}$ and $\mathbf{L_d}$ were made using 3-chloro-N-isopropylpropanamide.[17] However it was found that under the basic conditions used in the synthesis, the 3-chloro-N-isopropylpropanamide underwent an elimination reaction to form N-isopropylacrylamide (Figure 7.15).

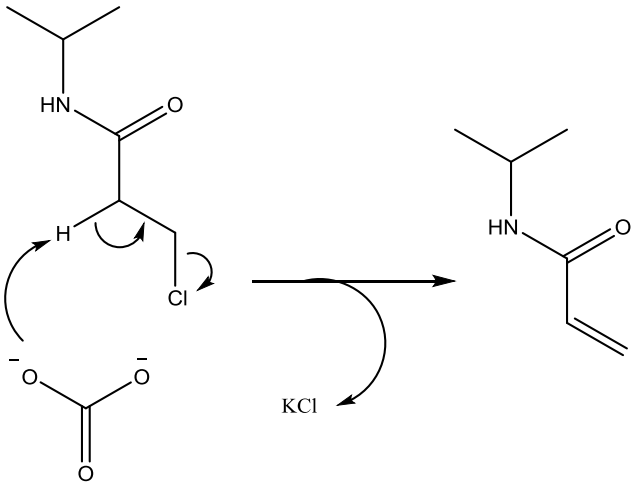

Figure 7.15: Proposed elimination pathway of 3-chloro-N-isoproylpropanamide to form N-isoproylacrylamide.[18]

This was shown in the ^{1}H NMR spectrum of the crude reaction mixture which revealed that the parent tacn resonances were unchanged after reaction. Further, three multiplets corresponding to a vinyl alkene were observed between δ = 5.5 and 6.5 ppm. Consequently, ligands $\mathbf{L_c}$ and $\mathbf{L_d}$ were accessed *via* a Mannich reaction using N-isopropylacrylamide in refluxing MeOH (Figures 7.16 and 7.17).[19]

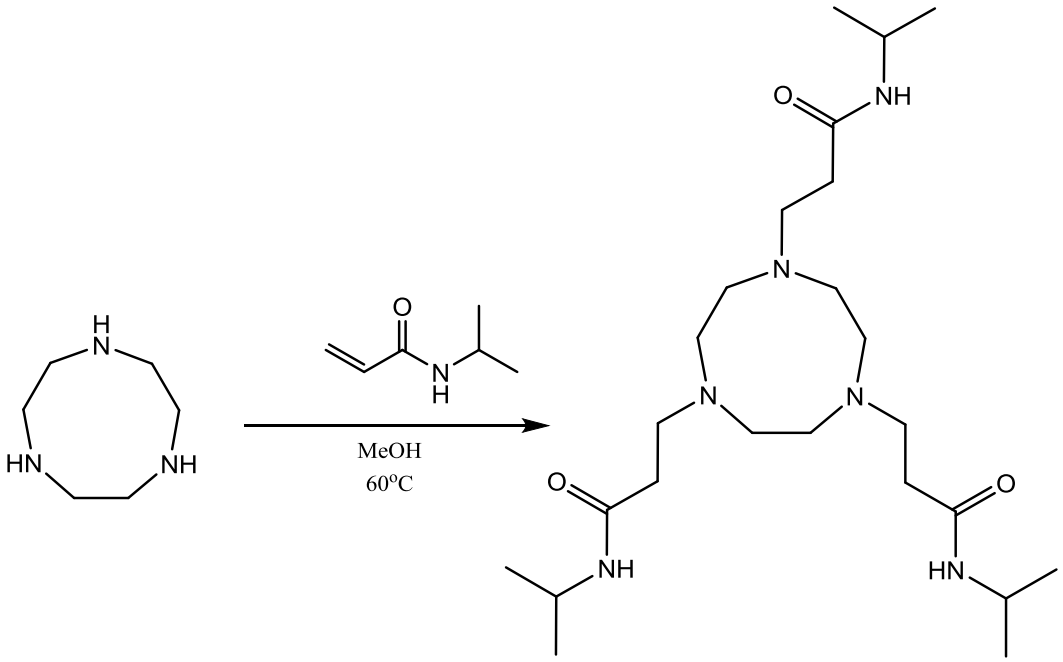

Figure 7.16: Synthesis of $((CH_2)_2CONH^iPr)_3$-tacn, $\mathbf{L_c}$.

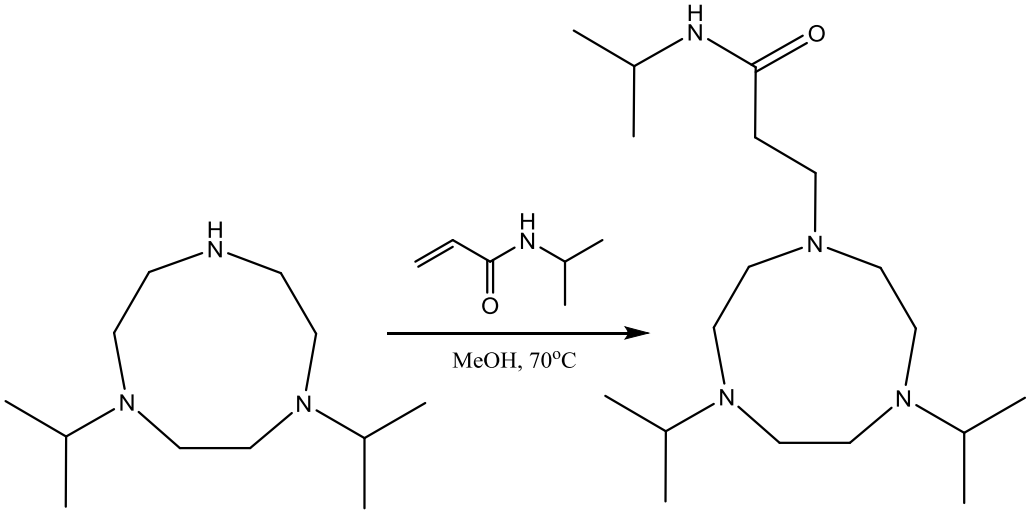

Figure 7.17: Synthesis of $^iPr_2((CH_2)_2CONH^iPr)$-tacn, $\mathbf{L_d}$.

The reactions were performed with an excess of N-isopropylacrylamide, which was removed from the crude reaction mixture using a pH adjusted work up. Treatment of the crude reaction mixture with 1.0 M HCl to pH 1 places the desired ligand in the aqueous phase. Repeated washings with $CHCl_3$ remove the unreacted N-isopropylacrylamide. Adjustment of the aqueous phase to pH 12 with 2.0 M KOH followed by extraction with $CHCl_3$ and drying gives the ligands $\mathbf{L_c}$ and $\mathbf{L_d}$ as very viscous yellow oils in high yield.[19]

The ^{1}H NMR spectrum of $\mathbf{L_c}$ showed a doublet at 1.16-1.14 ppm ($^{2}J_{HH}$ = 6.6 Hz) corresponding to the methyl CHs of the isopropyl groups on the amide pendant arms. A triplet at 2.30-2.27 ppm ($^{2}J_{HH}$ = 6.3 Hz) corresponds to the CH_2s on the dimethylene linker. The resonance corresponding to the tacn CH_2s and the other dimethylene linker CH_2s overlap one another, giving rise to a broad resonance at 2.78 ppm [18H]. A multiplet corresponding to the iso-propyl CH atoms is present at 4.12-4.02 ppm. The ^{1}H NMR spectrum also gave evidence of H-bonded water, shown by a broad resonance at 1.75 ppm. ESI MS of a sample of the ligand showed three peaks at *m/z*; 235.3 (100%) $[M + 2H]^{2+}$, 469.4 (40%) $[M + H]^{+}$ and 491.4 (35%) $[M + Na]^{+}$.

$\mathbf{L_d}$ gives a more complex pattern in the ^{1}H NMR spectrum, with two separate doublets at 1.00-0.99 ppm [12H] ($^{2}J_{HH}$ = 6.6 Hz) and 1.16-1.14 ppm [6H] ($^{2}J_{HH}$ = 6.6 Hz) corresponding to the two distinct isopropyl CH_3 environments. The other resonances corresponding to the dimethylene linker and the tacn CH_2 environments were very broad and difficult to assign. The $^{13}C\{^{1}H\}$ NMR spectrum was more conclusive, showing the expected resonances arising from ligand formation. The ESI mass spectrum gave two peaks at *m/z*; 164.1 (100%) corresponding to $[L + 2H]^{2+}$and 327.2 (40%) corresponding to $[L + H]^{+}$, providing further evidence for ligand formation.

7.2.3 Coordination Chemistry

Coordination Chemistry with Group 13 Metal Halides

The coordination chemistry of the ligands prepared in Chapter 7.2 was investigated to gain insight into the potential coordination modes the ligands might adopt. Due to time constraints only the coordination chemistry of the ligands $\mathbf{L_c}$ and $\mathbf{L_b}$ was investigated.

Initial reactions were performed with the Group 13 metal chlorides under anhydrous conditions. Treatment of a solution of MCl_3 (M = Ga, In) in anhydrous MeCN with a solution of the ligands $\mathbf{L_c}$ or $\mathbf{L_d}$ in anhydrous MeCN at room temperature rapidly precipitated a while solid. Analysis of the precipitate indicated the formation of a tetrachlorometallate salt of the form [H**L**][MCl_4]. The infra-red spectrum of the solids produced showed a broad band at 2812 cm^{-1} corresponding to protonated amine. This implies that the nitrogen in the macrocyclic ring is being protonated, rather than the amide nitrogen.[20] The infra-red spectra each also showed a sharp stretch at 370 cm^{-1} and 338 cm^{-1} corresponding to the $[GaCl_4]^{-}$ and $[InCl_4]^{-}$ respectively.[21, 22] The presence of $[GaCl_4]^{-}$ anion in the salt [H**L**][$GaCl_4$] was confirmed using ^{71}Ga NMR spectroscopy. The spectrum recorded in CD_3CN showed a resonance at 250 ppm, indicative of $[GaCl_4]^{-}$.[21] ^{1}H NMR spectrocopy of the products showed the formation of a series of sharp multiplets corresponding to the tacn CH_2 protons. The sharp multiplets arise from the inequivalency in the tacn ring due to the protonated nitrogen atom. Further evidence of

protonated ligand was also derived from the change in chemical shifts from the free ligand resonances. While the neutral RMe_2-tacn complexes discussed in Chapters 2 and 3 displayed a *ca.* 0.5 ppm shift upon coordination to the metal centre, the ^{1}H NMR spectra of the compounds discussed here only a 0.02 ppm shift was observed, further indicating that the ligand was protonated in solution rather than coordinated to a metal centre.

Confirmation of the formulation derived from the spectroscopic data was gained from the microanalytical measurements which were consistent with the salts $[HL][MCl_4]$. It is likely that the free ligand contains water which is H-bonded to the amide functionality. Treatment of the hydrolytically unstable MCl_3 salts with the ligand solution resulted in hydrolysis of the metal halide to form the stable tetrahedral anion.

An attempt was made to synthesis the trifluoride complexes *via* hydrothermal synthesis. Reaction of $GaF_3{\cdot}3H_2O$ with $\mathbf{L_a}$ under hydrothermal conditions resulted in the formation of a black solution. Removal of the volatiles *in vacuo* gave a very dark brown solid. Spectroscopic analysis (IR, NMR, ESI^+ MS) gave no evidence of complex formation. It was assumed that the amide pendant arms were hydrolysed under the aggressive reaction conditions employed in hydrothermal synthesis. The resulting hydrolysis promoted complete ligand decomposition. This implies that while the hydrothermal synthesis method is suitable for robust alkyl or carboxylate functionlised aza-macrocycles, the amide pendant arms are unable to tolerate hydrothermal conditions. This is a further factor which can be taken into account in future ligand designs.

Coordination Chemistry with Transition Metal Salts

Due to the inability to form identifiable complexes with the hydrolytically unstable Group 13 chloride salts, attempts were made to identify a suitable metal salt which would allow the coordination modes of the ligands to be ascertained under mild conditions, and which would not readily form anionic species such as $[MCl_4]^-$.

The transition metal salt $Ni(NO_3)_2{\cdot}6H_2O$ was identified as a suitable precursor in which the coordination modes of the ligands could be investigated. The complex exists as the dissociated salt $[Ni(H_2O)_6][NO_3]_2$ in the solution phase, meaning the labile water molecules are readily displaced by any co-ligands which may be introduced. The pale green salt is soluble and stable in alcohol (MeOH, EtOH) solution, allowing the coordination chemistry to be more readily accessed.

Treatment of a pale green solution of $Ni(NO_3)_2{\cdot}6H_2O$ in MeOH with one molar equivalent of $\mathbf{L_c}$ at room temperature gives a purple solution. Removal of the volatiles *in vacuo* gives an air and mositure stable purple solid which is readily recystallised in $MeCN/Et_2O$ in good yield (> 60%). The complex is soluble in MeOH, H_2O and MeCN but is insoluble in

chlorocarbons. The initial characteristics of the complex (colour and solubility) closely matched the related $[Ni(tcet)]^{2+}$ (tcet = 3,3′,3″-(1,4,7-triazacyclononane-1,4,7-triyl)tripropanamide)) cation prepared by Wang *et al*. suggesting hexadentate coordination of the ligand to the Ni(II) centre *via* an N_3O_3 donor set.[23] As expected for a metal complex containing paramagnetic Ni(II) ion, d^8, the ^{1}H NMR spectrum was uninformative.[24] Attempts to gain an ESI mass spectrum of the complex were also unsuccessful. However, the purple crystals were suitable for single crystal X-ray diffraction (Figure 7.18). This confirmed the formation of the Ni(II) salt $[Ni(\mathbf{L_c})][NO_3]_2$.

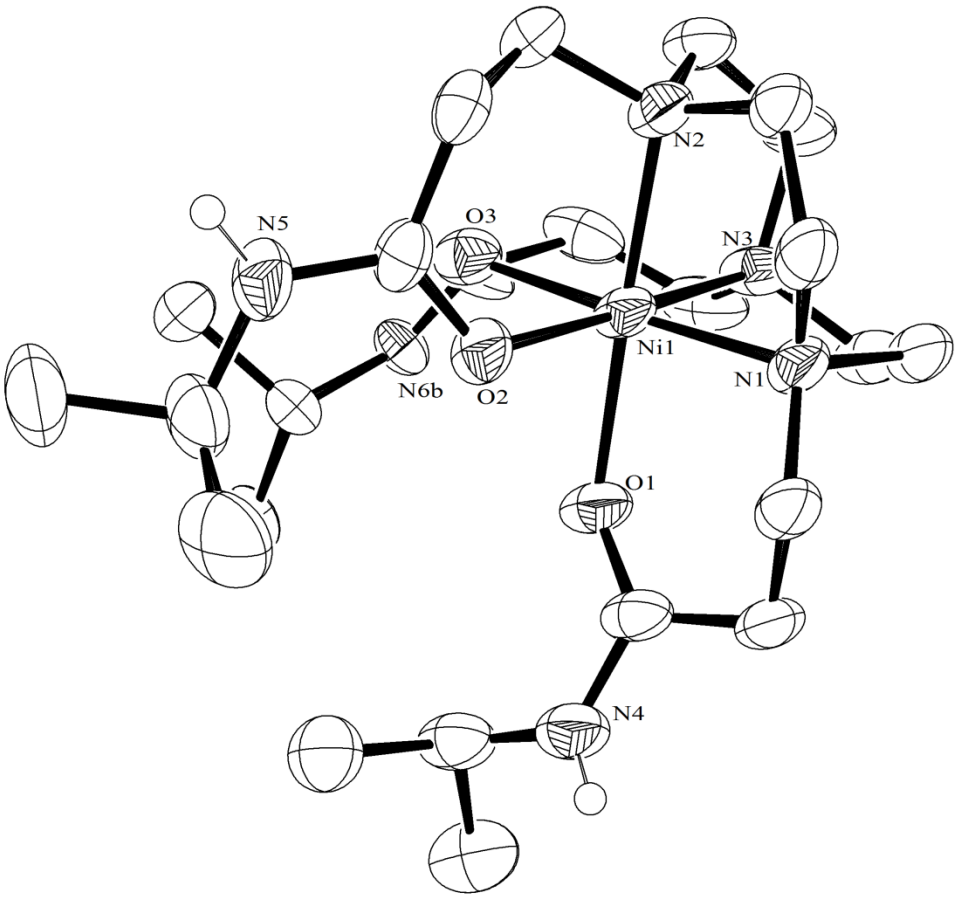

Figure 7.18: Crystal structure of the Ni containing cation in the complex $[Ni(\mathbf{L_c})][NO_3]_2$ with atom numbering scheme. Ellipsoids are drawn at 50% probability level. H-atoms (excluding those on the amide N-H) are omitted for clarity. Ni1-N1 2.059(3), Ni1-N2 2.074(2), Ni1-N3 2.070(3), Ni1-O1 2.059(2), Ni1-O2 2.036(2), Ni1-O3 2.040(2) Å. N1-Ni1-N2 85.65(10), N3-Ni1-N2 85.67(9), O3-Ni1-O1 89.19(9), O3-Ni1-N1 177.55(9), O3-Ni1-N3 92.19(10), O1-Ni1-N2 178.26(9)°.

The crystal structure shows that Ni(II) adopts a distorted octahedral coordination sphere. The ligand $\mathbf{L_c}$ coordinates in a hexadentate fashion. The tacn unit coordinates *facially* to the metal centre. The amide pendant arms fold over and coordinate through the amide carbonyl

groups forming a six-membered chelate ring. Comparison of the cation shown above with the $[Ni(tcet)]^{2+}$ reported by Wang *et al.* shows only small differences between the d(Ni-N) and d(Ni-O) bond lengths.[23] This is not unexpected since aside from the functional group attached to the amide nitrogen, the ligand architecture is essentially unchanged. This is also reflected in the bond angles, which show the N-Ni-O angles are very closely related to the complex reported previously.[23] The nitrate anions partake in O···H-N H-bonding interactions (2.984(2), 3.025(2) Å) with two of the amide pendant arms. This provides further evidence that the amide functionalised pendant arms may be able to form H-bonding interactions with a coordinated fluoride ligand, provided that the coordination of the amide group to the metal centre can be eliminated. Microanalytical measurements on the crystals obtained were consistent with the formulation derived crystallographically.[23]

The data obtained has demonstrated that even with longer ethylene bridged amide functionality there is a preference for both the tacn framework and the amide carbonyl groups to bind to the the metal centre as a hexadentate ligand containing six-memebered chelate rings. In alcohol solution, where the only competing ligands are labile, such as H_2O, $[NO_3]^-$ this is not unexpected as the chelate effect dominates.[4] It may be of interest to observe what would happen if a solution of fluoride was also added to the reaction mixture; would the formation of an M-F interaction be more favourable than the formation of a six-membered chelate.

Reaction of 1:1 molar equivalents of $Ni(NO_3)_2 \cdot 6H_2O$ with $\mathbf{L_d}$ in MeOH at room temperature gives a dark green solution. Removal of the volatiles *in vacuo* gives a very hygroscopic dark green solid. Rapid dissolution of this material in MeCN, followed by layering with Et_2O results in the formation of dark blue crystals suitable for single crystal x-ray diffraction.

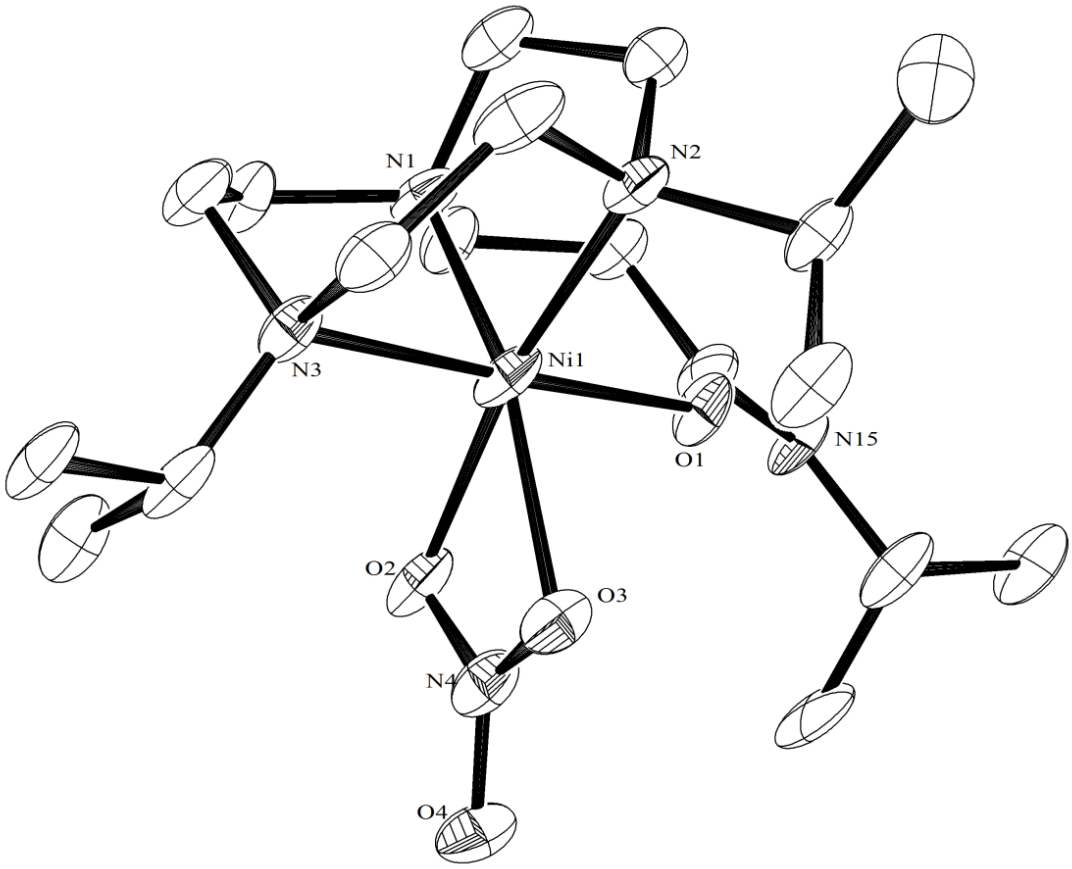

Figure 7.19: Crystal structure of the Ni containing cation in the complex $[Ni(NO_3)(\mathbf{L_d})]$ $[NO_3]$ with atom numbering scheme. Ellipsoids drawn at 50% probability level. The nitrate anion and H-atoms are omitted for clarity. Ni1-N1 2.042(4), Ni1-N2 2.086(5), Ni1-N3 2.151(5), Ni1-O1 2.047(4), Ni1-O2 2.157(4), Ni1-O3 2.124(4) Å. N1-Ni1-N2 85.40(2), N3-Ni1-N2 87.00(2), O2-Ni1-O3 83.35(17), N3-Ni1-O1 177.3(2), O1-Ni1-O3 86.89(17), O1-Ni1-N2 90.40(2), N2-Ni1-O3 112.11(17)°.

Figure 7.19 shows that the Ni(II) centre adopts a distorted octahedral geometry in which the $\mathbf{L_d}$ ligand coordinates in a tetradentate fashion with the tacn moiety bound *facially* to the metal centre. The amide pendant arm coordinates through the carbonyl oxygen to form a six-membered chelate. The coordination sphere around the metal is completed by κ^2 coordination of a nitrate anion. Comparison of the Ni-O bond lengths of the coordinated carbonyl group in $[Ni(NO_3)(\mathbf{L_d})]^+$ with the cation $[Ni(\mathbf{L_c})]^{2+}$ reveals very little difference between the two, however comparison of the d(M-N) of the nitrogen donor atoms from the tacn ring shows a slightly larger range in bond lengths for $[Ni(NO_3)(\mathbf{L_d})]^+$ (2.042(4)-2.151(5) Å) compared to $[Ni(\mathbf{L_c})]^{2+}$ (2.059(3)-2.070(3) Å). This is likely due to ligand distortion effects in order to allow coordination of the oxygen from the amide carbonyl group, and the requirement of κ^2

coordination of the nitrate anion to complete the octahedral coordination sphere around the nickel centre.

κ^2 Coordination of nitrate ions to a nickel centre is not unusual and there many examples in the literature.[25-28] The most relevant example was synthesised by Ochs *et al.* in which a tripodal tetramine ligand trpn (trpn = tris(2-aminopropyl)amine) reacts with $Ni(NO_3)_2 \cdot 6H_2O$ in MeOH to form the complex $[Ni(NO_3)(trpn)][NO_3]$.[29] They found that the Ni-O bond lengths from the coordinated nitrate were 2.173(11) and 2.224(10) Å.[29] The Ni-O bond lengths of the coordinated nitrate in the $[Ni(NO_3)(\mathbf{L_d})]^+$ complex above were found to be 2.124(4) and 2.157(4) Å, approximately 0.06 Å shorter than the most directly relevant literature example. This may infer that the nitrate is more strongly bound in the $[Ni(NO_3)(\mathbf{L_d})]^+$ complex above. This was a little unexpected as the more sterically demanding $\mathbf{L_d}$ ligand may have prevented the close approach of the nitrate anion.

It was presumed that the green solution and resulting hygroscopic solid was due to the complex $[Ni(OH_2)_2(\mathbf{L_d})]^{2+}$, and that the very hygroscopic nature was due to the coordinated water ligands. Dissolution of the material in MeCN and slow crystal formation likely promoted the coordination of the nitrate anion, and the subsequent formation of the blue crystalline material. As was the case for the $[Ni(\mathbf{L_c})]^{2+}$ cation, no peaks were observed in the ESI^+ mass spectrum for the dicationic species. Further confirmation of the formulation derived crystallographically was gained from microanalytical measurements.

The complex $[Ni(NO_3)(\mathbf{L_d})][NO_3]$ represents an exciting future ligand development towards ^{18}F labelled metal macrocyclic complexes supported by H-bond donor pendant arms. The use of a single amide pendant arm leaves vacant coordination sites on the metal in which the $^{18}F^-$ may coordinate. The coordination of the amide carbonyl oxygen rather than the amide nitrogen may allow the amide N-H to form H-bonding interactions with the coordinated fluoride ligands, forming a stronger interaction and aiding in directing the $^{18}F^-$ towards the metal centre. While direct comparisons between transition metals and main group metals (e.g. between nickel and gallium) should be treated with some caution, it is possible that the ligand will adopt the same coordination mode. This gives the possibility of reacting a Group 13 salt such as $Ga(NO_3)_3 \cdot 9H_2O$ (utilised in Chapters 3.2.4 and 4.2.2) with $\mathbf{L_d}$ and KF in aqueous MeOH to potentially produce the complex $[GaF_2(\mathbf{L_d})]$, which could have potential use in PET imaging applications.

7.3 Conclusions and Further Work

This chapter aimed to describe the synthesis of a series of azamacrocyclic ligands with amide functionalised pendant arms as models for future ligand frameworks which could act as intramolecular H-bond donors to coordinated ^{18}F. The ligands $\mathbf{L_a}$ – $\mathbf{L_d}$ were synthesised and purified in high yield and characterised fully. The ligands gave evidence of potential H-bonding interactions with anions, as shown by the crystal structure of $\mathbf{L_b}$·HCl, in which the amide N-H H-bonds to the chloride anion.

The potential coordination modes of the ligands $\mathbf{L_c}$ and $\mathbf{L_d}$ were investigated with the Group 13 metal chlorides. However reaction of the ligand with the metal halide under anhydrous conditions gave evidence of formation of the protonated ligand salt [H**L**][MCl_4] as evidenced by infra-red and NMR spectroscopy and microanalysis. It was concluded that trace H-bonded water in the ligand resulted in hydrolysis of the metal halide and the formation of the stable tetrahedral anion. Therefore the coordination chemistry was performed with a hydrolytically stable transition metal salt $Ni(NO_3)_2{\cdot}6H_2O$ in MeOH. Reaction of $\mathbf{L_c}$ with the nickel salt gives the octahedral Ni(II) cation $[Ni(\mathbf{L_c})]^{2+}$. The ligand forms a hexadentate interaction with the metal centre in an N_3O_3 donor set. The amide carbonyl oxygen preferentially binds to the metal centre over the amide N-H, in keeping with the general trends discovered previously.[8, 23] This ligand, in which there are three amide pendant arms is likely unsuitable for the proposed application of H-bond directed ^{18}F incorporation as it is likely that on the smaller Group 13 metals aluminium and gallium there would be no vacant coordination site in which ^{18}F could bind. However on larger trivalent metal centres such as indium, scandium or yttrium, in which higher coordination numbers may be accessed, this ligand may be of interest. In a departure from the proposed application, this ligand may be of interest as an alternative scaffold for ^{68}Ga and ^{111}In based imaging agents (Chapter 1.8).[30]

A more exciting alternative ligand scaffold was found by reaction of $\mathbf{L_d}$ with $Ni(NO_3)_2{\cdot}6H_2O$ in MeOH at room temperature. The resulting blue crystals of the octahedral cation $[Ni(NO_3)_3(\mathbf{L_d})]^+$ showed that the ligand coordinates as a tetradentate, with the amide carbonyl oxygen coordinated. κ^2 Coordination of the nitrate ligand completes the coordination sphere. The coordinated nitrate raises the possibility of performing a ligand exchange reaction with KF leading to the potential formation of $[MF_2(L_d)]^{n+}$. Complexes of this type may well prove to be very good agents for the incorporation of $^{18}F^-$ and subsequent PET imaging applications.

This account of the synthesis, characterisation and selected coordination chemistry of new amide functionalised pendant arm azamacrocycles has demonstrated a number of potential ligand architectures and provided synthetic methods. Future work could be aimed towards synthesising a large library of these ligand types, with amide pendant arms which could be

tuned to change the electronic and steric properties of the ligand. Although amide functionality was used exclusively as potential H-bond donors in this section of work, the synthesis could be extended to a number of differing H-bond donors such as amine, imidazole or pyrrole based pendant arms.

The coordination chemistry of these ligands could be explored in more detail, particularly with the Group 13 ions which as shown throughout this thesis have been highly successful in forming stable metal fluoride complexes with macrocyclic ligands. Of particular interest would be whether the metal fluoride complex could be made using **L_d**, and subsequently investigation whether the amide pendant arm does form an H-bonding interaction with the coordinated fluoride.

7.4 Experimental

For general synthetic methods see Appendix 1. The ligands 1,4,7-triazacyclonoane (tacn),[31] and 1,4-diisopropyl-1,4,7-triazacyclonoane ($^{i}Pr_2$-tacn)[14] were synthesised as described in the literature. The 2-chloro-N-phenylacetamide was synthesised as described in the literature and recrystallised from CH_2Cl_2/hexane before use.[32] N-isopropylyacrylamide (Aldrich) was used as supplied. Solvents used were of chromatography grade and where appropriate were thoroughly degassed with N_2 before use.

1,4,7-tris-N-phenylacetamide-1,4,7-triazacyclononane, L_a

To a rapidly stirring mixture of K_2CO_3 (3.25 g, 27 mmol) in 40 mL acetone was added H_3-tacn (0.253 g, 1.96 mmol). The mixture was stirred for ten minutes at room temperature. A solution of 2-chloro-N-phenyl acetamide (1.00 g, 5.90 mmol) in 20 mL acetone was added dropwise. The resultant mixture was stirred at room temperature for 18 hours. The mixture was filtered and the pH of the resulting pale yellow solution adjusted to 12 with 1.0 M NaOH. The filtrate was concentrated under high vacuum. This resulted a pale yellow solid which was purified by flash column chromatography (9:1 MeOH: CH_2Cl_2). Yield 0.75 g, 75%. ^{1}H NMR ($CDCl_3$, 298 K) δ = 2.91 (s [12H] tacn CH_2), 3.66 (s [6H] N-CH_2CO_2), 7.15 (m [3H] ArCH), 7.35 (m [6H] ArCH), 7.57 (m [6H] ArCH), 8.51 (br s [3H] N-H). $^{13}C\{^{1}H\}$ NMR ($CDCl_3$, 298 K) δ = 30.9, 42.9, 120.1, 125.1, 129.1, 136.8, 163.9. ESI+ (MeCN): *m/z* 529.2 (100%) [$M+H^+$]. Recrystallisation from MeCN/Et_2O furnished crystals suitable for single crystal X-ray diffraction.

1,4-diisopropyl-7-N-phenylacetamide-1,4,7-triazacyclononane, L_b

Powdered K_2CO_3 (0.200 g, 1.44 mmol) was added to a solution of 1,4-diisopropyl-1,4,7-triazacyclononane (0.200 g, 0.937 mmol) in 10 mL degassed acetone and stirred at room

temperature for 15 minutes. A solution of 2-chloro-N-phenylacetamide (0.158 g, 0.936 mmol) in 10 ml degassed acetone was added drop wise to the rapidly stirring mixture. The orange solution was stirred at room temperature overnight. The mixture was filtered through celite and the pH of the filtrate adjusted to 12 with 1.0 M NaOH. The solvent was removed under high vacuum to yield the product as a highly viscous yellow oil. Yield 0.316 g, 70%. ^{1}H NMR ($CDCl_3$ 298 K) δ = 1.23-1.19 (t [12H] $^{2}J_{HH}$ 15 Hz ^{i}Pr CH_3), 2.98 (br m [12H] tacn CH_2), 3.26 (m [2H] ^{i}Pr CH), 3.82 (s [2H] N-CH_2-CO), 7.04 (m [1H] Ar CH), 7.25 (m [2H] Ar CH), 7.88 (m [2H] Ar CH). $^{13}C\{^{1}H\}$ NMR ($CDCl_3$ 298 K) δ = 17.6, 18.2, 46.9, 47.9, 51.0, 54.5, 59.0, 120.0, 123.7, 138.7, 169.6. ESI^{+} (MeCN) *m/z*; 174.3 (100%) $[M + 2H]^{2+}$, 347.2 (45%) $[M + H]^{+}$.

1,4,7-tris-N-isopropylacrylamide-1,4,7-triazacyclononane, L_c

1,4,7-triazacyclononane (0.322 g, 2.50 mmol), and N-isopropylacrylamide (0.849 g, 7.50 mmol) were dissolved in 50 mL degassed MeOH and heated to 70 °C for 18 hours. The pale yellow solution was filtered through celite to remove particulates and the volatiles removed under high vacuum. The pale yellow oil was dissolved in 10 mL 1.0 M HCl, which was washed with 3 x 20 mL $CHCl_3$. The pH of the aqueous phase was adjusted to > 12 using *ca*. 30 mL 2.0 M KOH. The aqueous phase was extracted with 3 x 50 mL $CHCl_3$. The organic extract was dried over $MgSO_4$, filtered and concentrated under high vacuum to give the desired compound as a highly viscous brown oil. Yield 0.750 g, 80%. ^{1}H NMR ($CDCl_3$, 298 K) δ = 1.16-1.14 (d [18H] ^{i}Pr CH_3), 2.29 (t [6H] Et CH_2), 2.78 (s [12H] tacn CH_2), 2.81 (m [6H] Et CH_2), 4.07 (sextet [3H] ^{i}Pr CH), 6.66 (br s [3H] NH). $^{13}C\{^{1}H\}$ NMR ($CDCl_3$ 298 K) δ = 23.2, 35.0, 41.5, 55.5, 56.3, 171.6. ESI^{+} (MeCN): *m/z*; 235.3 (100%) $[M + 2H]^{2+}$, 469.4 (40%) $[M + H]^{+}$, 491.4 (35%) $[M + Na]^{+}$.

1,4-diisopropyl-7-N-isopropylacrylamide-1,4,7-triazacyclononane, L_d

1,4-diisopropyl-1,4,7-triazacyclononane (0.295 g, 1.38 mmol) and N-isopropylacrylamide (0.156 g, 1.38 mmol) were dissolved in 30 mL degassed MeOH and heated to 70 °C for 18 hours. The yellow-orange solution was filtered through celite to remove particulates and the volatiles removed under high vacuum. The orange oil was dissolved in 10 ml 1.0 M HCl, which was washed with 3 x 20 mL $CHCl_3$. The pH of the aqueous phase was adjusted to > 11 using *ca*. 30 mL 2.0 M KOH. The aqueous phase was extracted with 3 x 50 mL $CHCl_3$. The organic extract was dried over $MgSO_4$, filtered and concentrated under high vacuum to give the desired compound as a viscous orange-brown oil. Yield 0.324 g, 72%. ^{1}H NMR ($CDCl_3$, 298 K) δ = 1.00-0.99 (d [12H] ^{i}Pr CH_3), 1.16-1.14 (d [6H] ^{i}Pr CH_3), 2.30-2.27 (t [2H] Et CH_2), 2.49 (br s [4H] tacn CH_2), 2.71 (m [6H] tacn CH_2), 2.89-2.85 (sextet [2H] ^{i}Pr CH), 2.93 (br m [4H] tacn CH_2 and Et CH_2), 4.10-4.00 (sextet [1H] ^{i}Pr CH), 8.58 (br s [1H] NH) . $^{13}C\{^{1}H\}$ NMR ($CDCl_3$, 298 K) δ = 18.2, 22.8, 33.2, 40.6, 47.8, 50.6, 51.4, 52.2, 53.0, 54.8, 55.6, 163.6, 172.4. ESI^{+} (MeCN): *m/z*; 164.1 (100%) $[L + 2H]^{2+}$, 327.2 (40%) $[L + H]^{+}$.

[Ni(L_c)][NO_3]$_2$

A solution of $\mathbf{L_c}$ (0.094 g, 0.20 mmol) in 5 mL EtOH was added to a solution of $Ni(NO_3)_2 \cdot 6H_2O$ (0.056 g, 0.20 mmol) in 5 mL EtOH. Addition of the ligand solution produced a purple solution. The mixture was stirred at room temperature for one hour. The volatiles were removed *in vacuo* giving a lilac/purple solid. The solid was recrystallised from MeCN/EtOH which yielded large purple crystals suitable for single crystal X-ray diffraction. Yield 0.082 g, 63%. Required for $C_{24}H_{48}N_8NiO_9$: C, 44.3; H, 7.4; N, 17.2. Found: C, 44.6; H, 7.2; N, 16.6%. IR (Nujol, ν/cm^{-1}) 3272, 3094 1639, 1611, 1571.

[Ni(NO_3)(L_d)][NO_3]

A solution of L_d (0.087 g, 0.27 mmol) in 5 mL EtOH was added to a solution of $Ni(NO_3)_2 \cdot 6H_2O$ (0.078 g, 0.27 mmol) in 5 mL EtOH. An intense green solution formed. The mixture was stirred at room temperature for one hour. The volatiles were removed *in vacuo* giving a hygroscopic green solid. The solid was taken up in MeCN and layered with Et_2O. Over a period of about 4 days, a mass of blue crystalline material formed. These were isolated by filtration, washed with Et_2O and dried. Yield 0.064 g, 47%. Required for $C_{18}H_{38}N_6NiO_7$: C, 42.5; H, 7.5; N, 16.5. Found: C, 41.9; H, 8.0; N, 17.4%. IR (Nujol, ν/cm^{-1}) 3619, 3179, 1615, 1584.

Table 7.1: Table of crystallographic data for the compounds discussed in this chapter.[a]

Compound	**$(CH_2CONHPh)_3$-tacn·0.5 Et_2O**	**$^{i}Pr_2(CH_2CONHPh)$-tacn·HCl·H_2O**
Formula	$C_{32}H_{41}N_6O_{3.5}$	$C_{20}H_{37}ClN_4O_2$
M	565.71	400.99
Crystal system	Triclinic	Orthorhombic
Space group (no.)	P-1	$Pna2_1$
a /Å	8.093(5)	15.931(5)
b /Å	13.598(8)	9.731(3)
c /Å	14.091(9)	29.861(9)
α /°	101.570(15)	90
β /°	94.556(15)	90
γ /°	95.664(15)	90
U /Å^3	1503.9(16)	4629(3)
Z	2	8
μ(Mo-K$_\alpha$) /mm^{-1}	0.71073	0.71073
F(000)	606	1744
Total number reflections	14935	21600
Unique reflections	6903	9867
R_{int}	0.1023	0.0569
R_1 [$I > 2\sigma(I)$] [b]	0.093	0.063
R_1 (all data)	0.115	0.161
wR_2 [$I > 2\sigma(I)$] [b]	0.2043	0.1308
wR_2 (all data)	0.2193	0.1708

[a] Common items: T = 100 K; wavelength (Mo-Kα) = 0.71073 Å; θ (max) = 27.5°;

[b] $R_1 = \Sigma||F\sigma| - |Fc|| / \Sigma|Fo|$; $wR_2 = [\Sigma w(Fo^2 - Fc^2)^2 / \Sigma wFo^2]^{1/2}$.

Table 7.2: Table of crystallographic data for the compounds discussed in this chapter.[a]

Compound	**$[Ni(L_c)][NO_3]_2$**	**$[Ni(NO_3)(L_d)][NO_3]$**
Formula	$C_{24}H_{48}N_8NiO_9$	$C_{18}H_{38}N_6NiO_7$
M	509.21	651.41
Crystal system	Monoclinic	Triclinic
Space group (no.)	$P2_1/c$	P-1
a /Å	17.826(8)	9.897(6)
b /Å	11.407(4)	10.639(6)
c /Å	18.086(11)	12.956(9)
α /°	90	98.235(19)
β /°	119.181(7)	101.140(16)
γ /°	90	110.359(14)
U /Å^3	3211(3)	1221.5(13)
Z	4	2
μ(Mo-K$_\alpha$) /mm^{-1}	0.71073	0.71073
F(000)	1388	542
Total number reflections	30359	7945
Unique reflections	7348	4297
R_{int}	0.0749	0.1533
R_1 [$I > 2\sigma(I)$] [b]	0.053	0.056
R_1 (all data)	0.085	0.188
wR_2 [$I > 2\sigma(I)$] [b]	0.1377	0.1104
wR_2 (all data)	0.1577	0.1336

[a] Common items: T = 100 K; wavelength (Mo-Kα) = 0.71073 Å; θ (max) = 27.5°;

[b] $R_1 = \Sigma||F\sigma| - |Fc|| / \Sigma|Fo|$; $wR_2 = [\Sigma w(Fo^2 - Fc^2)^2 / \Sigma wFo^2]^{1/2}$.

7.5 References

1. Bhalla, R.; Darby, C.; Levason, W.; Luthra, S. K.; McRobbie, G.; Reid, G.; Sanderson, G.; Zhang, W., *Chem. Sci.* **2014,** *5*, 381-391.
2. Bhalla, R.; Levason, W.; Luthra, S. K.; McRobbie, G.; Sanderson, G.; Reid, G., *Chem. Eur. J.* **2015,** *21*, 4688-4694.
3. Wieghardt, K.; Bossek, U.; Chaudhuri, P.; Herrmann, W.; Menke, B. C.; Weiss, J., *Inorg. Chem.* **1982,** *21*, 4308-4314.
4. Sayer, B. A.; Michael, J. P.; Hancock, R. D., *Inorg. Chim. Acta.* **1983,** *77*, L63-L64.
5. Moore, D. A.; Fanwick, P. E.; Welch, M. J., *Inorg. Chem.* **1989,** *28*, 1504-6.
6. Schlager, O.; Wieghardt, K.; Grondey, H.; Rufinska, A.; Nuber, B., *Inorg. Chem.* **1995,** *34*, 6440-8.
7. Gahan, L. R.; Lawrance, G. A.; Sargeson, A. M., *Aust. J. Chem.* **1982,** *35*, 1119-31.
8. Weyhermüller, T.; Weighardt, K.; Chaudhuri, P., *J. Chem. Soc., Dalton Trans.* **1998**, 3805-3814.
9. Amin, S.; Marks, C.; Toomey, L. M.; Churchill, M. R.; Morrow, J. R., *Inorg. Chim. Acta.* **1996,** *246*, 99-107.
10. Tei, L.; Blake, A. J.; Lippolis, V.; Wilson, C.; Schroeder, M., *Dalton Trans.* **2003**, 304-310.
11. Zhang, Z.; He, Y.; Zhao, Q.; Xu, W.; Li, Y.-Z.; Wang, Z.-L., *Inorg. Chem. Commun.* **2006,** *9*, 269-272.
12. Scheuermann, J. E. W.; Sibbons, K. F.; Benoit, D. M.; Motevalli, M.; Watkinson, M., *Org. Biomol. Chem.* **2004,** *2*, 2664-2670.
13. Tsukube, H.; Adachi, H.; Morosawa, S., *J. Org. Chem.* **1991,** *56*, 7102-8.
14. Martin, A. E.; Ford, T. M.; Bulkowski, J. E., *J. Org. Chem.* **1982,** *47*, 412-415.
15. Winchell, H. S.; Klein, J. Y.; Simhon, E. D.; Cyjon, R. L.; Klein, O.; Zaklad, H. Compounds with chelation affinity and selectivity for first transition series elements for medical use. US5874573A, 1999.
16. Smith, R. M.; Martell, A. E., *Critical Stability Constants, Vol. 2: Amines*. Plenum: 1975.
17. Schlesinger, A. H.; Prill, E. J., *J. Am. Chem. Soc.* **1956,** *78*, 6123-6127.
18. Clayden, J.; Greeves, N.; Warren, S.; Wothers, P., *Organic Chemistry*. Oxford University Press: 2000.
19. Kataky, R.; Matthes, K. E.; Nicholson, P. E.; Parker, D.; Buschmann, H. J., *J. Chem. Soc , Perkin Trans 2* **1990**, 1425-32.
20. Nakamoto, K., *Infrared Spectra of Inorganic and Coordination Compounds*. J. Wiley & Sons: 1985; Vol. 1.
21. George, K.; Jura, M.; Levason, W.; Light, M. E.; Ollivere, L. P.; Reid, G., *Inorg. Chem.* **2012,** *51*, 2231-2240.

22. Gurnani, C.; Jura, M.; Levason, W.; Ratnani, R.; Reid, G.; Webster, M., *Dalton Trans.* **2009**, 1611-1619.
23. Liu, R.; Li, Y.-Z.; Zhang, Z.; Wang, Z.-L., *Acta Cryst. Section E.* **2006,** *62*, m1064-m1065.
24. Mason., J., *Multinuclear NMR*. Plenum Press: 1987; Vol. 1.
25. Broge, L.; Pretzmann, U.; Jensen, N.; Sotofte, I.; Olsen, C. E.; Springborg, J., *Inorg. Chem.* **2001,** *40*, 2323-2334.
26. Gorczynski, A.; Walesa-Chorab, M.; Kubicki, M.; Korabik, M.; Patroniak, V., *Polyhedron* **2014,** *77*, 17-23.
27. Kong, D.; Meng, L.; Song, L.; Xie, Y., *Transition Met. Chem. (Dordrecht, Neth.)* **1999,** *24*, 553-557.
28. Massoud, S. S.; Chun, H.; Wen, R.; Bernal, I., *J. Coord. Chem.* **2002,** *55*, 1065-1078.
29. Ochs, C.; Hahn, F. E.; Lügger, T., *Eur. J. Inorg. Chem.* **2001**, 1279-1285.
30. Blower, P. J., *Dalton Trans.* **2015**, DOI: 10.1039/C4DT02846E,.
31. Richman, J. E.; Atkins, T. J., *J. Am. Chem. Soc.* **1974,** *96*, 2268-2270.
32. Zhaowen, L.; Li, Z.; Chunfen, X.; Yong, Y.; Fanbo, Z.; Kaixun, H., *Med. Chem. Res.* **2007,** *16*, 380-391.

Chapter 8

Summary and Outlook

While the detailed conclusions and future work have been discussed at the end of each chapter, this short section summarises the conclusions drawn from the work presented and their potential further uses in PET imaging applications described.

This thesis aimed to develop a new generation of potential PET imaging agents using coordination complexes of the Group 13 metal halides. This involved the incorporation of the radioactive ^{18}F isotope into a preformed metal complex *via* a halide exchange reaction. In order to develop this class of compound further, the coordination chemistry of the Group 13 fluorides was investigated to further the understanding of this little explored area of coordination chemistry.

The mildly moisture sensitive adducts $[MCl_3(RMe_2tacn)]$ (M = Al, Ga, In) were synthesised in good yield from combination of the trivalent metal chloride MCl_3 with the neutral aza-macrocycles Me_3-tacn and $BzMe_2$-tacn. The complexes adopt a six-coordinate octahedral geometry with the tridentate tacn ligand bound *facially* to the metal centre. The complexes were characterised fully.

The neutral trifluoro complexes $[MF_3(Me_3\text{-tacn})]\cdot 4H_2O$ (M = Al, Ga, In) were synthesised hydrothermally. The complexes are hydrated in the solid state and display extensive F····H-OH and H····OH_2 H-bonding interactions. The trifluoro complexes are stable under a number of conditions. The spectroscopic fingerprint acquired for these compounds proved useful in identifying the other trifluoro complexes synthesised in this work.

The complexes $[MF_3(RMe_2\text{-tacn})]\cdot xH_2O$ were prepared *via* a halide exchange under both anhydrous conditions using R_4NF (R = Me, Bu) and with $KF_{(aq)}$. Unusually, under anhydrous conditions, the halide exchange reaction did not occur in the aluminium. This was due to the steric constraints of the aluminium as it underwent ligand substitution. The gallium and indium complexes were accessed in both cases, with the gallium analogue forming very quickly (10 minutes) at room temperature in aqueous solution. The indium analogue was significantly slower at room temperature (60 minutes) but accelerated with heating to 80 ^{o}C (30 minutes).

Based upon the halide exchange studies, the complex $[GaCl_3(BzMe_2\text{-tacn})]$ was radiolabelled with carrier added $^{18}F/K^{19}F$ to form $[Ga^{18}F^{19}F_2(BzMe_2\text{-tacn})]$ at room temperature in aqueous MeCN. The reaction showed 30% incorporation of $^{18}F^-$ into the complex, which leads to an exciting prospect of using this chelate type to label heat or temperature sensitive biomolecules. The labelled complex is remarkably stable under physiological conditions (PBS,

pH 7.5), showing no significant decomposition over at least 120 minutes. This shows that the use of a *fac*-trifluoride based metal chelate as a robust imaging agent is possible.

The radiolabelled complex [$Ga^{18}F^{19}F_2$(BzMe$_2$-tacn)] was identified by ESI MS, giving a peak in the mass spectrum corresponding to the unusual cationised species {[GaF_3(BzMe$_2$-tacn)] + NH_4}$^+$. This suggested that the highly electronegative trifluoride face of the complex was able to form weak interactions with any cations which may be introduced. This phenomenon was investigated with a series of ESI MS experiments, and supported with crystallographic examples. Combination of [GaF_3(BzMe$_2$-tacn)] with a series of alkali metal and ammonium cations gives species in the mass spectrum consistent with the ion {[GaF_3(BzMe$_2$-tacn)] + cat}$^+$ (cat = cation). This helped support the observations from the radiolabelling experiments. Unusually while alkali metal and ammonium cations showed this feature, Group 2 and Group 3 metal cations did not show this feature, likely a consequence of their high affinity for water. The observations from the mass spectrometry experiments was supported by a number of crystallographic examples which gave a series of very interesting supramolecular assemblies in which [GaF_3(BzMe$_2$-tacn)] acted as a metalloligand towards the alkali metal cations Li, Na and K. The metal size has a huge influence on the types of structure formed. The mixed NH_4^+/Na^+ metalloligand species was also formed.

Reaction of the water soluble $Ga(NO_3)_3{\cdot}9H_2O$ with the hydrochloride salt of the anionic ligand (Bz(CH_2CO_2)$_2$-tacn)$^{2-}$ at 85 ^{o}C leads to the formation of the neutral octahedral complex [GaCl(L)] in which L acts as a pentadentate ligand donor with an N_3O_2 donor set. The carboxylate pendant arms coordinate to the metal centre leaving a single halide site in which to perform an exchange reaction. The chloride from the ligand salt preferentially coordinates to the metal centre. The corresponding fluoride complex [GaF(L)] was synthesised *via* chloride/fluoride in aqueous KF at room temperature. The [GaCl(L)] complex was radiolabelled with carrier free $^{18}F^-$ at 85 ^{o}C leading to 80% incorporation of the $^{18}F^-$ to give [$Ga^{18}F$(L)]. The radiolabelled compound was purified by a cartridge based technique. While [$Ga^{18}F$(L)] was stable in acidic media, at neutral pH the compound rapidly hydrolysed liberating $^{18}F^-$. This is in contrast to the complexes discussed above, and perhaps further highlights just what a good class of chelate the neutral trifluorides might be. The subtle role of Lewis acidity and sterics were postulated to be the reason for the complexes decomposition. However, with appropriate tuning of the ligand architecture, this compound type may yet still have useful properties as future PET imaging agents.

The coordination chemistry of the poorly soluble Group 13 metal fluorides was investigated using hydrothermal synthesis. $MF_3{\cdot}3H_2O$ reacts with terpy to give the complexes [MF_3(terpy)]$\cdot3H_2O$. As is shown in all of the fluoride complexes discussed throughout this

thesis, there are extensive H-bonding interactions in the solid state. Reaction of $MF_3 \cdot 3H_2O$ with the bidentate imines 2,2'-bipy and phen gives rise to the complexes $[MF_3(L\text{-}L)(OH_2)] \cdot xH_2O$.

A series of amide based pendant arm tacn macrocycles were synthesised and characterised, and their coordination modes studied. These ligands may be of interest in future labelling applications.

The work described in this thesis represents a significant enhancement in the field of metal complex based PET imaging agents in with $^{18}F^-$. A new method was developed in which ^{18}F labelled compounds may be accessed *via* a halide exchange reaction under mild conditions from a preformed metal chelate complex. This could allow the labelling of heat or temperature sensitive biomolecules, and raises the prospect of a kit based radiopharmaceutical which could be prepared with minimal technical support. The stability of the labelled complex $[Ga^{18}F^{19}F_2(BzMe_2\text{-tacn})]$ in phosphate buffered saline in particular is a remarkable observation, and demonstrates that with careful ligand design, this compound type may have real utility in imaging applications.

The future development of this chemistry lies in the incorporation of bioactive molecules or peptides into the ligand framework so that post labelling, the bio distribution may be measured and if possible, the imaging quality tested *in vivo* on an animal subject. One may envisage preparing the neutral macrocycle RMe_2-tacn (where R = a peptide attached to the benzyl substituent). This bioactive ligand would then be conjugated to a Ga(III) centre, likely by reaction with $Ga(NO_3)_3 \cdot 9H_2O$ to allow very small quantities of the preformed complex to be prepared. The preformed chelate could then be radiolabelled utilising the methodology described in this thesis. This could lead to a bioactive, ^{18}F labelled radiopharmaceutical which is stable *in vivo* and can thus allow imaging studies.

If this route proves viable, and its utility shown with a number of bioactive molecules or peptides, then it is likely that a kit could be prepared which would then make the method highly suitable for clinical use as a stable compound in which late stage fluorination may occur under mild conditions.

It is strongly hoped that the work described in this thesis forms the basis for these exciting future developments in the field of PET imaging agents.

Appendix 1 – General Experimental Techniques

Where required all reactions were conducted using Schlenk, vacuum line and glove-box techniques under a dry dinitrogen atmosphere. The Group 13 metal chlorides MCl_3 (M = Al, Ga, In) and complexes thereof were handled and stored in a dry N_2 filled glove box. Solvents were dried and degassed prior to use. Et_2O and thf were distilled over Na/benzophenone ketyl; hexane and toluene over Na wire; CH_2Cl_2, $CHCl_3$ and MeCN were distilled over CaH_2 and MeOH was dried over Mg/I_2. Reactions performed under aqueous conditions utilised freshly distilled H_2O. Unless stated explicitly in each Chapter's experimental, all commercial reagents (obtained from Sigma-Aldrich, Strem, Alfa Aesar) were used as received. All ligands were prepared *via* literature methods or modifications thereof.

Infra-red spectra were recorded over a range of 4000-200 cm^{-1} using a Perkin Elmer Spectrum 100 spectrometer. Samples were prepared as Nujol mulls between CsI plates. NMR spectra were recorded on a Bruker AV400 or DPX400 spectrometers. ^{1}H and $^{13}C\{^{1}H\}$ NMR spectra were referenced to the solvent resonances. $^{19}F\{^{1}H\}$ spectra were referenced to $CFCl_3$, ^{27}Al to aqueous $[Al(OH_2)_6]^{3+}$, ^{71}Ga to aqueous $[Ga(OH_2)_6]^{3+}$ and ^{115}In to aqueous $[In(OH_2)_6]^{3+}$ at pH 1. ESI mass spectrometry was recorded using a Waters (Manchester, UK) ZMD mass spectrometer equipped with a single quadrupole analyser. Samples were introduced to the mass spectrometer via flow injection using a Waters 600 pump (flow rate 0.1 mL / min MeCN) and Waters 2700 autosampler. Microanalyses were performed by Medac Ltd or London Metropolitan University.

Single crystal X-ray data were collected using a Rigaku AFC12 goniometer equipped with an enhanced sensitivity (HG) Saturn724+ detector mounted at the window of an FR-E+ SuperBright molybdenum rotating anode generator with HF or VHF Varimax optics using Mo-Kα radiation (λ = 0.71073 Å). Crystals were held at 100 K under a nitrogen gas strem (Oxford Cryostream). Solution and refinement of structures was carried out using SHELX-97,[1-3] with hydrogen atoms added to the model in calculated positions using default C-H distances. Where additional restraints were required, details are provided in the cif file for each structure, or are discussed in the text.

Radiolabelling experiments were analysed on a Gilson 322 HPLC system with a Gilson 156 UV detector. Dionex Chromeleon 6.8 Chromatography data recording software was used to integrate the UV and radiochemical peak areas. ESI^+ mass spectra of radiolabelled species were recorded from direct injection of the products onto a Thermo Finnigan mass spectrometer fitted with an LCQ advantage MS pump.

References

1. Sheldrick, G. M. *SHELXL-97, program for crystal structure refinement*, University of Gottingen, Germany, 1997.
2. Sheldrick., G. M. *SHELXL-97, program for crystal structure solution*, University of Gottingen, Germany, 1997.
3. Flack, H. D., *Acta Crystallogr., Sect. A.* **1983,** *A39*, 876-81.

Appendix 2 – Crystallographic Information Files

Cif files are located on a CD attached to the back of the thesis.

‘The measure of who we are is what we do with what we have’